DOPING EXPERIMENTS ON MAGNETIC HEAVY FERMION SUPERCONDUCTORS

By

WEONWOO KIM

A DISSERTATION PRESENTED TO THE GRADUATE SCHOOL
OF THE UNIVERSITY OF FLORIDA IN PARTIAL FULFILLMENT
OF THE REQUIREMENTS FOR THE DEGREE OF
DOCTOR OF PHILOSOPHY

UNIVERSITY OF FLORIDA

1995

ACKNOWLEDGMENTS

I wish to express my sincere appreciation to Professor Gregory R. Stewart not only for his stimulating suggestions and valuable advice throughout the entire research of this work, but also for his patient encouragement when I had a hard time in my course work and research. In addition, I am very thankful not only to Professor P. Kumar for his delightful and clear discussions and comments in physics, but also to Professors Y. Takano, N.S. Sullivan, K. Ingersent, and T.J. Anderson for their valuable advice and suggestions.

Special thanks go to Dr. B. Andraka for his valuable discussions and cooperation, Dr. J.S. Kim for his help in experiments, R. Pietri, and S. Thomas for his proofreading of the manuscript as well as pleasant relationship.

The faculty, postdoctoral fellows, administrative, and technical support from the machine shop, cryogenics, and electronic shop have contributed a great deal to this work.

Finally, I dedicate my warm love and gratitude to my family including my wife Hea-Kyung for her consistent trust and encouragement, two sons Dong-Hwa and Dong-In, and relatives in Korea for their support and prayer.

HAPPY IS THE PERSON WHO REMAINS FAITHFUL UNDER TRIALS, BECAUSE WHEN HE SUCCEEDS IN PASSING SUCH A TEST, HE WILL RECEIVE AS HIS REWARD THE LIFE WHICH **GOD** *HAS PROMISED TO THOSE WHO LOVE HIM.* (James 1:12)

TABLE OF CONTENTS

pages

ACKKNOWLEDGMENTS....................ii

LIST OF TABLES....................v

LIST OF FIGURES....................vi

ABSTRACT....................ix

CHAPTERS

INTRODUCTION....................1

- 1.1 Overview of Heavy Fermion Systems....................1
  - 1.1.1 Classification of Heavy Hermion Systems....................2
  - 1.1.2 Mass Enhancement....................5
  - 1.1.3 Superconductivity....................6
  - 1.1.4 Magnetism....................6
- 1.2 Motivation....................9
- 1.3 Experimental Techniques....................10
  - 1.3.1 Sample Preparation....................11
  - 1.3.2 Measurement Techniques....................11

2 REVIEW OF THEORY....................20

- 2.1 Fermi Liquid Theory....................20
- 2.2 Non-Fermi Liquid Theory....................27
  - 2.2.1 Multichannel Kondo Effect....................27
  - 2.2.2 Phenomenological Theory of a Critical Point at $T = 0$ K....................38

3 NON-FERMI LIQUID BEHAVIOR OF MAGNETIC HEAVY FERMION SUPERCONDUCTORS....................42

- 3.1 Overview of Non-Fermi Liquid Systems....................42
- 3.2 Investigation of the Ground State in $U_XTh_{1-X}Ru_2Si_2$ for $x < 0.20$....................44
  - 3.2.1 URu_2Si_2....................45
  - 3.2.2 Doping Effects of URu_2Si_2....................48

3.2.3 Non-Fermi Liquid Behavior of $U_xTh_{1-x}Ru_2Si_2$ for $x \leq 0.07$ 49
3.2.4 Non-Fermi Liquid Behavior of $U_xTh_{1-x}Ru_2Si_2$ for $0.07 \leq x \leq 0.17$ 51
3.3 Magnetism and Its Connection to Non-Fermi Liquid Behavior in $U_{1-x}M_xNi_2Al_3$ {M = Th, Pr, and Y} 65
3.3.1 UNi_2Al_3 65
3.3.2 Non-Fermi Liquid Behavior in $U_{1-x}M_xNi_2Al_3$ {M = Th, Pr, and Y} 71

4 HYDROGEN DOPING EFFECTS ON UPd_2Al_3 92

4.1 Review of Hydrides 92
4.1.1 Electronic Properties 93
4.1.2 Magnetic Properties 95
4.1.3 Concentration Determination 96
4.1.4 Isotope Effects 96
4.1.5 Pressure-Composition Isotherms 97
4.2 Overview of UPd_2Al_3 99
4.2.1 Normal State 100
4.2.2 Superconducting State 108
4.2.3 Electron Subsystems 109
4.3 Experimental Apparatus 111
4.4 Sample Preparation 113
4.4.1 Polycrystalline Sample 114
4.4.2 Activation of Sample 115
4.4.3 Passivation of Sample 117
4.5 Hydrogen Effects on UPd_2Al_3 119
4.5.1 Hydrogen Effects on Uranium 119
4.5.2 Hydrogen Effects on $UPd_2Al_3H_x$ 122

5 SUMMARY AND CONCLUSION 148

5.1 $U_xTh_{1-x}Ru_2Si_2$ for $x \leq 0.17$ 148
5.2 $U_{1-x}M_xNi_2Al_3$ {M = Th, Pr, and Y} 150
5.3 $UPd_2Al_3H_x$ 151

APPENDIX : PRELIMINARY RESULTS OF $UNi_2Al_3H_x$, $CeCu_{2.2}Si_2H_x$, AND UPt_3H_x 154

REFERENCES 166

BIOGRAPHICAL SKETCH 177

LIST OF TABLES

Tables   Pages

2-1 The physical quantities of two channel spin 1/2 and electric quadrupolar (*pseudospin* 1/2) Kondo effect....38

3-1 Kondo temperature T_K in $U_XTh_{1-X}Ru_2Si_2$ for $0.07 \leq x \leq 0.17$....55

3-2 Physical parameters for $U_{0.9}M_{0.1}Ni_2Al_3$ (M = Ce, Th, La, Y, and Pr)....73

3-3 Physical relations between the U and the doped elements....73

4-1 Parameters for hydrogen doped $UPd_2Al_3H_X$ 127

LIST OF FIGURES

Figures Pages

1-1 Classification of heavy fermion and intermediate valence compounds..............4

1-2 Diagram of heat flow in the system used for thermal relaxation method.........13

1-3 The sample platform and copper-ring heat reservoir.....................................14

1-4 Block diagram of experimental setup for the specific heat measurements.......16

2-1 Specific heat as a function of T/T_K in constant magnetic field and $n = 1$ for $S = 1/2$ and $S = 3/2$...32

2-2 Magnetic susceptibility as a function of T/T_K in constant magnetic field and $n = 1$ for $S = 3/2$...33

2-3 Entropy, specific heat, and specific heat divided by temperature as a function of T/T_K in constant magnetic field for $S = 1/2$ and $n = 2$...............................34

3-1 Crystal and spin structure of antiferromagnetic superconductor URu_2Si_2.......46

3-2 Magnetic susceptibility of $U_XTh_{1-X}Ru_2Si_2$ for $x \leq 0.07$.................................52

3-3 Low temperature resistance normalized to the room-temperature value R_o of $U_{0.17}Th_{0.83}Ru_2Si_2$ 57

3-4 The anomaly T_A in terms of concentration x..58

3-5 C_{5f}/T as a function of ln T in $U_XTh_{1-X}Ru_2Si_2$ for $0.07 \leq x \leq 0.17$...................59

3-6 C/T vs. T^2 for $U_{0.1}Th_{0.9}Ru_2Si_2$ in two different magnetic fields......................60

3-7 Classification of Kondo system by T_K and T_{RKKY}..61

3-8 χ of polycrystalline sample $U_{0.14}Th_{0.86}Ru_2Si_2$ as a function of T for ZFC and FC measurements in $H = 0.004$ T..63

3-9 Hexagonal $PrNi_2Al_3$ crystal structure observed in UNi_2Al_3...........................67

3-10 T dependence of χ_{dc} as measured for UNi_2Al_3 68

3-11 ρ as a function of temperature for UNi_2Al_3 69

3-12 C/T vs. T for UNi_2Al_3 between 0.5 K and 9 K 70

3-13 $\chi(T)$ between 1.8 K and 300 K for four samples of UNi_2Al_3 75

3-14 C/T vs. T^2 for four samples of UNi_2Al_3 and $U_{0.9}Ce_{0.1}Ni_2Al_3$ 76

3-15 C/T vs. T^2 in $U_{0.9}M_{0.1}Ni_2Al_3$ for M = La, Th, Pr, and Y 77

3-16 C_{5f}/T vs. ln T for $U_{0.9}M_{0.1}Ni_2Al_3$ (M = Pr, Th, La, and Y) 78

3-17 C_{5f}/T vs. ln T for $U_{1-X}Th_XNi_2Al_3$ (x = 0.015, 0.1, 0.2, and 0.3) 79

3-18 C/T vs. T^2 for $U_{1-X}Th_XNi_2Al_3$ (x = 0.015, 0.1, 0.2, and 0.3) 80

3-19 χ vs. $T^{1/2}$ for $U_{0.9}M_{0.1}Ni_2Al_3$ (M = Pr, Th, and Y) 82

3-20 χ vs. ln T for $U_{0.9}Y_{0.1}Ni_2Al_3$ 83

3-21 ρ as a function of temperature in $U_{0.9}M_{0.1}Ni_2Al_3$ (M = Pr, Th, and Y) 84

3-22 C/T vs. T^2 for $U_{1-X}Th_XNi_2Al_3$ (x = 0.0, 0.0025, 0.005, and 0.015) 86

3-23 $\chi(T)$ at low temperatures in $U_{1-X}Th_XNi_2Al_3$ (x = 0.0025 and 0.005) 87

3-24 C/T vs. T for $U_{0.9}Th_{0.1}Ni_2Al_3$ in two different magnetic fields 89

4-1 Two pressure-composition isotherms of a hydride 98

4-2 Hexagonal $PrNi_2Al_3$ crystal structure observed in UPd_2Al_3 101

4-3 $\rho(T)$ and $\chi(T)$ in UPd_2Al_3 below T = 25 K and up to T = 300 K 102

4-4 C/T vs. T of UPd_2Al_3 H = 0 T and in several magnetic fields 104

4-5 $\chi(T)$ of UPd_2Al_3 along the a- and c-axes 107

4-6 Hydriding apparatus 112

4-7 Valence-band XPS spectra for β-UD_3 121

4-8 χ vs. T of $UPd_2Al_3H_x$ for $0 \leq x \leq 1.30$ 126

4-9 Magnetization M vs. magnetic field H for $UPd_2Al_3H_x$ for x = 0 and 1.30 128

4-10 Low-temperature C/T vs. T of $UPd_2Al_3H_x$ for $0 \leq x \leq 1.30$ 129

4-11 $\gamma(\equiv C/T$ as $T \rightarrow 0)$ vs. χ in a ln-ln plot for a number of heavy systems 132

4-12 Schematic model of XPS for $UPd_2Al_3H_x$ 133

4-13 Curie-Weiss temperature $\theta_{C.W.}$ vs. concentration x for $UPd_2Al_3H_x$ 136

4-14 χ(as $T \rightarrow 0$) vs. x for $UPd_2Al_3H_x$ 138

4-15 $\gamma((\equiv C/T$ as $T \rightarrow 0)$ vs. x for $UPd_2Al_3H_x$ 139

4-16 χ vs. temperature T for $UPd_2Al_3H_{0.64}$ in magnetic field 141

4-17 χ vs. $\sqrt{T}$ of $UPd_2Al_3H_x$ for x = 1.09 and 1.30 142

4-18 $\Delta C/T$ vs. ln T of $UPd_2Al_3H_x$ for x = 1.09 and 1.30 143

4-19 Specific heat of $UPd_2Al_3H_x$ as C/T vs. T at the superconducting state 145

A-1 C/T vs. T of $UNi_2Al_3H_x$ (x = 0.0, 0.23, 0.30, and 0.39), ... 155

A-2 $\chi(T)$ of $UNi_2Al_3H_{0.30}$ in different magnetic fields 157

A-3 $\chi(T)$ of $CeCu_{2.2}Si_2H_x$ for x = 0.0 and 0.07 160

A-4 $M(H)$ of $CeCu_{2.2}Si_2H_x$ at T = 1.8 K for x = 0.0 and 0.07 161

A-5 χ of the polycrystalline sample of UPt_3 as a function of temperature 162

A-6 $\chi(T)$ of UPt_3H_x for x = 0.0 and 0.17 (both systems are pellets) 164

A-7 C/T vs. T of UPt_3H_x for x = 0.0 and 0.17 (both systems are pellets) 165

Abstract of Dissertation Presented to the Graduate School
of the University of Florida in Partial Fulfillment of the
Requirements for the Degree of Doctor of Philosophy

DOPING EXPERIMENTS ON MAGNETIC HEAVY FERMION SUPERCONDUCTORS

By

Weonwoo Kim

August, 1995

Chairman: Gregory R. Stewart
Major Department: Physics

We present experimental results of non-Fermi liquid (NFL) behavior in $U_XTh_{1-X}Ru_2Si_2$ and in $U_{0.9}M_{0.1}Ni_2Al_3$ (M = Y, Th, and Pr), and the hydrogen effects on UPd_2Al_3. The objective of this work is to understand the origin of the NFL behavior and how hydrogen changes the heavy fermion system.

In $U_XTh_{1-X}Ru_2Si_2$, we have observed the NFL behavior in thermodynamic, transport, and magnetic measurements for $0.07 \leq x \leq 0.17$. We report a temperature T_A in electrical resistivity ρ measurements which measures the onset of intersite correlations between local magnetic moments. The increase of ρ with T for $0.3\ K < T < 20K$, the approximately linear decrease of T_A for $0.1 \leq x \leq 0.14$, and the spin glass behavior in χ_{dc} seem to tell us that the origin of the NFL behavior in $U_XTh_{1-X}Ru_2Si_2$ for $0.07 \leq x \leq 0.17$

may be due to magnetic fluctuations at $T = 0$ K or collective modes of excitations at low temperatures rather than the single-site two channel Kondo effect (TCKE).

We have found another new system $U_{0.9}M_{0.1}Ni_2Al_3$ (M = Th, Pr, and Y) which exhibits the NFL behavior. We observe a positive linear ρ with T for 1.0 K $\leq T \leq$ 20 K in Th- and Y-doped samples (less wide range in T for the Pr-doped sample). For susceptibility χ_{dc}, $T^{1/2}$ (Th and Pr doped) and ln T (Y doped) dependences are observed as a sign of NFL behavior. The ln T dependence of C_{5f}/T as an NFL characteristic following the destruction of the magnetic order as observed in C measurements, seemed to imply that the NFL behavior may be due to the proximity of magnetic instability, where a Kondo-compensated nonmagnetic state and the long range magnetic order are nearly degenerate.

We have succeeded in doping UPd_2Al_3 with hydrogen by improving the activation and poisoning of the parent samples. In the normal state, the increase in both $\chi(0)$ and $\gamma(0)$ with hydrogen uptake can be interpreted as an enhancement of the effective mass supported by the Sommerfeld free-electron behavior of these physical values. On the other hand, magnetic correlations are proposed as a possible origin of the behavior in both $\chi(0)$ and $\gamma(0)$ based on the observed relations among $\theta_{\text{C.W.}}$, $\chi(0)$, and $\gamma(0)$ around the critical hydrogen concentration C_C. The peak in χ for UPd_2Al_3 seems to be due to the short range magnetic correlations; we observe the shift of the peak to lower T for more hydrogen uptake and at higher magnetic fields for a given hydrogen concentration. In the superconducting state, T_C decreases with hydrogen uptake along with a broadening of the transition width.

CHAPTER 1
INTRODUCTION

In this chapter, we will summarize heavy fermion systems based on not only a coupling constant between local moment and conduction electron at each lattice site, but also essential topics in this area while keeping in mind the magnetic and superconducting ground states. Our motivation to study non-Fermi liquid behavior by alloying experiments and to perform hydrogen doping experiments on these HFS will be given below. We also describe experimental techniques used to get our data in our laboratory. We are going to explain separately experimental techniques and apparatus for the hydrogen doping experiments in chapter 4.

1.1 Overview of Heavy Fermion Systems

Heavy fermion systems (HFS), which are usually intermetallic compounds of certain lanthanides or rare-earth elements (notably Ce 4f one-electron and Yb 4f one-hole) and actinides (notably U, Pu, and Np), have attracted physicists for more than a decade because of their fascinating physical properties [Stewart, 1984; Lee *et al.*, 1986; Ott and Fisk, 1987; Fulde *et al.*, 1988; Grewe and Steglich, 1991]. The highly correlated electronic systems of HFS can be regarded as a lattice of f-ions being embedded in a Fermi sea of conduction electrons. In many aspects, they behave as a gas of strongly renormalized quasiparticles with a Fermi surface and enormously enhanced effective mass.

Although both the Kondo effect [Kondo, 1964] occurring at each lattice site and the strong low-lying magnetic fluctuations seem to play a central role, there is no accepted microscopic theory for either the mass renormalization or the pairing mechanism. However, we are briefly going to describe the main topics in HFS so that we may reduce any conceptual gap to understand following chapters.

1.1.1 Classification of Heavy Fermion Systems

Each of these HFS can be characterized by a Kondo-lattice temperature, T^* (this temperature corresponds to the Kondo temperature T_K for an isolated Kondo impurity). For $T >> T^*$, f-ions carry local f-electron-induced magnetic moments which are coupled very weakly to the conduction electrons. For $T < T^*$, however, this coupling becomes strong enough to give rise to a nonmagnetic low temperature state [Grewe and Steglich, 1991].

The ground states of the HFS with lanthanide ions depend heavily on the competition between the magnetic intersite interaction, i.e., the indirect Ruderman-Kittel-Kasuya-Yoshida (RKKY) exchange interaction, and the on-site Kondo interaction reducing the local magnetic moments [Doniach, 1977]. If we use the dimensionless coupling constant, $g = N_F \cdot |J|$, we can express two energies ($k_B \equiv 1$) as $T^* \sim \exp\{-1/g\}$ and $T_{RKKY} \sim g^2$. N_F is the conduction-band density of states at the Fermi energy E_F, and J is the exchange coupling constant between the local f-spin and the conduction-electron spin with $J < 0$. The coupling constant g represents the degree of delocalization of f-states. For the HFS with actinide ions with almost no direct 5f-wave function overlap, hybridization between 5f and ligand valence-electron states is usually stronger than that for the more localized 4f electrons. Thus, two adjacent 5f configurations ($5f^2$ and $5f^3$) may be nearly degenerate, and one single parameter g may not be sufficient to classify the various ground states of the HFS with 5f-ions.

In Figure 1-1, we show a schematic classification of HFS and intermediate valence (IV) compounds with 4f-ions. For $g << 1$, there is a stable moment regime of an ordinary rare-earth magnetism, and for $g > 1$ there is a *charge* fluctuation between the f-shell and the conduction band exhibiting a nonmagnetic Fermi-liquid ground state. HFS exist between the above two regimes, i.e., for $0 << g < 1$. For the 4f heavy-fermion compounds, valence fluctuations are usually ignored so that local *spin* fluctuations, which have essentially the same origin as in dilute Kondo alloys, exist for the weaker local exchange coupling. Thus, HFS characterize both the 'magnetic limit' of the IV compounds and the 'concentrated limit' of the Kondo alloys.

There also exists a critical value g_c, where the on-site and the intersite interactions have the same strength [Steglich *et al.*, 1994]. For $g_c < g < 1$, the strong hybridization between 4f and conduction electrons fully compensates the local f-derived moments well below T^* resulting in Fermi liquid behavior. However, these Fermi liquids appear to be unstable against AFM and/or superconducting phase transitions at $T_N/T_C << T^*$. Also there is a very interesting regime around $g = g_c$, i.e., at the magnetic instability, where it seems that non-Fermi liquid (NFL) behavior takes place [Kim J.S. *et al.*, 1992; Kim W.W. *et al.*, 1993; Andraka and Stewart, 1993; Löhneysen *et al.*, 1994; Steglich *et al.*, 1994]. We are going to discuss the origin and physical properties of the NFL behavior more thoroughly in chapter 3.

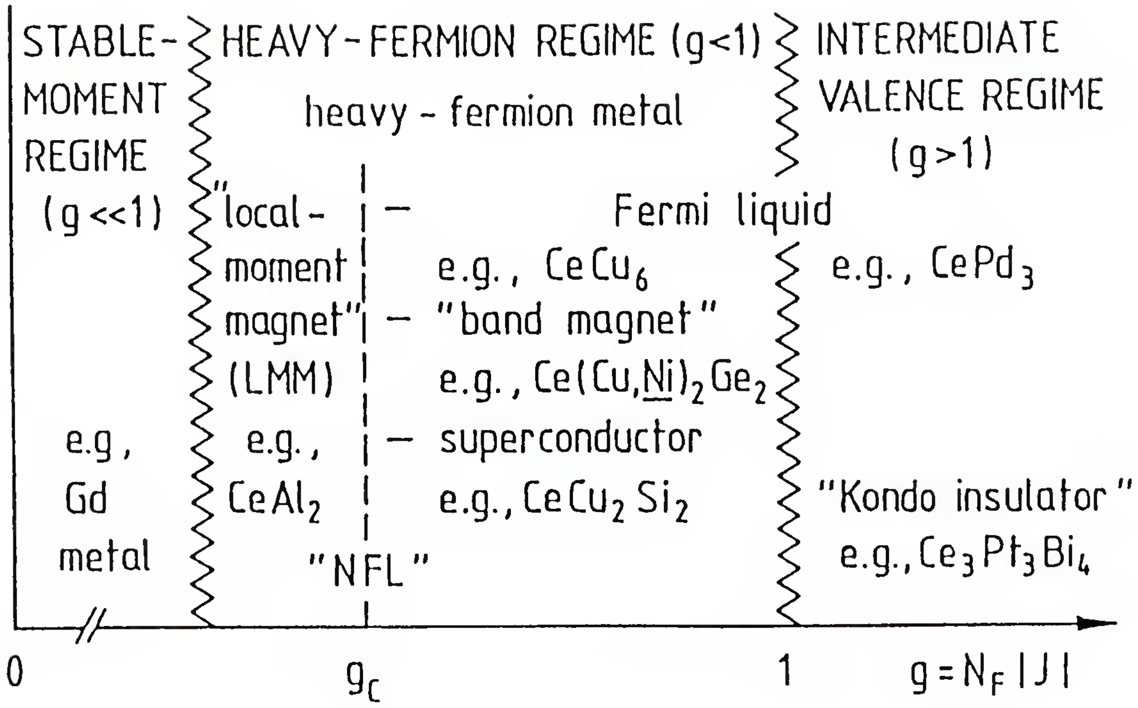

Figure 1-1. Schematic classification of heavy fermion and intermediate valence compounds using exemplary Ce-intermetallics. They are classified based on the indirect local exchange-coupling constant, $g = N_F \cdot |J|$, which represents the degree of delocalization of 4f-states (see text for detail). Note that non-Fermi liquid effects have been postulated for systems with $g \sim g_c$. This is from Steglich *et al.* [1994].

1.1.2 Mass Enhancement

The origin of heavy quasiparticles may be due to either a single electron interaction or a many body resonance (we already know that we can not simply apply the theory of a single electron interaction, because we can not understand the development of the large effective mass m* of quasiparticles at low temperatures simply based on the single electron theory). The single electron interaction is a coupling between initially well localized f-electrons and light conduction (itinerant) electrons. This coupling or hybridization makes the localized f-electrons delocalized, and the f-electrons contribute to the Fermi level with a low Fermi velocity. A large part of the mass enhancement is obtained by local magnetic fluctuations reminiscent of the single impurity Kondo effect. This large effective mass is observed by a large coefficient γ_o of the electronic specific heat for $T \rightarrow 0$ K, a large 'Pauli-like' spin susceptibility χ_o, and a large coefficient ζ from the Fermi liquid behavior in resistivity, i.e., $\rho = \zeta T^2$ ($\zeta \sim \gamma_o^2$). Despite these large physical values, the Sommerfeld-Wilson ratio χ_o/γ_o with proper normalization is of the same order as in simple metals.

At the same time, there exists an intersite magnetic coupling J_{ij}, which is comparable in magnitude to the local Kondo temperature T_K, between magnetic moments induced by the partially filled f-electron shells. One of the consequences of this interplay is that heavy fermion compounds exist near magnetic instability, i.e., around the transition between a long range magnetic order and a Pauli paramagnetic ground state.

1.1.3 Superconductivity

A possible origin of the superconducting mechanism in HFS can be a large magnetic fluctuating medium which furnishes an attractive potential to form the quasiparticle pairs. Since the quasiparticles exist for $T < T^* \leq T_F/10$, i.e., in the Fermi liquid region, such a magnetic fluctuating medium observed in $\chi(\mathbf{q}, \omega)$ can be the origin of the SC. Here, the parity of the pairing depends on the nature of the magnetic spin fluctuations, e.g., ferromagnetic spin fluctuations (for odd parity) and antiferromagnetic spin fluctuations (for even parity). Thus, we can change the pairing strength by, e.g., changing the hydrostatic pressure. For instance, the Grünesien parameter Ω is given by

$$\Omega = -\partial \log T_F / \partial \log V \tag{1.1}$$

where V is a volume. Under pressure, T_F increases causing a decrease of the pairing strength which gives rise to a decrease of T_C ($\zeta \sim \gamma^2 \sim \eta^2 \sim T_F^{-2}$, where η is related to the strength of the quasiparticles pairing). Another possibility is to apply a magnetic field to change the pairing potential, e.g., UBe_{13} [Brison *et al.*, 1988].

1.1.4 Magnetism

About the origin of magnetism in HFS, it seems to be basically similar to a general magnetism which has been constructed on the Heisenberg model [Heisenberg, 1928] and the Stoner model [Stoner, 1938]. The first model describes magnetism in terms of local magnetic moments, and the other one describes magnetism in terms of itinerant electrons with spins where magnetic moments are determined by the number of unpaired electrons in the exchange-split spin-up and spin-down bands.

There has been a proposed picture [Doniach, 1977; Nozières, 1985] for a magnetic state with well localized moments and only moderate enhancement of γ, i.e., of order 0.1 J $K^{-2}mole^{-1}$ as in $CeAl_2$. Starting from band electrons and ionic f-states, there is an end to the quasiparticle renormalization when the spin order of renormalized moments occurs. The corresponding RKKY interactions with energy scale T_{RKKY} are mediated by renormalized band electrons. From then on, spin-flip scattering is frozen out and the band electrons move in the fixed modulated exchange field provided by the magnetic moments. For instance, T_{RKKY} exceeds T_M by more than an order of magnitude for $CeAl_2$ [Steglich *et al.*, 1979b] (the long range magnetic ordering temperature, T_M, is usually responsible for an antiferromagnetic ordering, but it can be a ferromagnetic ordering one, e.g., $CeCu_2$ [Gratz *et al.*, 1985]). The intermediate γ-values above T_M point to moderate renormalization for band electrons well above the Kondo lattice temperature $T^* < T_M < T_{RKKY}$. γ_o is usually lower due to the reduced density of excitations in the magnetically ordered phase. The ordered moments are correspondingly smaller than the free-ion values in the proper CEF ground state. Even though the density of states (DOS) near the Fermi energy E_F changes due to an exchange-split incipient Abrikosov-Suhl resonance (ASR) [Abrikosov, 1965; Suhl, 1965], no electronic excitation gap develops anywhere on the Fermi surface. In general, the specific heat well below T_N follows $C = \gamma T + \beta T^3$ with a cubic magnon contribution.

On the other hand, the quasiparticle band theory can describe heavy fermion magnets in the itinerant regime where there is a considerable influence of quasiparticle renormalization. The magnetic degrees of freedom, originally related to the local moments, have been transferred to the itinerant heavy quasiparticles. Thus, this system shows a strongly reduced magnetic moment and a large γ-value in the electronic specific heat. In particular, a spin density wave (SDW) instability [Doniach, 1987] may open an electronic excitation gap on parts of the Fermi surface, a situation strongly favored by the nesting properties. In that case, the density of quasiparticle excitations is reduced at low temperatures and an exponential decrease of $\gamma(T)$ can take place below T_N, e.g., for $U_{1-X}Th_XPt_3$ [Ramirez *et al.*, 1986; Stewart *et al.*, 1986].

However, most of HFS are typically in a crossover regime between the class of local moment systems and of itinerant systems. Also, when both superconducting and antiferromagnetic ground states coexist, there is a larger coupling between magnetic and superconducting order parameters in the local moment system than in the itinerant system because of the its larger ordered moment.

Before we close this section, we would like to classify a large variety of ground states in the HFS based on superconductivity (SC) and magnetism. The first group has a nonmagnetic ground state, i.e., paramagnetism without SC, e.g., $CeCu_6$ [Stewart *et al.*, 1984b]. The second group has a magnetic ground state without SC, e.g., UCu_5 [Ott *et al.*, 1985]. The third group has an SC ground state without magnetism, e.g., UBe_{13} [Ott *et al.*, 1984]. The fourth group has SC and magnetism in its ground state, and we can divide the fourth group into two subgroups: One is the system where the two ground states coexist, e.g., UPd_2Al_3 [Geibel *et al.*, 1991b], the other is the system where the two ground states compete with each other rather than coexist, e.g., $CeCu_{2.2}Si_2$ [Steglich *et al.*, 1995].

1.2 Motivation

We can change external physical parameters such as temperature and pressure to study a system more thoroughly. Alloying experiments with different elements (which have different electronic configurations, atomic sizes, and local magnetic moments) are also a very interesting and effective method in gaining more understanding and insight into condensed matter physics. In principle, alloying can vary the band structure and the chemical potential causing changes of DOS at E_F. It is crucial to vary the DOS at E_F to understand HFS, because the DOS at E_F in HFS (the DOS is proportional to γ from specific heat measurements) is one of the most important topics to be understood. Alloying also changes the lattice constants inducing a variation in hybridization. It causes a change in the interaction mechanism, and sometimes even induces a phase transition.

Since NFL behavior studies have been a newly developing field [Seaman *et al.*, 1991; Andraka and Tsvelik, 1991], we have focused on the magnetic HF superconductors (which would have a relatively small ordered moment below antiferromagnetic transition) out of the family of HFS to find new NFL systems, because as we described briefly in section 1.1.1, the magnetic instability can be the origin of NFL behavior. We will discuss this in detail in chapter 3.

As we all agree, one of the unavoidable results of alloying experiments is to disturb the occupation of the sublattice. Physicists have an idea to overcome such a disadvantage by doping hydrogen rather than the usual doping method (with transition elements, lanthanides, and actinides) in these HFS. The other possible advantage of hydrogen doping experiments is that we can keep the crystalline structure of a hydrogen doped system unchanged, even at a relatively high doping concentration, (which is an essential point for a systematic study) because hydrogen atoms can go into the lattice interstitially as a proton (which is in size several orders smaller than the atom) by donating its electron to the Fermi level. Even though hydrogen atoms get extra electrons from the Fermi level in some cases, the effect on the crystalline structure is still smaller than other usual doping elements.

However, there are also very difficult problems, which we will describe in detail in section 4.4, that we need to overcome in order to enjoy the advantages mentioned above. After we studied several hydrided systems (usually for hydrogen storage), the hexagonal crystalline structure of $LaNi_5$ (one of most studied systems and a possible candidate for hydrogen storage) stimulated our research on the HFS hydrides. Hydrogen doping experiments can not only give more information about the parent system, but also induce a new ground state in the hydrided system as will be discussed in chapter 4.

1.3 Experimental Techniques

We are going to describe in this section briefly how we made our samples and what experimental techniques we used. There is already a very detailed description about this in J.S. Kim's dissertation [1992]. However, we will describe in detail how we made our hydrided samples and what apparatus we used in the hydriding system in sections 4.3 and 4.4.

1.3.1 Sample Preparation

We synthesized each polycrystalline sample with stoichiometric amounts of elements within 0.3 % accuracy using a Bühler arc melter. Each sample was melted several times followed by flipping each time to increase the homogeneity of the sample. We especially have kept some air-sensitive elements, e.g., some transition elements and all lanthanides, in sealed Pyrex tubes to have the highest quality samples. We sometimes used a pressure casting technique [Crow and Sweedler, 1973] in the arc melter to make some resistivity samples. If necessary, we sealed the samples in evacuated quartz tubes and annealed them in a temperature-controlled furnace for a few days or a few weeks. Then, we characterized the samples using a Philips X-ray diffractometer to see if there is any second phase and to determine the lattice constants.

1.3.2 Measurement Techniques

Measurements of resistivity and specific heat down to about 1.1 K have been performed in a ^{4}He cryostat by pumping the dewar or an inner ^{4}He pot. Even lower temperature measurements for resistivity, specific heat, and ac magnetic susceptibility were done by using ^{3}He cryostat with a movable charcoal rod, which absorbs and releases ^{3}He depending on the temperature and pressure (boiling point of ^{3}He is 3.2 K at 1 bar). For the probe used, refer to J.S. Kim's dissertation [1992] for a schematic drawing. If necessary, high magnetic fields up to 14 T for these experiments were used for thermodynamic measurements.

1.3.2.1 Specific heat

Specific heat measurements can be classified into two groups, i.e., adiabatic and diabatic methods, depending on the isolation of the system from its surroundings. Adiabatic methods attempt to isolate the sample system completely from heat sources or heat leaks so that a sample with an internal heat source, e.g., radioactive material is not suitable for this method. On the other hand, diabatic methods in principle accept the fact that no sample can be completely isolated from its environment. The thermal conductance of the main links between the sample system and its surroundings (or heat reservoir) is measured and used to get the specific heat, and this is in contrast to a heat switch used in adiabatic methods in order to stop heat flowing. Thus, we may regard adiabatic methods as special cases of more general diabatic methods, because we can regard the thermal conductance in adiabatic methods as becoming zero. Diabatic methods improve the precision of specific heat measurements while they lose accuracy relative to the adiabatic methods.

We used a thermal relaxation (or time constant) method [Bachmann *et al.*, 1972; Stewart, 1983] which is one of the diabatic methods. This method is especially good for small sample calorimetry in HFS. In HFS, samples can be as small as 1 mg because of the large specific heat at low temperatures resulting in a much smaller ratio of the addenda contribution to the total specific heat than low γ-value samples.

As we show in Figures 1-2 and 1-3, after we are in equilibrium temperature T_o, we apply power P through the platform heater to increase the temperature of sample and platform (sapphire) to a stable temperature $T_o + \Delta T$. When the power is turned off,

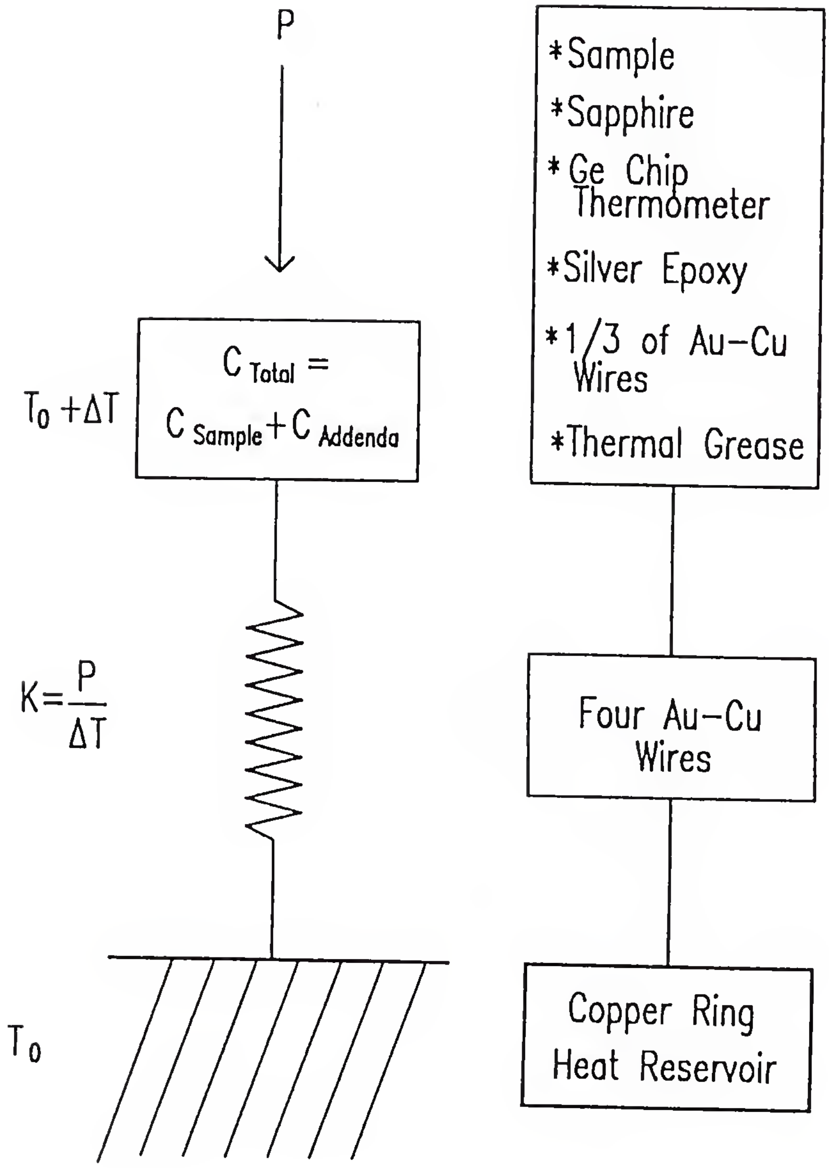

Figure 1-2. Schematic diagram of heat flow in the system used for thermal relaxation method. The sample and addenda (sapphire, Ge-alloy platform thermometer, H31LV silver epoxy, 1/3 of link wires, and thermal grease) are linked to copper-ring heat reservoir with Au-Cu alloyed wires (for detail, see Figure 1-3). This is from J.S. Kim [1992].

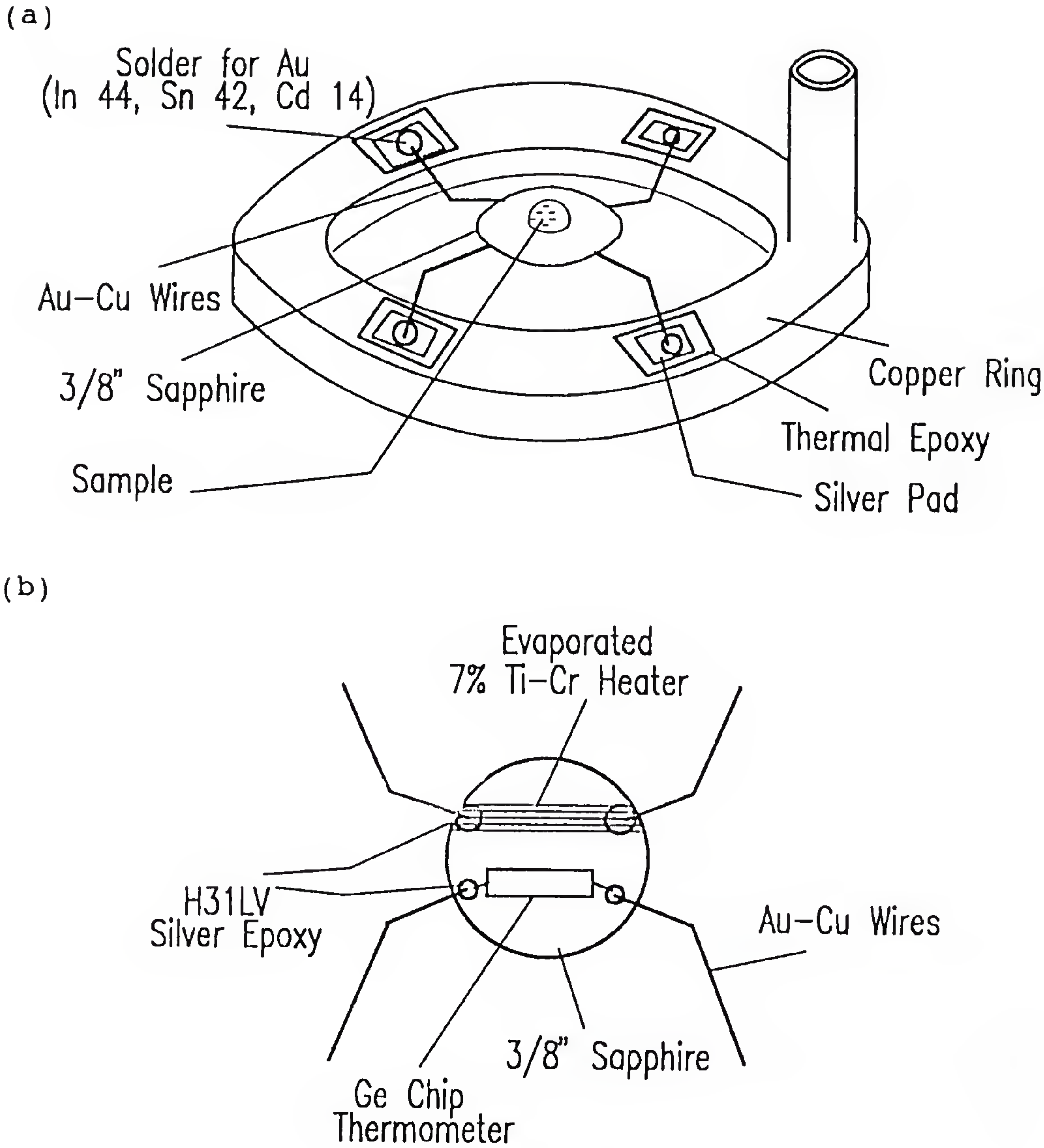

Figure 1-3. The sample platform and copper-ring heat reservoir are linked by four Au-Cu wires and shown in (**a**) in detail. We show the bottom side of the sample holder in (**b**). A Ge-alloy (or Ge-chip) platform thermometer and an evaporated platform heater are mounted, and four wires are electrically connected with EPO-TEK H31LV epoxy. This is from J.S. Kim [1992].

the temperature of sample and platform decays exponentially with a time constant τ_1 (a measure of the time for the sample and platform to reach thermal equilibrium) which is inversely proportional to the conductance of the wire links. We can express the relation as follow:

$$T(\mathrm{t}) = T_0 + \Delta T \exp(-\mathrm{t}/\tau_1). \qquad (1.2)$$

The conductance $K(T)$ of the wire links should be measured and calibrated vs. temperature for the later specific heat measurements using a relation $K = P/\Delta T$. We use K_o, the K-value at $T_o + \Delta T/2$, to get the specific heat $C = K_o \cdot \tau_1$ at $T_o + \Delta T/2$ followed by subtracting the addenda contributions. Here, the thermal conductance of sample and platform should be much larger than that of the wire links. Otherwise, there should be some corrections due to the so-called τ_2 effect [Bachmann *et al.*, 1972] to get a correct value of the specific heat.

We would like to describe briefly how to measure specific heat using Figure 1-4. We set the frequency of an ac excitation in the lock-in amplifier (LIA) around $f_o = 2700$ Hz such that it is not the multiple of 60 Hz to avoid any unwanted noise. This frequency setup in the LIA increases the signal-to-noise ratio by filtering out frequencies other than f_o with a width of frequencies. We then set up the phase to get the maximum sensitivity of the platform-thermometer resistance and thereby a best time-constant value. We achieve this by firstly finding a phase, where the LIA voltmeter shows no response for varying the resistance of the resistance-box implying that the impedance is only a function of capacitance. Subsequently, we get the right phase by going 90° off to have the impedance as a function of only resistance.

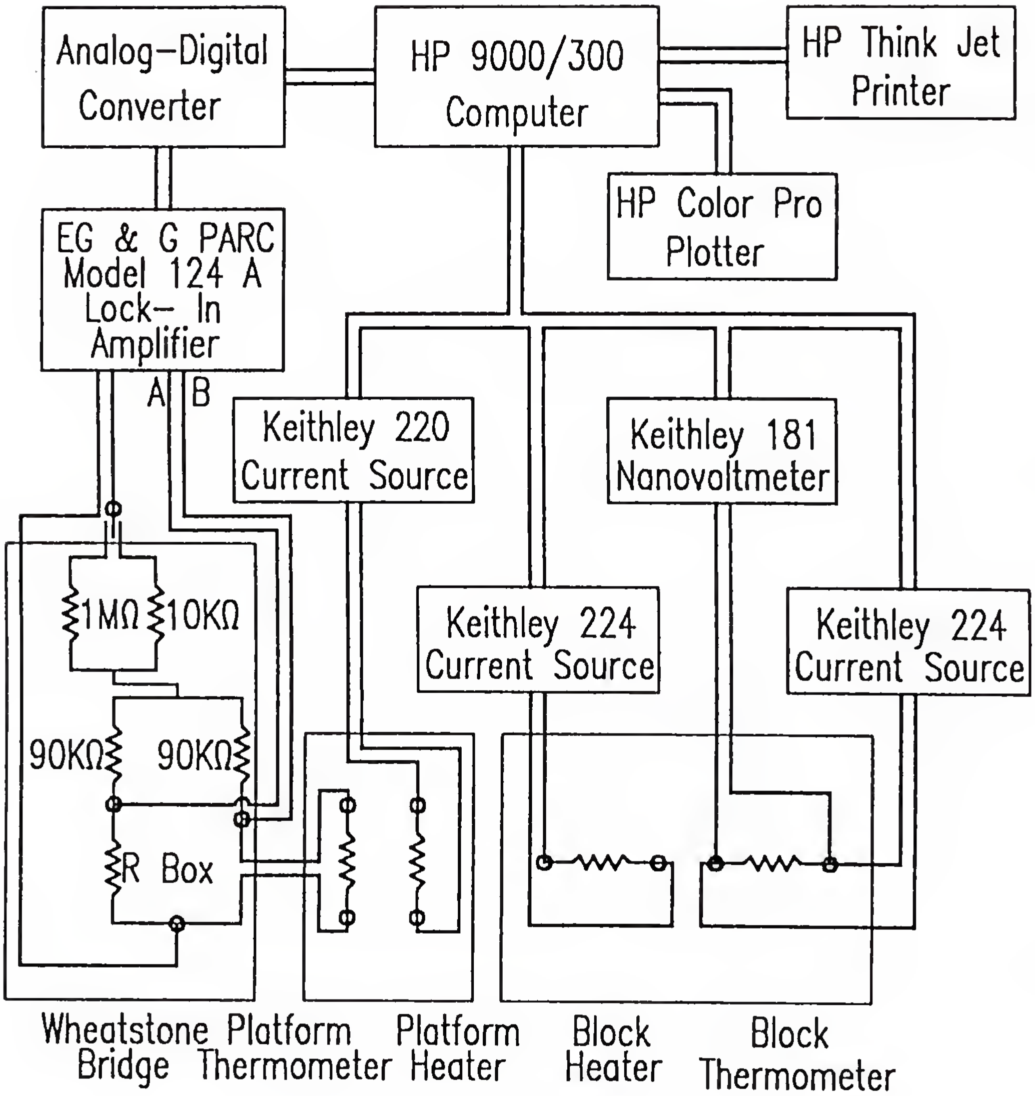

Figure 1-4. Block diagram of our experimental setup for the specific heat measurements. HP-computer is interfaced with current sources, voltmeter, and lock-in amplifier through analog-digital converter. This is from J.S. Kim [1992].

The block temperature is controlled by a block heater and measured by a block thermometer at T_0. We apply power P increasing the temperature of the platform-sample assembly to $T_0 + \Delta T$ ($\Delta T/T_0 < 1$ %). The resistance of the platform thermometer is measure by an ac Wheatstone bridge, and the resistance value is used to get the new platform temperature based on the precalibrated data. After we are at a stable temperature, we turn off the platform heater. We get the time constant τ_1 by digitizing the signal from the Wheatstone bridge using an analog-digital converter and subsequent signal average. With the K-value at this temperature, we have the specific heat after correcting for the addenda contribution. Overall absolute accuracy of our measurements is approximately within 5 %. For detailed descriptions, see the J.S. Kim's dissertation [1992].

We used a Ge-thermometer for the block thermometer, and a home made evaporated Ge-alloy was used for ac calorimetry to the platform thermometry (see J.S. Kim's dissertation [1992] for detailed process). When we measured the specific heat in magnetic fields up to 14 T (we can go up to 16 T if we lower the temperature of magnet below 2.2 K by pumping the λ-plate), we used Speer carbon-resistor thermometer for the block-temperature measurements down to 0.3 K. We calibrated it in zero magnetic field with the block Ge-thermometer, then did a field correction according to Naughton *et al.* [1983]. We also used a capacitive thermometer above 1 K as a thermometer in magnetic field, because it is not sensitive below 1 K [Naughton *et al.*, 1983] (Speer thermometers are very sensitive, especially below 4 K and their magnetoresistance is small relative to Ge-thermometers [Andraka and Stewart, 1991 and references therein]). We recalibrated the platform thermometer based on the precalibrated thermometers in magnetic field, and subsequently corrections to the thermal conductance with the help of these two (block and platform) field-calibrated thermometers in order to get the right specific heat were made.

1.3.2.2 Magnetic Measurements

For the ac magnetic susceptibility, we used a low frequency (around 86 Hz) mutual inductance technique using home-made primary (superconducting wire) and secondary (Cu wire) coils [J.S. Kim, 1992]. After we put a specimen into the primary coil, we applied an ac voltage using a lock-in amplifier (EG & G Model 124 A) to the coil. The signal detected by the secondary coil is amplified by the lock-in and gives a voltage difference due to the magnetic flux change in time, $d\Phi/dt$ (the secondary coil is wound in opposite directions so that there is no electromagnetic force due to unintended fluctuations of the applied voltage or field.). This voltage difference is proportional to the magnetization, and therefore the magnetic susceptibility [Signore, 1995]. We used this technique to measure the superconducting transition temperatures of our HFS for $0.3\ \mathrm{K} < T < 2.5\ \mathrm{K}$.

For dc magnetic susceptibility, we used a superconducting quantum interference device (SQUID) from Quantum Design for $1.7\ \mathrm{K} < T < 400\ \mathrm{K}$ in magnetic fields up to 5.5 T in two opposite directions. The basic idea of the dc measurement [Rose-innes and Rhoderick, 1980] is similar to that of the ac method. We move the specimen in the steady magnetic field applied by a dc powered solenoid (corresponding to the primary coil excited by ac voltage in the ac method) to induce a change of magnetic flux in time, then the secondary coil detects the signal with a high sensitivity due to the SQUID. We also measured magnetization vs. magnetic field at a given temperature.

1.3.2.3 Electrical Resistivity

We used a standard four probe dc technique to measure the resistance of a specimen for 0.3 K < T < 70 K. If necessary, we measured the dimension of the specimen to get resistivity. All measurements are automatically performed with computer controlled equipment and data collection [J.S. Kim, 1992].

CHAPTER 2
REVIEW OF THEORY

We are going to review briefly the basic concepts and the physical quantities of the Fermi liquid (FL) theory as a function of temperature, because it explains relatively well the phenomena in heavy fermion systems. However, unusual behavior, which can not be understood by the FL theory, has been observed in recent years. There have been very extensive theoretical developments both in a microscopic, e.g., the exact Bethe ansatz and conformal field theory, and in a phenomenological theory to understand the origin of the new behavior. We will concentrate on the physical quantities for which unusual behavior has been observed in, e.g., thermodynamics, transport, and magnetic susceptibility. There is no conclusive theory explaining all of the new phenomena.

2.1 Fermi Liquid Theory

The model of non-interacting fermions or a Fermi gas has worked relatively well in a system of Fermi particles, even though the interaction among the fermions is rather strong. Electrons in a metal serve as a classic example. The reason why it does so well is that the scattering rate of electrons is dramatically reduced because of the Pauli exclusion principle.

Landau argued that the non-interacting fermion model discussed above was not a valid starting point. Instead, he emphasized that the above model is applicable if we assume a non-interacting *quasiparticle* model as a good first approximation and the quasiparticles obey the exclusion principle. He proposed a semiphenomenological method [Landau, 1956]. He assumed firstly the interaction between the particles is adiabatically turned on such that the Fermi gas gradually transits into the excited Fermi gas resulting in a Fermi liquid. Here, there is a one-to-one correspondence between the eigenstates of the Fermi liquid and those of the non-interacting Fermi gas. Secondly, he assumed that the temperature is much lower than the Fermi energy, so excitations are confined to with an energy of T ($k_B \equiv 1$) near the Fermi surface, and those excitations have a sufficiently long relaxation time to be well defined. The excitations of the Fermi gas are called *quasiparticles*. Like the bare particles, they obey Fermi statistics and have momentum (or crystal momentum) as a good quantum number. However, since the quasiparticles can be considered as particles in a self-consistent field, they have a renormalized effective mass, and the energy of the whole system is no longer the same as the sum of the energy of each particle in isolation. Instead, the energy is a functional of the distribution function $n(k)$.

If the distribution function is changed by an infinitesimal quantity $\delta n(k)$,

$$\delta n(k) = n(k) - n_0(k), \tag{2.1}$$

where $n_0(k)$ is the distribution function of quasiparticles in the ground state, then the total energy of the system changes by an amount

$$\delta E = \sum_k \varepsilon_k \delta n(k), \tag{2.2}$$

where $\varepsilon_k = \delta E/\delta n(k)$ is the first functional derivative of E with respect to $n(k)$. When one quasiparticle is surrounded by a gas of other quasiparticles, its energy becomes

$$\varepsilon_k = \varepsilon_k^{\circ} + \sum_{k'} f(k,k')\delta n(k'), \tag{2.3}$$

where $f(k,k')$ is the *interaction energy* of the quasiparticles and of order $1/V$, the volume of the system. From Eqs. (2.2) and (2.3), we have

$$\delta E = \sum_k \varepsilon_k^{\circ}\delta n(k) + \frac{1}{2}\sum_k\sum_{k'} f(k,k')\delta n(k)\delta n(k'). \tag{2.4}$$

If the system is isotropic for k and k' on the Fermi surface, $f^{s(a)}(k,k')$ depends only on the angle θ between the directions k and k'. Here $f^{a}(k,k')$ and $f^{s}(k,k')$ are the spin antisymmetric and symmetric parts of the quasiparticle interactions, respectively. They can be expanded in a series of Legendre polynomials as follows:

$$f^{s(a)}(k,k') = \sum_{l=0}^{\infty} f_l^{s(a)} P_l(\cos\theta) \tag{2.5}$$

where f is completely determined by the set of coefficients f_l^{s} and f_l^{a}. It is convenient to express f in reduced units by setting $N(E_F)\, f_l^{s(a)} = F_l^{s(a)}$, where $N(E_F)$ is the density of states at the Fermi level. After using elementary thermodynamics, we can relate the physical quantities obtained from experiments to the Landau parameters $F_l^{s}(\theta)$ and $F_l^{a}(\theta)$ as follows [Nozières, 1963; Pines and Nozières, 1989]:

$$C_v = \frac{\pi^2 k_B{}^2 N(E_F)}{3V} T \tag{2.6}$$

$$N(E_F) = \frac{V k_F m^*}{\pi^2 \hbar^2} \tag{2.7}$$

$$S^2 = \frac{\hbar^2 k_F^2}{3mm^*}(1 + F_o^s) \tag{2.8}$$

$$\frac{m^*}{m} = 1 + \frac{F_1^s}{3} \tag{2.9}$$

where V is the volume of the system, C_v is the specific heat, m is the bare mass of a Fermi particle, m^* is the effective mass of quasiparticle, and S is the sound velocity. The electrical resistivity due to the impurity at low temperatures can be derived by applying a Fermi liquid approach to the Anderson model for degenerate orbitals assuming electron-hole symmetry near the Fermi level, and it is proportional to T^2 [Yoshimori, 1976; Mihály and Zawadowski, 1978].

Landau's theory was constructed for a *neurtal* Fermi gas in which there are no long range interactions. The only neutral Fermi liquid found in nature is the quantum liquid ^{3}He, and it becomes degenerate at very low temperatures. If there was no interaction between the ^{3}He atoms, the Fermi temperature or the degeneracy temperature would be given by

$$T_{\mathrm{F}} = \frac{E_{\mathrm{F}}^{\circ}}{k_{\mathrm{B}}} = \frac{\hbar^2 k_{\mathrm{F}}^2}{2mk_{\mathrm{B}}} \cong 5\mathrm{K}. \tag{2.10}$$

with $m \sim 5\times10^{-24}$g and, from the particle density σ, $k_{\mathrm{F}} = 3\pi^2\sigma^{1/3}$. Such quantum behavior as a linear T dependence in specific heat and T independent magnetic susceptibility are experimentally found at about 0.05 K. This reduction in T_{F} by two orders of magnitude comes from the interaction between the ^{3}He atoms, i.e., the enhancement in the effective mass of the quasiparticles.

Now let us consider the *charged* Fermi liquid rather than the *neutral* Fermi liquid. Let us consider a system of *noninteracting* electrons which move in the periodic potential of the crystalline lattice of a solid. The single particle eigenstates are Bloch wave with a wave function

$$\psi_{kj}(r) = e^{ik\bullet r}u_{kj}(r), \tag{2.11}$$

where u_{kj} has the periodicity of the lattice. Both j, the band index, and $\mathbf{k}$, a wave vector, are good quantum numbers. When we take account of the Coulomb interaction between electrons, we can again establish a one-to-one correspondence between the eigenstates of the real system and those of the noninteracting system by using the adiabatic switching procedure as discussed in the neutral Fermi liquid.

A Bloch wave possesses an energy ε^{o}_{kj}, and a velocity on the Fermi surface is given by $\mathbf{v}^{o}_{k} = \nabla(\varepsilon^{o}_{kj})$ which is different from the velocity of a free electron k/m. After we turn on the interaction adiabatically, the quasiparticles have an energy $\varepsilon_{kj} = dE/\delta n(k)$. ε_{kj} is constant over the Fermi surface, and is equal to the chemical potential μ. We can again define at every point of the Fermi surface a velocity $\mathbf{v}_{k}$, which will be different from $\mathbf{v}^{o}_{k}$. Now, we know that the difference between $\mathbf{v}_{k}$ of interacting electrons and k/m of a free electron is due to firstly, the influence of the periodic lattice on each electron and secondly, the "many body" effect arising from the Coulomb interaction. Thus, Landau's theory of a Fermi liquid as applied to a spatially homogeneous state is suitable in the case of the Coulomb interaction between electrons [Silin, 1958].

Just as for the neutral Fermi liquid, we can now define an interaction energy between quasiparticles $f(\mathbf{k},\mathbf{k}')$ as the second derivative of the energy with respect to $n(\mathbf{k})$. Since the Fermi surface of a metal is generally not isotropic (e.g., due to the anisotropy of the crystalline lattice), ε_{k} depends on the direction of $\mathbf{k}$ and $f(\mathbf{k},\mathbf{k}')$ depends on both $\mathbf{k}$ and $\mathbf{k}'$. Also, the divergence of $f(\mathbf{k},\mathbf{k}')$ due to, e.g., the inhomogeneity of the system or the Coulomb interaction between the electrons, can be removed if $f(\mathbf{k},\mathbf{k}')$ refers to the interaction between *screened* quasiparticles, i.e., the quasiparticle plus its associated screening cloud [Pines and Nozières, 1989].

However, the Fermi surface is almost spherical, as in the alkali metals for example, if the system's behavior is nearly isotropic. Thus, we can introduce a *crystalline mass* or a *band mass* m_c such that

$$j_k = \frac{k}{m_c} . \tag{2.12}$$

where j_k is the current carried by a quasiparticle with wave vector k, and m_c is different from the bare electron mass m because of the periodic potential acting on the electron ($\hbar \equiv 1$). The real quasiparticle effective mass m^* due to the quasiparticle interaction is defined by

$$\mathrm{v}_k = \frac{k}{m^*}, \tag{2.13}$$

where v_k is the velocity of a quasiparticle on the Fermi surface. The relation between m^* and m_c is given by

$$m^* = m_c(1 + F_1^s/3). \tag{2.14}$$

We can also express the spin susceptibility χ_s in terms of the paramagnetic susceptibility χ_P due to the noninteracting free electron gas as follows:

$$\chi_s = \chi_P \frac{m^*}{m(1+F_0^a)}. \tag{2.15}$$

Equation (2.15) is meaningful only when

$$1 + F_0^a > 0 . \tag{2.16}$$

Otherwise, the long wavelength fluctuations of the magnetic moment become unstable giving rise to a ferromagnetic correlation.

Phenomena that are not influenced by quasiparticle interactions can be described in terms of a one electron model with renormalized energies. The de Haas-Van Alphen effect and the low frequency Hall-constant in a high magnetic field are examples. On the other hand, phenomena affected by the quasiparticle interaction $f(k,k')$ can not be exactly described by the one electron model. Instead, they can be expressed in terms of the Landau parameters above.

Some properties of heavy electron systems (HFS), e.g., the Pauli-like magnetic susceptibility and the linear temperature dependence of the specific heat at low temperatures can be explained by the Landau FL theory even if there are strong on-site correlations at low temperatures for $T << T_F$. An analogy has been drawn between liquid ^{3}He and the HFS, and it seems that there is relatively good agreement with experiments. The Landau Fermi liquid theory is likely to work well in metals as long as there is no critical behavior such as a phase transition.

Before we finish this Section, let us mention that there are some problems in translating the ^{3}He results directly to the HFS. One of those [Lee *et al.*, 1986] is the lack of Galilean invariance in the HFS, so that the effective mass is not simply related to the Landau parameter F_1^s as shown in Eq.(2.14). Furthermore, the Fermi liquid theory does not consider the effects of spin-orbital coupling, crystal symmetry, and band structure.

2.2 Non-Fermi Liquid Theory

We define non-Fermi liquid (NFL) behavior as that deviating from Fermi liquid results, e.g., a logarithmic divergence of C/T at low temperatures instead of saturation. One possible theory to explain the NFL behavior is the multichannel Kondo effect. We will discuss the multichannel Kondo effect mostly based on the exact Bethe ansatz solution [Schlottmann and Sacramento, 1993]. Subsequently, we will summarize another proposed phenomenological theory, which is based on the scenario of magnetic quantum fluctuations at $T = 0$ K, to explain the NFL behavior.

2.2.1 Multichannel Kondo Effect

The n-channel Kondo model for an impurity spin S and an integer n-number of orbital conduction electron channels is given by Nozières and Blandin [1980]

$$H_{\mathrm{K}} = \sum_{k,m,\sigma} \varepsilon_k a^{+}_{km\sigma} a_{km\sigma} + J \sum_{k,k',m,\sigma,\sigma'} \mathbf{S} \cdot a^{+}_{km\sigma} \boldsymbol{\sigma}_{\sigma\sigma'} a_{k'm\sigma'} \,. \tag{2.17}$$

where S is the spin operator describing the magnetic impurity, J is the antiferromagnetic coupling constant, σ are the Pauli matrices, and m labels the orbital channels.

The different orbital channels are strongly correlated close to the impurity and form an orbital singlet; i.e., the spins of the conduction electrons at the impurity site are glued together to form a total spin $n/2$ [Nozières and Blandin, 1980; Andrei and Destri, 1984; Tsvelik and Wiegmann, 1984]. In general, three qualitatively different situations can arise when this effective spin $n/2$ couples to an impurity spin S:

(i) If $n = 2S$, the number of conduction electron channels is exactly sufficient to compensate the impurity spin into a singlet giving rise to the Fermi liquid behavior. Classic examples are FeCu, FeAg, and CrCu.

(ii) If $n < 2S$, the impurity spin is only partially compensated (undercompensated spin), because there are not enough conduction electron channels to yield a singlet ground state. An effective degeneracy of $\{2S+1-n\}$ remains at low temperatures (and in zero field). This case may describe the integer valent limit of impurities with two magnetic configurations like Tm.

(iii) If $n > 2S$, the impurity is said to be overcompensated. A critical behavior is obtained as the temperature and the external field tend to zero. The quadrupolar Kondo effect [Cox, 1987a] is one possible realization of this case.

2.2.1.1 Compensated Impurity Spin

The basic model describing the interaction of a transition metal (or magnetic) impurity with a metallic host is the orbitally degenerate Anderson model:

$$\begin{aligned} H = &\sum_{km\sigma} \varepsilon_k c^+_{km\sigma} c_{km\sigma} + \varepsilon_d \sum_{m\sigma} d^+_{m\sigma} d_{m\sigma} \\ &+U \sum_{m\sigma \neq m'\sigma'} d^+_{m\sigma} d_{m\sigma} d^+_{m'\sigma'} d_{m'\sigma'} + \sum_{km\sigma} V_k (d^+_{m\sigma} c_{km\sigma} + c^+_{km\sigma} d_{m\sigma}) \end{aligned} \tag{2.18}$$

where $c^+_{km\sigma}$ ($c_{km\sigma}$) creates (annihilates) a conduction electron with momentum $k=|\boldsymbol{k}|$ in the partial wave $l = 2$ with z-component m ($|m| \leq l$) and spin σ, and $d^+_{m\sigma}$ ($d_{m\sigma}$) creates (annihilates) an d-electron with quantum numbers m and σ, ε_k is the conduction-state dispersion relation and V_k is the hybridization matrix element without spin-orbit coupling.

There are several competing energy scales, all restricting the orbital degrees of freedom. First, Hund's second rule maximizes the orbital angular momentum. Second, crystalline electric field (CEF) quenches the orbital angular momentum. Third, the rather large hybridization width of the 3d levels smears out the energy splitting of the ionic term. Lastly, the direct orbital exchange, which leads to an orbital singlet, is expected to occur at $T >> T_K$ [Okada and Yosida, 1973].

This model can also be applied to rare earth (4f) or actinide (5f) impurities. The spatial extension of the wave function is reduced in such cases: 4f < 5f < 3d. This decreases the magnitude of the hybridization V_k.

At low temperatures ($T << T_F$), the Fermi liquid properties can be extracted resulting in the singlet ground state, where the coefficient γ of the linear T term in the specific heat can be obtained via the Sommerfeld expansion as follows:

$$\gamma = \frac{\pi n}{(n+2)T_K}, \tag{2.19}$$

and the zero magnetic field susceptibility is given by

$$\chi_s = \frac{n}{2\pi T_K}. \tag{2.20}$$

The Wilson ratio for the impurity is given by

$$(\frac{4\pi^2}{3})\frac{\chi_s}{\gamma} = \frac{2(n+2)}{3}, \tag{2.21}$$

which is same as $(\Delta\chi/\chi)/(\Delta C/C)$ [Nozières and Blandin, 1980], where $\Delta\chi$ and ΔC are the contribution of impurities in the susceptibility and specific heat, respectively. As we see, Eq. (2.21) reduces to the Wilson ratio of the ordinary Kondo problem for $n = 1$. The electrical resistivity due to the impurity at low temperatures can be derived within a Fermi liquid approach assuming electron-hole symmetry near the Fermi level [Yoshimori, 1976; Mihály and Zawadowski, 1978] as follows:

$$\rho_{\text{imp}} = \rho_o\{1-\frac{1}{8}[\frac{5\pi T}{(n+2)T_{\text{K}}}]^2\} . \qquad (2.22)$$

Thus, we see the T independent specific heat divided by temperature and susceptibility along with T^2 dependence of resistivity at low T in the compensated impurity spin.

2.2.1.2 Undercompensated Impurity Spin

Let us compare the compensated case, $n = 1$ and $S = 1/2$, with the case $n = 1$ and $S = 3/2$ (all cases with $S > n/2$ are qualitatively the same). The specific heat as a function of temperature is shown in Figure 2-1. For spin $S = 1/2$ and $n = 1$, see Figure 2-1*a*, the height of the peak grows with field and asymptotically approaches the value of a free spin Schottky anomaly. For $S > 1/2$, if $H << T_{\text{K}}$, e.g., $H = 0.01\ T_{\text{K}}$ in Figure 2-1*b*, the specific heat has two independent peaks; the peak at lower T corresponds to the Zeeman splitting of the ground multiplet and the one at higher T to the Kondo screening.

For $S = 1/2$ and $n = 1$, the susceptibility has a maximum at low T due to the singlet ground state in $H << T_{\text{K}}$. On the other hand, its maximum at about $H \sim T$ is reminiscent of free spin behavior. For $S > 1/2$ and $H = 0$, the Curie law as a straight line is shown in Figure 2-2. However there is a smooth change in the Curie constant due to the change of the effective spin from S at high T to $\{S-1/2\}$ at low T. The magnetic field lifts the degeneracy at low T and reduce the susceptibility to a finite value resulting from the Kondo spin-compensated degrees of freedom.

2.2.1.3 Overcompensated Impurity Spin

Since there are more conduction electron channels to compensate the impurity spin, the remaining conduction electron spin of $\{n-2S\}$ is delocalized giving rise to a critical behavior. The magnetic susceptibility in small field, $H \ll T_K$, diverges with a power law given by Wiegmann and Tsvelik [1983] and Sacramento and Schlottmann [1991a]

$$\chi = H^{(-1+2/n)};\ n > 2,\ S < n/2\ . \tag{2.23}$$

For $n = 2$ and $S = 1/2$, the susceptibility diverges with a logarithmic dependence on the field [Desgranges, 1985]. Note that the critical exponent in Eq. (2.23) only depends on the number of channels, but not on the spin. The entropy, s, of the impurity in $H = 0$ and at $T = 0$ is given by Tsvelik [1985], Desgranges [1985], and Sacramento and Schlottmann [1991b]

$$s(T=0, H=0) = \ln \frac{\sin[\pi(2S+1)/(n+2)]}{\sin[\pi/(n+2)]}\ . \tag{2.24}$$

In the presence of a magnetic field, the ground state is a singlet giving the corresponding entropy equal to zero. At high temperature the impurity spin behaves like a free spin in a magnetic field.

At low temperatures, the zero field susceptibility $\chi(T)$ and the specific heat divided by temperature $C(T)/T$ diverge with critical behavior given by Schlottmann [1991c], Tsvelik [1985], Desgranges [1985], and Sacramento and Schlottmann [1991a]

$$\chi \sim C/T \sim (T/T_K)^{\frac{2-n}{n+2}}\ . \tag{2.25}$$

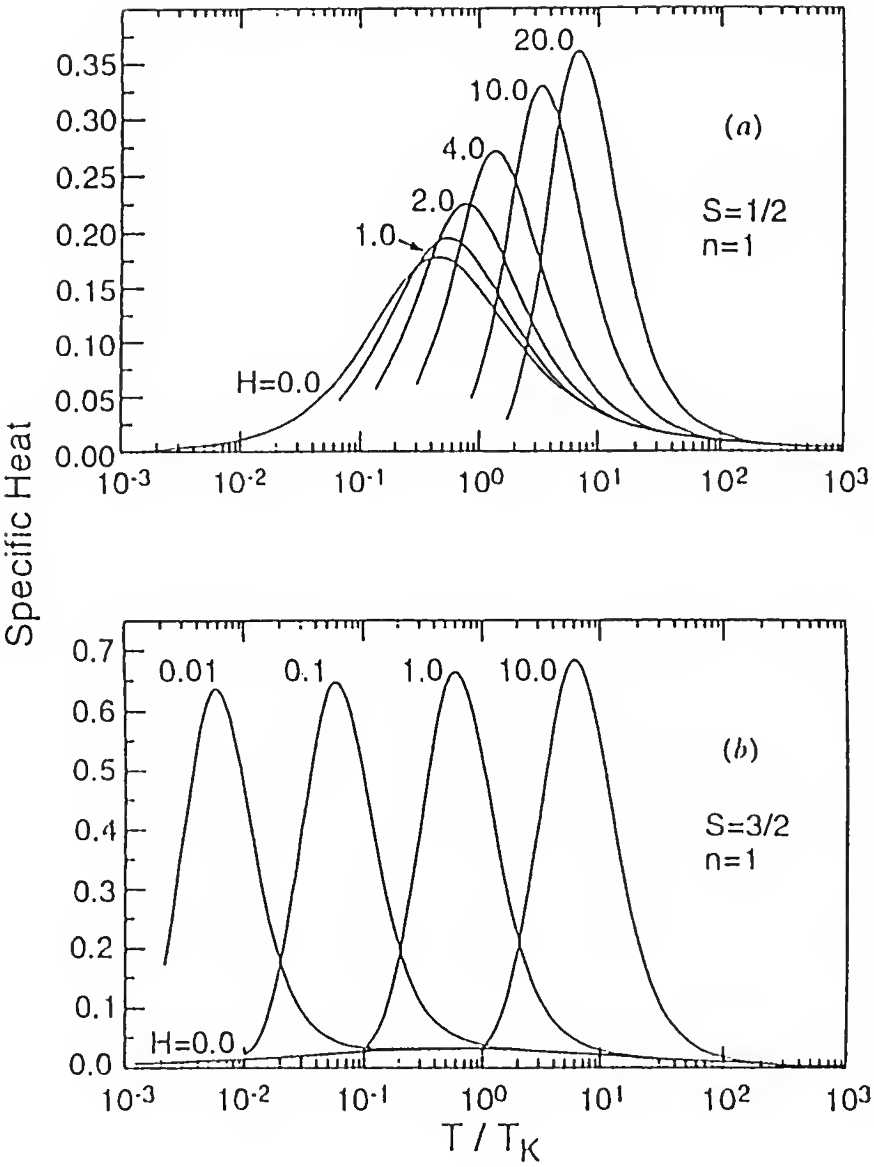

Figure 2-1. Specific heat as a function of T/T_K in constant magnetic field and $n = 1$ for (*a*) $S = 1/2$ and (*b*) $S = 3/2$. The field intensity H is given in units of T_K. This is from Sacramento and Schlottmann [1989a].

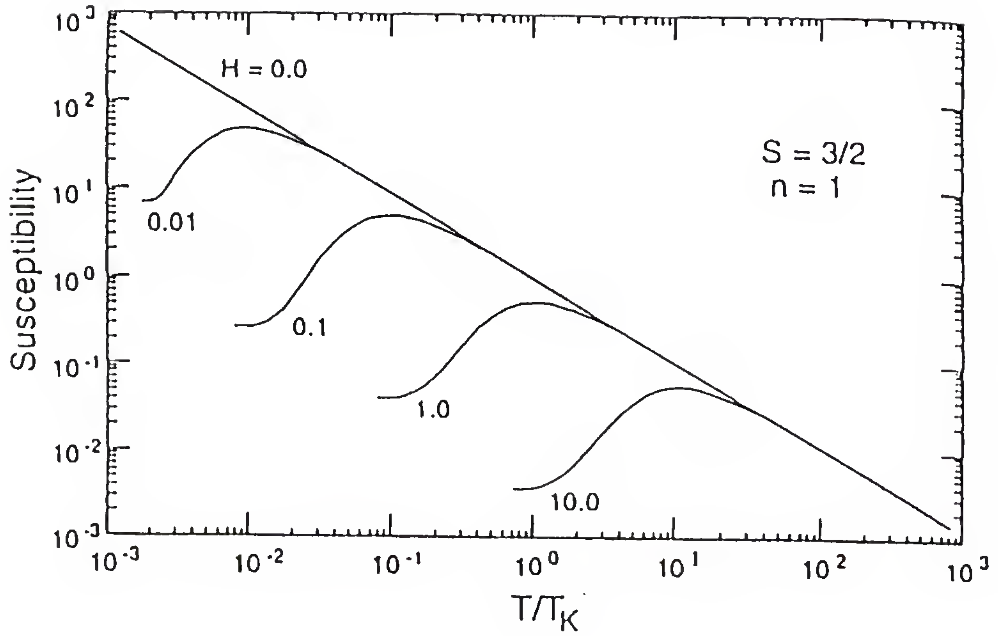

Figure 2-2. Magnetic susceptibility as a function of T/T_K in constant magnetic field and $n = 1$ for $S = 3/2$. The field intensity H is given in units of T_K. This is from Sacramento and Schlottmann [1989a].

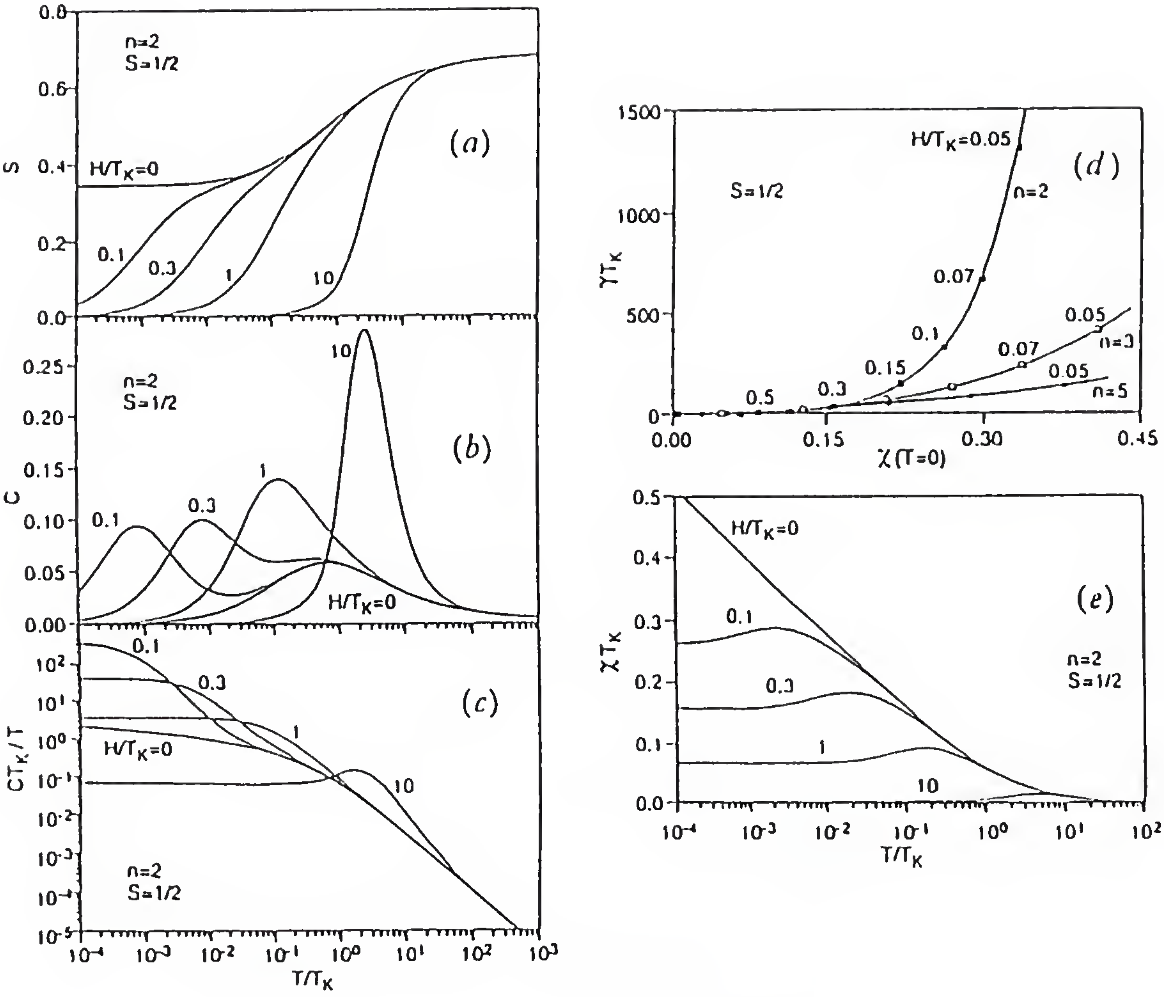

Figure 2-3. (*a*) Entropy, (*b*) specific heat, and (*c*) specific heat divided by temperature as a function of T/T_K in constant magnetic field for $S = 1/2$ and $n = 2$. The entropy is singular at $H = T = 0$. (*d*) γ values as a function of the zero temperature magnetic susceptibility for $n = 2,3$, and 5 with the field as a parameter. Note the rapid increase of γ as H approaches zero. (*e*) Magnetic susceptibility as a function of T/T_K in constant magnetic field for $S = 1/2$ and $n = 2$. The shoulders correlate with the field-dependent peak in the specific heat. This is from Schlottmann and Sacramento [1993].

For $n = 2$ and $S = 1/2$ (two channel Kondo model, see Figure 2-3), the critical exponent vanishes and again a logarithmic dependence on the temperature arises [Tsvelik, 1985; Desgranges, 1985; Sacramento and Schlottmann, 1989b, 1990, 1991a].

In Figure 2-3*a*, we see that in zero field the entropy changes smoothly between the value $\{\ln 2\}/2$ given by Eq. (2.24) for low T and the asymptotic free spin entropy, ln 2, at high T. The results for the entropy for $n \geq 2$ is qualitatively different from the traditional Kondo problem ($n = 1$), where there is only one energy scale T_K, because as n increases the Kondo screening is less pronounced and another field dependent energy scale $T_K(H/T_K)^{1+2/n}$ exists.

The specific heat as a function of T/T_K in constant field for $n = 2$ and $S = 1/2$ is shown in Figure 2-3*b*, and these curves just correspond to the slope, $C_v = T(\partial s/\partial T)_v$, of those in Figure 2-3*a*. The $H = 0$ specific heat curve shows the Kondo resonance. In a small magnetic field and at low T, another peak develops due to the second energy scale and the two peaks merge into one characterized by a Schottky anomaly at intermediate fields $H \sim T_K$. For $H \neq 0$ the specific heat at low T is proportional to T, and can be characterized by a coefficient γ. In Figure 2-3*c*, we see that the value γ for $H = 0$ does not saturate as $T \rightarrow 0$ K, but it becomes finite for $H \neq 0$. Also a maximum in C/T arises for larger fields as a consequence of the developing Schottky anomaly. In Figure 2-3*e*, we see the logarithmic divergence of χ in T for $H = 0$ and $n = 2$, and χ decreases with field but has a maximum which correlates with the low T peak of the specific heat.

Quadrupolar Kondo Effect. The model of the quadrupolar Kondo effect was introduced [Cox, 1987a] as a possible mechanism to quench the orbital and spin degrees of freedom of the U 5f-shell in the heavy fermion compound UBe_{13}. It can explain the lack of a magnetic field dependence of the electronic specific heat and magnetic susceptibility, but cannot explain the strong negative magnetoresistivity.

The main assumptions of the model are the following: Firstly, the stable 5f-shell configuration of the U ions is $5f^2$ and this leads to a ground multiplet with total angular momentum J = 4 according to Hund's rule. Secondly, the CEF splits the J = 4 multiplet into a Γ_1 singlet, Γ_3 doublet, and Γ_4 and Γ_5 triplets. The Γ_3 non-Kramers doublet is assumed to be the ground state. Thirdly, the excited Γ_4 triplet explains a Schottky anomaly in the specific heat, and the coupling to the Γ_3 via the magnetic field gives rise to the van Vleck susceptibility.

The Kondo effect is incorporated by hybridizing the 5f electrons with the conduction states and by considering virtual excitations into the $5f^1$ configuration with a J = 5/2 ground multiplet, which is split into a ground state Γ_7 doublet and Γ_8 quartet in cubic symmetry. A nonvanishing matrix element between the Γ_3 states of $5f^2$ and the Γ_7 states of the $5f^1$ can be obtained via the J = 5/2 partial wave, in particular with the conduction electron states having Γ_8 symmetry. By projecting the $5f^1$ states out, one obtains the following exchange interaction,

$$H_{ex} = \frac{1}{2} J S \cdot [\sigma_8(0) + \sigma_8'(0)] \,, \tag{2.26}$$

where $J > 0$, S are the *pseudospin* operators for S = 1/2 of the *electric* quadrupole moments representing the Γ_3 doublet and σ is the vector of Pauli matrices. σ_8 and σ'_8 denote two pseudospins representing the four Γ_8 states at the U site. Hamiltonian (2-26) has the general form of the spin-1/2 two channel Kondo model. Here we should be aware that the magnetic field in the Kondo Hamiltonian corresponds to the tetragonal (quadrupolar) splitting related to a deformation of the cubic symmetry. The magnetization is the *electric* quadrupolar moment, thus the magnetic susceptibility represents actually the *electric* quadrupolar susceptibility [Cox, 1987a, 1988a, and 1988b]. Also we should keep in mind that even if the concentration of U ions is very small, they are going to interfere with each other at low T due to a *divergent* correlation length associated with a critical behavior. This interference competes with the local lattice distortion induced by a single quadrupolar Kondo ion.

At low T ($T << T_K$), the resistance is given by Ludwig and Affleck [1991]

$$R(T)/R(0) = 1 - (T/T_K)^{1/2}\ . \tag{2.27}$$

The specific heat divided by temperature, C/T, and the electric quadrupolar susceptibility χ_q are proportional to $-\ln T$. However, the proportionality coefficient of χ_q is usually very small so that we do not see the effect. Instead, we do see the van Vleck magnetic susceptibility which is not due to the ground state, but due to the coupling between the ground state and the excited CEF level via the magnetic field. It is given by

$$\chi_m = \chi_{vV}[1 - \eta(T/T_K)^{1/2}]\ , \tag{2.28}$$

where χ_{vV} is the T-independent van Vleck magnetic susceptibility. The coefficient η is inversely proportional to the CEF splitting. We now summarize the basic physical quantities in Table 2.1 as a function of temperature between the two channel spin 1/2 (or *magnetic dipole*) Kondo effect and the two channel *electric quadrupole* (*pseudospin* 1/2) Kondo effect.

Possible examples of quadrupolar Kondo effect systems are $U_XY_{1-X}Pd_3$ for x = 0.2 [Seaman *et al.* 1991], $U_XTh_{1-X}Ru_2Si_2$ for $x \le 0.07$ [Amitsuka *et al.*, 1993; Amitsuka and Sakakibara, 1994], and $Ce_{0.1}La_{0.9}Cu_{2.2}Si_2$ [Andraka, 1994c].

Table 2.1. The physical quantities as a function of temperature of the two channel spin 1/2 Kondo effect and the two channel electric quadrupole (*pseudospin* 1/2) Kondo effect.

	Two Channel *Spin* 1/2 Kondo Effect	Two Channel *Electric Quadrupole* Kondo Effect
ρ	$-T^{1/2}$	$-T^{1/2}$
C/T	$-\ln T$	$-\ln T$
χ_q		$-\alpha \ln T$, $\alpha \ll 1$
χ_m	$-\ln T$	$-\eta T^{1/2}$, $\eta \sim \chi_{vv}$; for nonmagnetic ground state. $-\ln T$; for a magnetic ground state.

2.2.2 Phenomenological Theory of a Critical Point at $T = 0$ K with a Scaling Analysis

Even though there are several experimental results [Andraka and Stewart, 1993; Löhneysen *et al.*, 1994] which reveal a magnetic nature in the vicinity of a critical point at $T = 0$ K as an origin of the NFL behavior, there is no microscopic theory explaining the NFL behavior. However, recently there was a report [Tsvelik and Reizer, 1993] of a possible explanation for the NFL behavior not based on a microscopic theory but on a phenomenological theory.

Tsvelik and Reizer proposed a phenomenological theory to explain the NFL behavior, which exhibits strong deviations from the Fermi liquid theory, observed in the heavy fermion metallic alloys $U_{0.2}Y_{0.8}Pd_3$. Their theoretical development is based on the following experimental results in $U_{0.2}Y_{0.8}Pd_3$ [Andraka and Tsvelik, 1991] and $UCu_{3.5}Pd_{1.5}$ [Andraka and Stewart, 1993]. Firstly, a ln T dependence of C/T and a linear T behavior of the resistivity are observed. Secondly, there is a scaling in the magnetization M in the following form,

$$M = \frac{H}{T^{\gamma}} f(\frac{H}{T^{\beta+\gamma}}) \tag{2.29}$$

where $\gamma = 0.25 \sim 0.3$, $\beta + \gamma = 1.2 \sim 1.3$, and $f(x)$ is a nonsingular function. Thirdly, the same scaling of H holds for the specific heat,

$$\frac{C_v(H,T)}{T} - \frac{C_v(0,T)}{T} = g(\frac{H}{T^{\beta+\gamma}}) \ . \tag{2.30}$$

Lastly, the behavior of the thermodynamic quantities becomes even more singular in UCu_4Pd, which is closer to the antiferromagnetic (AFM) part of the phase diagram. All these properties hold below $T \sim 10$ K. The materials behave like Kondo alloys well above this temperature (~ 100 K) with the ln T dependence of ρ [Seaman *et al.*, 1991] originating from the scattering of conduction electrons off U ions.

The Fermi liquid (FL) theory is based on the assumption that the low energy excitations are dominated by fermionic excitations. This assumption via the Pauli principle implies a natural energy scale exists in the theory, the chemical potential ε_F and all thermodynamic properties depend on T/ε_F and H/ε_F. The dependences of C and M to the magnetic field and temperature behave as described in Eqs. (2.29) and (2.30). Their scaling clearly demonstrates the absence of a natural energy scale and thus the irrelevance of NFL behavior with fermionic excitations.

Therefore, Tsvelik and Reizer suggested that the low T thermodynamics in the above alloys is dominated by collective bosonic modes. These modes arise due to the fact that the system is in the vicinity of a phase transition which occurs at $T = 0$ K. If a phase transition occurs at a finite critical temperature T_c, the notation T in Eqs. (2.29) and (2.30) should be changed $T - T_c$. Although the nature of the $T = 0$ K instability remains obscure, spin glass fluctuations are suggested as an essential origin based on the observed experimental results in the alloys.

The free energy is given by

$$F = -Tf\,(\frac{T}{T_K}, \frac{h_i}{T^{\delta_i}})\ , \tag{2.31}$$

where h_i are external fields and δ_i are dimensions. The fields are relevant if their dimensions are positive $\delta_i > 0$. In the scaling region, one must consider only the leading singularity of the free energy F and then perform the limit $T_K \to \infty$. Suppose that the excitation spectrum ω at the critical point is given by $\omega \sim q^z$, then the dimensional analysis gives $F \sim T^{1+d/z}$. In the limit $T_K \to \infty$ and $h_i << 1$, the indices of the singular χ are given by

$$\chi_i(0) \sim T^{-\gamma_i} \equiv T^{-2\delta_i+1+d/z}\ . \tag{2.32}$$

If $\chi_i(0)$ are related to the thermodynamic correlation functions of the operators $\Phi_i(t,x)$ as a function of time and real space and the concept that the correlation must decay at t = 0 and x → ∞ is applied at finite temperature to restrict γ's (see the paper by Tsvelik and Reizer [1993]), the following relation is obtained:

$$\delta_i < 1 + d/z\ . \tag{2.33}$$

The comparison of the specific heat result, $C \sim T \ln T$, with the specific heat from the free energy, first derivative of $F \sim T^{1+d/z}$ in terms of T, gives $d = z = 3$ (the scaling arguments do not control logarithms), and the excitation spectrum at the critical point scales as $\omega \sim q^3$.

This result along with Eq. (2.33) means that $\delta_i < 2$ and this simple inequality is very important, because in both a spin glass transition and a quadrupolar fluctuation a magnetic field couples to a relevant field quadratically, i.e., $h = H^2$. The data from the alloys show that the magnetic field scales as T^δ with $\delta = 1.3 \pm 0.1$, which means that H^2 has the scaling dimension $\delta(H^2) = 2\delta = 2.6 \pm 0.2 > 2$. This estimate contradicts the requirement $\delta_i < 2$, so that it rules out not only the scenario related to a spin glass transition but also the one of an impurity quadrupolar fluctuations. Recently, there was a study of two channel Kondo effect with two impurities to consider a more realistic system where intersite and on-site interactions compete all the time [Ingersent *et al.*, 1992].

CHAPTER 3
NON-FERMI LIQUID BEHAVIOR OF MAGNETIC HEAVY FERMION SUPERCONDUCTORS

There has been a lot of interest in a non-Fermi liquid (NFL) behavior in f-electron (Ce and U) heavy fermion materials for the past few years. The physical properties of the NFL usually exhibit a weak power law or logarithmic divergence at low temperatures. A critical point at $T = 0$ K has been suggested as an origin. The possible origins of a 0 K critical point are an unconventional single ion effect and fluctuations of the order parameter near 0 K resulting in a second order phase transition. Our attention will be given to the NFL systems whose parent systems have the antiferromagnetic (AFM) state and superconductivity (SC) at low T. A more thorough emphasis will be given to the $U_XM_{1-X}Ni_2Al_3$ (M = Th, Pr, and Y) and $U_XTh_{1-X}Ru_2Si_2$ systems with experimental data to suggest a possible ground state of these systems.

3.1 Overview of Non-Fermi Liquid Systems

Almost a dozen NFL systems have been discovered in recent years (see the review papers, e.g., Maple *et al.* [1995], Andraka [1994], and Steglich *et al.* [1994a]). These systems are Ce or U intermetallics doped with a nonmagnetic element with a few exceptions. Since the Ce and the U have a partially filled f electron shell, they carry magnetic dipole (or spin) or electric quadrupolar moments depending on the ground state of the CEF levels. While the magnetic dipole moments interact with the *spins* of the conduction electrons resulting in magnetic order, the nonmagnetic quadrupolar moments interact with the *charges* of the conduction electrons participating in a quadrupole ordering at low T. The NFL materials exhibit several unusual physical properties in, e.g., specific heat C, electrical resistivity ρ, and magnetic susceptibility χ_m in contrast to the local Fermi liquid theory with which we can describe some of the heavy fermion systems.

For instance, C/T is expressed in terms of ln T dependence rather than constant in temperature, ρ is linear in $T^{1/2}$ or T or ln T rather than in T^2, and χ_m is linear in ln T or $T^{1/2}$ rather than constant at low temperatures. Thus, the existence of a critical point at $T = 0$ K has been suggested. One of the possible origins comes from an unconventional moment screening process such as multichannel Kondo effect [Schlottmann and Sacramento, 1993]. Another possibility is a $T = 0$ K second-order phase transition such as a long range magnetic order [Andraka and Tsvelik, 1991; Tsvelick and Reizer, 1993] (another possibility is due to dilute magnetic impurities in a disordered metal where a singularity comes from the probability distribution for Kondo temperatures [Dobrosavljevic *et al.*, 1992]).

There have been very extensive experimental studies to confirm the above theoretical suggestions. The parent heavy fermion materials, of which doped ones exhibit NFL behavior, vary from the nonmagnetic ($CeCu_6$) to the magnetic system (UCu_5), from the superconductor (UBe_{13}) to Kondo insulator (CeRhSb), and even systems in which SC and antiferromagnetic states coexist (URu_2Si_2). We can roughly divide these systems into three different groups: The first group members, considered to exhibit the $T = 0$ K long range phase transition or collective modes of excitation, are $CeCu_{5.9}Au_{0.1}$ [Löhneysen *et al.*, 1994], $CeCu_{5.7}Au_{0.3}$ at pressure [Bogenberger and Löhneysen, 1995], $UCu_{3.5}Pd_{1.5}$ [Andraka and Stewart, 1993], $Ce_XTh_{1-X}RhSb$ (may be disorder) [Andraka, 1994b], and $CePtSi_{0.9}Ge_{0.1}$ and $UCu_{5.6}Al_{6.4}$ [Steglich *et al.*, 1994]. The second group members, being described to exhibit the single ion two channel Kondo effect (TCKE), are $U_{0.9}Th_{0.1}Be_{13}$ [Aliev *et al.*,1995] and maybe $U_XTh_{1-X}Pd_2Al_3$ [Maple *et al.*, 1995]. The last group members may be described by either the first collective modes or the second single particle excitation, e.g., $Ce_{0.1}La_{0.9}Cu_2Si_2$ [Andraka, 1994c], $U_XM_{1-X}Pd_3$ (M = Y, Sc) [Seaman *et al.*, 1991; Andraka and Tsvelick, 1991; Gajewiski *et al.*, 1994], $Pr_XY_{1-X}Cu_2Si_2$ [Sampathkumaran, 1993], and $U_XTh_{1-X}Ru_2Si_2$ [Amitsuka and Sakakibara, 1994].

So we present here some experimental results for $U_XTh_{1-X}Ru_2Si_2$. It seems to us that possible collective modes at low temperatures dominate over the single ion excitations in the system. Furthermore, we will present another new NFL materials $U_{0.9}M_{0.1}Ni_2Al_3$ (M = Th, Pr, and Y) and in the end we hope to convince that our new systems are more related to a $T = 0$ K long range phase transition than other possible origins.

3.2 Investigation of the Ground State in $U_XTh_{1-X}Ru_2Si_2$ for $x < 0.20$

There has been a very interesting report [Amitsuka *et al.*, 1993] such that they have found non-Fermi liquid behavior in $U_XTh_{1-X}Ru_2Si_2$ for $x \leq 0.07$. The experimental results of C/T, ρ, and χ due to U-ion exhibit a ln T dependence for one or two decades of temperatures. They have attempted to explain the results of χ and C/T in terms of the TCKE [Nozieres and Blandin, 1980; Tsvelick and Wiegmann, 1985b; Sacramento and Schlottmann, 1991a] with a single impurity. In contrast to χ and C/T, the present theories predict [Tsvelick, 1990; Ludwig and Affleck, 1991] that the resistivity subtracted from the residual one, $\rho(T) - \rho(0)$, increases as $-T^{-\alpha}$ with a positive α for $T \rightarrow 0$.

We firstly summarize briefly the parent system URu_2Si_2 and its doping experiments on the U-site with Th, Y, La, and Ce. We then describe the main points of $U_XTh_{1-X}Ru_2Si_2$ experiments for $x \leq 0.07$ by Amitsuka *et al.*, [1993] with their recent new interpretation [Amitsuka and Sakakibara, 1994]. Our emphasis will be given to the possibility of a magnetic transition at low T with the resistance, specific heat, and magnetic susceptibility measurements in $U_XTh_{1-X}Ru_2Si_2$ for $0.07 \leq x \leq 0.17$.

3.2.1 URu_2Si_2

The physical properties of the superconductivity (T_C = 1.5 K) and antiferromagnetism (T_N = 17.5 K) in URu_2Si_2 [Palstra *et al.*, 1985; Schlabitz *et al.*, 1986; Maple *et al.*, 1986] have attracted condensed matter physicists. Its structure is body-centered tetragonal $ThCr_2Si_2$ with lattice parameters a = 4.219 Å and c = 9.575 Å as shown in Figure 3-1. The spins on the U-sites are aligned antiferromagnetically to the c-direction with alternate ferromagnetic sheets in $a/2$ apart. It is a semi-heavy electron system with γ, the coefficient of electronic specific heat, being 64 mJ $K^{-2}mole^{-1}$ [Palstra *et al.*, 1985]. It also shows a large slope of the upper critical magnetic field H_{C2} at the superconducting critical temperature T_C, $(-dH_{C2}/dT)_{Tc}$, which is about 7.6 T/K [Rauchschwalbe, 1987]. $ThRu_2Si_2$ has the same crystalline structure as URu_2Si_2, and γ is about 10 mJ $K^{-2}mole^{-1}$ with a constant $\rho = 1$ $\mu\Omega$-cm for $T < 20$ K.

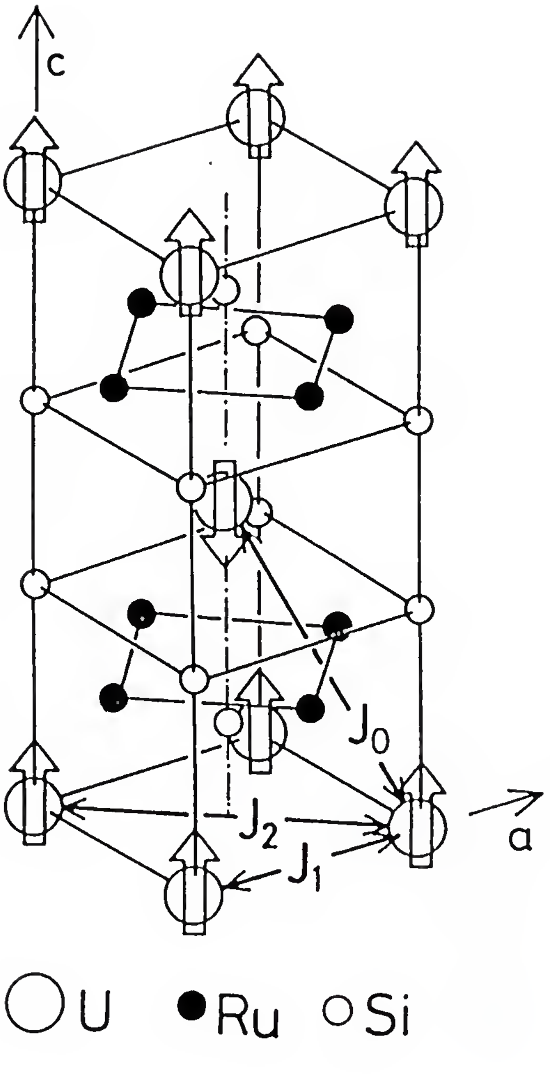

Figure 3-1. Crystal and spin structure of antiferromagnetic superconductor URu_2Si_2. It is tetragonal with parameters a = 4.219 Å and c = 9.575 Å. This figure is from Date and Kindo [1993].

For the AFM ordering there are several possibilities. Firstly, it may be due to the development of a charge density wave (CDW) or spin density wave (SDW) with a gap of 11 meV from specific heat measurements [Maple *et al.*, 1986] or a gap of 7.5 meV produced by the hybridization of U-5f states with conduction-electron states from the inelastic neutron scattering [Walter *et al.*, 1986]. In this case, the nonmagnetic singlet ground state is responsible for the transition. However, there is a maximum around 30 K in the electronic specific heat vs. temperature in addition to the anomaly at T_N. The total entropy connected with both peaks is close to R ln2 implying the magnetic low temperature state of URu_2Si_2 is formed by localized 5f electrons in a CEF doublet ground state [Schlabitz *et al.*, 1986]. Secondly, it may be due to the long range Ruderman-Kittel-Kasuya-Yoshida (RKKY) interaction of the localized U-5f magnetic moments supported by X-ray resonance magnetic scattering [Isaacs *et al.*, 1990] and magnetic neutron scattering [Mason *et al.*, 1990]. But, there is no indication of a Schottky anomaly in specific heat up to 350 K even if most of the CEF levels should be populated at 200 K. The entropy released below T_N is about $0.17R$ ln2 although the ordered moment is as small as 0.03 μ_B [Broholm *et al.*, 1987].

In the magnetic susceptibility χ_m, there is a broad peak around 55K, which is interpreted as being due to a short range magnetic correlation [Schlabitz *et al.*, 1986], or the coherence effect in the Kondo lattice [Mydosh, 1987], or AFM fluctuations of 5f state [Amitsuka *et al.*, 1992]. High field magnetization experiments reveal several sharp transitions at 35-40 T [de Boer *et al.*,1986] indicating a possible crossing of CEF levels. More interesting result comes from the fact that the SC and antiferromagnetism coexist

[Palstra *et al.*, 1985; Schlabitz *et al.*, 1986; Broholm *et al.*, 1987]. This invokes the possibility of elucidating the interplay between the two ground states.

3.2.2 Doping Effects of URu_2Si_2

There have been several doping experiments of $U_{1-X}M_XRu_2Si_2$ (M = Th, Y, La, and Ce) into U-site to understand the fascinating properties of the parent system mentioned above [Torre *et al.*, 1992; Park, 1994; Park *et al.*, 1994; Amitsuka *et al.*, 1992; Mihalik *et al.*, 1993]. In $U_{1-X}La_XRu_2Si_2$ for $0 \leq x \leq 0.3$ [Amitsuka *et al.*, 1992], T_N decreases for $x < 0.07$ and starts to increase for $0.07 < x < 0.3$ as the lattice parameters gradually expand. Their argument is that 5f character continuously changes from an itinerant to a localized nature with doping based on χ_m experiments. There is a linear correlation between T_m, where χ_m shows a maximum peak, and T_N for $0.07 < x < 0.3$, indicating the same nature of both T_N and T_m. So they concluded the maximum peak in χ_m around 55K is related to the AFM fluctuations of the 5f state.

In the U-rich case of $U_{1-X}Th_XRu_2Si_2$ for $0.0 \leq x \leq 0.05$ [Torre *et al.*, 1992], small doping of Th suppresses both T_N and T_C, and it can be explained in terms of the decreased coupling constant J between the 5f and conduction electrons. In other words, the expanding of the lattice parameters causes a suppression of hybridization as shown in Eq. (3.1) assuming the energy difference between the Fermi level and 5f level is unchanged based on tetravalent character of U and Th. Thus, both decrease of J and increase of R_{ij} due to the lattice expansion cause the depression of T_{RKKY} illustrated by Eq. (3.2):

$$J \sim -\frac{|V_{sf}|^2}{|E_F - E_f|} \tag{3.1}$$

$$T_{\mathrm{RKKY}} \sim [JN(E_{\mathrm{F}})]^2 / R_{ij}^{\ 3} , \qquad (3.2)$$

where V_{sf} is the hybridization matrix, E_{F} the Fermi level, E_{f} the energy of the 5f-level, $N(E_{\mathrm{F}})$ the density of states at the Fermi level, and R_{ij} the distance between lattice sites *i* and *j*. Torre *et al.* [1992] use the concept of "Kondo *hole*" to explain the minimum in the resistivity. However, it might be ruled out as shown by Y-doping experiments [Park, 1994], specifically, the minimum in ρ at low temperatures exists up to 50 % doping. On the other hand, there have been a lot of interesting phenomena in the U-dilute case, namely "non-Fermi liquid" behavior which we will describe in more detail in the following section.

3.2.3 Non-Fermi Liquid Behavior of $U_XTh_{1-X}Ru_2Si_2$ for $x \leq 0.07$

A Japanese group has reported [Amitsuka *et al.*, 1993; Amitsuka and Sakakibara, 1994] that they have found non-Fermi liquid behavior in a single crystal of $U_XTh_{1-X}Ru_2Si_2$ for $x \leq 0.07$, i.e., U-dilute case, such that C/T, ρ, and χ due to the U-ions show a ln T dependence. They have attempted to explain the experimental results in terms of the two channel Kondo effect (TCKE) [Nozieres and Blandin, 1980; Tsvelick and Wiegmann, 1985; Sacramento and Schlottmann, 1991a; Seaman *et al.*, 1991] with a single impurity based on the tetragonal $5f^2$ configuration even though the resistivity data is totally in disagreement with the model, which predicts the $-T^{1/2}$ dependence of electrical resistivity.

They have claimed that the T independence of χ^{a}_{m}, magnetic susceptibility along the basal plane or *a*-axis, originates from the van Vleck paramagnetism due to the transverse coupling between Γ_{5t} doublets and five $\Gamma_{(1\text{-}4)t}$ singlets. But the divergence of χ^{c}_{m}, the magnetic susceptibility along the c-direction, forced them to conclude the ground state was a magnetic doublet Γ_{5t} ($^3H_4$, U^{4+}, $5f^2$) rather than a nonmagnetic doublet. Thus, the TCKE in this U-dilute system $U_XTh_{1-X}Ru_2Si_2$ for $x \leq 0.07$ is caused by *dipolar* fluctuations in the ground state. This ruled out the possibility of the TCKE caused by *quadrupolar* fluctuation in the ground state of Γ_3 nonmagnetic doublet for the cubic and tetragonal U-compounds [Cox, 1988b].

For instance, there is no such magnetic ground state phenomena in the cubic symmetric systems such as $U_{0.9}Th_{0.1}Be_{13}$ [Aliev *et al.*, 1993; Aliev *et al.*, 1995] and $U_{0.2}Y_{0.8}Pd_3$ [Seaman *et al.*, 1991] which are also believed to exhibit non-Fermi liquid behavior (there has been polarized inelastic neutron scattering in which they observed the critical fluctuations around the antiferromagnetic position in the $U_{0.2}Y_{0.8}Pd_3$ similar to that of the $U_{0.45}Y_{0.55}Pd_3$ whose ground state is a magnetic Γ_5 triplet). In cubic symmetry, e.g. $U_{0.2}Y_{0.8}Pd_3$, the selection rules used [Cox, 1993] restrict the lowest CEF state to the Γ_3 doublet that couples to the Γ_7 excited doublet via the Γ_8 symmetry conduction states. In this case the degeneracy of Γ_3 comes only from the quadrupolar degrees of freedom. On the other hand, in the tetragonal symmetry, e.g. $U_XTh_{1-X}Ru_2Si_2$ for $x < 0.2$, the TCKE is expected only when the Γ_{5t} ($5f^2$) lowest doublet couples to the Γ_{7t} ($5f^1$) excited doublet via the hybridization effects with the Γ_{6t}+ Γ_{7t} symmetry conduction states at the U-site. So the ln T dependence of χ^c_m of $U_XTh_{1-X}Ru_2Si_2$ for $x \leq 0.07$ is the very case not in the *electric quadrupolar field* but in the *magnetic field* [Amitsuka and Sakakibara, 1994]. The above result is true only when the doublet Γ_{5t} given by $\{\alpha|+3> + \beta|-1>\}$ and $\{\alpha|-3> + \beta|+1>\}$ in the $^3H_4$ ($5f^2$) is mag-netically degenerate in z-component of the total angular momentum J_Z for $3\alpha^2 - \beta^2 \neq 0$. However, it is still possible for quadrupolar susceptibility,

χ_q, to show ln T divergence at low temperatures because Γ_{5t} is doubly degenerate with the quadrupolar moment in the c-plane. To investigate this possibility ultrasound measurements, from which the quadrupolar (or strain) susceptibility can be extracted, are desired.

3.2.4 Non-Fermi Liquid Behavior of $U_XTh_{1-X}Ru_2Si_2$ for $0.07 \leq x \leq 0.17$

A purely logarithmic temperature dependence of χ^c_m (χ_c^{imp} in Figure 3-2) in the c-direction breaks down at low temperatures (T < 100 mK) for x ≥ 0.03 resulting in a peak anomaly at temperature T_m of the order of 0.1 K as shown in Figure 3-2. The anomaly may come from an intersite magnetic correlation between U-ions, e.g., spin glass ordering. While we were doing the doping experiments in $U_XTh_{1-X}Ru_2Si_2$ for $0.07 \leq x \leq 0.17$, we found a kink below 2 K in the resistance data. This fact allowed us to speculate that the ln T dependence of χ^c_m for about two decades of temperature observed in $U_{0.01}Th_{0.99}Ru_2Si_2$ might correspond to magnetic fluctuations near $T = 0$ critical point [Andraka and Tsvelik, 1991], proposed already for other U-based alloys displaying similar low temperature properties. Since the temperature of the anomaly increases with U-concentration x, we have focused our investigation [Kim W.W. *et al.*, 1994] on the less dilute systems corresponding to x ≥ 0.07 to operate at more accessible temperatures in our laboratory, but we limited x ≤ 0.17 to avoid the problem of a miscibility gap for 0.2 < x < 0.9 [Torre *et al.*, 1992].

Polycrystalline samples of $U_XTh_{1-X}Ru_2Si_2$, with x = 0.07, 0.1, 0.125, 0.14, and 0.17, were made with Los Alamos U, 99.9 % Th from Los Alamos, 99.95 % Ru from

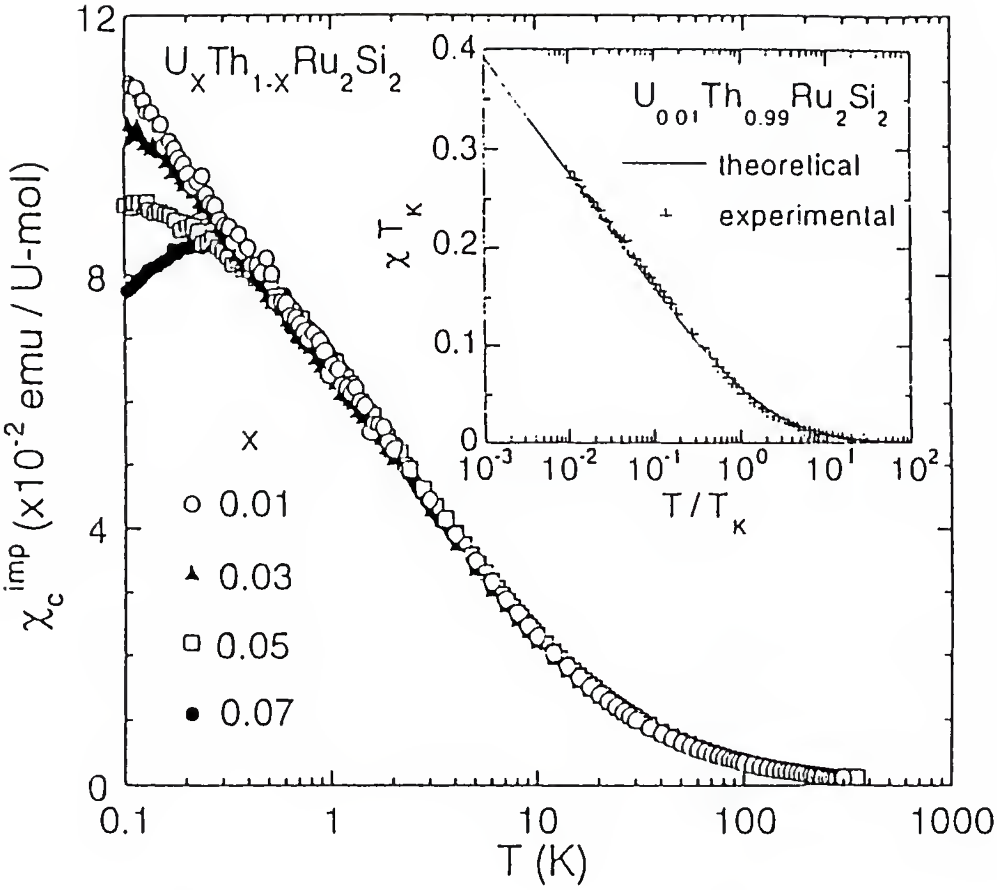

Figure 3-2. Magnetic susceptibility along the c-axis in terms of ln T of the $U_XTh_{1-X}Ru_2Si_2$ single crystals, x = 0.01, 0.03, 0.05, and 0.07. The inset shows the comparison between the χ_c^{imp} data for x = 0.01, scaled by using $\mu = 1.7\ \mu_B$ and $T_K = 11.1$ K, and the numerical calculations based on the S = 1/2 TCKE model (solid line). This figure is from Amitsuka and Sakakibara [1994].

Johnson Matthey Inc. (JMI), and 99.999 % Al from JMI as we described in section 1.3.1 in detail. Some resistivity samples were cast into a particular shape in a water-cooled crucible by using a pressure casting technique inside of an arc furnace [Crow and Sweedler, 1973]. After we took the sample out of the arc furnace, we subsequently annealed it at 900 °C for one week. All samples showed single phase according to X-ray powder diffraction data taken on a Philips diffractometer with a scan of 6 ° per minute in 2θ.

Resistance. These measurements were performed via a standard dc four-probe method to temperature as low as 0.3 K. If we look at the resistance data shown in Figure 3-3 in terms of T, we see a kink below 2 K for all our concentrations. The position of the kink anomaly decreases as we dilute U-concentrations for $x \leq 0.14$ as shown in Figure 3-4, and decreases abruptly for $x > 0.14$. We think the peak at 250 mK in χ^c_m from single crystalline sample [Amitsuka *et al.*, 1993; Amitsuka and Sakakibara, 1994] corresponds to an anomaly T_A in the resistance for $x = 0.07$. Although the T_A for $x = 0.07$ was not clear in our polycrystalline sample, it is interesting to note that the T_A approaches zero for $x \rightarrow 0$ if we assume the linear decrease of T_A for $x < 0.1$—we can see such a possibility for $0.1 \leq x \leq 0.14$. Thus, it is desirable to check this behavior with single crystalline samples for $x < 0.1$. This possibility allows us to speculate that the ln T dependence of χ^c_m observed in $U_{0.01}Th_{0.99}Ru_2Si_2$ may correspond to magnetic fluctuations near $T = 0$ critical point.

We do also see a linear T dependence of ρ below T_A, except the saturation region of ρ as $T \rightarrow 0$, which can not be explained by Fermi liquid theory. Moreover, we do see a increasing resistivity with temperature for $0.3 \text{ K} < T < 20 \text{ K}$ (even up to room temperature

[Amitsuka and Sakakibara, 1994]) in contradiction to the TCKE, which predicts an decrease in ρ with temperature caused by Kondo scattering. Thus, it seems that the behavior of ρ is closely related to the onset of coherence and correlated scattering. In other words, the NFL behavior of the resistivity in the $U_XTh_{1-X}Ru_2Si_2$ for U-dilute region ($x \leq 0.14$) seems to be related to the intersite interaction of U (short range correlation or even long range one as $T \rightarrow 0$) rather than the single site two channel Kondo effect.

Specific heat. Specific heat measurements did not reveal any signature consistent with a phase transition at T_A. Only the specific heat for the 'most magnetic' alloy of x = 0.14 showed a change of slope or a peak in C/T at about 0.45 K shown in Figure 3-5; this temperature is roughly three times smaller than the corresponding T_A. Since we saw the NFL behavior in ρ measurements at low temperatures, we can expect an unusual Fermi liquid behavior in specific heat rather than Fermi liquid behavior, in which we usually observe a saturation of C/T at low temperatures. We show specific heat due to the U-5f contribution divided by temperature C_{5f}/T vs. ln T for $0.07 \leq x \leq 0.17$ in Figure 3-5. C_{5f}/T for a given concentration is fairly linear in ln T scale over more than one decade implying again NFL behavior (the ln T dependence of C_{5f}/T for x = 0.07 holds for only one decade of T deviating for $T > 3$ K and this is also observed by Amitsuka *et al.* [1994]).

When we applied a magnetic field, C/T monotonically decreased as we increased the field up to 14 T. For instance, C/T at 1 K is decreased by about 42 % at $H = 14$ T compared to the value in the $H = 0$ for x = 0.1, and it follows surprisingly well Fermi liquid behavior with $\gamma = 178$ mJ $K^{-2}mole^{-1}$ as shown in Figure 3-6. Thus, we think that the system in the vicinity of magnetic instability at zero field approaches Fermi liquid region

[Steglich *et al.*, 1994] as we apply magnetic fields, because a single-site interaction is induced by the magnetic fields which destroy the weak long range correlations between local magnetic moments. A similar behavior of the magnetic field dependence has been reported [Löhneysen *et al.*, 1994] in system $CeCu_{5.9}Au_{0.1}$, which is believed to have an antiferromagnetic transition at $T = 0$ K in $H = 0$, and comes back to the Fermi liquid behavior in the magnetic field $H = 6$ T. According to TCKE [Schlottmann and Sacramento, 1993] as we described in Figure 2-3c, however, C/T should increase from the zero field value for the magnetic field roughly comparable to T_K. For instance, C/T for x = 0.1 should increase at least by a factor of five at $H = 10$ T and $T = 1$ K for $T_K = 10$ K, i.e., $T/T_K = 0.1$ and $H/T_K = 1$ (see Table 3-1). T_K listed in Table 3-1 has been obtained from the slope of the linear fit of Figure 3-5 using the formula (3.3) from TCKE model and assuming T_K is independent of magnetic field:

$$C_{5f}/T = -\frac{0.251R}{T_K}\ln\left(\frac{T}{0.41T_K}\right) + A\,, \tag{3.3}$$

where A is a constant and R is a gas constant 8.314 J $K^{-1}mole^{-1}$. But, we did not see such an increasing behavior of C/T implying the ineligibility of the TCKE in this system.

Table 3-1. Summary of Kondo temperature T_K using Eq. (3.3) for all our concentrations $0.07 \leq x \leq 0.17$.

concentration (x)	T_K (K)
0.07	6
0.10	10
0.125	11
0.14	14
0.17	20

As we dilute the U-concentration from 0.17 to 0.07, the lattice constants increase due to the larger atomic size of Th than U giving rise to a decrease of both T_K and T_{RKKY}. If we assume that the T_A corresponds to a magnetic phase transition, we see in Figure 3-7 that the long range correlations (T_{RKKY}) are *dominant* over the on-site interaction (T_K) in our system because T_A decreases as the coupling constant between the local magnetic moments and the conduction electrons decreases.

Amitsuka *et al.* [1994] also suggested a possibility of "channel reduction" such that there is a cross-over from the TCKE with a magnetic ground state Γ_{7t} to the usual one-channel Kondo effect in high magnetic fields and at low temperatures. But it is not probable, because it always generates the Kramers doublet as the lowest state so that a Curie-law susceptibility is expected even along the hard axis (in this case *a*-axis) and this contradicts the almost T independent behavior of χ^a_m. Thus, such a magnetic field dependence of the specific heat can not be explained by the simple TCKE as shown by both the decrease of C/T with fields and the inadequate argument of the channel reduction to explain the FL behavior in magnetic field.

There is another NFL system of $U_{0.2}Y_{0.8}Pd_3$, where the physical properties such as specific heat and magnetic susceptibility were suggested to obey TCKE [Seaman *et al.*, 1991; Maple *et al.*, 1995]. Also, as the theory [Tsvelik, 1985; Sacramento and Schlottmann, 1989b] predicts, there seems to be a remnant entropy $\{R \ln 2\}/2$ at $T = 0$ K [Seaman *et al.*, 1991]. Thus, C/T should increase at low temperatures, i.e., $T/T_K < 0.1$, in magnetic field $H < T_K$, e.g., $H < 50$ T for $T_K \sim 50$ K [Maple *et al.*, 1995] in $U_{0.2}Y_{0.8}Pd_3$ due to the release of the residual entropy. However, the decrease of C/T by 37 % is

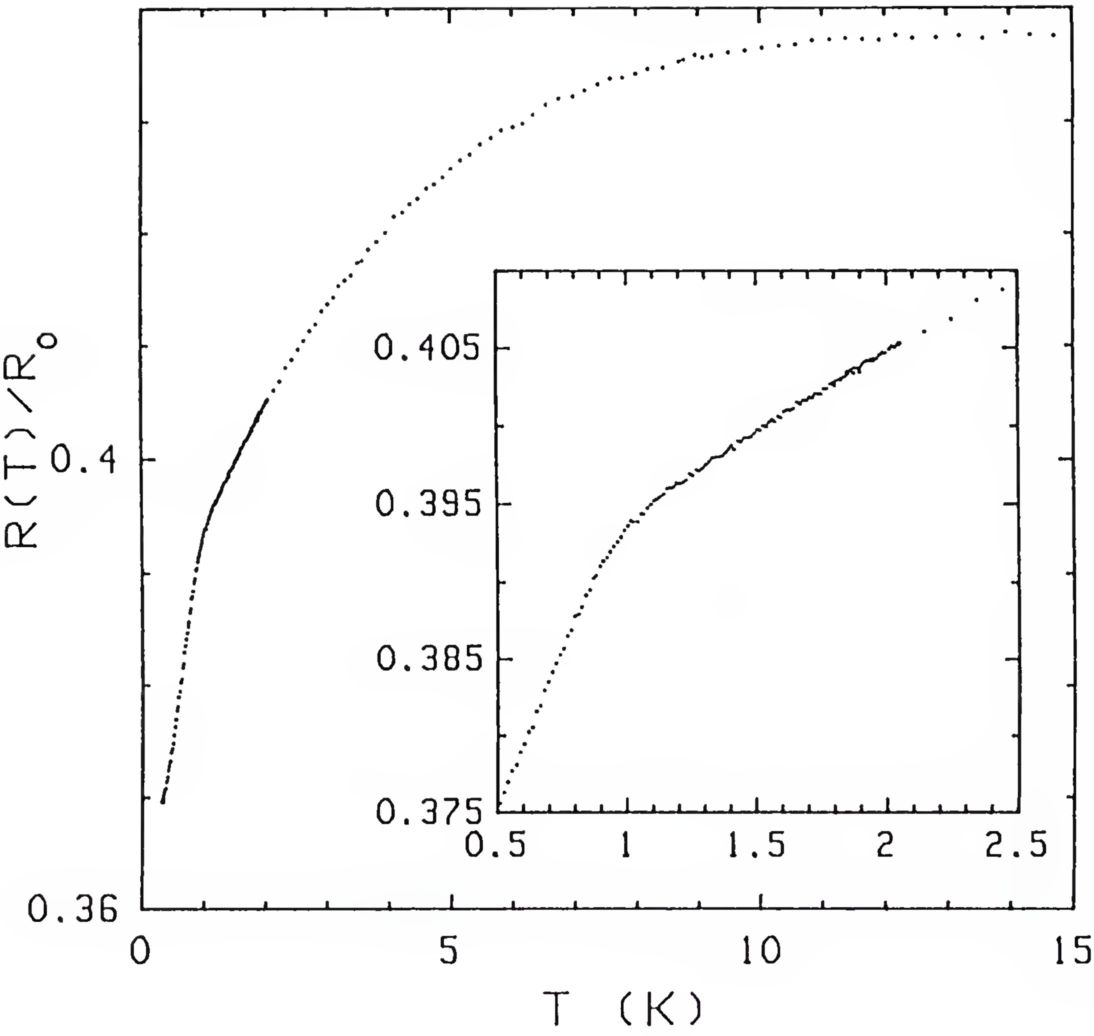

Figure 3-3. Low temperature resistance normalized to the room-temperature value R_o of $U_{0.17}Th_{0.83}Ru_2Si_2$. The inset shows anomaly at around T_A where the low and high T slopes cross each other.

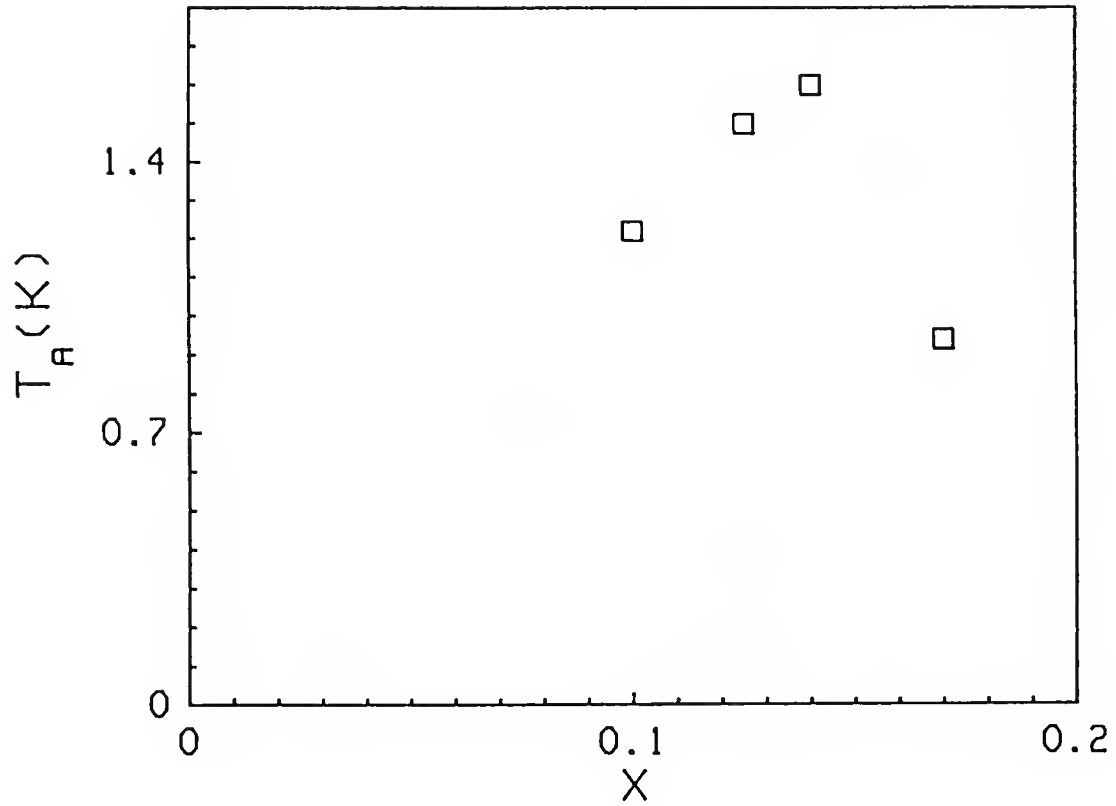

Figure 3-4. The anomaly T_A in terms of uranium concentration x. There is a linear decrease in T_A for decreasing x for $0.1 \leq x \leq 0.14$ for the polycrystalline samples (open triangles).

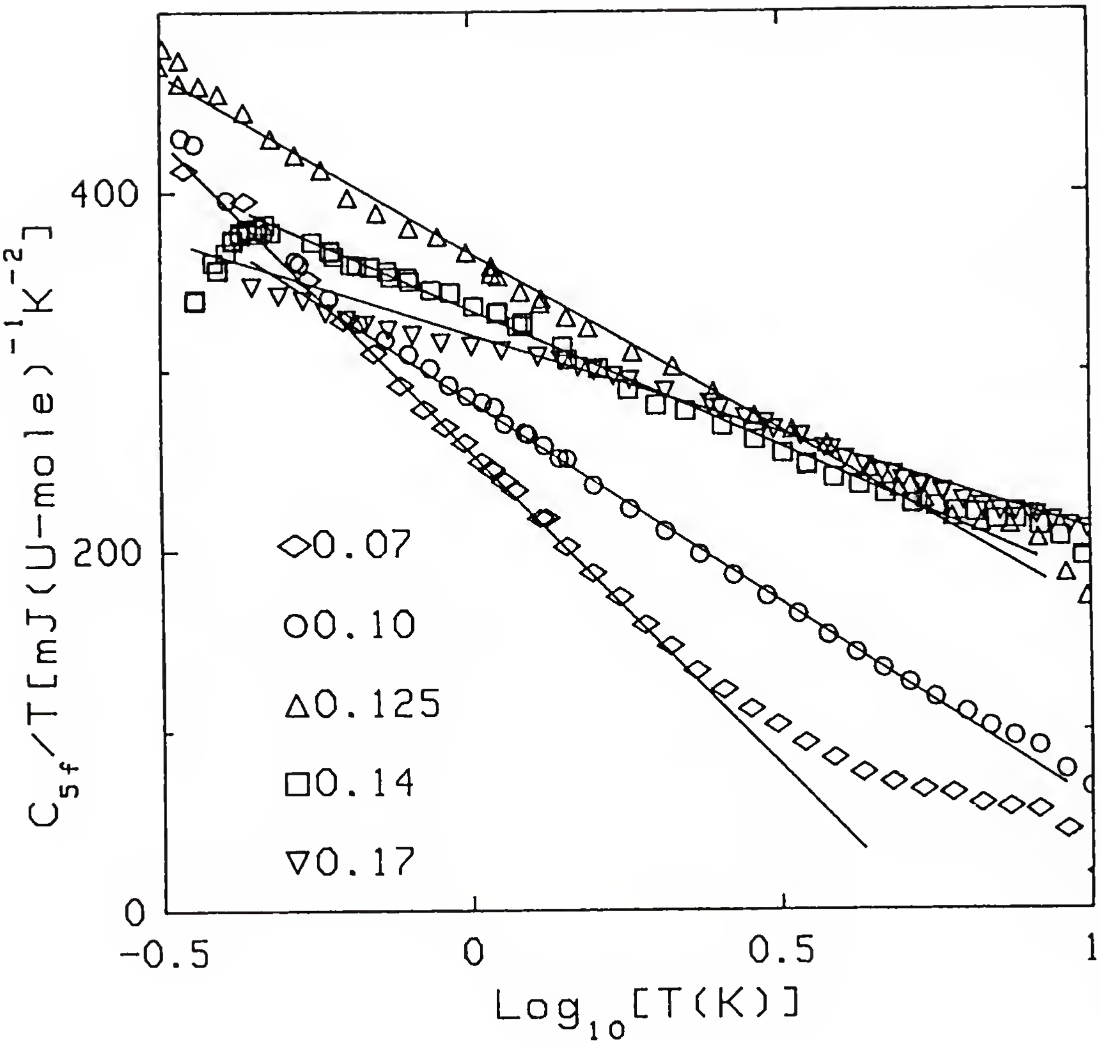

Figure 3-5. Specific heat of U-5f contribution divided by temperature, C_{5f}/T,as a function of ln T. We obtain the specific heat of U-5f by ,firstly, subtracting the specific heat of $ThRu_2Si_2$ from that of $U_xTh_{1-x}Ru_2Si_2$ and ,secondly, multiplying 1/x to the subtracted specific heat. The 'most magnetic' alloy of x = 0.14 shows a peak at about 0.45 K (open squares). All, except for x = 0.07, C_{5f}/T data show a ln T dependence for more than one decade in a good approximation. The lines are a guide to the eye.

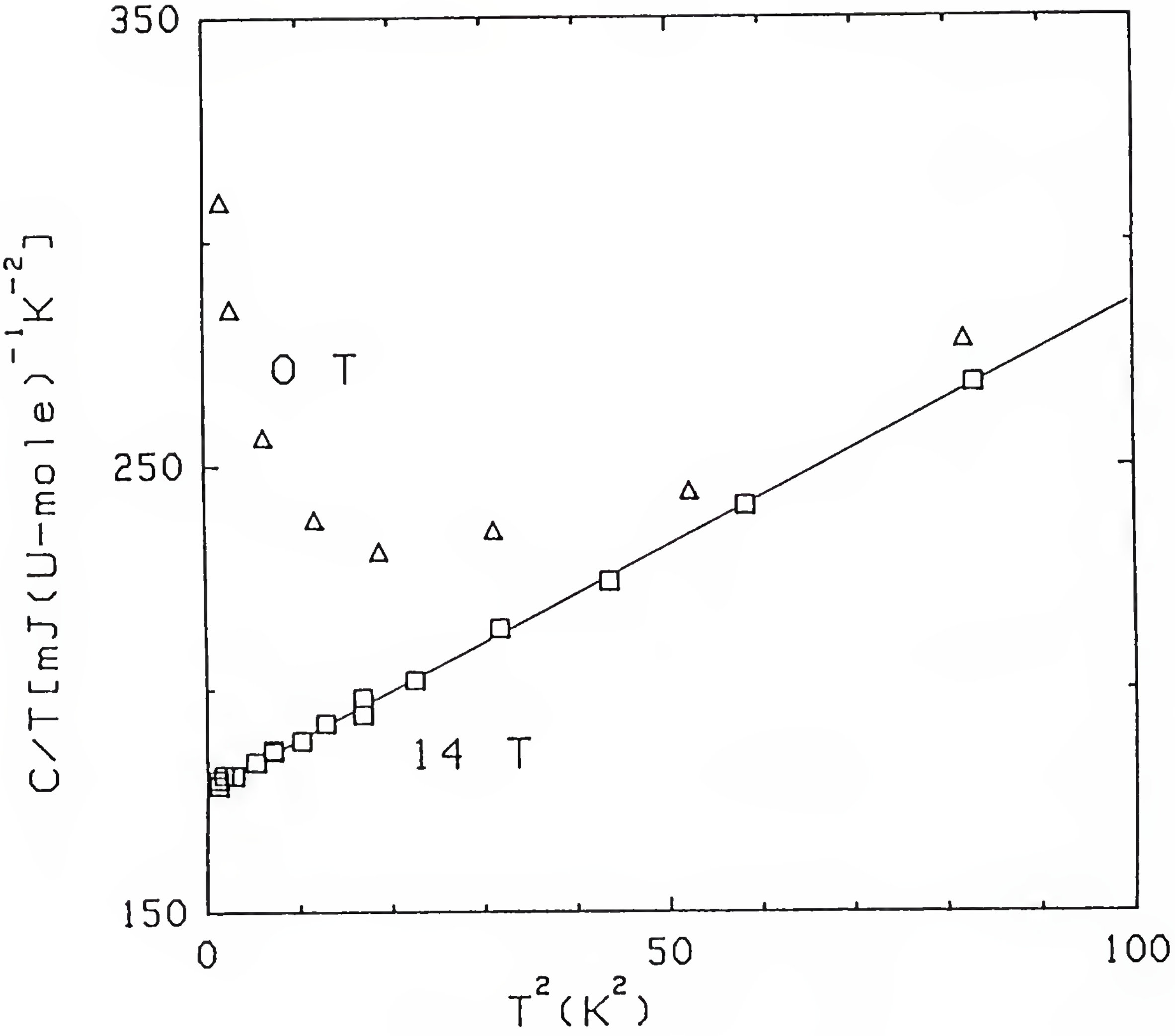

Figure 3-6. Specific heat divided by temperature vs. temperature squared for $U_{0.1}Th_{0.9}Ru_2Si_2$ in two different magnetic fields. The data in zero magnetic field (open triangles) at 1 K was reduced about 42 % when it was measured in H = 14 T (open squares). Notice the linear behavior of C/T in terms of T^2 in the field. The line is a linear fit to $C/T = \gamma + \beta T^2$ with γ = 178 mJ K^{-2} (U-mole)$^{-1}$ and β = 1.09 mJ K^{-4} (U-mole)$^{-1}$.

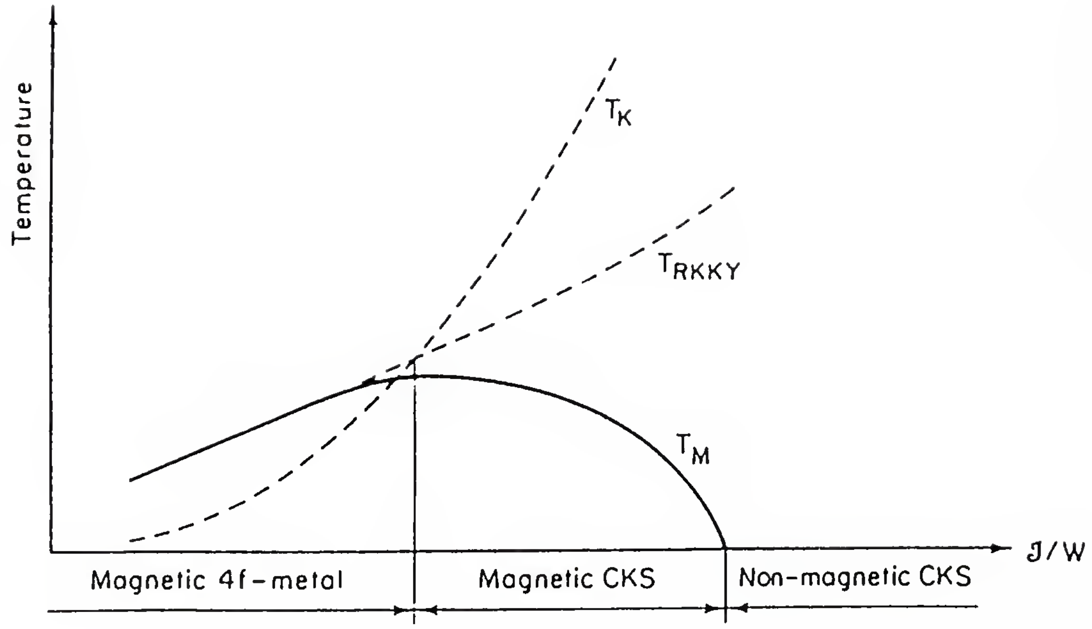

Figure 3-7. The classification of concentrated Kondo system by the relation between two characteristic temperatures— T_K and T_{RKKY}. T_M is a magnetic transition temperature. This figure is from Brandt and Moshchalkov [1984].

observed by Andraka and Tsvelik [1991] at 0.35 K and 14 T (there should be about order of one increase in C/T for $T/T_K < 0.01$ and $H/T_K \sim 0.3$ from the Figure 2-3c) indicating the ineligibility of the TCKE theory to $U_{0.2}Y_{0.8}Pd_3$.

Susceptibility. Dc magnetic susceptibility measurements were performed from room temperature down to 1.8 K in a commercial SQUID magnetometer. No apparent signature consistent with a magnetic anomaly was found in our samples in the investigated range of temperatures—this is not surprising if we accept the possible relation between T_A and T_m, i.e., $T_A \approx (3 \sim 4)\ T_m$ so that T_m is expected below 1 K. However there was a distinct difference between the zero-magnetic-field-cooled (ZFC) and field-cooled (FC) susceptibilities χ_m for all concentrations investigated. Moreover, ZFC χ_m for some concentrations flattened out at the lowest temperature investigated indicating that there might be a possibility of an anomaly at temperatures lower than 1.8 K. This tendency is depicted in Figure 3-8 for x = 0.14.

It has been reported [Amitsuka and Sakakibara, 1994] that there was an excellent scaling behavior in the χ^c_m for $x \leq 0.07$ implying a single site Kondo effect and a fairly good fitting of χ^c_m data was possible by the TCKE as shown in the inset of Figure 3-2. However, we suggest that it may be interesting to look if there is a one-to-one correspondence between T_A and T_m by measuring χ^c_m (even T_A for better resolution) with single crystalline samples for $0.07 \leq x \leq 0.14$. Because, if such a correspondence exists, it means that the ln T dependence at low temperatures in χ^c_m is due to the collective modes of excitation rather than single ion excitations.

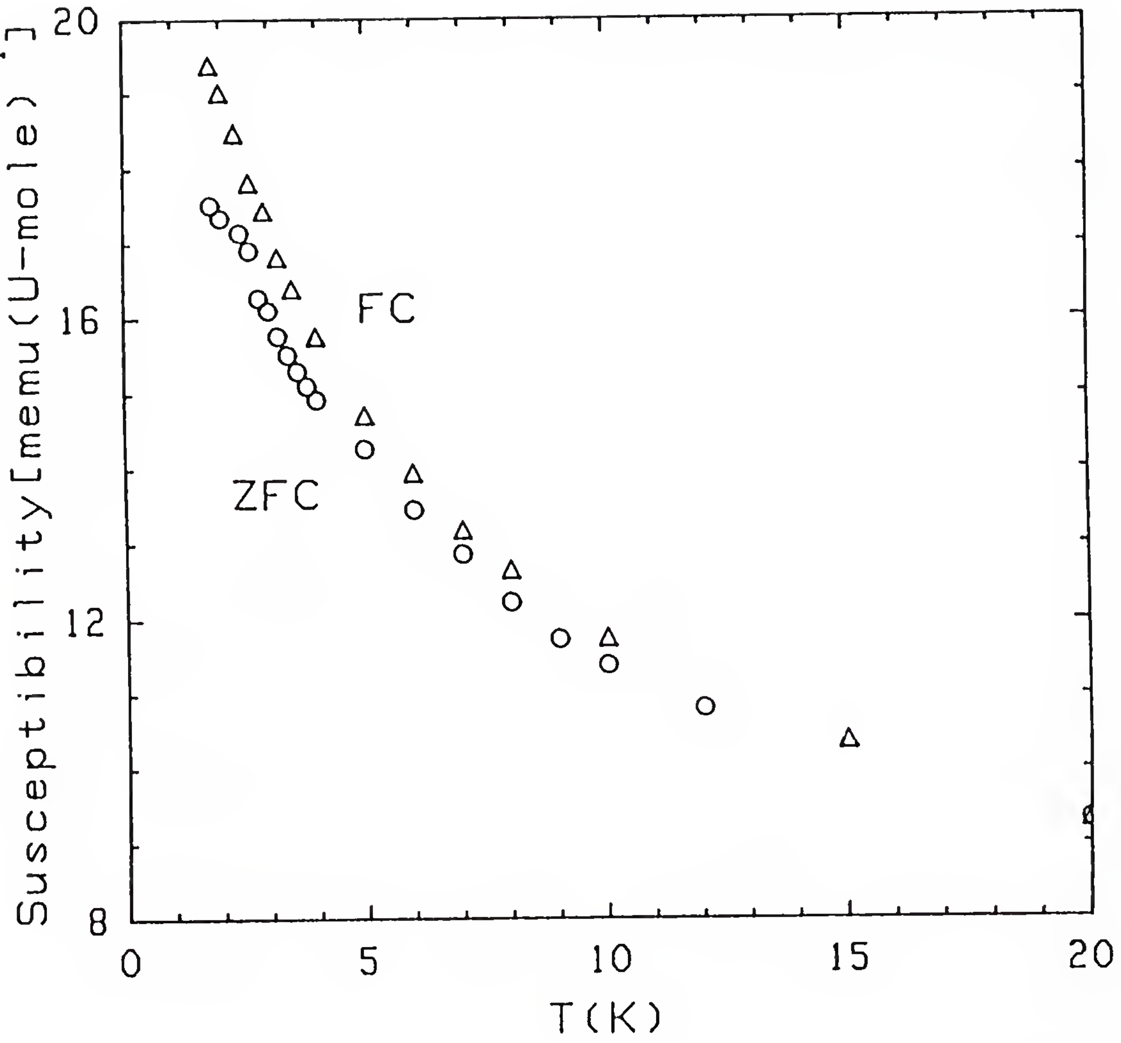

Figure 3-8. Magnetic susceptibility of polycrystalline sample $U_{0.14}Th_{0.86}Ru_2Si_2$ as a function of temperature for zero magnetic field cooled (ZFC, open circles) and field cooled (FC, open triangles) measurements in H = 0.004 T. A kink around 2.3 K is shown in the ZFC data, however it is gone in the FC data.

In summary, firstly we observed T_A in ρ measurements, below which the intersite interactions between local magnetic moments occur, for $0.1 \leq x \leq 0.17$ at low T. This anomaly at T_A seems to be related to the onset of coherence, and can not be explained by the single-site TCKE interpretation. Furthermore, the increase of resistivity with temperature for 0.3 K < T < 20K contradicts the TCKE, instead implying the onset of coherence. Thus, the NFL behavior in $U_xTh_{1-x}Ru_2Si_2$ for $0.1 \leq x \leq 0.17$ seems to be due to magnetic fluctuations at $T = 0$ K or collective modes of excitations at low temperatures rather than the single-site TCKE. Secondly, we know the specific heat of $U_xTh_{1-x}Ru_2Si_2$ in the U-dilute regime exhibits the NFL behavior. Also, thermodynamic measurements in magnetic fields reveal that these systems transforms to the Fermi liquid regime from the magnetic instability or magnetic intersite correlation regime caused by the destruction of the intersite interactions between local magnetic moments. Thirdly, we observed a spin-glass anomaly for concentrations $0.07 \leq x \leq 0.17$ in the FC and ZFC χ_m measurements using the polycrystalline samples.

Also, the confirmation of the relation between T_m and T_A using single crystalline samples is desirable to understand the origins of T_m and the logarithmic behavior of $U_{0.01}Th_{0.99}Ru_2Si_2$ in χ_m. Although we have focused on the anomaly of T_A and T_m in the resistivity and magnetic susceptibility, it is desirable to check if our system obeys the scaling behavior in the specific heat and magnetization measurements at several magnetic fields as a further work.

3.3 Magnetism and its Connection to Non-Fermi Liquid Behavior in $U_{1-X}M_XNi_2Al_3$ {M = Th, Pr, and Y}

Since there was a report of the discovery of a new heavy fermion system UNi_2Al_3 [Geibel *et al.*, 1991c], there have been several studies to understand the system. While we were conducting doping experiments on the U-site in UNi_2Al_3, we found unusual temperature dependence of the physical properties inconsistent with Fermi liquid behavior indicating a possible NFL system. Thus, we are going to investigate the doped system more thoroughly and give a possible explanation for the origin of our newly discovered [Kim W.W. *et al.*, 1993] NFL system.

3.3.1 UNi_2Al_3

It took several years for physicists to discover the new heavy-fermion superconductor, UNi_2Al_3, [Geibel *et al.*, 1991c] after discovering the previous ones such as $CeCu_2Si_2$ [Steglich *et al.*, 1979a], UBe_{13} [Ott *et al.*, 1983], UPt_3 [Stewart *et al.*, 1984a] and URu_2Si_2 [Schlabitz *et al.*, 1986]. Superconductivity takes place at T_C = 1 K in UNi_2Al_3, and the AFM transition at T_N = 4.6 K reflects a weak delocalization of 5f electrons. It has a hexagonal $PrNi_2Al_3$ crystalline structure, shown in Figure 3-9, with the lattice parameters a = 5.207 Å and c = 4.018 Å. As we see in Figure 3-9, the U-U distance is already larger than the Hill limit (3.4 Å) [Hill, 1970] to exhibit heavy fermion behavior. The sample is annealed to remove secondary phases (usually UAl_2) which exist in the unannealed sample.

If we look at χ vs. temperature as shown in Figure 3-10, there is a cusp at T_N and a broad maximum around $T_m = 100$ K. There is a flat region for $T > T_m$ in electrical resistivity ρ vs. T, which is shown in Figure 3-11. Also, Geibel *et al.* [1991c] found a corresponding maximum in ρ around T_m after they subtracted the contribution from the electron-phonon part, and suggested a transition from localized to weakly delocalized 5f behavior in the spirit of the Kondo lattice concepts.

The AFM transition is not clear in ρ, but is exhibited by a mean-field-type relatively sharp transition at T_N and a broad curve below T_N down to the onset of T_C in C/T vs. T as shown in Figure 3-12. The T_N is weakly depressed by an external magnetic field as high as $H = 8$ T as shown in the inset of Figure 3-12, resembling the case of, e.g., the heavy fermion antiferromagnet $CeCu_2Ge_2$ [de Boer *et al.*, 1987]. Magnetic entropy released at T_N gives a value of $S = 0.13\ R$ ln2 indicating a rather small ordered U-moment. This has been confirmed by neutron scattering measurements [Schröder *et al.*, 1994] which give ordered moments $\mu_{ord} = (0.24 \pm 0.10)\ \mu_B$/U-atom in the basal plane, which is incommensurate with the nuclear lattice. However, positive-muon spin rotation (μ^+SR) measurements [Amato *et al.*, 1992b] were reported such that the $\mu_{ord} = 0.1\ \mu_B$/U-atom along the c-direction (perpendicular to the basal plane) with a commensurate AFM ordering.

The superconductivity is exhibited by a sharp transition in ρ, shown in the inset of Figure 3-11, and by a broadened jump in the specific heat around at $T_C = 1$ K, shown in Figure 3-12. The electronic specific heat coefficient $\gamma = 120$ mJ $K^{-2}mole^{-1}$ is deduced, shown in Figure 3-12, by extrapolation of the $H = 1$ T data to $T = 0$ K. The resistivity

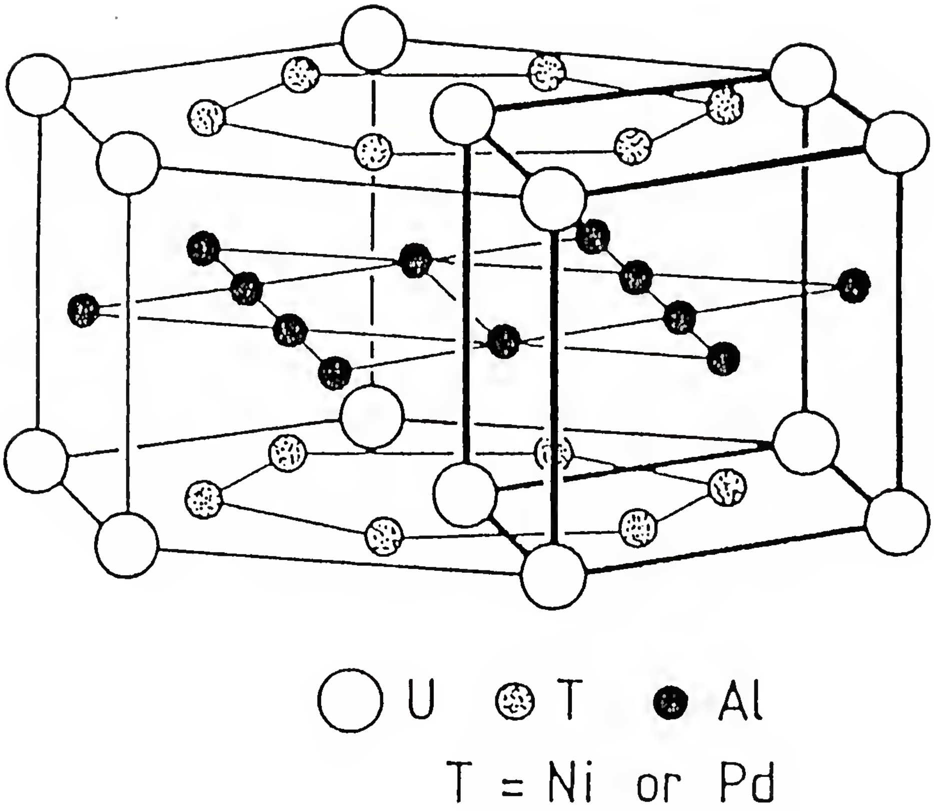

Figure 3-9. Hexagonal $PrNi_2Al_3$ crystal structure observed in UNi_2Al_3 and UPd_2Al_3. Heavy lines show unit cell. U-atoms carry magnetic moment. This figure is from Sticht and Kübler [1992].

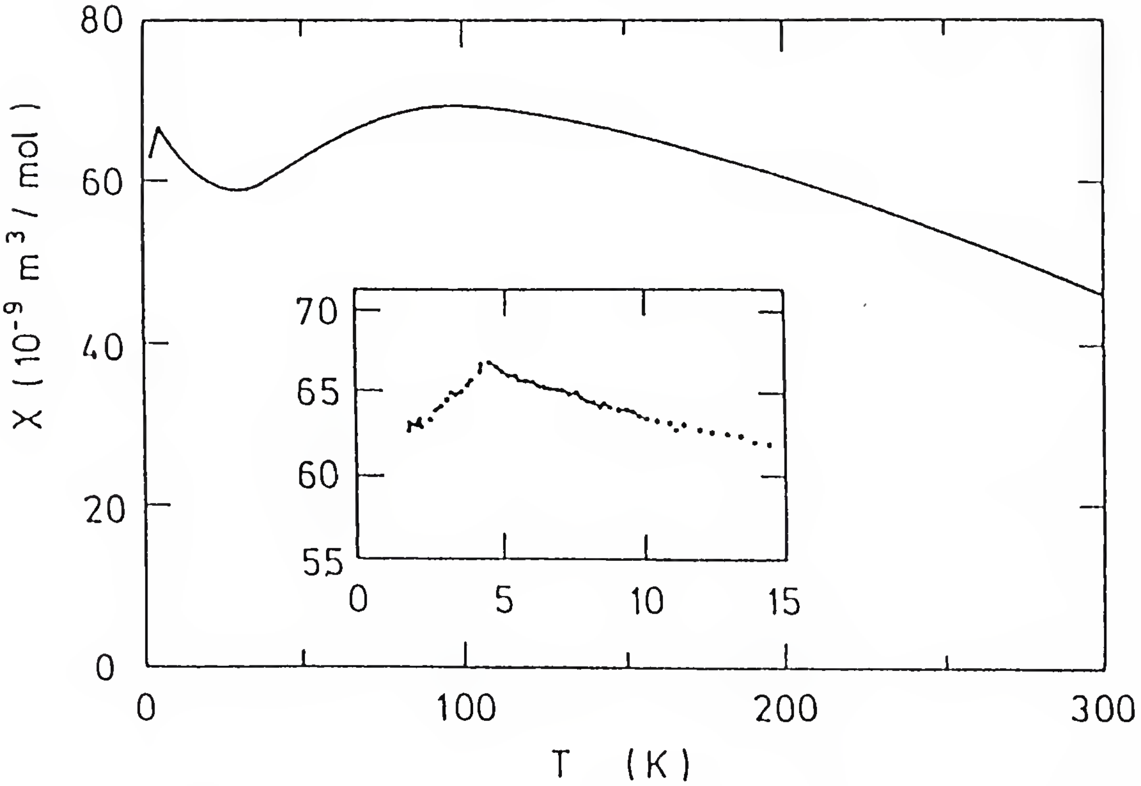

Figure 3-10. Temperature dependence of the magnetic dc-susceptibility, χ_{dc}, as measured for UNi_2Al_3 in a magnetic field of 20 mT using a SQUID magnetometer. Inset displays the AFM transition at $T_N = 4.6$ K. This figure is from Geibel *et al.* [1991c].

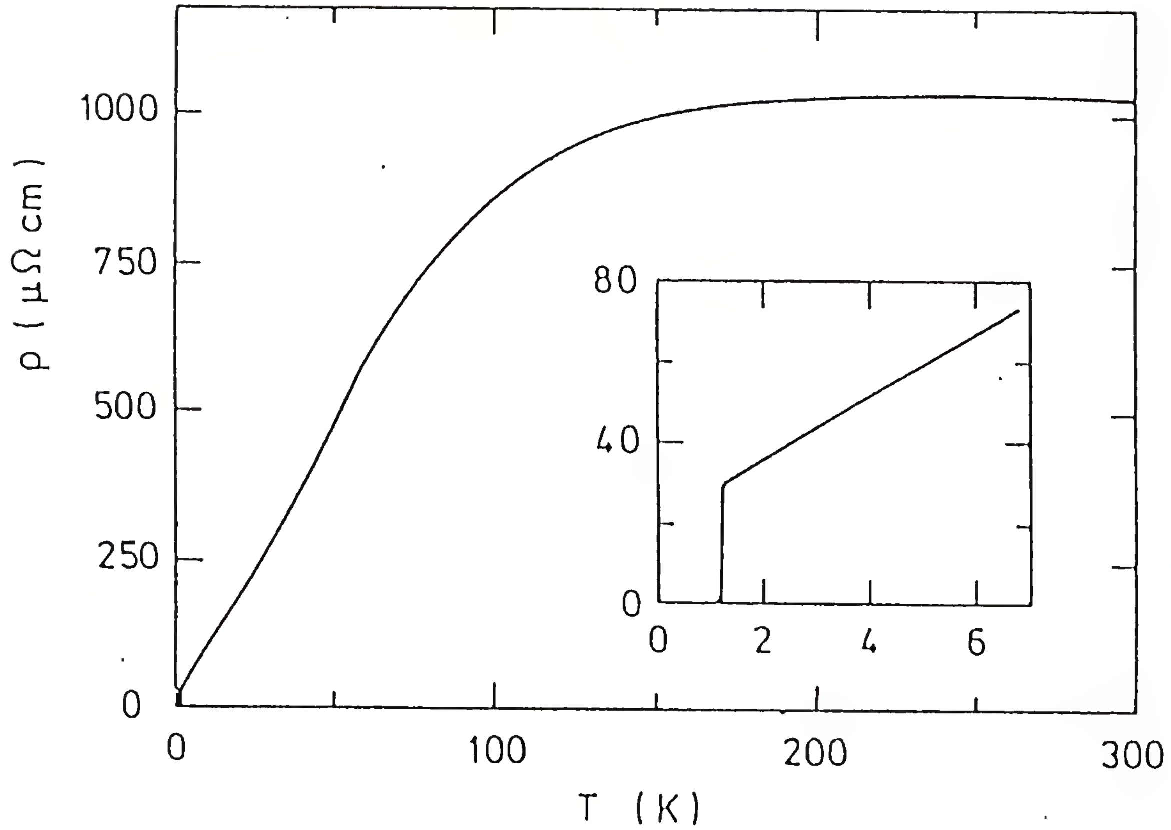

Figure 3-11. Electrical resistivity, ρ, as a function of temperature for UNi_2Al_3. It is estimated that the true resistivity values are lower by a factor of five. (The data points shown represent an upper limit caused by a large number of microcracks in the sample.) Inset shows data below 7 K, and note the linear *T* dependence of ρ. This figure is from Geibel *et al.* [1991c].

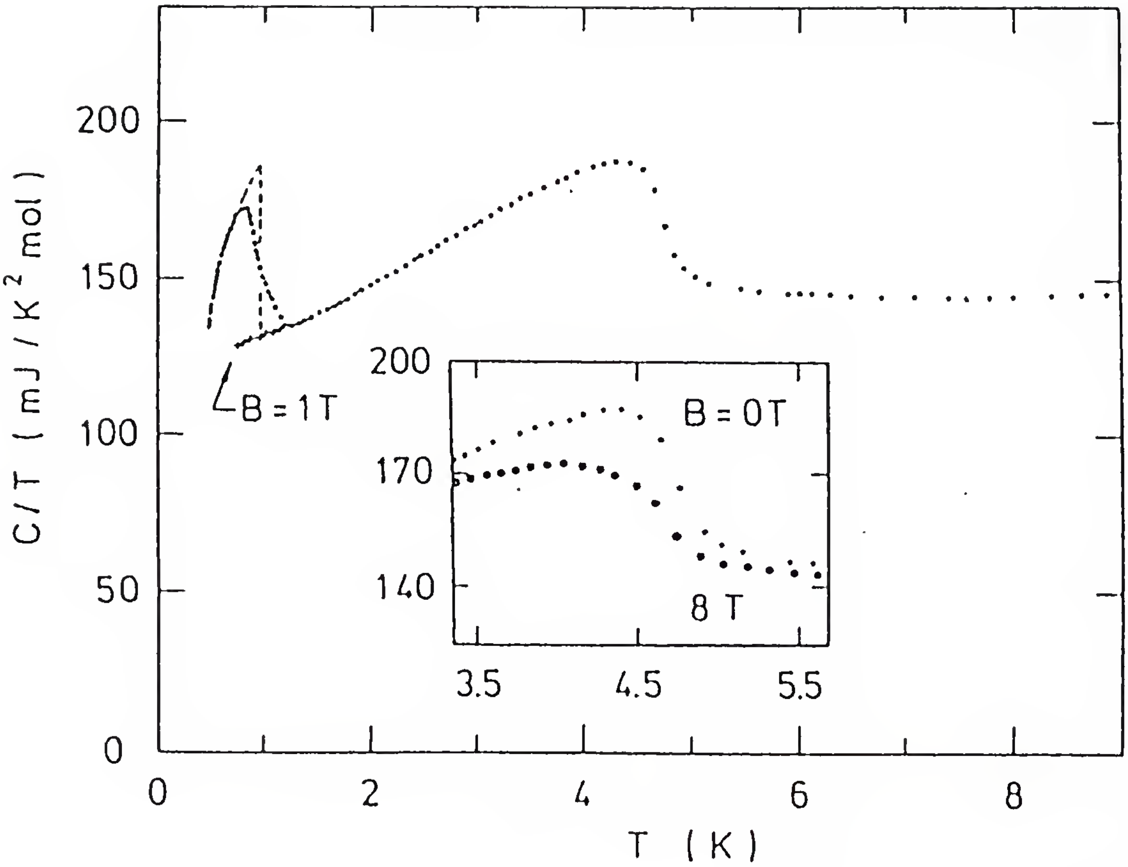

Figure 3-12. Specific heat for UNi_2Al_3 in a plot C/T vs. T between 0.5 K and 9 K. H (or B) = 1 T data shown represent the normal state. Dashed lines are used to replace, under conservation of total entropy, the broadened anomaly at T_C by an idealized jump. Inset shows a slight shift of the AFM transition in a magnetic field of 8 T. This figure is from Geibel *et al.* [1991c].

measurements of T_C with magnetic fields, the initial slope of the upper critical mag data between T_C and 7 K shows a linear behavior, shown in the inset of Figure 3-11, usually preceding the asymptotic low T behavior, $\rho \sim T^2$, of Fermi liquid. From the netic field, $H'_{c2} = -(\partial H_{c2}/\partial T)_{Tc}$, is also reported to be 1.4 T/K. From γ_o, T_C, ρ_o, H'_{c2}, and assuming an isotropic one band model, they estimate [Geibel *et al.*, 1991c] the effective carrier mass $m^* \approx 70\ m_o$, where m_o is the mass of the bare electron.

3.3.2 Non-Fermi Liquid Behavior in $U_{1-x}M_xNi_2Al_3$ {M = Th, Pr, and Y}

Since our group has found a possible separation of single ion effects from correlation effects in doping experiments [Kim J.S. *et al.*, 1991; Jee *et al.*, 1990], we doped the parent system UNi_2Al_3 on the U-site with Ce, La, Y, Th, and Pr in order to vary the observed behavior. While we were doing our experiments, we found unusual temperature dependence of the physical properties in, e.g., C/T, χ, and ρ inconsistent with the FL behavior. Thus, we performed systematic studies to understand the origin of the NFL behavior.

Samples were prepared via arc melting together the starting elements, followed by (with exception of the sample #1 in UNi_2Al_3 discussed below) annealing for one week at 900 °C. All samples maintained the $PrNi_2Al_3$ crystalline structure with the lattice parameters shown in Table 3-2. We also compare the physical properties of U and the doped elements in Table 3-3 to help the understanding of the doping effects in these systems.

The dc magnetic susceptibility χ_{dc} was measured for all samples. The value obtained at 1.8 K for our UNi_2Al_3 sample #1 was about 8 % less than that found in the discovery work by Geibel *et al.* [1991c]. In addition, they saw a small (about 6 %) peak at 4.8 K in χ_{dc} (see the inset in Figure 3-10), whereas our data for sample #1 are, within 2 %, featureless in this region as shown in Figure 3-13. As will be discussed below more thoroughly, the sample dependence of the magnetic transition at T_N is an important point. Thus, weprepared three additional samples of UNi_2Al_3, whose χ_{dc} ($1.8\text{ K} \leq T \leq 300\text{ K}$) and C/T ($1\text{ K} \leq T \leq 10\text{ K}$) were measured (see Figures 3-13 and 3-14). We see a significant orientational dependence (~ 20 – 30 %) for χ_{dc} in these samples as shown in Figure 3-13. The only difference between the sample #1 and the samples #2, 3, and 4 is that sample #1

Table 3-2. Parameters for $U_{0.9}M_{0.1}Ni_2Al_3$.

M =	a (Å)	c (Å)	χ (1.8 K) [memu/formula unit]
U (parent)	5.184	4.023	4.55, 3.30, 3.95, 3.50 [a]
La	5.200	4.023	4.20
Y	5.184	4.024	5.35
Ce	5.188	4.030	4.20
Th	5.182	4.032	5.15
Pr	5.184	4.027	8.35

a) The values correspond to the sample #1 through #4 from the left.

Table 3-3. Comparison of U and the doped elements.

atomic size	electronic configuration	effective magnetic moments
U ~ Y	tetravalent (4+) : Th	U > Pr, U > Ce
U < La, Pr, Th, Ce	trivalent (3+) : La, Y, Pr, Ce	Y, La, Th = 0

was annealed at 1000 °C for six days, while the subsequent samples were annealed in a different furnace at 900 °C for seven days. Unless the furnace used for sample #1 was defective, the absence of the AFM transition shown in the *C/T* and χ_{dc}, seems unusual. Recently, there was a report [Schank *et al.*, 1994] of the influence of off-stoichiometry on UNi_2Al_3. They did see the absence of AFM transition and superconductivity down to 40 mK in $UNi_{2.05}Al_{2.95}$, while they found about a 10 % suppression of T_N, and $T_C^{onset} = 0.66$ K with a much broader transition width in $UNi_{1.95}Al_{3.05}$. From these results we see that the off-stoichiometry of the Ni (the excess) and Al (the deficiency) is very crucial to the magnetic order and the superconductivity in UNi_2Al_3.

We show *C/T* vs. T^2 for $U_{0.9}Ce_{0.1}Ni_2Al_3$ in Figure 3-14 and for $U_{0.9}M_{0.1}Ni_2Al_3$ (M = Y, Th, La, and Pr) in Figure 3-15. The 10 % doping destroys the AFM order completely and the *C/T* at low temperatures seems to diverge (except for Ce doping). For the small peak around 2.5 K in the 10 % Ce-doped sample, shown in *C/T* vs. T^2, we do not see a corresponding anomaly in χ_{dc} down to 1.8 K. We checked the temperature dependence of the 5f electronic contribution of specific heat over temperature C_{5f}/T of 10 % Y, Th, La and Pr doped systems. As shown in Figure 3-16, a ln *T* dependence for more than one decade of temperatures is observed in the 10 % Th- and Pr-doped systems. Even though we did not see a broad ln *T* dependence of C_{5f}/T for the 10 % Y-doped systems for $T >$ 2.5 K, we saw a ln *T* dependence down to about 0.3 K leaving about a decade of NFL temperature behavior, shown in Figure 3-16 (all NFL systems mentioned in section 3-1 show the logarithmic temperature dependence of *C/T* due to magnetic ions). The 10 % La-doped sample shows a ln *T* behavior with different slopes for narrow temperatures. If we estimate Kondo temperature using the formula (3.3), we have 77 K, 69 K, and 53 K for Pr, Th, and Y 10 % doped systems, respectively.

The question arises: how does this unusual behavior change upon further doping? For instance, the shrinking of the T range, where ln T dependence of C/T is observed, is seen upon further U-doping in $U_{0.2}Y_{0.8}Pd_3$ [Seaman *et al.*, 1991]. In $UCu_{3.5}Pd_{1.5}$ [Andraka and Stewart, 1993], varying the Pd to UCu_4Pd totally destroys the ln T dependence; instead giving rise to $C/T \propto T^{-0.32}$ from 1 to 10 K. In our systems, the temperature range over which this ln T behavior is observable, on the other hand, shrinks upon increasing Th (or decreasing U) content, up to 3.2 K for 20 % Th and 2.2 K for 30 % Th as shown in Figure 3-17. In other words, the unusual behavior is too limited in T to give any significant credence. As seen in Figure 3-18, using Th doping as a representative example, the temperature at which the upturn in C/T begins is depressed with more doping and the negative slope at low temperatures is steeper for more Th doping resulting in the deviation from the ln T dependence in C/T.

The low T values of χ_{dc} vary as detailed in Table 3-2. The χ_{dc} results for $1.8 \text{ K} \leq T \leq 9\text{K}$ of x = 0.1 Th and Pr obey $T^{1/2}$ dependence, shown in Figure 3-19, as predicted by TCKE for the nonmagnetic ground state [Cox, 1987a and 1987b]. The theory says that we can express magnetic susceptibility χ_m as $\chi_m \sim -\eta T^{1/2}$ (refer to Eq. 2.28) where η is proportional to the T independent van Vleck susceptibility, χ_{vv}, and inversely proportional to the CEF splitting. The coupling via conduction electrons between the nonmagnetic ground state and excited magnetic states gives rise to the T dependence of χ_m. Because

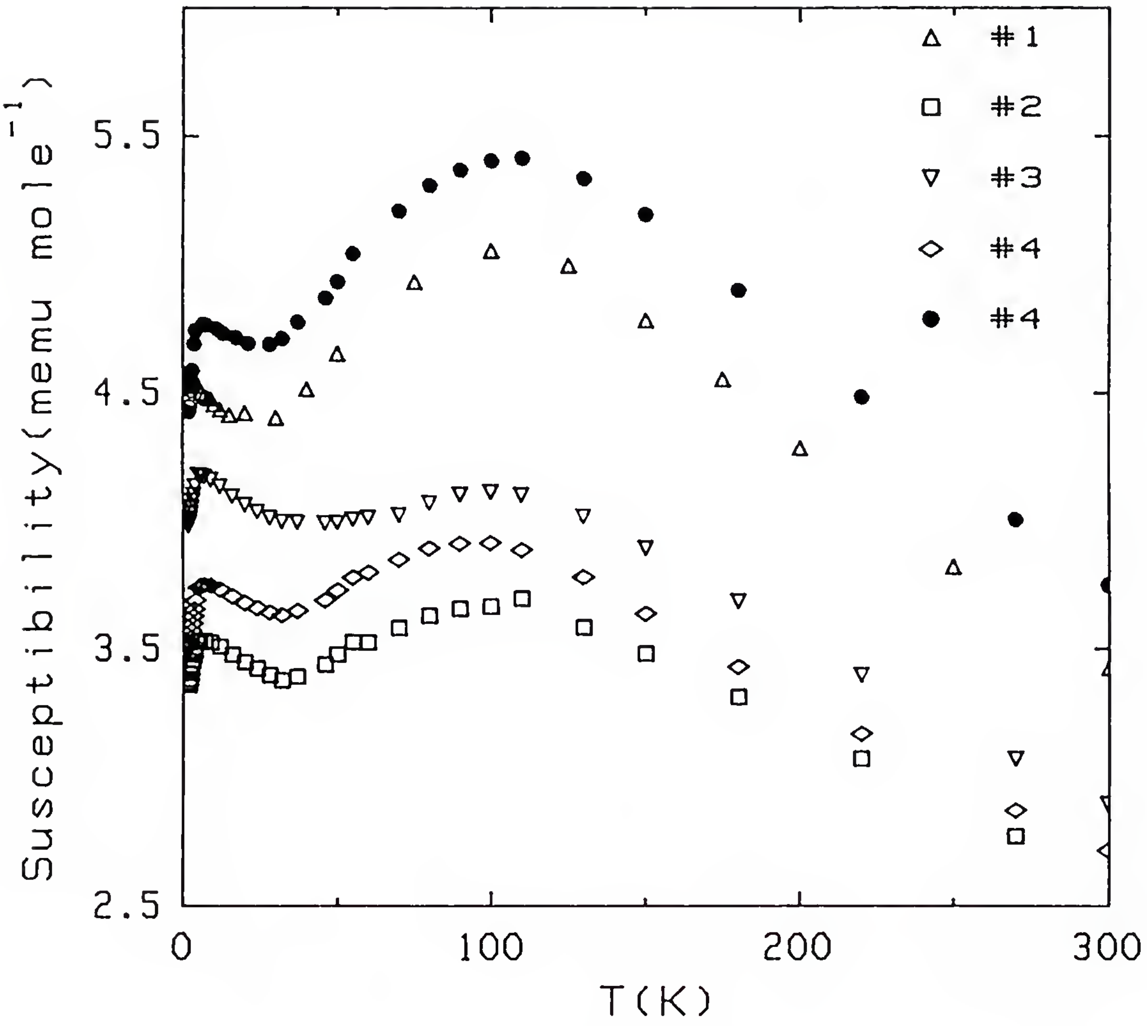

Figure 3-13. Magnetic susceptibility as a function of *T* between 1.8 K and 300 K for four samples of UNi_2Al_3. As discussed in the text, sample #1 shows no peak at low temperatures, while samples #2, #3, and #4 do. The difference in magnitude of susceptibility between the samples is not significant due to the orientational dependence of the samples. It is clearly exhibited in sample #4 which we measured in one direction (open diamonds) and in 90 ° off direction (filled circles).

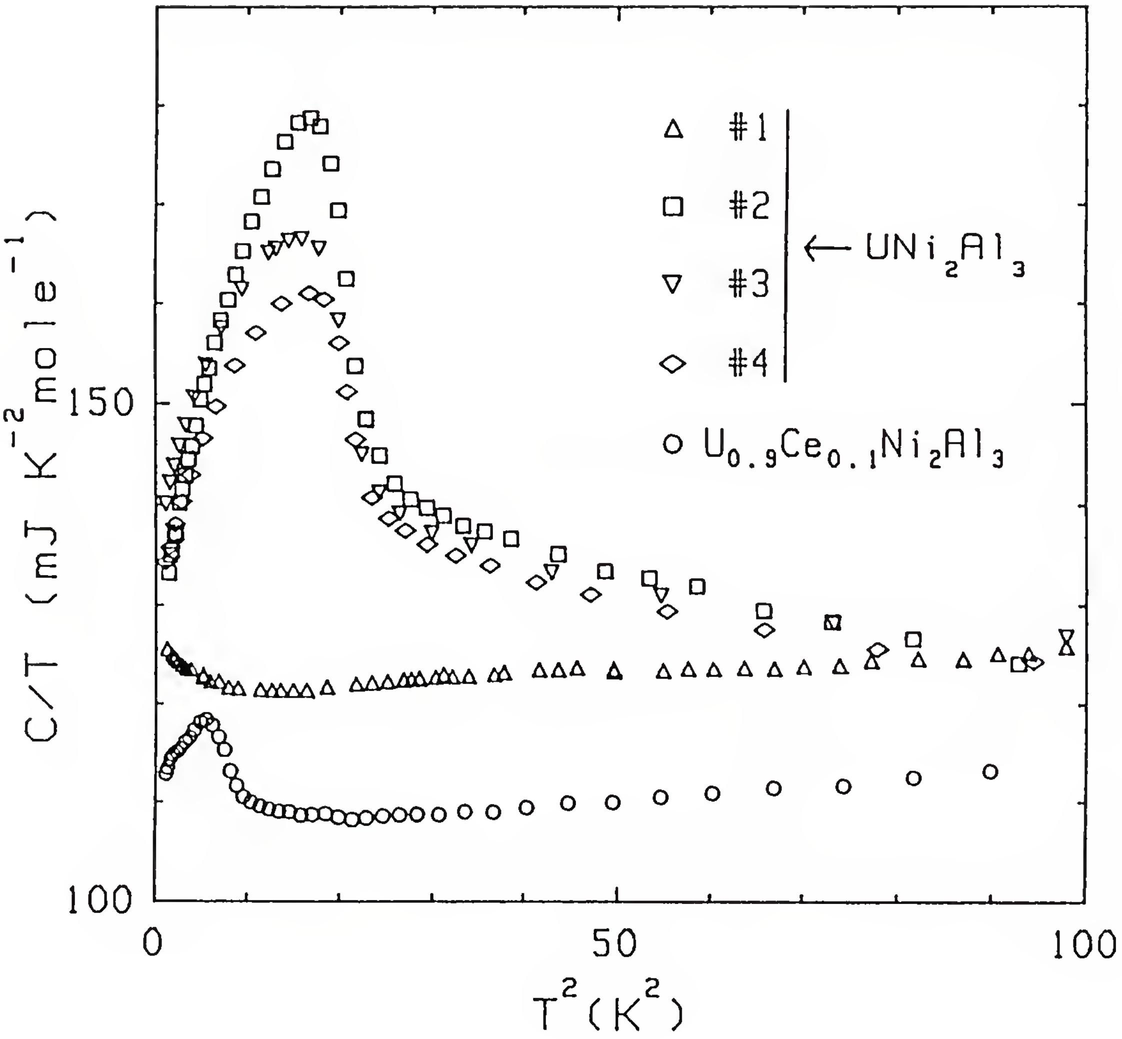

Figure 3-14. *C/T* vs. T^2 for four samples of UNi$_2$Al$_3$ and U$_{0.9}$Ce$_{0.1}$Ni$_2$Al$_3$. Note the small peak at 2.5 K for the Ce-doped sample and the varying magnitude of the peak in the samples of UNi$_2$Al$_3$. No anomaly is shown at low temperatures for sample #1 of UNi$_2$Al$_3$.

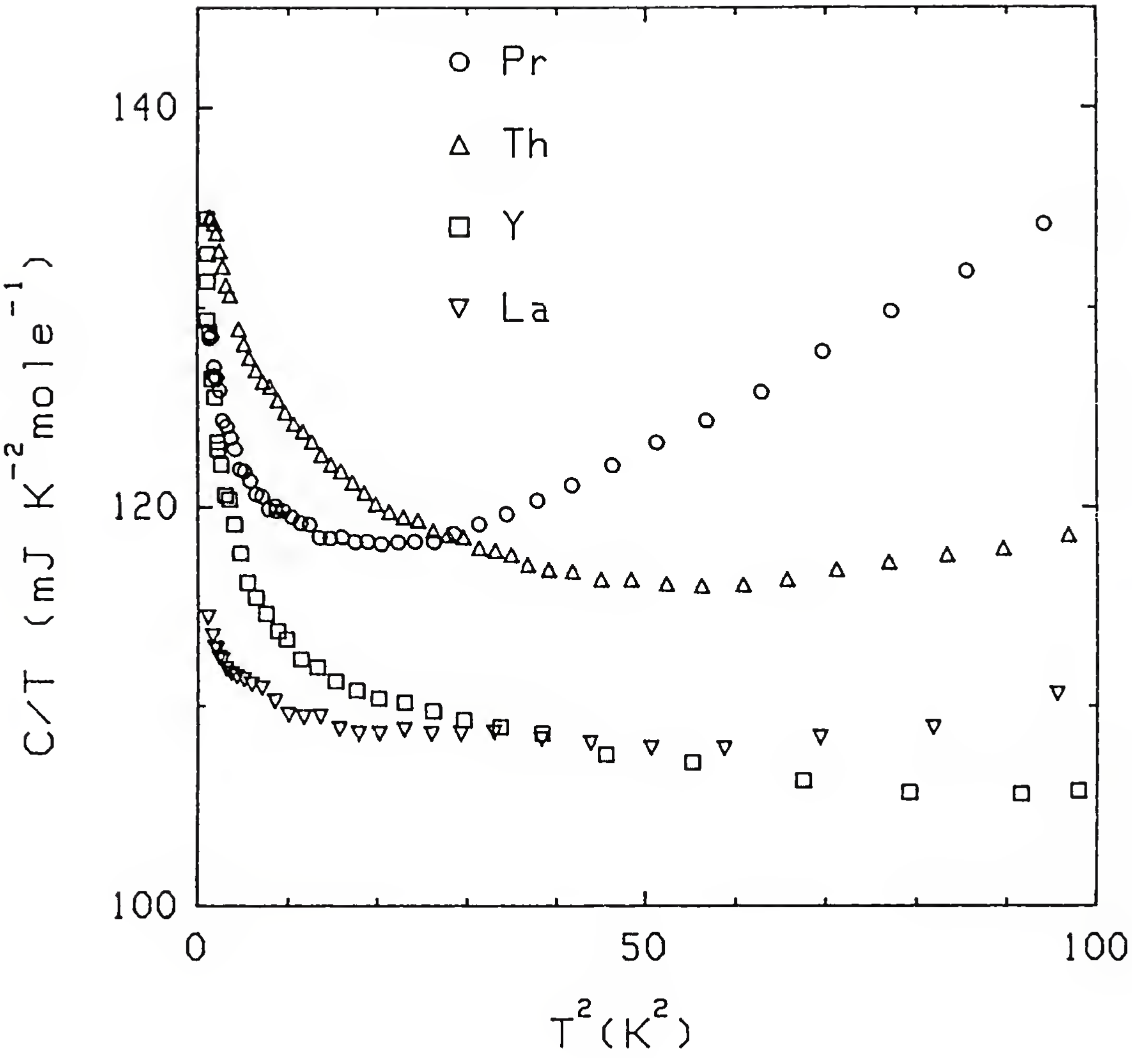

Figure 3-15. *C/T* vs. T^2 in $U_{0.9}M_{0.1}Ni_2Al_3$ for M = Pr, Th, Y, and La. The absolute error of the specific heat data is ± 3 %, based on measurements of a standard. Note the upturn at low temperatures for Pr, Th, Y, and—to a lesser extent for La.

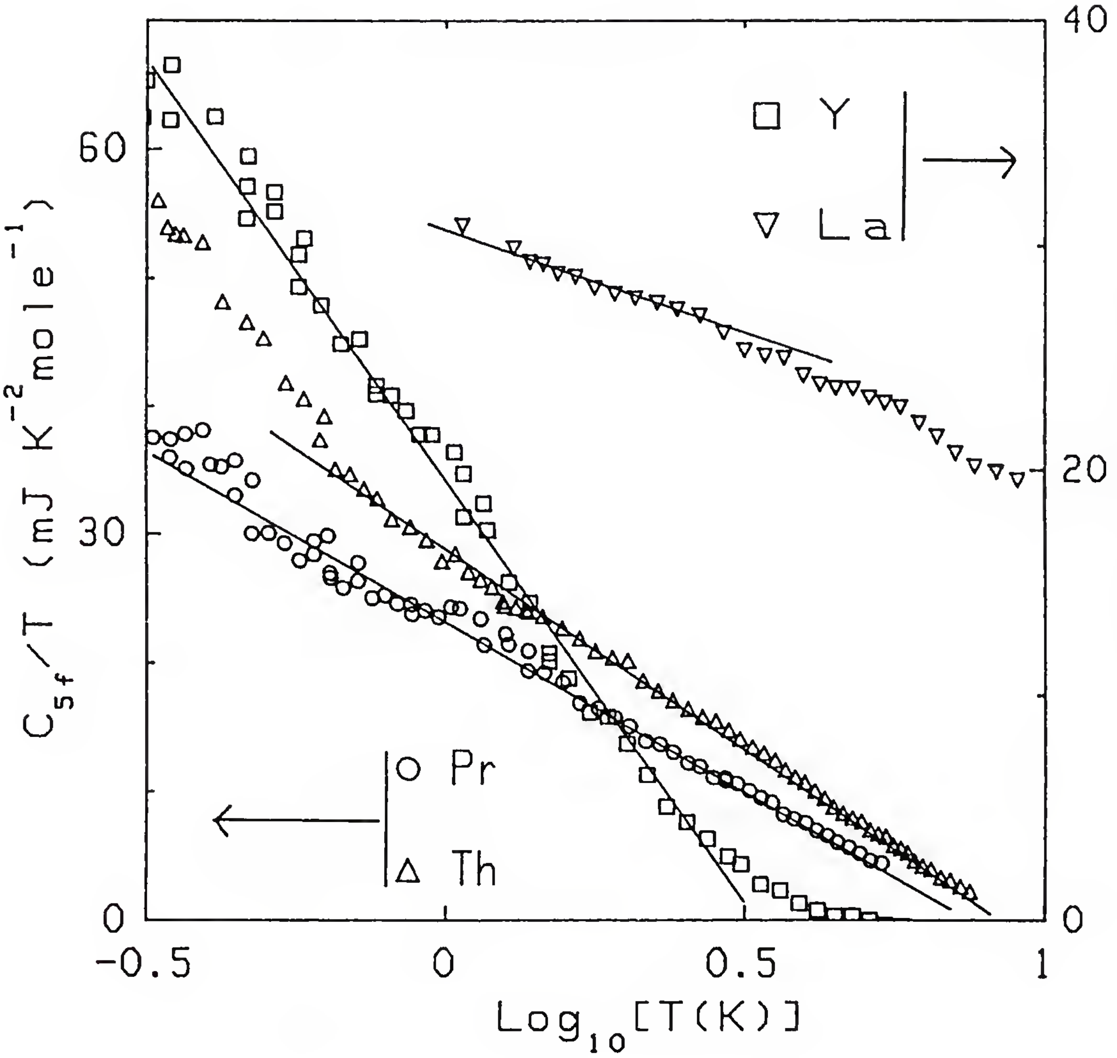

Figure 3-16. The 5f electronic contribution of specific heat over temperature, C_{5f}/T, measured for $U_{0.9}Pr_{0.1}Ni_2Al_3$, $U_{0.9}Th_{0.1}Ni_2Al_3$, $U_{0.9}Y_{0.1}Ni_2Al_3$, and $U_{0.9}La_{0.1}Ni_2Al_3$ is plotted in a logarithmic temperature scale. Subtraction of the background consisting simply of a two term ($C/T = \gamma + \beta T^2$) fit to the data above the upturn. The logarithmic behavior displayed in this figure is not sensitive to the background fit used. The data of La-doped sample are shifted by +20 mJ K^{-2}mole^{-1} for the clear figure. The lines are a guide to the eye.

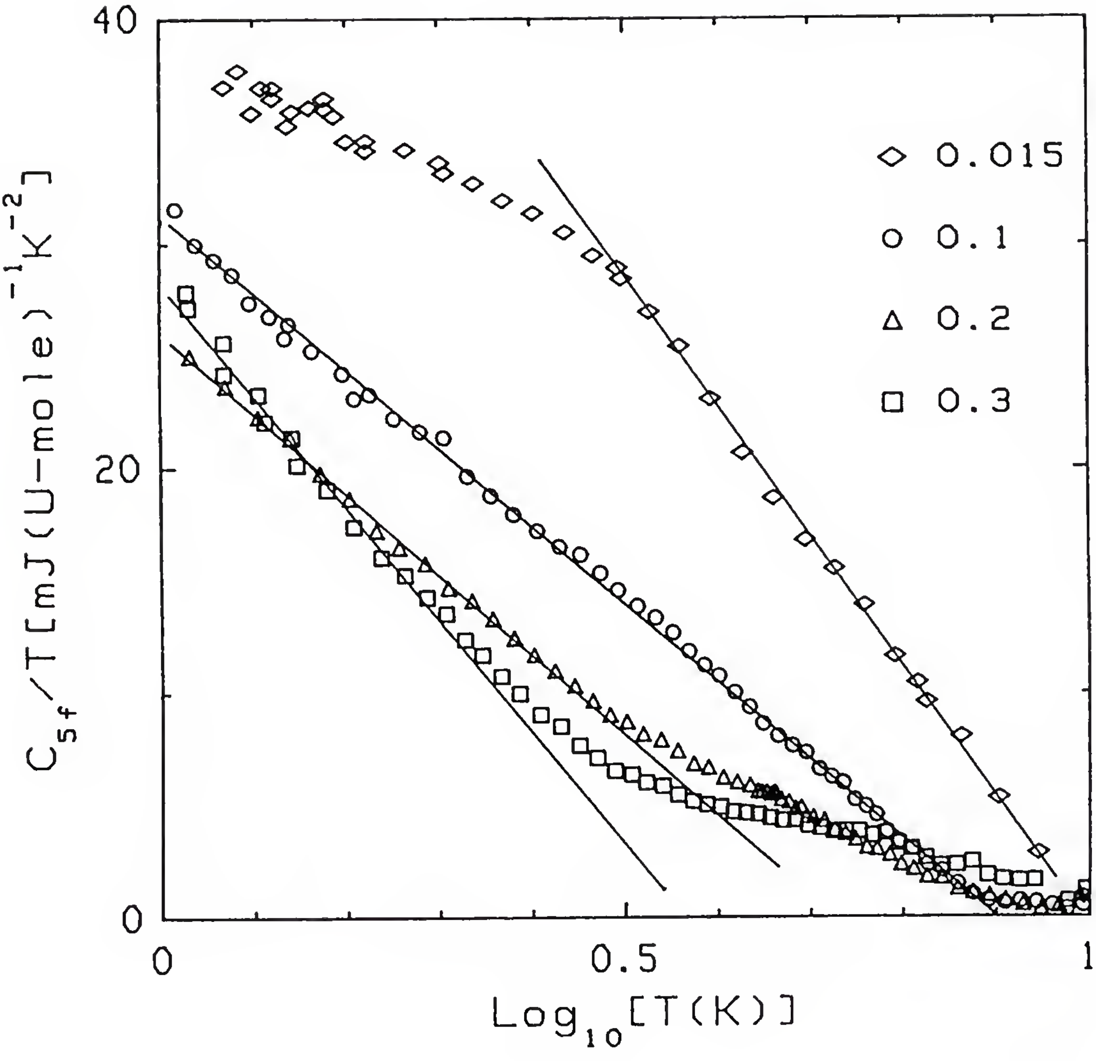

Figure 3-17. C_{5f}/T vs. ln T for $U_{1-x}Th_xNi_2Al_3$, x = 0.015, 0.1, 0.2, and 0.3, normalized per U-mole. The data for x = 0.03 (not shown) agree with those for x = 0.015 within our error bar of ±3 %. As we dope more Th from the low concentration, e.g., x = 0.015, a ln T dependence of C_{5f}/T is recovered around x = 0.1 in wider temperature range. The system deviates from the ln T dependence for more Th dopings.

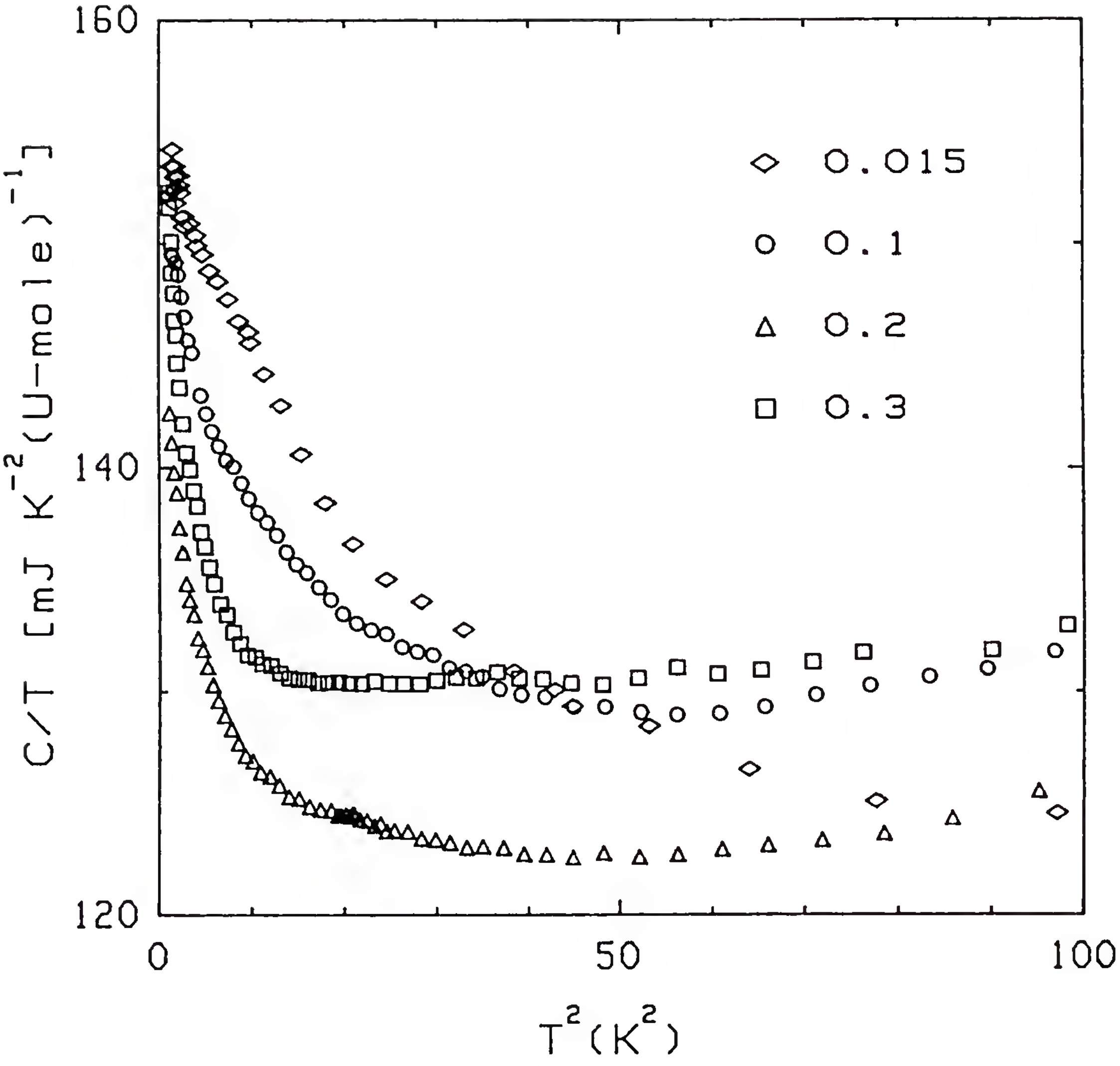

Figure 3-18. *C/T* vs. T^2 for $U_{1-x}Th_xNi_2Al_3$, x = 0.015, 0.1, 0.2, and 0.3, normalized per U-mole. The data for x = 0.03 (not shown) agree with those for x = 0.015 within our error bar of ±3 %.

we have seen the sample dependence in the parent system, we prepared a second sample of $U_{0.9}Th_{0.1}Ni_2Al_3$. The data also show $\chi_{dc} \sim T^{1/2}$ dependence. On the other hand, we found that χ_{dc} of the 10 % Y-doped system exhibits a more singular behavior in the $T^{1/2}$ scale than the Th- and Pr-doped systems as shown in Figure 3-19. Thus, the 10 % Y-doped system follows the logarithmic temperature dependence rather than the $T^{1/2}$ dependence as shown in Figure 3-20. Since the quadrupolar susceptibility, where aspherical charge distribution of the 5f ions play the role of a *pseudospin*, is usually too small to see a response, χ_{dc} for Y-10 % doped sample may be described by the effect of magnetic ground state as also suggested [Amitsuka and Sakakibara, 1994] in the U-dilute $U_XTh_{1-X}Ru_2Si_2$. However, as we will discuss thoroughly in the specific-heat measurements by a small amount of doping, it seems to be unlikely that we could ignore the intersite correlations in the U-concentrated (90 %) systems.

As we showed in Table 3-2, there are differences for Th, Pr, and Y. Non-magnetic Th and Y doped systems exhibit a smaller χ_{dc} values at low temperatures than the magnetic Pr doped one. Also, the different T dependence in χ_{dc} seems to be more related to the atomic size of doped elements, i.e., Th and Pr are larger than Y (which is almost same in size with U) as shown in Tables 3-2 and 3-3 rather than the electronic configuration and the magnetic moment of each element.

Furthermore, we measured the electrical resistivities of 10 % Th, Pr, and Y doped systems, and they all show a linear T dependence ($\rho = \rho_o + \delta T$) with a positive δ for 1.0 K $\leq T \leq$ 20 K in Th and Y doped ones, while the Pr doped one exhibits the linear behavior

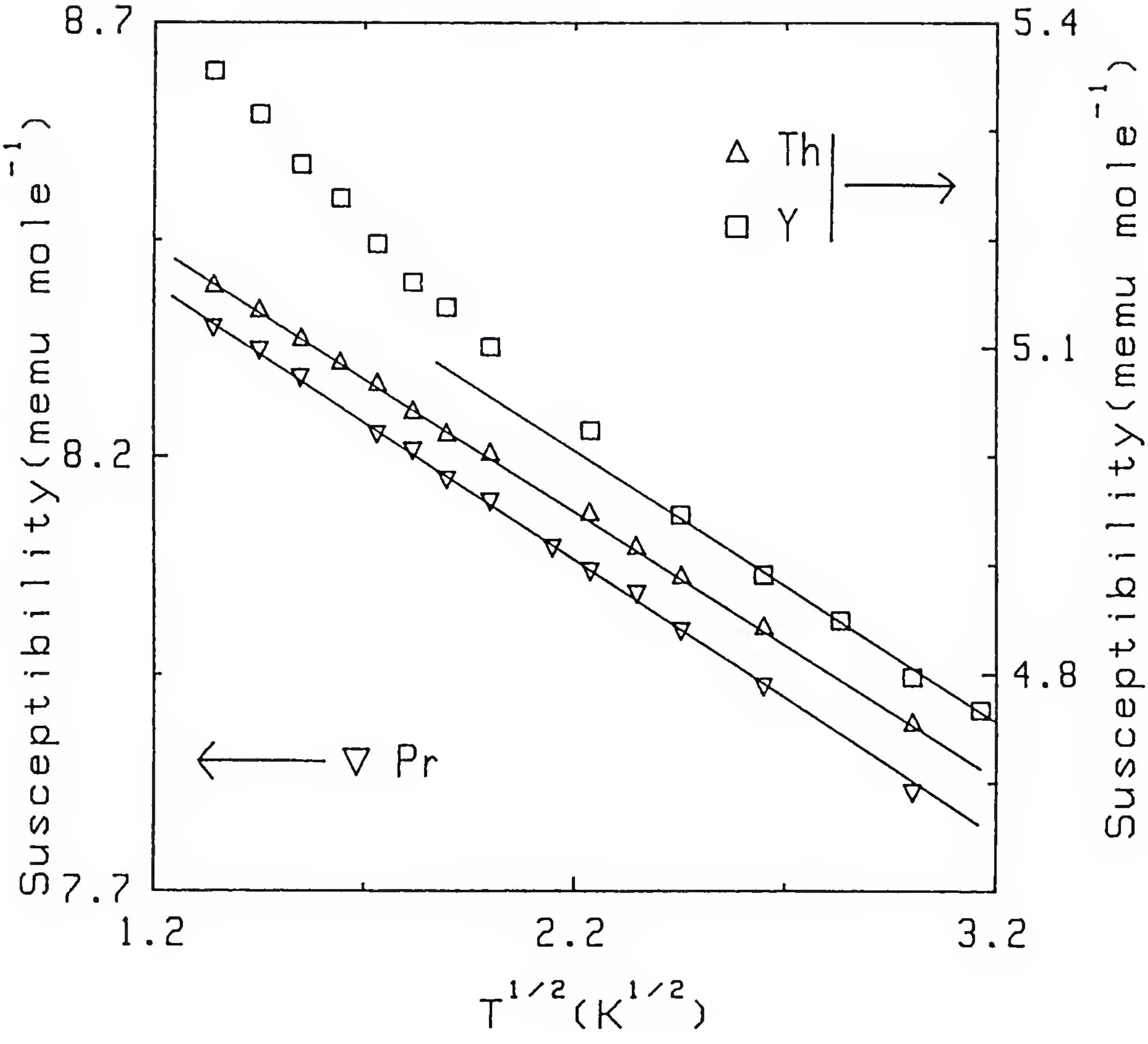

Figure 3-19. The low temperature magnetic susceptibility of $U_{0.9}Th_{0.1}Ni_2Al_3$, $U_{0.9}Pr_{0.1}Ni_2Al_3$, and $U_{0.9}Y_{0.1}Ni_2Al_3$ plotted vs. $T^{1/2}$. Data for a second sample of $U_{0.9}Th_{0.1}Ni_2Al_3$ (not shown) display similar behavior. Above 9 K, the data of the Th- and Pr-doped samples begin to deviate from the $T^{1/2}$ dependence. The 10 % Y-doped sample is more singular than the other two systems. No background subtraction from the data is made. The lines are for a guide to the eye.

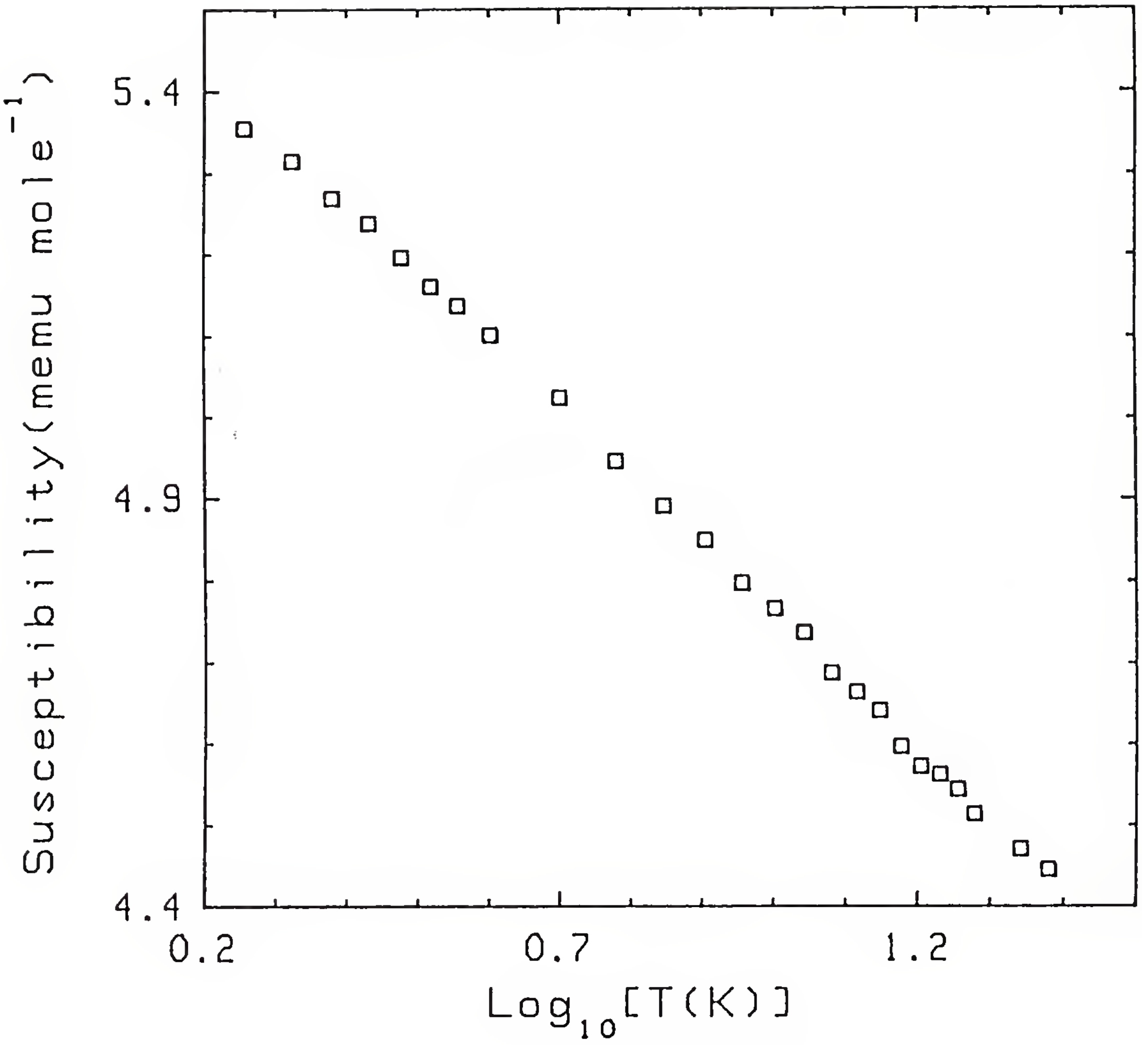

Figure 3-20. The low temperature magnetic susceptibility of $U_{0.9}Y_{0.1}Ni_2Al_3$ plotted in logarithmic *T* dependence for more than one decade in temperature (1.8 K ≤ *T* ≤ 25 K). No background subtraction from the data is made.

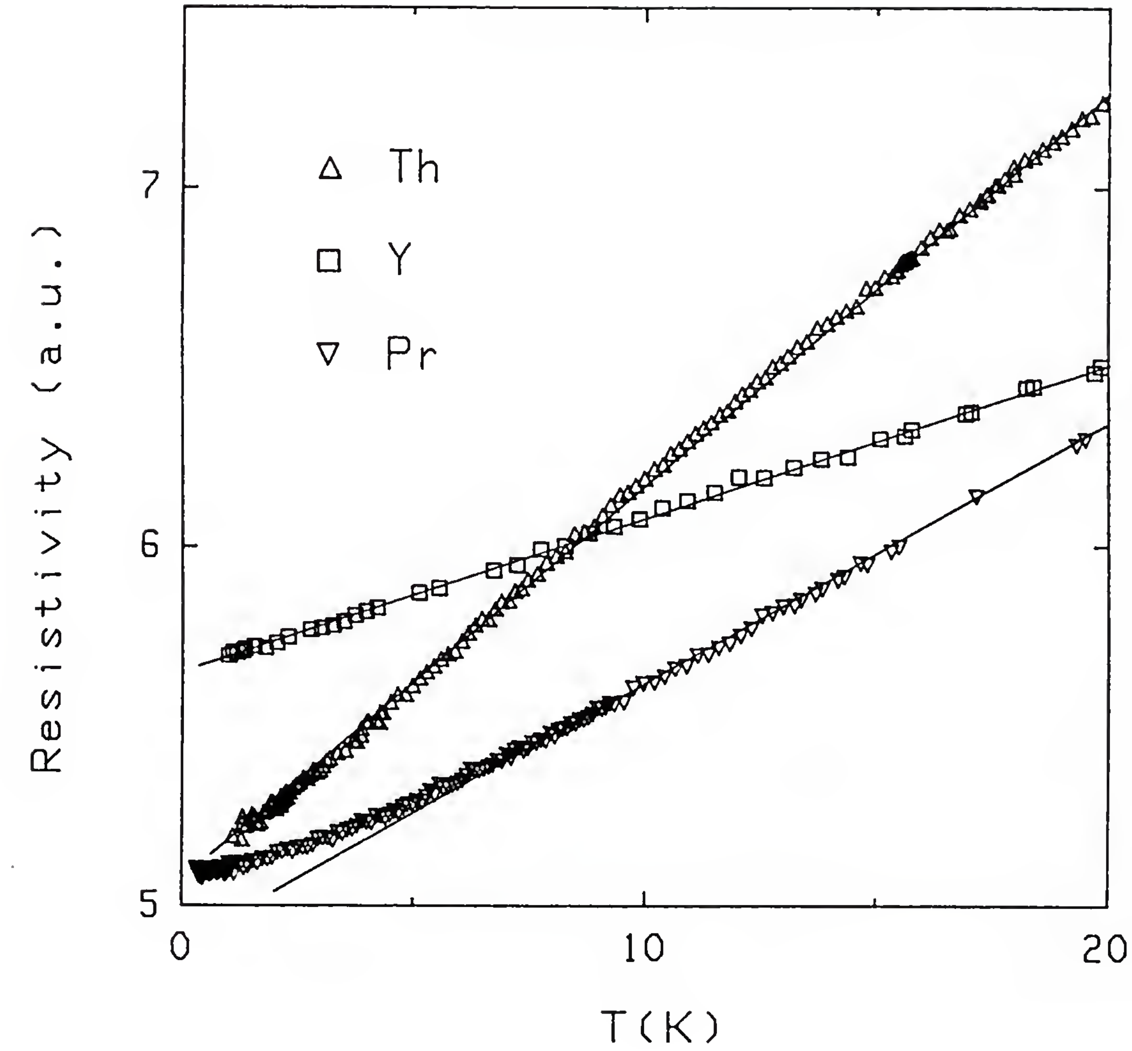

Figure 3-21. Resistivity in arbitrary unit as a function of temperature in $U_{0.9}Th_{0.1}Ni_2Al_3$ (triangles), $U_{0.9}Y_{0.1}Ni_2Al_3$ (squares), and $U_{0.9}Y_{0.1}Ni_2Al_3$ (deltas). The lines are a guide to the eye.

for about 8.0 K $\leq T \leq$ 20 K saturating at lower temperatures as shown in Figure 3-21. The decrease of resistivity at lower temperatures contradicts the TCKE, where the opposite behavior is expected because of Kondo scattering. Thus, the observed positive δ seems to be related to the onset of coherence and the correlated scattering rather than a single-ion scattering. This kind of behavior having positive δ is observed in $CeCu_{5.9}Au_{0.1}$ [Löhneysen *et al.*, 1994] out of the several NFL systems, and also observed in high-T_C superconducting oxides over a wide temperature range leading to the proposal of a marginal Fermi liquid [Varma *et al.*, 1989]. The resistivity ρ for the above three systems of 10 % doped with Th, Pr, and Y varies linearly in T with a smaller positive δ value for 0.3 K $\leq T \leq$ 1.0 K approaching residual resistivity (the data of ρ for 0.3 K $\leq T \leq$ 1.0 K were indistinguishable in the T and T^2 scales due to the scatterings of data).

To understand the origin of the NFL behavior in our systems, we doped small amount of Th in $U_{1-X}Th_XNi_2Al_3$ (x = 0.0025, 0.005, and 0.015) as shown in Figure 3-22. The magnetic transition temperature, as may be measured by the position of the maximum in the specific heat anomaly, decreases with increasing doping at the rate of about 2 K/%Th, while the size of the anomaly, ΔC, decreases by 40 % for x = 0.005. Magnetic susceptibility, χ_{dc}, for these series of samples shows a maximum at about 4.2 K (3.7 K) for x = 0.0025(0.005) as shown in Figure 3-23, while there is a peak at about 5 K for the undoped UNi_2Al_3. If the decreasing rate of T_N is linear for Th doping, estimated about 2 K/%, we should see the disappearance of T_N at around 3 % Th-doped system along with a ln T dependence of C_{5f}/T. However the data for 3 % Th-doped sample, which agree with those for x = 0.015 sample within our error bar of ±3 % for $T > 3$ K, deviates from the

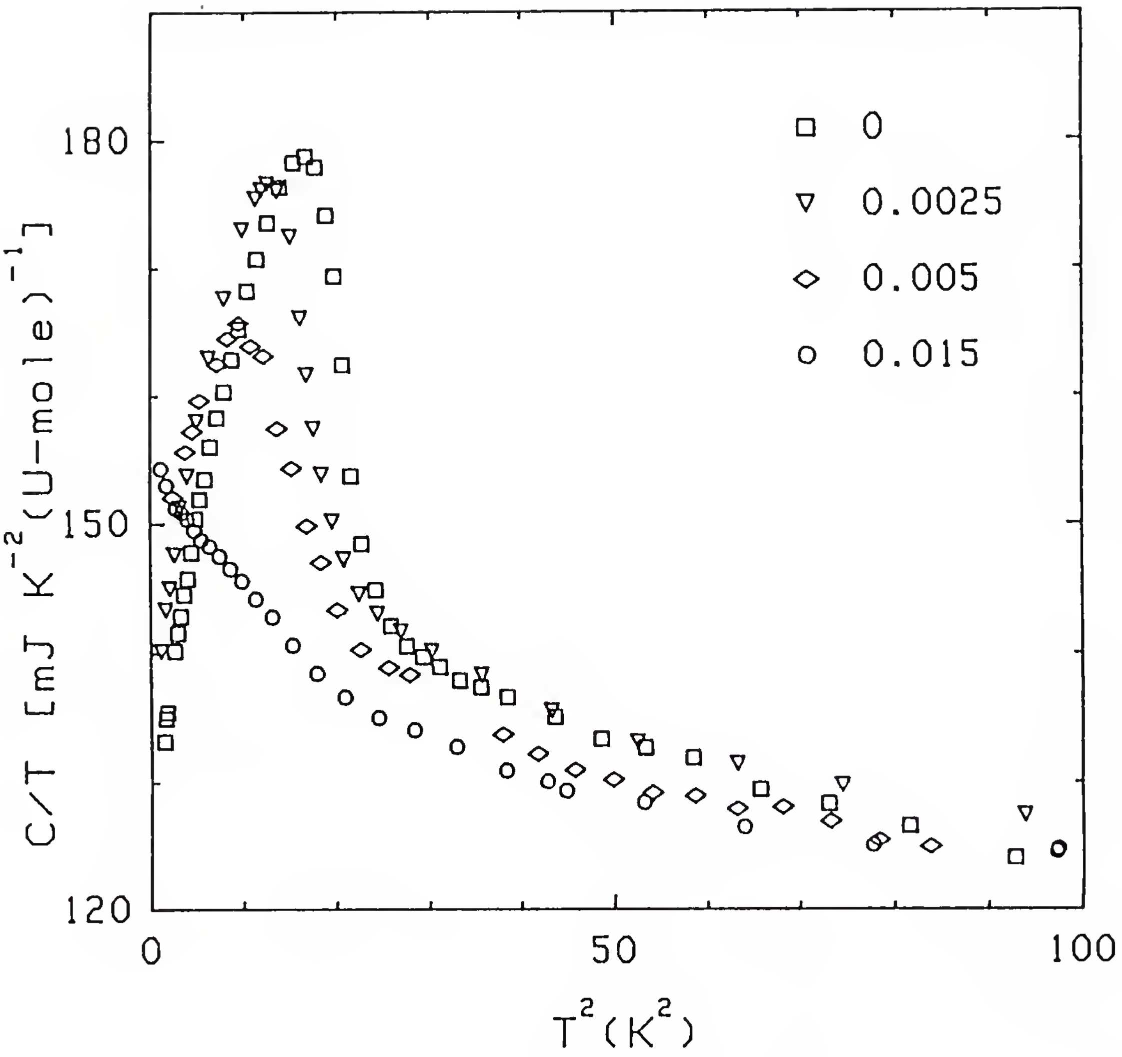

Figure 3-22. C/T vs. T^2 for $U_{1\text{-}x}Th_xNi_2Al_3$, x = 0.0 (sample #2), 0.0025, 0.005, and 0.015, normalized per U-mole. The suppression of magnetism is clearly seen to be achieved with extremely small doping levels. Note the divergence in C/T as $T \rightarrow 0$ is already present in the undoped compound (see text for more descriptions). If the suppression of the magnetic transition were linear with doping, one would expect $T_{peak} \approx 1$ K for x = 0.015. Instead, data down to 0.3 K in specific heat show no anomaly other than the change in slope seen at about 3 K, which may be a sign of sample inhomogeneity and not a bulk transition.

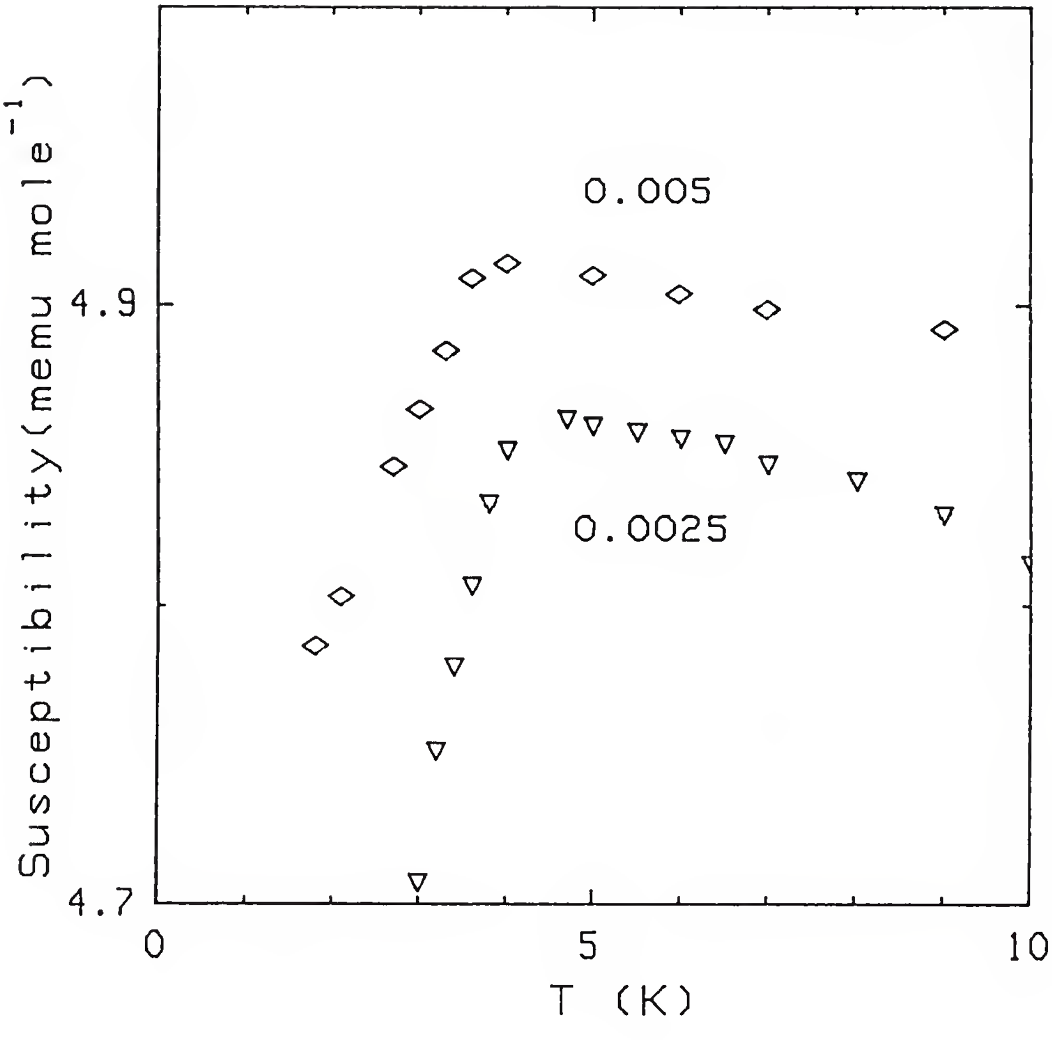

Figure 3-23. Temperature dependence of the magnetic dc-susceptibility, χ_{dc}, as measured for $U_{0.9975}Th_{0.0025}Ni_2Al_3$ (deltas) and $U_{0.995}Th_{0.005}Ni_2Al_3$ (diamonds) in a magnetic field of 0.01 T using a SQUID magnetometer.

ln T dependence below about 3 K resulting in a more saturation than the x = 0.015 data which are shown in Figure 3-17.

We also performed specific heat C measurements on $U_{0.9}Th_{0.1}Ni_2Al_3$ in magnetic field. We found about a 2 % decrease of C at $H = 14$ T at 1 K and almost no change for 4 K $\leq T \leq$ 10 K as shown in Figure 3-24. This small magnetic field dependence of C in the doped system is not surprising if we remember there is almost no magnetic field dependence of the AFM anomaly in the parent system, shown in Figure 3-12. If this system follows the TCKE, where we estimated $T_K \sim 70$ K using Eq. (3.3), there should be an increase of C/T of order of one at 14 T and 1 K as can be seen in Figure 2-3c ($T/T_K \sim 0.014$ and $H/T_K \sim 0.2$, where we assumed there is no change of T_K in magnetic field) which was not observed. However, we can not explain our system in terms of the scaling theory suggested by Tsvelick and Reizer [1993], either. For instance, we do not see a power law dependence of χ_{dc} as a function temperature which is necessary to obey the scaling properties.

It is also interesting to note that the upturn in C/T observed at low temperatures in $U_{1-X}M_XNi_2Al_3$ with several doping elements, is already present above T_N in the parent compound, as seen in Figures 3-14 and 3-22. The broad upturn above T_N is apparently not due simply to a broadened AFM transition with entropy spread out to higher temperatures due to sample inhomogeneity. Instead, we see in Figure 3-22 that the magnetic transition stays relatively unbroadened as it is suppressed to lower temperatures, while the C/T upturn above the anomaly is, within 5 %, the same for the given four

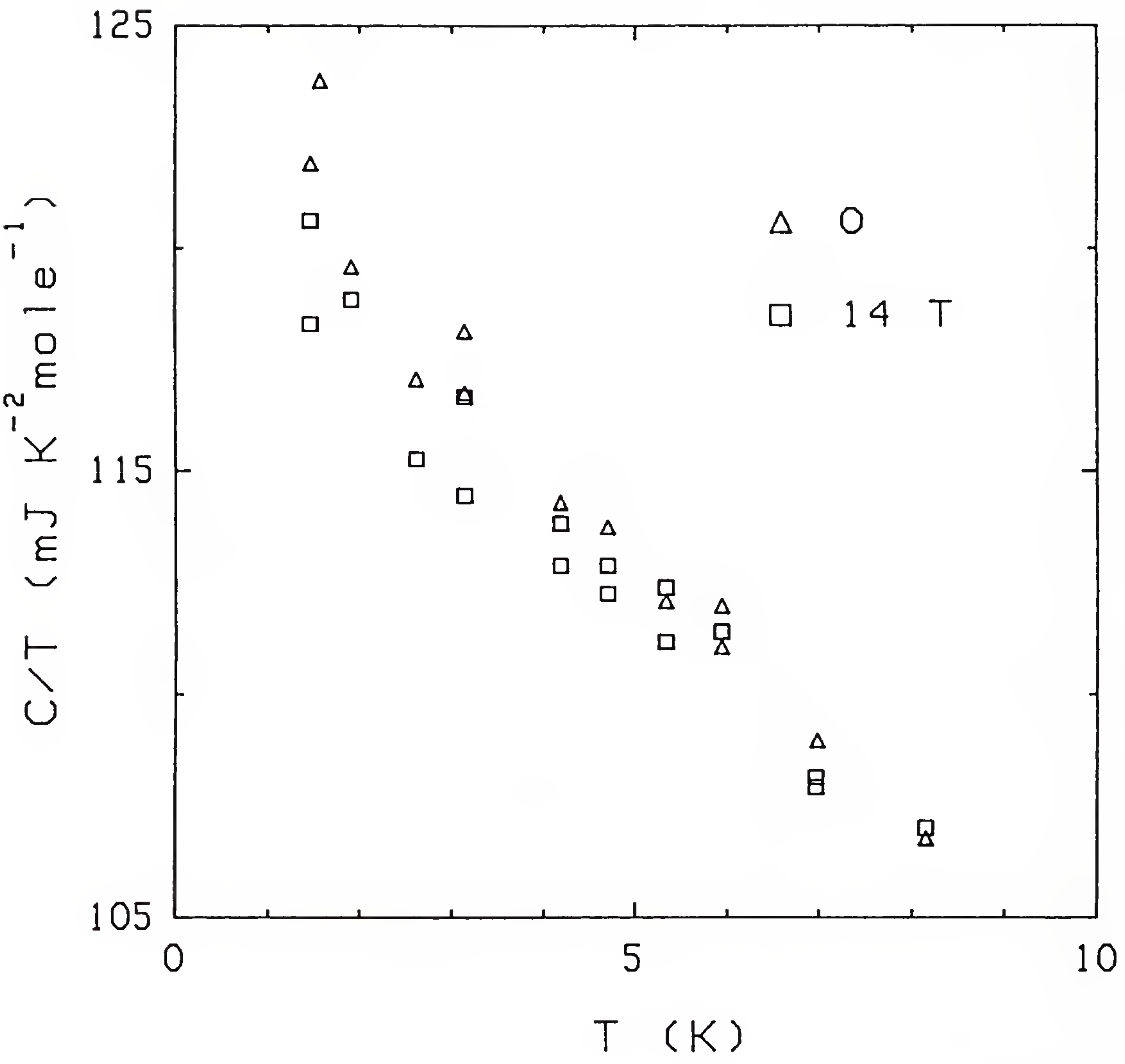

Figure 3-24. Specific heat divided by temperature vs. temperature for $U_{0.9}Th_{0.1}Ni_2Al_3$ in two different magnetic fields. The data in zero magnetic field (open triangles) at 1.5 K was reduced about 2 % when it was measured in *H* = 14 T (open squares).

concentrations. Thus, this fact indicates that the disorder interpretation [Dobrosavljevic *et al.*, 1992] seems not to be correct, because for weak disorder—as one would expect for the parent compound—the theory predicts unusual temperature dependence only at ultralow temperatures.

Thus, we see that dilution of the U causes a suppression of T_N to lower temperatures and results in a disappearance of T_N for more doping. Our 90 % U-concentration, where we found the NFL behavior of C/T, ρ, and χ at low T, seems to be still close to the magnetic instability region. Therefore, it seems to us that there may be a relatively broad crossover region between (weakly) magnetic and non-ordering in which we are finding the NFL behavior in C, χ, and ρ in the $U_{1-x}M_xNi_2Al_3$ (M = Th, Pr, and Y) systems.

In summary, we found the new system $U_{0.9}M_{0.1}Ni_2Al_3$ (M = Th, Pr, and Y) which exhibits the NFL behavior in thermodynamic, transport, and magnetic properties. Firstly, the resistivity being linear in temperature at least for $1.0 \text{ K} \leq T \leq 20 \text{ K}$ (the Pr-doped one exhibited the same behavior in a less wide range) contradicts the Fermi-liquid theory. Also, the monotonic increase of resistivity with temperature for $0.3 \text{ K} < T \leq 20 \text{ K}$ can not be explained by the single-ion TCKE, but seems to be related to the onset of coherence and the correlated scattering. Secondly, the $T^{1/2}$ (Th and Pr doped) and $\ln T$ (Y doped) dependence in χ_m were observed as a sign of the NFL behavior. The difference between the Th and Pr doped systems and the Y doped sample seems to be mainly the atomic size of the dopants. Also, it seems to be unlikely that the TCKE is an origin of the NFL behavior in such a U-concentrated (90 %) system, even though the data can be fitted to the theory in the specific heat and magnetic susceptibility measurements. Lastly, the ln T dependence of C_{5f}/T is observed in the above systems as a sign of the NFL behavior. The broad upturn above T_N in the parent system and the change of T_N without the broadening of the AFM transition , e.g., in $U_{1-X}Th_XNi_2Al_3$ for $x \leq 0.005$, may rule out the possibility of the disorder interpretation as an origin of the NFL behavior.

The NFL behavior observed in $U_{0.9}M_{0.1}Ni_2Al_3$ (M = Th, Pr, and Y) did not follow the scaling properties, which were suggested as an evidence of a long range phase transition at $T = 0$ K. However, the fact that the NFL behavior follows the destruction of magnetic order observed in the specific-heat measurements of Th-doped samples seems to tell us that the NFL behavior may be due to the proximity to magnetic instability. In other words, the doping makes the magnetic parent system approach a critical point, where a Kondo-compensated nonmagnetic state and the long range magnetic order are nearly degenerate.

CHAPTER 4
HYDROGEN DOPING EFFECTS ON UPd_2Al_3

In this chapter we introduce the general and simple overview of hydrides including electrical and magnetic properties. The motivation for hydrogen doping experiments on UPd_2Al_3 will be given below. Then we will summarize the physical properties of UPd_2Al_3 briefly to understand its hydrides and to get more insight into the parent system UPd_2Al_3 from the experimental results of its hydrides. Emphasis is placed on the preparation of hydrided UPd_2Al_3 and the effect of hydrogen on UPd_2Al_3 with its interpretations.

4.1 Review of Hydrides

A special attention has been given to the hydrides of intermetallic compounds with rare earth elements (R) in comparison to other hydrided systems [Alefeld and Völkl, 1978; Ward, 1985a; Schlapbach, 1988, 1992; Wiesinger and Hilscher, 1991], where we define the term "hydride" as a material which hydrogen is in. Because some of them were found to be good for high performance permanent magnets (RCo_5 and $Nd_2Fe_{14}B$) as well as hydrogen storage ($LaNi_5$), they are considerably important in industrial applications. Also, the studies of hydrides of intermetallic compounds frequently have led to a deeper insight into the fundamental properties of the parent system. A variety of techniques have been applied to elucidate the mechanism of hydrogen uptake in spite of its complexity in intermetallic compounds. They can be roughly divided into two areas. One is surface-sensitive methods such as photoemission spectroscopy, to some extent susceptibility, and

NMR. The other is surface-insensitive experiments like neutron scattering and X-ray diffraction.

There are some general statements, despite the complex hydrogen absorption, about the influence of hydrogen upon physical properties. Although the hydrogen uptake leads to a considerable lattice expansion, the overall crystal structure is usually retained. The hydrogen induced increase in volume implies narrower electronic bands which may reduce the hybridization having perhaps been present in the host or parent compound. When a transition metal (TM) is alloyed to a rare earth metal (RM), the exchange interaction (overlap between 3d electrons of TM and 5d electrons of RM) leads to a significant suppression of the TM magnetic moment. However the strong hydrogen affinity of the RM brings about a decrease of the 3d-5d overlap in the hydride giving rise to the cancellation of this moment depression to a certain degree. So this partial restoration of the 3d moment is interpreted as a hydrogen-induced screening effect [Wiesinger and Hilscher, 1991].

4.1.1 Electronic Properties

It is essential to have a knowledge of the electronic properties for materials (band structure and density of states) to understand hydrides. In the theoretical point of view, the accuracy of density of states (DOS) and Fermi energy calculations has grown very much. However, the electronic charge transfer calculations on hydrogenation are still at their beginning. There are a number of experimental methods to compare theory and experiment in the field of the electronic properties. The Pauli contribution of the magnetic susceptibility and the linear coefficient of specific heat γ are proportional to DOS at the

Fermi level, $N(E_F)$. Spectroscopy techniques such as electron and X-ray photoemission (XPS) are the most powerful methods to study the electronic properties. Charge transfer is indicated by XPS core level and Mössbauer isomer shifts, and the X-ray absorption near-edge structure contains information about the partial DOS.

Even though electrical resistivity measurements yield valuable results for binary hydrides, this method is rarely applied because of experimental difficulties such as contacting brittle samples or disintegration of the specimens into powder. The introduction of interstitial hydrogen particles into a metallic lattice creates new scattering centers. This leads to an increase of the residual resistance which can manifest itself even at room temperature. Approaching stoichiometry, a new ordered phase is formed causing a decrease of resistivity at low T. The charged hydrogen can influence the band structure of the electrons, and in the TM the filling up of the d-band vacancies reduces the s-d scattering resulting in the depression of resistivity. However we should be careful here, because the effective resistivity measured may include changes due to creation of cracks, microcrystallites, and other mechanical defects. Also, from the measurements of resistivity vs. hydrogen pressure, we may get information about ordered alloys versus disordered state such as Pd_3Fe. The ordered alloys absorb hydrogen at a much lower pressure than the same one in the disordered state. In general, hydrogen ions usually occupy both tetrahedral and octahedral interstitial positions. It seems (for instance in rare earths hydrides [Ward, 1985a]) that they prefer the tetrahedral positions in low concentrations, because the octahedral hydrogens are bound less strongly.

4.1.2 Magnetic Properties

The rare earth elements form binary hydrides RH_X with the stoichiometries x = 2 and 3. When x approaches 3, electrical conductivity disappears. This has been attributed to the formation of a low lying s-band with the capacity to hold six valence electrons [Switendick, 1978]. In fact, this is equal to the number of electrons supplied to the conduction band by one R and three H atoms. Since this low lying bonding band is completely filled up with electrons, no conduction electrons are present in RH_3 prohibiting the RKKY interaction. This accounts for the suppression of the magnetic interaction and it is usually observed experimentally.

Now let us consider R-3d intermetallics and their hydrides. Firstly, if both the R and 3d elements carry a magnetic moment, we can distinguish between three types of magnetic interactions: i) the localized moment 4f-4f interaction; ii) the more itinerant moment 3d-3d interaction; iii) the 4f-3d interaction. In general, it is observed that these interactions decrease in the following sequence: 3d-3d > 3d-4f > 4f-4f. In addition to that, a disturbance of the lattice periodicity takes place in the hydrides reducing the mean free path of the conduction electrons. This leads to a damping of the RKKY conduction-electron polarization which in turn decreases the magnetic coupling strength. Secondly if 4f magnetism is dominant in the R-3d compounds, the concept of an R-H charge transfer may be suitable. Thirdly, if the magnetic ordering in R-intermetallics is dominated by the 3d moments there is no general rule. Hydrogen absorption leads to a loss in the 3d moment in Ni- and Co-based intermetallics, but to an enhancement of the Fe moment. For

Mn-intermetallics either changes from paramagnetism to ferromagnetism or vice versa are observed.

Considering the hydrogen induced change of the magnetic properties, one frequently faces a difficulty finding reliable magnetic moment data. One usually has to rely on magnetization measurements, thereby achieving incomplete saturation because of the lack of high magnetic field facilities. Thus, high magnetic field measurements are desirable in this area.

4.1.3 Concentration Determination

One of the widely used and simple methods to determine the concentration of dissolved hydrogen is measuring the mass change of hydride. Since we poison the surface of bulk or powder samples with impurities in order to keep the sample sealed after doping with hydrogen, where the influence of impurities is mainly within a surface layer, the accuracy of measuring the mass change decreases with increasing surface to volume ratio of the sample. Another method often used is to measure the pressure increase during a high temperature vacuum extraction of hydrogen. Once a reliable calibration exists, measuring the relative lattice parameter change gives the hydrogen concentration.

4.1.4 Isotope Effects

The reaction of a metal with deuterium or tritium is generally similar to that of the same metal with hydrogen. Minor differences exist in such physical properties as smaller mass density and larger lattice parameters of hydrides than those of deuterides and tritides. The heats of formation in the metal deuterides and tritides are usually less than those of the corresponding metal hydrides resulting in a less stable ground state. So, the dissociation pressures of deuterides and tritides are always greater than those of the corresponding hydrides. For the isotope effects on superconductivity, T_C is usually inversely proportional to $M^{1/2}$ thereby decreasing with increasing isotope mass M. Neutron diffraction is especially suitable method to study the positions of both metal and hydrogen atoms in the hydrides lattices, because neutrons are scattered by nuclei giving rise to the same magnitude of scattering factor between light and heavy atoms. Also neutron scattering experiments with deuterides give much better results in a noise to signal ratio than those with hydrides, because deuterium has a higher coherent scattering amplitude and lower spin diffuse scattering than does hydrogen [Blackledge, 1968].

4.1.5 Pressure-Composition Isotherms

The hydrogen absorption in metal systems has been studied by the isothermal measurements of the hydrogen pressure P_{H2} as a function of the hydrogen concentration x. In Figure 4-1, we see a relatively strong increase of the hydrogen pressure from the beginning up to point 1, it is called α_1 phase, where a small fraction of hydrogen is absorbed without changing the crystal structure. After the plateau from point 1 to point 3, there is another increase of hydrogen pressure up to point 4 and so on. We call the region from point 3 to point 4 as β_1 phase, and there is a mixed region of α_1 and β_1 phases between point 1 and point 3. In the mixed region, a reaction $\alpha_1 + H_2 \leftrightarrow \beta_1$ happens and this plateau is called a miscibility gap. So we can not get a given hydride which has a concentration, say x_2 at point 2, on the plateau where two phases are in equilibrium with each other. One of these is the α_1 phase with composition x_1, and the other phase is the

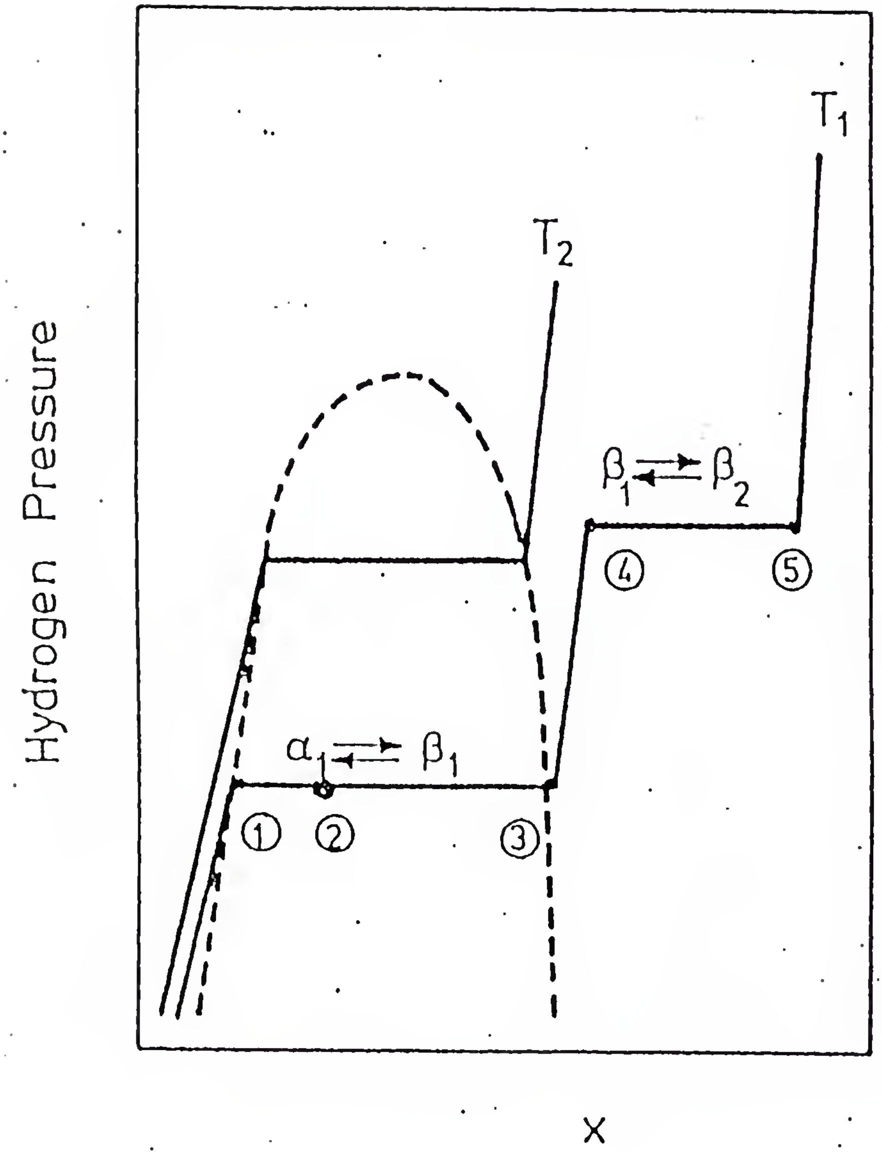

Figure 4-1. Schematic representation of two pressure-composition isotherms of a hydride. At the temperature T_1 (< T_2) the two-phase regions (miscibility gaps) are confined to within the concentrations denoted by 1 and 3 and by 4 and 5, respectively. The miscibility gap corresponding to the formation of the first hydride β_1 is indicated by a broken line. This figure is taken from Buschow [1984].

hydride β_I with composition x_3. The miscibility gap comes from the fact that the heat of solution in the sample decreases (becomes increasingly negative) with increasing H concentration. Thus, the process of solution in the plateau becomes more exothermic as we go from point 1 to point 2 so that it is energetically more favorable for the H atoms to be concentrated locally (hydride) than to be distributed in a uniform manner (solution) throughout the metal. In the plateau of α_I and β_I phases, hydride of β_I phase starts to form resulting in the decrease of α_I phase region and the full β_I phase is reached at point 3. As we increase temperature from T_1 to T_2 and so forth, the miscibility gap or plateau decreases until the gap finally disappears. However the influence of entropy will counteract this trend to form two separate phases. Such a behavior is represented by the broken line in Figure 4-1 [Buschow, 1984]. The absence of the plateau does not always means a homogeneity of the hydride though.

4.2 Overview of UPd_2Al_3

After there was a report [Geibel *et al.*, 1991b] of the discovery of a record high T_C = 2 K for a heavy fermion system with antiferromagnetic (AFM) ordering at T_N = 14.5 K in UPd_2Al_3, there has been a great deal of excitement [Steglich, 1994 and references therein] because of its large magnetic moment below T_N which is of order of two larger than the previous AFM heavy fermion superconductors (HFS), e.g., URu_2Si_2 and UPt_3. This large magnetic moment invoked physicists to search for the possible understanding of the interaction between magnetic and superconducting ground states which coexist below

T_C. We would like to review here the system UPd_2Al_3 by giving attention to the physical properties which are closely related to the hydrided system $UPd_2Al_3H_X$.

4.2.1 Normal State

UPd_2Al_3 [Geibel *et al.*, 1991b] crystallizes in the hexagonal $PrNi_2Al_3$ structure, and the lattice constants are a = 5.365 Å and c = 4.186 Å. The lattice perfection can be improved by annealing the sample at 900 °C for 1 week. We show in Figure 4-2 the crystal structure of UPd_2Al_3. The magnetic moments at each U-atom site are aligned ferromagnetically in the hexagonal basal plane and coupled antiferromagnetically along the c-axis. We see, in figure 4-3*a*, that there is a kink at T_N in χ and ρ which is totally different from that of URu_2Si_2 where the anomaly of the magnetic transition shows a peak in both χ [Roy *et al.*, 1994] (Roy *et al.* did see it in field cooling measurements below 0.05 T and interpreted it as resulting from stacking faults, and our measurements, not shown, exhibit a peak even in zero field cooling around the AFM transition and the peak becomes broader and lower in temperature for a field cooling at 0.02 T) and ρ being interpreted as due to spin density wave [Maple *et al.*, 1986]. Dalichaouch *et al.* [1992] suggest that in UPd_2Al_3 an energy gap of 40 K opens up over 30 % of the Fermi surface below T_N from the resistivity measurement. Recently, tunneling spectroscopies along the ab-plane [Aarts and Volodin, 1995] revealed evidence for a 10 meV, which is corresponding to about 110 K, energy gap. As we show in Figure 4-3b, there is a peak at 35 K in the magnetic susceptibility χ and at 70 K in the electrical resistivity ρ, where χ for $T > 100$ K follows Curie-Weiss behavior and gives an effective moment μ_{eff} of 3.2 μ_B/U-atom deduced from the plot of χ^{-1} vs. T.

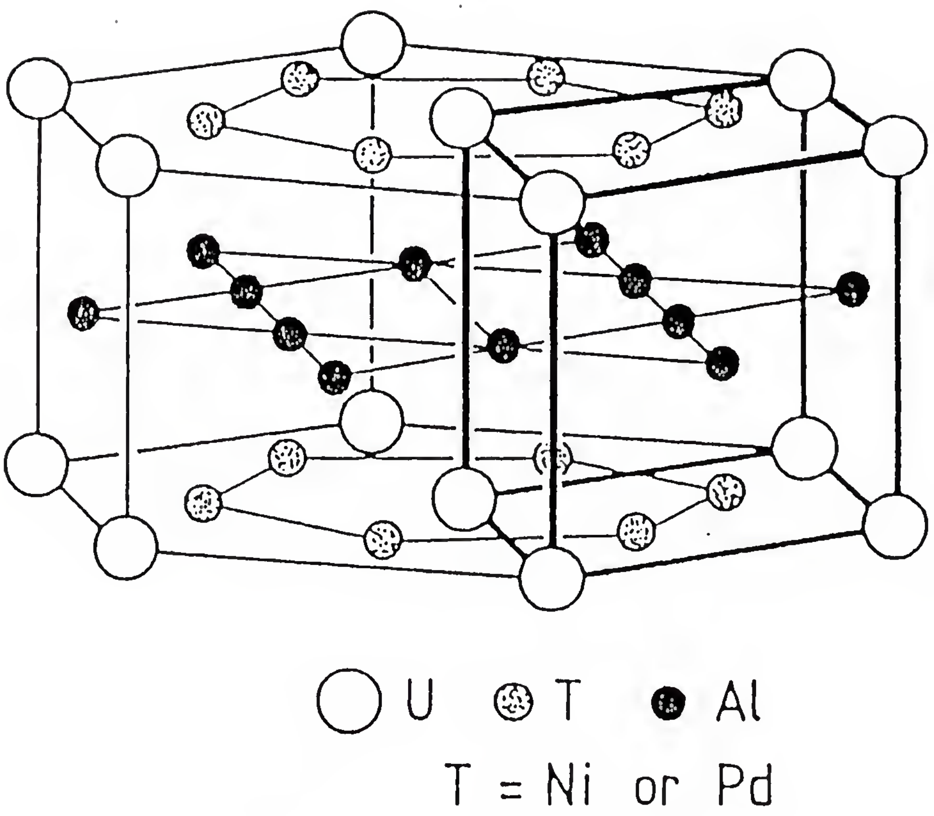

Figure 4-2. Hexagonal PrNi$_2$Al$_3$ crystal structure observed in UNi$_2$Al$_3$ and UPd$_2$Al$_3$. Heavy lines show unit cell. U-atoms carry magnetic moment. This figure is from Sticht and Kübler [1992].

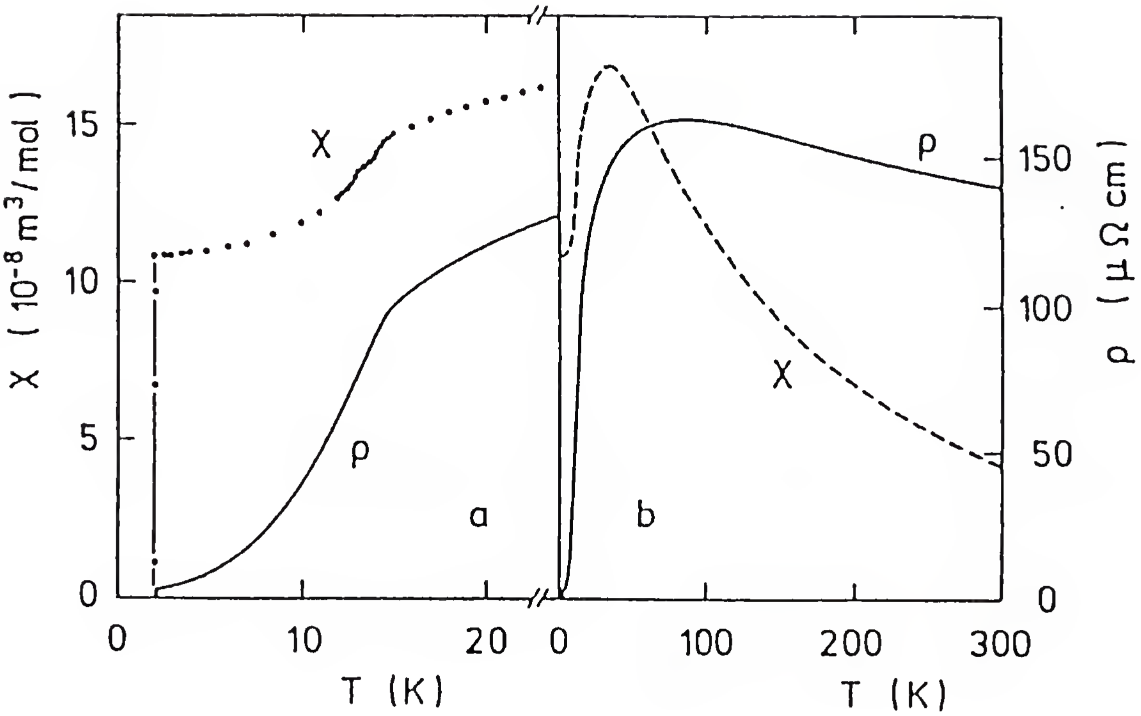

Figure 4-3. Temperature dependence of the electrical resistivity and of the dc magnetic susceptibility (at H = 10mT) for UPd_2Al_3 below T = 25 K in (*a*) and up to T = 300 K in (b). Thin solid line in (*a*), indicating only half of the transition, is a guide to the eye. This figure is from Geibel *et al.* [1991b].

In Figure 4-4b, we show the specific heat divided by temperature C/T vs. T where we see a large jump at the Néel temperature T_N. In the normal state for $T_C < T < T_N/2$, we can express the specific heat as $C_{el}(T) = C_n(T) - \beta T^3 = \gamma(T)\cdot T$, where the cubic term with $\beta = 2.4$ mJ K^{-4}mole^{-1} is mainly due to magnons. The γ_o as $T \rightarrow 0$ extrapolated for $T_C < T < T_N/2$ gives about 150 mJ K^{-2}mole^{-1}, and this value is reduced compared to $\gamma_p = 210$ mJ K^{-2}mole^{-1} which is extrapolated from the paramagnetic region ($T > T_N$). Such a reduction in γ has been found in magnetic heavy Fermions [Stewart, 1984; Grewe and Steglich, 1991]. Careful measurements of specific heat C below T_C has shown that C is described well by the linear and cubic terms in T [Caspary *et al.*, 1993] implying unconventional superconductor. The entropy released below the magnetic transition is 0.67R ln 2, where R is the gas constant in unit of 8.31 J K^{-1}mole^{-1}. The ordered magnetic moment below T_N is 0.85 ± 0.03 μ_B/U-mole [Krimmel *et al.*, 1992] from the neutron elastic scattering which is the highest value among the heavy Fermion superconductors. This has interested many physicists, because we have a much better chance to study the interplay between superconducting and magnetic ground states which coexist in this system.

After single crystalline specimens of UPd_2Al_3 became available [Geibel *et al.*, 1991a], there have been several interesting experiments. Magnetization experiments at high magnetic fields on a single crystalline sample at $T = 4.2$ K [de Visser *et al.*, 1993] suggest that there is a spin flip on the basal planes at a magnetic field $H_C = 18$ T along the basal plane. Because the jump of M at H_C is equal in magnitude to the ordered moment, this implies the magnetic phase transition from AFM to paramagnetic state. Anisotropy on the plane has been reported [de Visser *et al.*, 1994] from ρ measurements by rotating

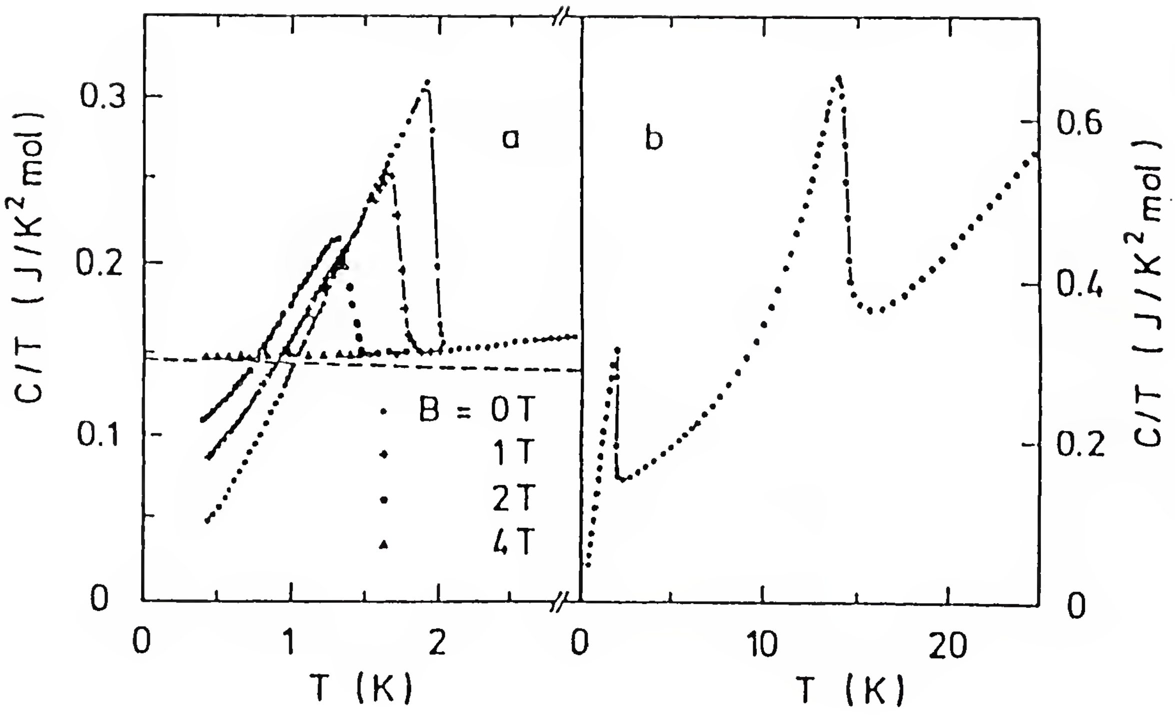

Figure 4-4. Specific heat of UPd_2Al_3 as C/T vs. T measured between 0.4 K and 3 K at H = 0 T and in several magnetic fields in (*a*) as well as up to 25 K at H = 0 T in (b). Dashed curve in (*a*) represents electronic contribution, $C_{el}(T)/T$. Thin solid lines are guides to the eye. This figure is from Geibel *et al.* [1991b].

the magnetic field in the hexagonal plane to determine the antiferromagnetic (AFM) phase diagram and suggested neutron diffraction experiments for confirmation. These have been done [Paolasini *et al.*, 1994] and their results are consistent with the idea of reorientation of the AFM domains. The domains of moments are aligned perpendicularly to the applied magnetic field for $H < 5$ T, where {100} seemed to be the easy axis, and for higher fields at $H \sim 18$ T the moments start to turn towards the direction of the applied field in the normal state. Also magnetization M vs. magnetic field H at $T = 4.2$ K [Sato *et al.*, 1992] has shown that M is linear for H being parallel to the c-axis, and an increase of slope at $H = 2.5$ T for H along the a-axis or basal plane. This break of slope presumably suggests the domain ordering within the hexagonal plane. There has been found an anisotropy in the magnetic susceptibility χ as shown in Figure 4-5, where we see a similar behavior reported in the polycrystalline specimen for a magnetic field along the basal plane. However, almost constant χ has been found for a magnetic field along c-axis as shown in Figure 4-5 [de Visser *et al.*, 1992]. Single crystal measurements of χ along the plane give $\mu_{eff} = 3.2$ μ_B for $100 \text{ K} < T < 300$ K and 3.4 μ_B for $350 \text{ K} < T < 650$ K [Grauel *et al.*, 1992] so that we should be careful about the temperature regions to deduce the effective moment which are well recognized in UPt_3 [Frings *et al.*, 1983].

Even though there are several interpretations about the peak in χ of UPd_2Al_3 [Geibel *et al.*, 1991b and references therein], no conclusive proof was given. For the crystalline electric field (CEF) structures there are two electronic configurations of U-5f^2 and U-5f^3 suggested, where 5f^1 was ruled out because of its small magnetic moment ($\mu_{eff} = 2.54$ μ_B) compared to the measured value $\mu_{eff} = 3.2 \sim 3.6$ μ_B. The theoretical fit based on both configurations seemed fine in specific heat *C* and χ data in the ab-plane. However, the $5f^3$ configuration with a doublet ground state and first excited doublet state separated by about 100 K showed a divergence of χ along the c-axis at low *T* contrary to experiments [Radwanski and Franse, 1993; Grauel *et al.*, 1993]. The $5f^2$ configuration with a singlet ground state and first excited singlet state separated by 32 K seems to be most probable from the evidence. For instance, there have been doping experiments on the U-site of UPd_2Al_3 with several lanthanide and actinide elements such as Y, La, Gd, Th, and Pr [Giebel *et al.*, 1994]. They studied how T_N depends on the electronic configurations, the atomic volume, and the local magnetic moment of the doping elements. Their conclusion was that the electronic configuration of U is $5f^2$ (or U^{4+}), because only the tetravalent Th doped system shows a much slower decrease (by a factor of about 4) of T_N relative to the other trivalent doped systems. More evidence comes from the similar behavior of χ in UPd_2Al_3 and $PrNi_5$, where Pr has the $4f^2$ or Pr^{3+} configuration [Grauel *et al.*, 1992]. Sato *et al.* [1993] has suggested the important role of CEF by analyzing the jump of *M* at 18 T based on the level crossing of the ground singlet with the first excited singlet with the reduction of level splitting from 33 k to 6 K. It has also been claimed in UPd_2Al_3 and UNi_2Al_3 that CEF splitting are proportional to the temperature of χ maximum, T_m. And the splitting are inversely proportional to the ordered moments and the intersite interaction between the local moments [Schank *et al.*, 1993].

Polarized neutron experiments are interpreted such that the magnetization density is totally associated with the U-atom and there is no spin transfer on the Pd atom, which

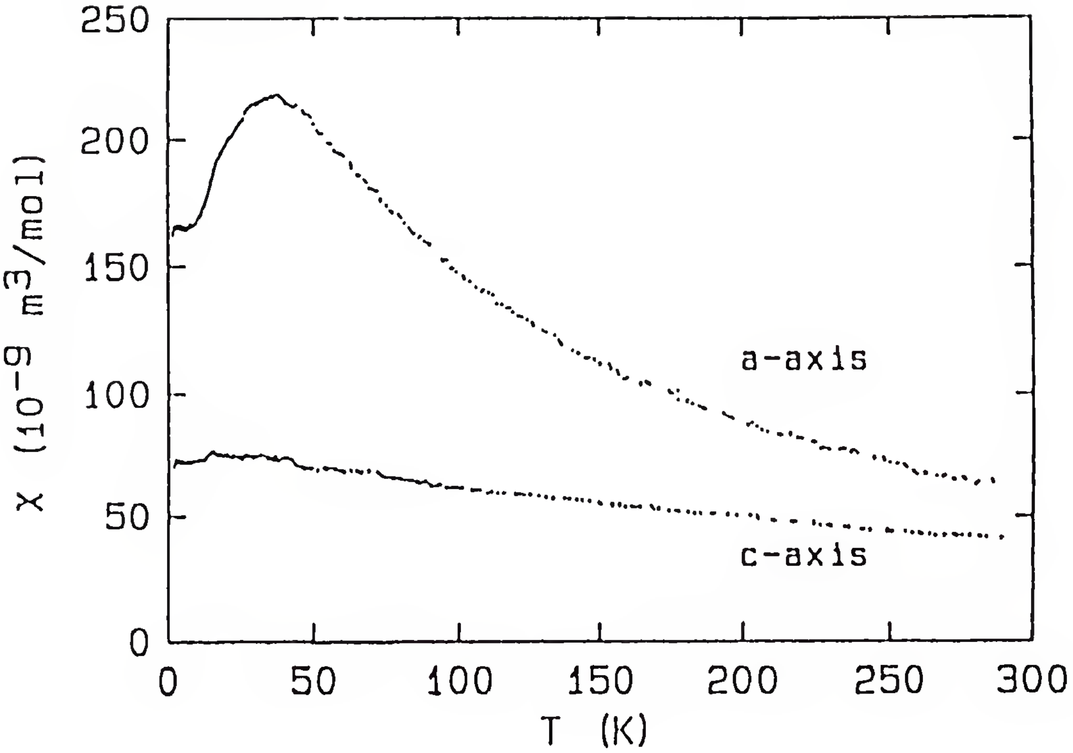

Figure 4-5. Magnetic susceptibility χ of UPd_2Al_3 for a magnetic field (H = 2 T) along the *a*- and c-axes as indicated. This figure is from de Visser *et al.* [1992].

means no hybridization between U(5f) and Pd(4d) [Paolasini *et al.*, 1994]. This is far different from URhAl and URuAl where there is about 35 % polarization of d-electrons giving rise to the 5f-4d hybridization. This seems to be true if the Pd-4d band is filled so that there is little overlap in the energy of the U(5f) and Pd(4d) bands. Magnetization M measurements with the analysis of the form factor reveal the moment at U atom is 0.14 μ_B/mole out of the total moment 0.16 μ_B/mole. Since we know that there is no moment at either the Pd or the Al sites, the difference of 0.02 μ_B/mole must be ascribed to plane waves, i.e., the conduction electron polarization. This seems to be consistent with the μSR experiments at magnetic fields, where there is a 16 % contribution to χ from the conduction electrons [Feyerherm *et al.*, 1994].

4.2.2 Superconducting State

Superconductivity is suppressed at least down to 0.5 K at 4 T as shown in Figure 4-4*a*. From the measurements of T_C with magnetic fields [Geibel *et al.*, 1991b], the initial slope of the upper critical magnetic field, $H'_{c2} = -(\partial H_{c2}/\partial T)_{Tc}$, is reported to be 4.3 T/K. They also conclude from the large jump of C and large value of H'_{c2} at T_C that the superconducting transition takes place out of the heavy Fermi liquid state [Steglich *et al.*, 1991]. From γ_o, T_C, ρ_o, H'_{c2}, and assuming an isotropic one band model, they estimate [Rauchschwalbe *et al.*, 1982] the effective carrier mass $m^* \approx 66\ m_o$, where m_o is the mass of the bare electron. In addition to that they calculate a Bardeen-Cooper-Schrieffer (BCS) coherence length $\xi \approx 85$ Å, magnetic penetration depth $\lambda \approx 4000$ Å, and elastic carrier mean free path $l \approx 720$ Å. Thus this system behaves as type II superconductor because the

Ginzburg-Landau parameter $\kappa \equiv \lambda/\xi \approx 50$, and as we see from $l/\xi \approx 10$ this is a clean superconductor. The effective cyclotron mass of UPd_2Al_3 is estimated to be about 10 m_o ~ 30 m_o from the de Haas-van Alphen (dHvA) experiments [Inada *et al.*, 1994], where it is usual to have a smaller value of effective mass in this measurement than that from the thermodynamic measurement. ^{27}Al nuclear magnetic resonance (NMR) studies [Kyogaku *et al.*, 1993] have shown a reduction of the Knight shift irrespective of the direction of the crystal axes indicating the singlet nature of the Cooper pairing. The behavior of the nuclear spin-lattice relaxation time T_1 below T_C is consistent with a model with gap zeros on lines at the Fermi surface and this also appears true from the ^{27}Al nuclear quadrupole resonance [Kohori and Kohara, 1994].

4.2.3 Electron Subsystems

In this section we review briefly recent developments in UPd_2Al_3 which we think may give some experimental results to understand hydrided UPd_2Al_3. There have been several papers about "two rather independent electron subsystems in UPd_2Al_3". According to this model, itinerant or less localized heavy quasiparticles mostly due to 5f electrons are responsible for superconductivity and more localized ones are identified with the AFM state. There have been experiments of specific heat and electrical resistivity under pressures up to 11 kbar [Caspary *et al.*, 1993]. There is an increase of $\Delta T_N/T_N$ by about 9 % and a decrease of $\Delta T_C/T_C$ by about 4 %. Also ΔC at T_C is not changed by the pressures. A most surprising fact comes from the pressure dependence of γ. The same change of γ below and above T_C let the authors obtain the following relation; $\gamma_n(p) = \gamma_1 + \gamma_S(p)$, where γ_n is for $T > T_C$, γ_S is for $T < T_C$, and γ_1 is 115 mJ $K^{-2}mole^{-1}$. They have argued that pressure independent γ_l is associated with the itinerant 5f electrons, and pressure dependent γ_n and γ_S are responsible for the localized ones. There has been another pressure experiment up to 65 kbar, where ΔT_N in pressures is about –0.09 K/kbar in contrast to the previous result. However, there is almost no change in T_C. Also Ehrenfest's equation

$$(\partial T_C / \partial p_h)_0 = T_C V_{mol} \Delta\beta / \Delta C \tag{4.1}$$

with the thermal expansion results has shown that the hydrostatic pressure derivative of T_C nearly vanishes [Geibel *et al.*, 1991a]. There has been a nice experiment of zero magnetic field muon spin rotation (μSR) [Amato *et al.*, 1992a; Uemura *et al.*, 1993], where they do not see any change of the internal magnetic field at the transition from the normal state to the superconducting state. This is totally different from the results for $CeCu_{2.2}Si_2$ where there is a decrease of the internal magnetic field when the normal state transforms into the superconducting state. So antiferromagnetism and SC in $CeCu_{2.2}Si_2$ compete with each other [Steglich *et al.*, 1995] rather than coexist as we have seen in UPd_2Al_3.

Another experiment of μ^+ Knight shift with different magnetic fields has shown an isotropic change ($\Delta\chi_\parallel = \Delta\chi_\perp$) of χ for $T \rightarrow 0$, which is associated with the itinerant electrons thereby to the superconductivity. However, $\chi_\parallel$ and $\chi_\perp$ are anisotropic by a factor of 3 ($\chi_\perp \approx 3\chi_\parallel$), where $\chi_\parallel$ and $\chi_\perp$ are the magnetic susceptibility χ along and perpendicular to c-axis respectively. Also $\Delta\chi_\parallel$ (or $\Delta\chi_\perp$) is smaller for a larger applied field. The magnetic field caused the breaking of Cooper pairs in the intervortex region, hence inducing an increase of unpaired electrons which contributes to χ_{5f} [Feyerherm *et al.*, 1994]. The residual susceptibility ($\chi_{5f} - \Delta\chi_{5f}$) for $T \rightarrow 0$ is associated with the local moment (responsible for the AFM ordering), which is not affected by the superconducting transition.

4.3 Experimental Apparatus

In this section we would like to describe the hydriding apparatus briefly and refer to Figure 4-6. There is a high pressure bomb or vessel series 4742 from Parr Instrument Company made of T316 stainless steel (SS) whose volume is 21 m*l*. We load the sample to be hydrided into the bomb, and an analogue pressure-gauge main-block-assembly (series 4316) is connected to the bomb. We install a main block to which several pieces of equipment are connected by a needle valve made of T316 SS. A 1/16 inch SS-gas-tube-assembly is used between the main block and the bomb as well as a hydrogen gas cylinder. We also install two wire cloths, each has 7 μm and 0.5 μm pores, between the main block and the bomb to prevent the sample powder from coming out of the bomb when we pump the bomb. The cylinders of hydrogen and passivating gas CO_2 are connected to the main block along with a mechanical pump. An argon gas cylinder is connected to the pumping line to ensure the safe pumping of hydrogen which will be explained in detail in section 4.4.2. We install a digital pressure transducer to the main block and we read the pressure through Hewlett Packard 85 interfaced to a Keithley 177 by converting the voltage output into pressure. The pressure transducer Model SA from Data Instruments with an accuracy of ±1 % is connected to the dc voltage source of 10 V and to a Keithley 177 Microvolt DMM as a voltmeter. We have calibrated the transducer with respect to the analogue pressure-gauge-main block-assembly. An exhaust line with a check valve is installed to

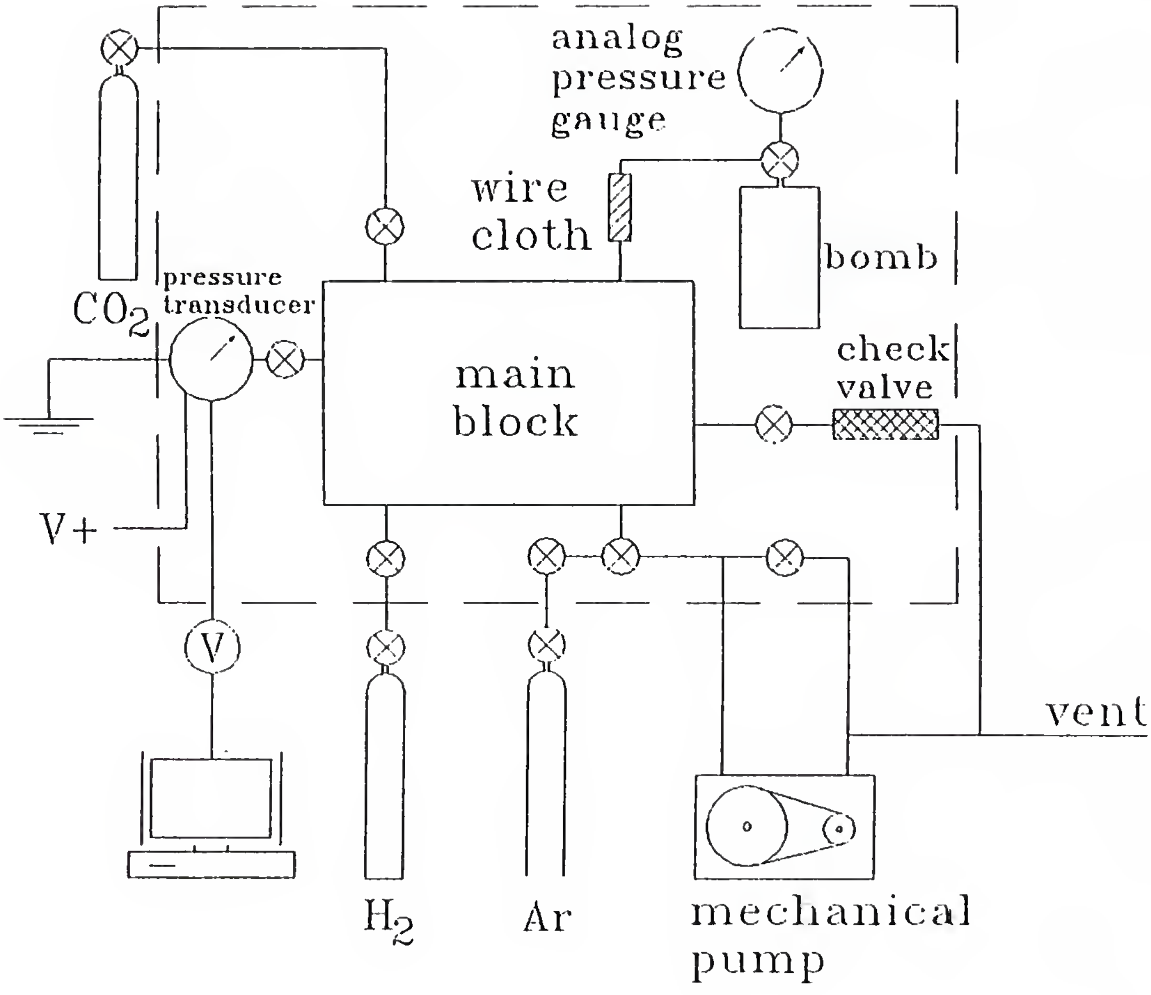

Figure 4-6. Hydriding apparatus. All equipment is connected to a main block where most of the control valves are installed. We can record the pressure change as a function of time on the HP screen (see the text for more detail). The safety box (broken line) contains most of the high pressure parts to avoid accidents.

the main block and we have the line go out from the building for the sake of good ventilation to reduce any possible explosive danger.

When we heat the bomb we use the heating mantle STM 900 from Glas-Col containing sand from Ottawa Sand Standard manufactured by Fisher, where sand works as a thermal media between heater and bomb. We use a digital thermometer from Fisher to measure the temperature of the bomb, and the temperatures of the heater is controlled by a power regulator MC 228 from Electrothermal.

We also have prepared a thick safety box made of aluminum and Plexi-glass (only front side to see inside) in which we put main block, bomb, and main control valves except those of the gas cylinders to prevent any serious accident. We tested our hydriding system with the well known hydride-host material $LaNi_5$, and we got good agreement with the phase diagram of the equilibrium hydrogen pressure vs. hydrogen concentration [van Vucht *et al.*, 1970; Buschow and van Mal, 1972 and references therein].

4.4 Sample Preparation

Before doping hydrogen into a polycrystalline specimen, we made several polycrystalline samples of UPd_2Al_3 and made sure that they had the right crystalline structure using a Philips X-ray diffractometer. Then they were powdered in a ceramic mortar without touching any metal to avoid possible magnetic ion effects other than the stress effect due to the grinding chunk. We synthesized the hydride in the bomb by pressurizing and pumping the hydrogen at several temperatures from –80 °C up to 450 °C. We will describe it in detail in subsequent sections by noting how we prepared the parent system UPd_2Al_3, how we activated the sample, and how we poisoned or passivated the hydrided sample. We then made the powders into pellets to measure the specific heat and magnetic susceptibility as well as to promote safety, because a radioactive element U is in the sample.

4.4.1 Polycrystalline Sample

We made UPd_2Al_3 polycrystals with each element according to the stochiometry as we have described in the experimental techniques in section 1.3.2. We used uranium from Los Alamos, 99.9985 palladium wire from Johnson & Matthey Inc., and 99.999 aluminum from Johnson & Matthey Inc.. We then annealed the chunk at 900 °C for 1 week followed by the X-ray and χ measurements to confirm the right crystalline structure (or any second phase if any) and to check the sample quality from the T_C and T_N, respectively.

Since the bulk chunk of UPd_2Al_3 does not absorb hydrogen in our experimental conditions, we have to grind it to increase the surface to volume ratio. At this point we should be very careful to reduce any possible unwanted effects such as magnetic impurities from iron pestle and mortar which we have used to crush the chunk into the rough size (about order of mm) of powder. For instance we did see a difference in χ measurements for UBe_{13} between the crushed powder by iron tools and that by the ceramic pestle and mortar. Thus, we crushed the parent chunk sample into a rough powder (size of order of mm) and subsequently ground it in the ceramic mortar with ceramic pestle into an average size of 50 μm. Sometimes we let the powder go through the metal cloth smaller than 50 μm to check if there was any unhydrided part in this size of material. At the average powder size of 100 μm and smaller, it seems to us that there is no unhydrided portion in it by firstly doing X-ray analysis with that size, and then grinding it into about 20 μm followed by another X-ray measurement. Therefore we think that the diffusion length of hydrogen in this material is at least larger than 100 μm. Here we have to be very cautious when we handle the very fine powder because of the radioactivity of sample.

4.4.2 Activation of Sample

It is unusual for a sample to absorb hydrogen gas spontaneously after it has been brought into a bar of hydrogen gas. Hydrogen absorption generally takes place only if the sample has been subjected to a so-called "activation treatment". The activation process consists of two steps [Sandrock, 1978]. In the first step, the thin surface oxide film is destroyed and a direct contact is established between the hydrogen gas H_2 and the metallic surface. For instance, it can be done by heating hydrogen gas in the bomb to a few hundred degrees °C, e.g., TiFe, or by applying a H_2 pressure considerably in excess of the corresponding plateau pressure of most compounds based on rare earth metals, e.g., $LaNi_5$. The second step of activation is that the hydride initially grows as an envelope around the partially activated particles of the compound. This volume increase of hydrides causes a stress giving rise to cracks which provide new surfaces and canals to the hydrogen gas, and results in a much faster activation process. In brittle intermetallic compounds, the first hydrogenation process already breaks the sample into an assembly of tiny particles. Further charging-discharging (or hydriding-dehydriding) cycles make the mean particle diameter even smaller.

We could not reach an activation state for our chunk sample of UPd_2Al_3 by just applying a high pressure of hydrogen up to 120 bar at 450 °C, which we can reach without any possible dangers. So, we powdered the sample to increase the surface area to the surrounding hydrogen. We then put the powdered sample into the bomb and connected the vessel to the main block where all control valves are located, see Figure 4-6. When we seal the bomb with a nickel gasket and a gage-assembly, we use a lubricant from Bostic composed of copper, aluminum, and zincoxide powder with oil. The lubricant works below 1000 °C to avoid any leak, which is very critical not only in high pressure experiments but also a possible oxidization of the sample at the elevated temperatures during pumping the bomb (the surface oxidization of sample in the bomb prevents hydrogen gas from activating the sample). Before we began each hydriding experiment we *always checked for leaks* by applying a hydrogen pressure of a few hundred bars, and then closing all valves and watching the pressure change on both the analogue and the digital gauges. If there is no indication of a leak, for instance the continuing decrease of pressure, we increase the pressure to a factor of two higher and do the same processes as before up to 100 bar. After we have confirmed the good seal, we exhaust the hydrogen gas very slowly through the exhaust line to the outside of the building down to about 1 bar of hydrogen. It is very crucial not to pump a high pressure of hydrogen directly because it may cause an explosion in the vacuum pump which is usually at an elevated temperature. After exhausting the high pressure hydrogen to room pressure, we let argon gas flush through the pumping line for few minutes to reduce oxygen in the pumping line. We then open the vacuum valve in the main block very slowly to avoid both any sucking of the powdered sample, even though we installed two sizes of wire cloth between the bomb and the main block, and any abrupt pumping of the remaining room pressure of hydrogen.

While we are pumping, we keep the bomb at the high temperature of about 450 °C to promote the cleanness of sample surface. We also use a cold trap in the pumping line with nitrogen liquid to reduce the back flowing of oil vapor which we think might prevent hydrogen gas from seeing the surface of the sample, because we pump the bomb from an hour to a day for one cycle of hydriding and dehydriding if necessary. After pumping we apply a high pressure of hydrogen gas up to 120 bar, which is allowed in our apparatus at 450 °C, and leave it for an hour to few days at 450 °C depending on the situation. Then we release the gas through the exhaust line very slowly, and complete one cycle of hydriding and dehydriding. We repeat these steps about 30 ~ 40 cycles to get a good activation of the sample. However, we can get a little activation for only about 5 cycles. Here we usually check the activation by watching the pressure decrease in the main block and bomb caused by the sample uptake of hydrogen after we apply a high pressure of hydrogen quickly and close the gas valve.

4.4.3 Passivation of Sample

After we activate the sample we keep the sample at a high pressure of about 120 bar of hydrogen and a high temperature of about 450 °C for a day. We decrease the temperature from 450 °C to room temperature at a rate of about 40 °C/hour, and pressurize it up to 140 bar at room temperature. Our apparatus is designed to work up to 200 bar at room temperature and we can get a pressure of ultra high purity hydrogen (99.999 %) up to 150 bar. However we go up to 2/3, about 140 bar, of our maximum allowance for the safety. Then we close the bomb valve between the bomb and the gauge main block, and release the hydrogen gas in the main block down to 1 bar through the exhaust line. We fill the main block with carbon dioxide (CO_2) up to 70 bar and increase the pressure in the main block with hydrogen up to 140 bar. After waiting for a few minutes until the mixed gases are stable in the main block, we open the bomb valve very slowly for the CO_2 to see the sample in the bomb at room temperature. It chemically reacts with the sample surface so as to prevent the hydrogen inside the powder or particle from coming out. We repeat this process with the CO_2 about 10 ~ 20 cycles, then put the bomb above a liquid nitrogen pot lowering the bomb temperature down to –80 °C to stabilize the hydrogen inside the passivated surfaces for a day. We release the gas mixture of CO_2 and H_2 at a slow rate of 15 bar/hour down to 1 bar to reduce any unwanted evolution of hydrogen due to the sudden change of equilibrium pressure at low temperature. We disconnect the tube to the bomb from the main block so that passivated or poisoned powder is exposed to air at low T for a few hours. We warm the bomb up to room temperature in a few hours, and open the bomb and collect the powder. At this point it is a much better idea to spread the hydrided powder on a plate immediately after we take the powder out of the bomb, because there may be *an ignition at room conditions* if lots of hydrogen comes out of the hydrided sample in a short time due to bad poisoning of the surface. For instance, we experienced such an ignition when we handled $LaNi_5$ without passivating it at low temperatures with air. However we do not see such a phenomena in the UPd_2Al_3 hydride, because it seems to us very stable in ambient conditions.

We then perform an X-ray diffraction measurement to find out the change of the lattice parameters and a second phase if any. We make pellets with hydrided powder at the pressure of about 1200 bar using a laboratory press and a home made pellet maker. Afterwards we measure specific heat and magnetic susceptibility with these pellets having a maximum hydrogen-concentration of 1.30 within 5 %. Up to this concentration of hydrogen we do not see any second phase from X-ray analysis in our hydrided UPd_2Al_3. We have dehydrided a given amount of hydrogen by measuring the pressure change of a known volume by heating the pellet hydride in a quartz tube. Here we should be aware that hydrogen exists outside of the sample as molecules H_2, but as atoms H inside of the sample to estimate the concentration of hydrogen. So the right concentration of hydrogen is 2x if we see a molar change x from the increase of hydrogen pressure.

4.5 Hydrogen Effects on UPd_2Al_3

Before we talk about the hydrogen effects on UPd_2Al_3, we would like to note some basic effects of hydrogen on uranium. The reason of this attempt is that it seems to us that we may explain the hydrogen effects on UPd_2Al_3 with approximations in terms of the hydrogen effects on uranium based on some experimental facts. As will be described in more detail in the following sections, the effects of hydrogen on UPd_2Al_3 perhaps seems to be similar to the hydrogen effects on uranim in χ, γ at low temperatures, μ_{eff}, and T_C. We then try to interpret $UPd_2Al_3H_X$ results with a thorough analysis of those data.

4.5.1 Hydrogen Effects on Uranium

Let us think about the uranium hydride UH_X which usually crystallizes in the *A*15 structure with x close to 3 called β phase [Ward, 1985a]. It belongs to the *Pm*3*n* group with two uranium sublattices—we are not going to talk about α phase because of the difficult synthesis. The hydride is stoichiometric up to 700 °C, and there are very complicated allotropic (α,β,γ) phase transitions in the uranium metal. In the β phase the U-U distance is increased by about 10 %. The positions of the hydrogen atoms using neutron diffraction of deuteride have been determined such that they are located near the center of a distorted tetrahedron equidistant from one type-*A* and three type-*B* uranium atoms, where the metal-hydrogen distance is 2.32 Å. The U-U distances are: *A-A* (bcc lattice), 4.05 Å; A-B, 3.70 Å and *B-B* (face chain lattice), 3.31 Å. The first two distances are clearly in the magnetic region of the Hill diagram for uranium compounds, whereas the third one is well within the nonmagnetic region. Also electronic energy bands have been calculated [Switendick, 1982] and there is evidence for considerable bonding between uranium 5f and hydrogen 1s. Both localized (magnetic) and itinerant (metallic) 5f characters are identified with the largest contribution from the linear chain atoms. X-ray photoemission studies [Ward *et al.*, 1979] on solid samples of β-UD_3 have been performed and a massive conduction band is made up of uranium f, d, and some s electrons, see Figure 4-7. It also shows a hydrogen-derived valence band in the region of 5 ~ 8 eV below the Fermi level and the main peak of uranium 5f electrons is nearly 2 eV below the Fermi level, indicating a considerable localization in comparison to the 5f pinned at the Fermi level of the uranium metal spectrum. Core-level 4f spectra are relatively well defined and without satellites, and energies indicate a uranium valence somewhere between U^{4+} and the metal. The effective magnetic moment per formula unit of β phase is 2.79 μ_B, which is still below the expected paramagnetic moment of 3.68 μ_B for U^{3+} or 3.62 μ_B for U^{4+}, implying a partial quenching or a configurational reduction of the free ion

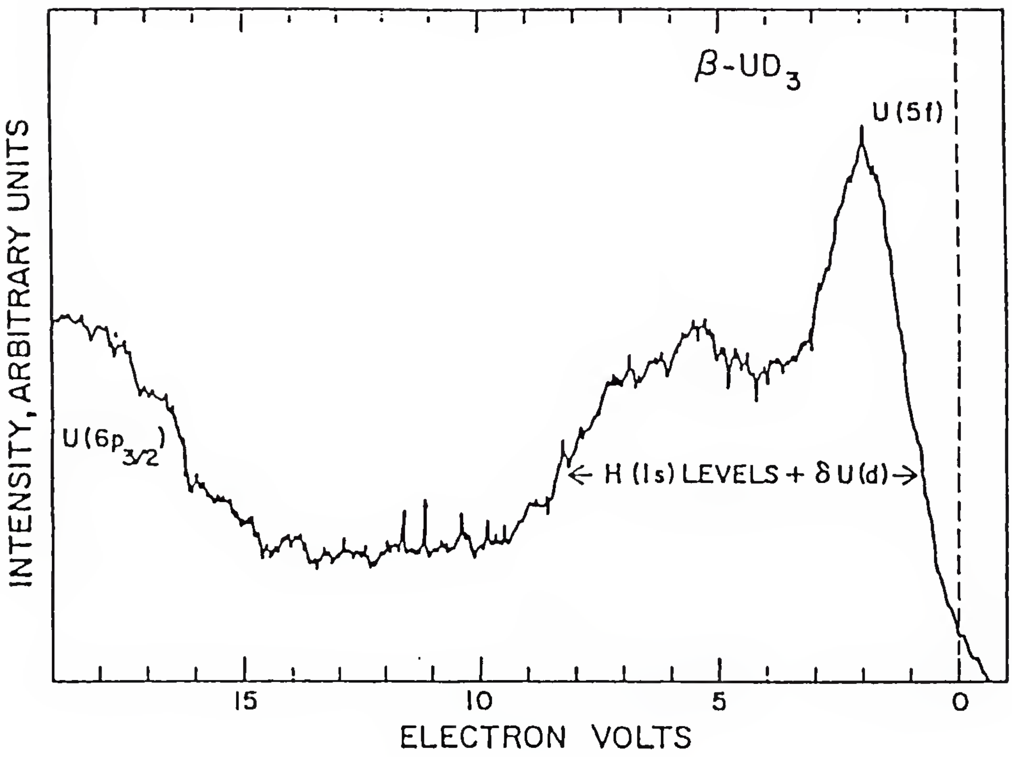

Figure 4-7. Valence-band XPS spectra for β-UD_3. The 5f electrons are pinned at the Fermi level of the uranium metal spectrum. This figure is from Ward *et al.* [1979].

moment. A Knight shift *K*, which is proportional to the change of the magnetic susceptibility, is defined as $K = (0.40 \pm 0.03)\chi_m$, where χ_m is the magnetic susceptibility [Grunzweig-Genossar *et al*, 1970]. This large shift is due to the polarization of conduction electrons via the RKKY coupling interaction accounting for the ferromagnetic ordering. The energy gap of about 80 K in the ferromagnetic spin wave spectrum [Fernandes *et al.*, 1985] strongly indicates a high magnetocrystalline anisotropy. Also the electronic specific heat coefficient of β phase ($\gamma = 28.7$ mJ K^{-2}mole^{-1}) [Wiesinger and Hilscher, 1991] is nearly by a factor of three larger than that of uranium metal. The uranium hydride orders ferromagnetically at about 180 K [Ward, 1985a and references therein], thereby no superconducting state observed in contrast to the superconductivity of U metal at an order of 1 K. The electrical resistivity of solid samples of β-UD_3 shows a ten times larger value than that of uranium metal, and it has been postulated [Ward *et al.*, 1979] that the atoms in the bcc sublattice would act as scattering centers giving rising to the increase of resistivity.

4.5.2 Hydrogen Effects on $UPd_2Al_3H_X$

We describe here $UPd_2Al_3H_X$ for $0 \le x \le 1.30$ where the hydrogen remains stable in the lattice under ambient pressure and temperature. Even though there has been a report [Alekseeviskii, 1985] on exposing UBe_{13} to 1 bar of hydrogen at 700 °C for two hours giving a different electrical resistivity, there were no details on how much, if any, hydrogen was retained. So we provide a particularly rich complement of hydrogen effects on heavy fermion systems. In $UPd_2Al_3H_X$ we think the hydrogen proton goes into the lattice interstitially by making itself several orders smaller than atomic size by giving its electron to the Fermi sea.

However we have found that hydrogen uptake in a bulk chunk, which has been found in the one of the most promising hydrogen storage systems $LaNi_5$ [van Mal, 1973], was not happened in UPd_2Al_3 under our experimental conditions mentioned in section 4.4.2. Thus we powdered our sample before loading it in the pressure bomb. This grinding has been found to affect the properties of the host materials, as already seen [Stewart *et al.*, 1986, 1984a] in $U_{1-X}Th_XPt_3$, $UPt_{3-X}Pd_X$, and UPt_3. Thus, T_C onset (as determined by ac susceptibility χ_{ac}) in UPd_2Al_3 is depressed about 20 % and ΔT_C is broadened by powdering. The $H'_{C2} = -(\partial H_{C2}/\partial T)_{Tc}$ is depressed by a factor of four and the antiferromagnetic anomaly in the specific heat is made 30 % smaller and broadened by grinding. All results presented here have been taken on the same sample to rule out sample dependent effects. As expected, hydrogen uptake in UPd_2Al_3 leads to a slight lattice expansion, with the hexagonal lattice parameter "a" increased by 0.52 % and "c" decreased by 0.31 % as a result of the maximum doping $UPd_2Al_3H_{1.30}$ we were able to achieve. This results in a unit cell volume, see Figure 4-2, $((\sqrt{3}/2)a^2c)$ increase of 0.75 %.

In order to determine the hydrogen concentrations of the various samples prepared, we first attempted to measure the weight gain of the powder in the bomb, where the accuracy was limited by our ability to gather all of the powder after hydriding. Thus after all measurements were finished, each sample (the powder was pressed into pellets for ease of handling and for improved thermal contact for low temperature measurements) was dehydrided by heating, using a weak hydrogen flame, in an evacuated quartz tube hooked to a pumping plenum. The temperature where hydrogen begins to come out of the lattice is about 225 °C. Samples of stoichiometry intermediate between $x = 0$ and 1.30 were prepared by partially dehydriding the material with a higher hydrogen concentration using controlled heating in the quartz tube-plenum arrangement while watching the pressure rise. In this fashion, we prepared $x = 1.09$, 0.77, 0.64, 0.34, 0.20, 0.17, and 0.13. Although we have no exact method to measure the homogeneity of the hydrogen in the lattice, we estimate the homogeneity to be ±10 % for $x = 1.30$ from the line broadening of X-ray measurements.

4.5.2.1 Normal State

The magnetic susceptibility χ of $UPd_2Al_3H_X$, $0 \le x \le 1.30$, is shown in Figure 4-8 and summarized numerically in Table 4-1. The feature in χ for $x = 0$ at 35 K is depressed to lower temperatures with increasing x, and decreases even linearly for more hydrogen uptake until it disappears for a hydrogen concentration larger than about 1 mole. Thus, it enables us to use the linear response as a calibration to estimate the hydrogen concentration for $x < 1$.

More useful information on the influence of hydrogen doping on the magnetic behavior can be gleaned from the behavior of the higher temperature Curie-Weiss effective moment μ_{eff} and the magnitude of the low temperature χ (see Table 4-1). The effective moment falls monotonically with increasing x for concentrations larger than 0.4 or 0.5, while χ at 1.8 K first remains relatively constant for $x \le 0.34$ as we may see in Table 4-1. A further parameter which we have measured is the magnetization M as a function of magnetic field H shown in Figure 4-9. In pure UPd_2Al_3, there exists an inflection point in the M vs. H curve near $H = 2$ T, where M rises more rapidly than linearly with H over a small region of H, which has been explained [Grauel *et al.*, 1992] as a rearrangement of the spins in the basal plane. Hydrogen doping for $x > 1.0$ destroys this inflection point as shown in Figure 4-9, at least up to our maximum field of 5.5 T, giving a linear M vs. H behavior.

In order to more completely discuss magnetism in $UPd_2Al_3H_x$, we need also to consider the behavior of T_N, which is visible as an inflection point below 15 K in χ vs. T shown in Figure 4-8, but it is much more readily apparent in the low T specific heat. Considering these data, shown in Figure 4-10, we see that the peak position (see also Table 4-1) shifts downward in temperature rather quickly with hydrogen doping, and is already below 5 K for $UPd_2Al_3H_{0.64}$. Thus, these specific heat data combined with the magnetic susceptibility and magnetization data present a consistent picture of the effect on UPd_2Al_3 of hydrogen doping: the magnetism, as judged by the size of χ at 1.8 K, μ_{eff}, and T_N, is suppressed and becomes weaker with increasing x. This effect is consistent with the added electrons in the Fermi sea increasing hybridization between 5f electrons and conduction electrons, thus lowering the effective 5f local magnetic moment.

As we see in Figures 4-8 and 4-10, χ and C/T in the limit of $T \rightarrow 0$ increase with higher hydrogen uptake. In fact, one can already observe in $UPd_2Al_3H_{0.17}$ that C/T between T_C and T_N is larger than that for $x = 0$, a trend that accelerates for higher hydrogen concentrations. The upturn at low temperatures observed in C/T and χ for the very same sample for $x > 1.0$ is itself the dominant feature. Data for $x = 1.30$, see Figure 4-10 for C/T and not shown here for χ, show no sign of saturation or anomaly down to

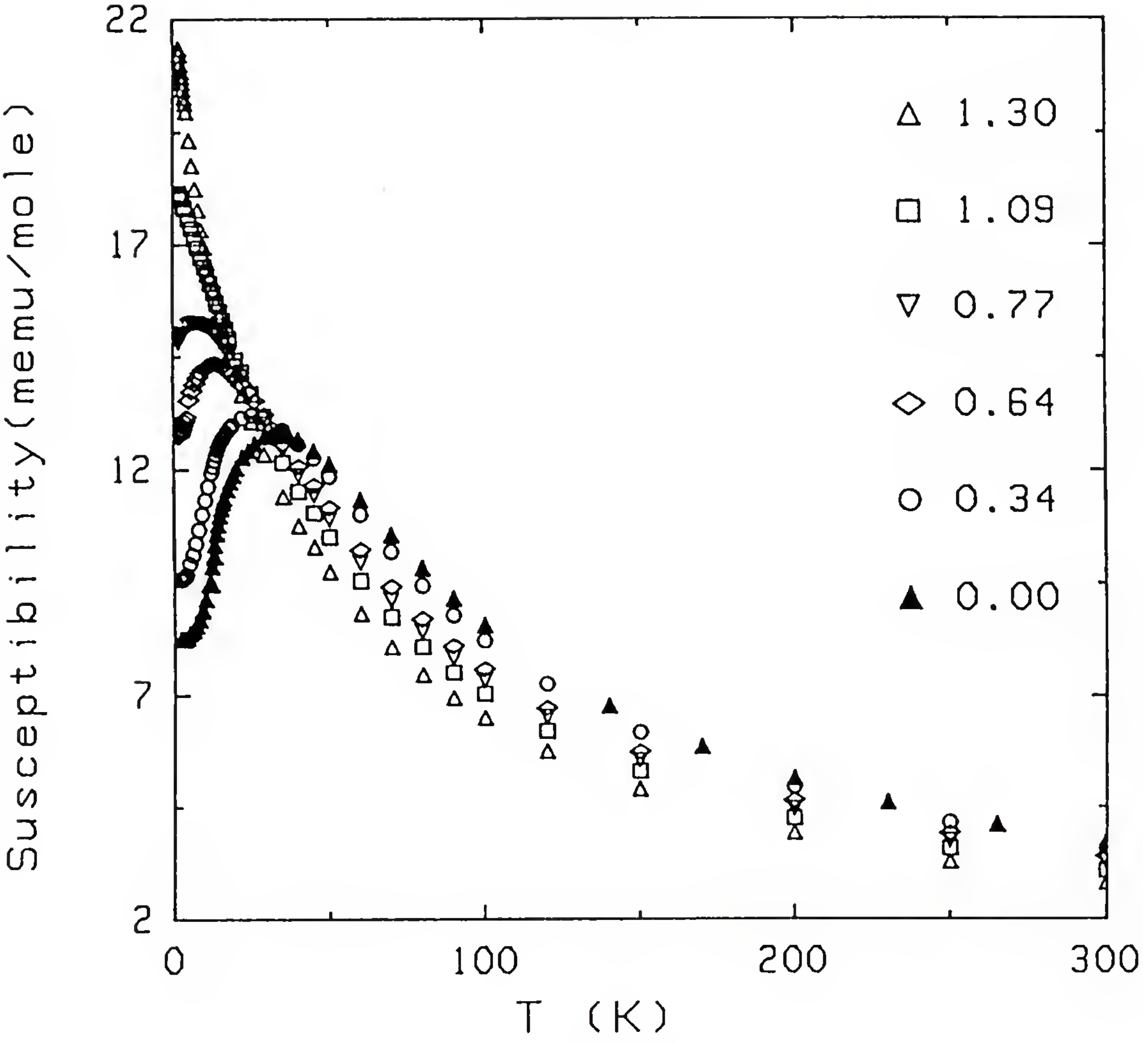

Figure 4-8. Magnetic susceptibility χ vs. T of $UPd_2Al_3H_x$ for $0 \leq x \leq 1.30$ are shown with different symbols for x. For clarity, data for x = 0.13, 0.17, and 0.20 are not shown. The peak at 35 K for x = 0 linearly decreases to low temperatures and gradually decreases in size with more hydrogen uptake.

Table 4-1. Parameters for hydrogen doped $UPd_2Al_3H_X$.

x =	0	0.13	0.17	0.20	0.34	0.64	0.77	1.09	1.30
T_χ^{max} [K]	35	32	30	29	26	13	7	—	—
μ_{eff} [μ_B]	3.39	3.21	3.23	3.21	3.19	3.14	3.08	2.96	2.82
χ (1.8 K) [memu $mole^{-1}$]	8.3	8.2	8.6	8.8	9.6	12.7	14.8	18.2	21.4
$T\,(C_{max}/T)$ [K]	13.6	12.6	12.7	12.2	10.8	4.9	—	—	—
$C/T(T \rightarrow 0)$ [mJ $K^{-2}mole^{-1}$]	155[a]	—	180[a]	—	220[b]	380	425	610	740
χ (1.8K)/$\{C/T(T \rightarrow 0)\}$ [memu K^2 mJ^{-1}]	0.054	—	0.048	—	0.044	0.033	0.035	0.030	0.029
S(17K) [mJ K^{-1} $mole^{-1}$]	5600	—	5600	—	5800	6100	6100	6200	6100
T_C^{onset} {from χ_{ac}(K)}[K]	1.78[c]	1.73	1.37	1.33	—	—	—	—	—
$H_C(0)$ [gauss][d]	450	300	430	230	—	—	—	—	—
$-(dH_{C2}/dT)_{Tc}$ [T/K]	0.47	0.23	0.45	0.48	—	—	—	—	—

[a] Sample is superconducting, value given is C/T at 2 K.

[b] Since this sample shows a slight superconducting anomaly in C, $C/T\,(T \rightarrow 0)$ is somewhat smaller than it otherwise would be.

[c] This value, as well as those for all the hydrided samples, is measured on ground powder. For a nonground sample, T_C^{onset} = 1.97 K.

[d] As discussed in, e.g., [Lynton, 1962], $H_C(0)$ is found from $\int_0^{Tc}[S_n(T)-S_s(T)]dT = VH_C(0)^2/8\pi$, is the normal (superconducting) state entropy.

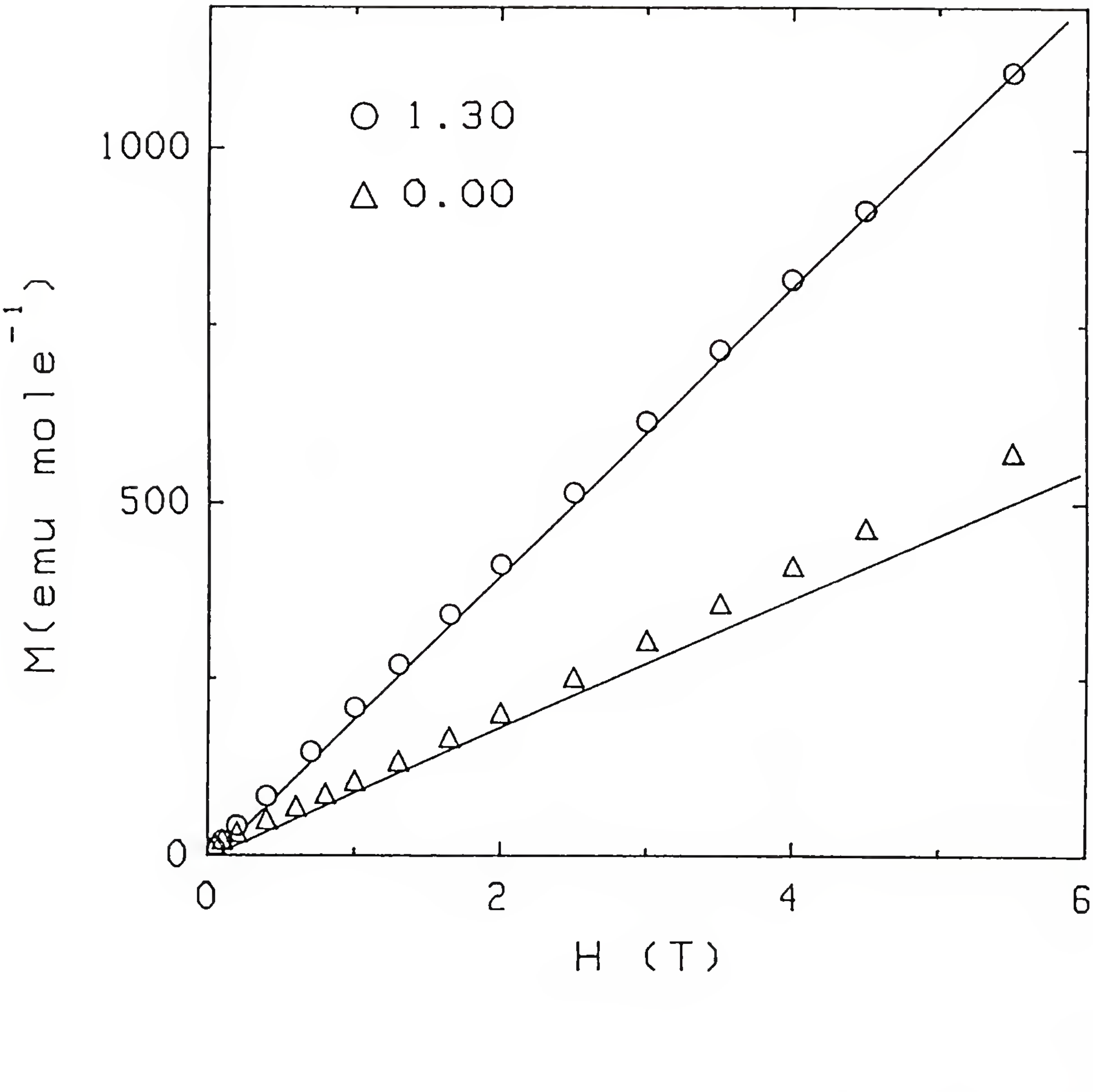

Figure 4-9. Magnetization *M* vs. magnetic field *H* up to 5.5 T for $UPd_2Al_3H_x$ for x = 0 and 1.30 at 1.8 K. The change of slope around 2 T for x = 0 seems to disappear for x = 1.30 up to 5.5 T.

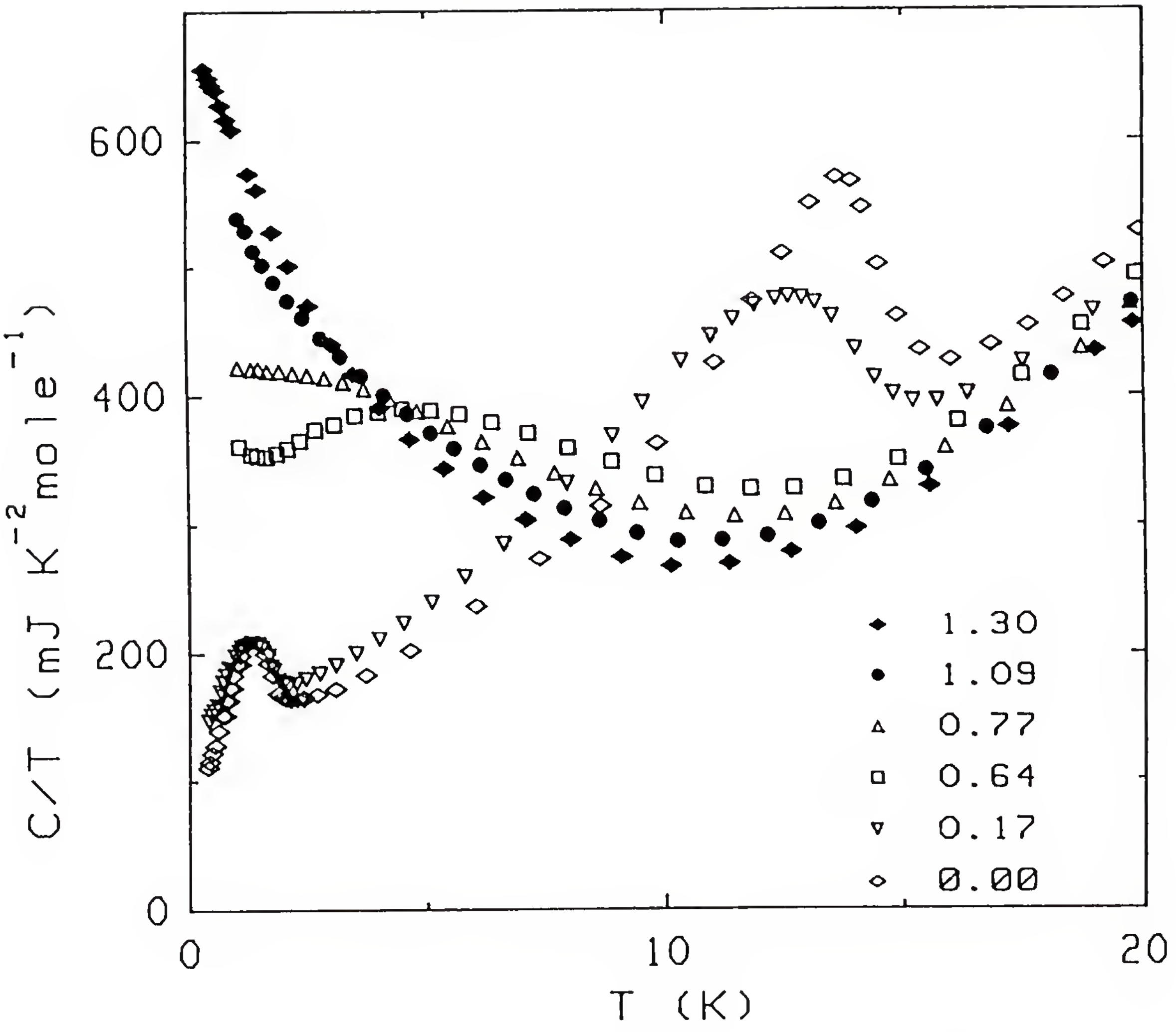

Figure 4-10. Low-temperature specific heat as *C/T* vs. *T* of $UPd_2Al_3H_x$ for $0 \leq x \leq 1.30$ is shown with different symbols for x. For clarity, data for x = 0.13, 0.20, and 0.34 are not shown. Low-*T* data below 1 K were measured only for x = 1.30.

our lowest temperature 0.3 K of measurement. We see in Figure 4-8 that χ at high T decreases and χ at low T increases as we dope more hydrogen. Here we think the smaller effective moment induces a smaller χ at high T, and a larger χ due to the weaker antiferromagnetic correlation at low T.

Effective Mass. One possible explanation for these data is that these increasing values of C/T ($T \rightarrow 0$), Figure 4-10 and Table 4-1, are coupled to the increasing low temperature magnetic susceptibility values through the Wilson ratio χ/γ, i.e., both the increase in χ (1.8 K) and C/T ($T \rightarrow 0$) are due to an increased effective mass, m*. This χ/γ ratio is shown in Table 4-1, and shown graphically in Figure 4-11 in a Fisk plot of γ as a function of χ. It is apparent from these data that the values we observe for $UPd_2Al_3H_X$ approach nicely the Sommerfeld free electron line shown in Figure 4-11, i.e., are consistent with an m* increasing with x interpretation [Kim W.W. and Stewart, 1994].

However, more thorough studies are desirable whether $N(E_F)$ increases or decreases for hydrogen uptake. The XPS data show [Ejima *et al.*, 1994] that the Fermi level resides at the negative slope in the photoelectron intensity vs. energy plot. Thus, $N(E_F)$ will increase if hydrogens take out the electrons from the Fermi level, resulting in a decrease of Fermi energy.

When one considers the low temperature entropies, S, of the samples in Table 4-1, we see that all samples have S (17 K) = 5900 $\mathrm{mJmole^{-1}K^{-1}}$ within 5 %, or about R ln2. For x < 0.7 $UPd_2Al_3H_X$ samples, this entropy (simply the area under the data in Figure 4-10) contains a large contribution from the magnetic anomaly and a small contribution from the γ_o ($\equiv C/T$ as $T \rightarrow 0$) term in the specific heat. As the magnetic anomaly is suppressed, the upturn in *C/T* begins and contributes a growing share of the (essentially) constant entropy. Thus, this consideration of shifting entropy from magnetism to creating a large γ would support the idea that χ/γ remaining approximately constant as x increases is due to an increasing m* simultaneously enhancing χ and γ [Kim W.W. and Stewart, 1994].

Magnetic Correlation. We would like here to describe another possible interpretation to understand the increase of *C/T* and χ at low *T*. We propose a model based on "two electron-subsystems in UPd_2Al_3" (see section 4.2.3) and on the X-ray photoemission spectrum (XPS) of UPd_2Al_3 [Ejima *et al.*, 1994]. We describe the model schematically in Figure 4-12. The total 5f ($5f^T$) electrons consist of localized 5f ($5f^L$) and rather itinerant 5f ($5f^I$) electrons. We define the terminology "localized" and "itinerant" based on the band width as $W_f << W_C$ and $W_f \leq W_C$ respectively, where W_f is the band width of 5f electrons and W_C is the band width of conduction electrons. We assume that the $5f^L$ band is centered around 0.5 eV below the Fermi energy with a narrow band width and the $5f^I$ band is asymmetric with a long tail, and the superposition of those two bands gives the $5f^T$.

Where do the electrons of hydrogen, 1s(H), go? We assume, for the sake of argument, that the 1s(H) electrons reside off the peak of U-5f intensity, e.g., around 5.5 eV below the Fermi energy E_F based on the Photoemission result [Ward *et al.*, 1979] of UD_3 as shown in Figure 4-7 (we already mentioned the isotope effects in section 4.1.4 such that most physical properties due to the isotopes of hydrogen are very similar). We assume, at a low concentration of hydrogen, that perhaps the 1s(H) electrons seem to be centered around 5.5 eV below E_F with a well defined momentum vector (or with a narrow

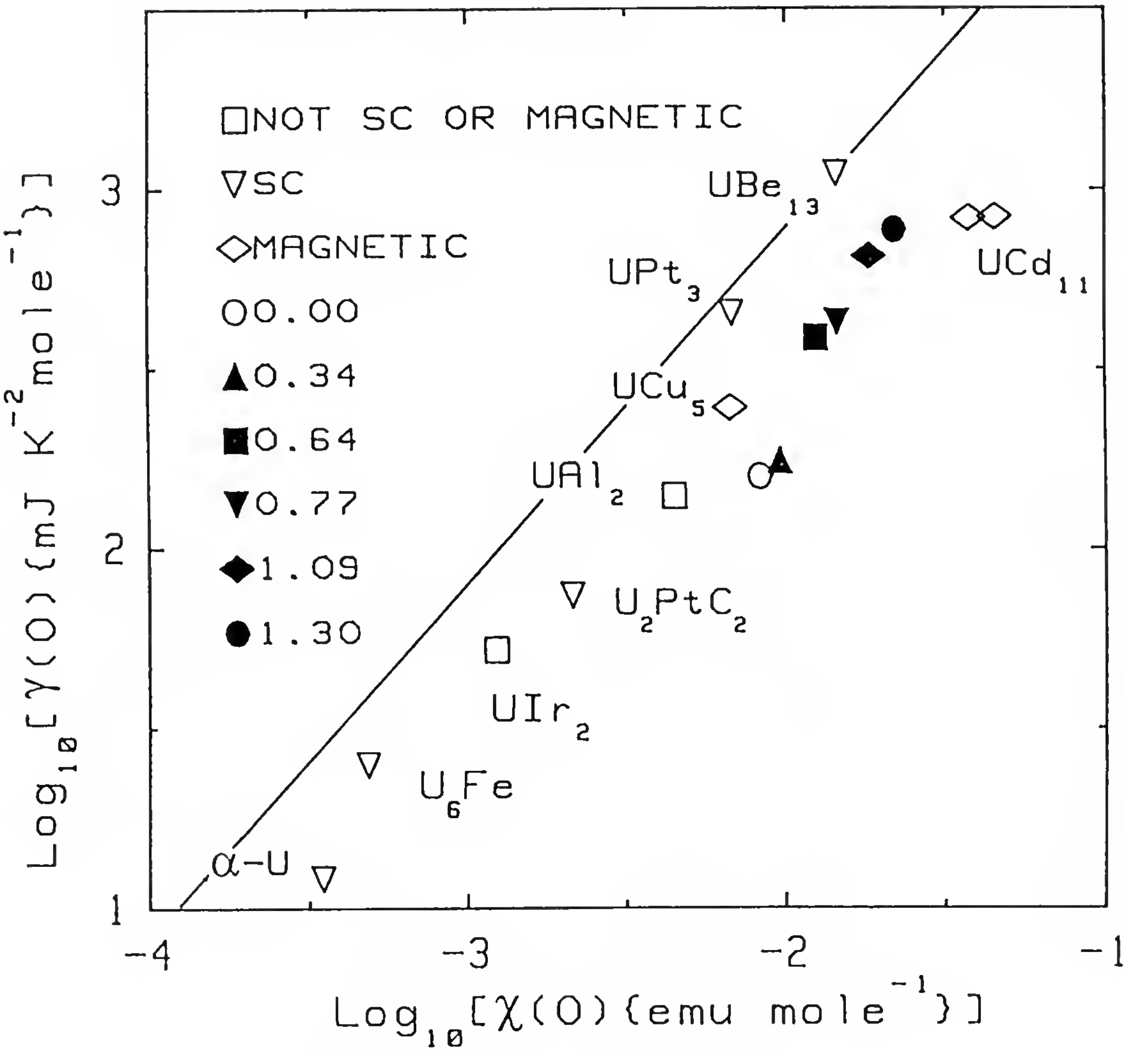

Figure 4-11. γ (≡ C/T as $T \to 0$) vs. magnetic susceptibility χ in a ln-ln plot for a number of heavy systems. The Sommerfeld free-electron line corresponds to superconductivity and the maximum γ possible for a given χ. Note that the systems of $UPd_2Al_3H_X$ for $x \geq 0.64$ exist in the series of magnetic systems.

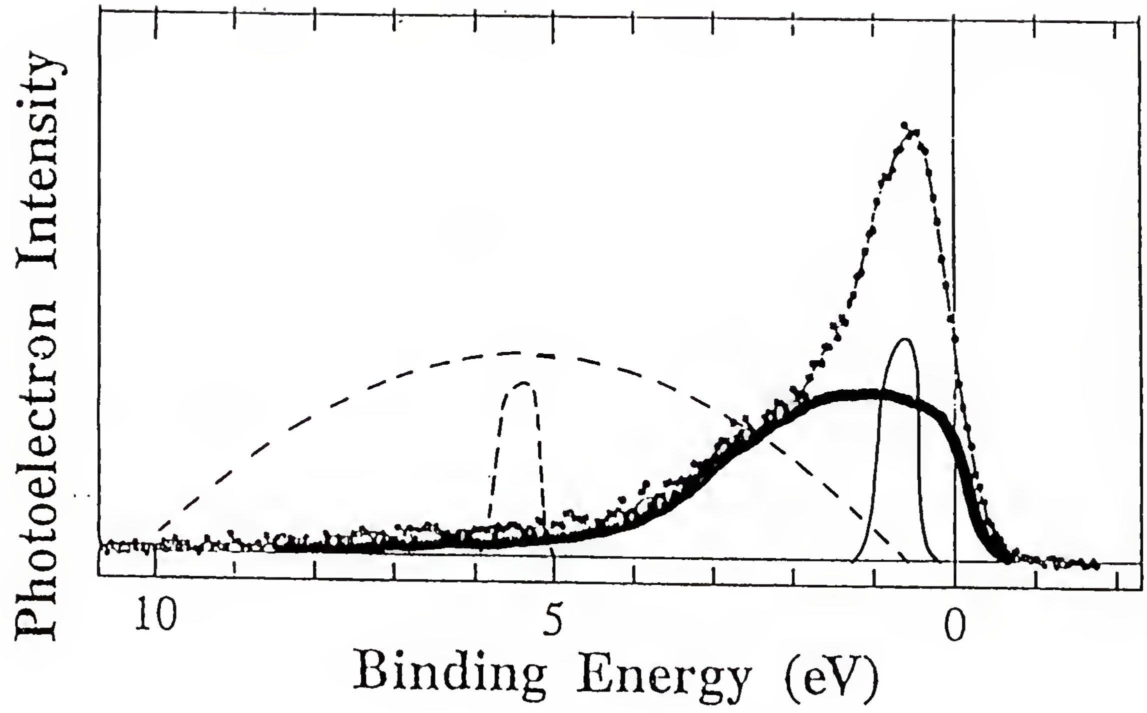

Figure 4-12. The filled circles are data for UPd_2Al_3 from XPS measurement by Ejima *et al.* [1994]. Thin solid line around 0.5 eV represents the intensity of $5f^L$ and thick line is for $5f^1$, see text for details. The superposition of $5f^L$ and $5f^I$ gives the total intensity of 5f electrons, $5f^T$. We assume that for low concentrations (x < 0.4) 1s(H) localizes around 5.5 eV below E_F. For x > 0.4, the shape of intensity of 1s(H) becomes broader and higher around the center 5.5 eV with more hydrogen uptake.

energy band). As we dope more hydrogen, the band width of 1s(H) seems to get broader with increasing the density of states. In other words, at low concentration of hydrogens, the 1s(H) electrons hybridize only with $5f^I$, but hybridize with $5f^L$ at higher concentrations of hydrogen. The critical concentration (C_C), above which 1s(H) begins to hybridize with $5f^L$, seems to be about 0.4~0.5 moles of hydrogen in $UPd_2Al_3H_X$ from the experimental results which we are going to explain below.

Experimental evidence supporting this model are: Firstly, the T_C onset (since we used a pellet out of hydrided powder, there is a broad superconducting transition) and T_N from magnetic susceptibility measurements show that T_C onset decreases 3 times faster than T_N at low concentration of hydrogen. Because the $5f^L$ is responsible for the magnetic correlation, at low concentrations of hydrogen there is much less interaction between 1s(H) and $5f^L$ resulting in the less effect of hydrogen on magnetism; Secondly, when we plot the Curie-Weiss temperature $\theta_{\text{c.w.}}$ vs. hydrogen concentration x, it looks almost constant up to C_C and monotonically or even linearly decreases after an abrupt enhancement of $\theta_{\text{c.w.}}$ happens around C_C, shown in Figure 4-13. Thus it seems to us that the 1s(H) mainly interacts with $5f^I$ for $x < C_C$ and with $5f^L$ for $x > C_C$. Here we use the $\theta_{\text{c.w.}}$, inferred from χ^{-1} vs. T plot, and the Curie-Weiss temperature is considered as a kind of estimation of the intersite magnetic interaction.

We also have measured the low temperature specific heat, $0.3\text{ K} < T \leq 1.4\text{ K}$, in 14 T on our $UPd_2Al_3H_{1.30}$. What we observe is a uniform shift downward by about 20 ~ 25 % of the data with applied field, with C/T (14 T) as $T \rightarrow 0$ equal to 590 $\text{mJmole}^{-1}\text{K}^{-2}$. This result is similar to the results for other known heavy fermion system [Andraka *et al.*, 1989] like non-superconducting $CeCu_2Si_2$ where there has been about 22 % decrease of C/T in 12 T at 2.4 K. It is known [Steglich *et al.*, 1994] that the superconducting state and magnetic "*A*-phase" are always separated in real space in $CeCu_2Si_2$, thus, they do compete with each other. Since the above $CeCu_2Si_2$ sample was non-superconducting in bulk, it seems to have a magnetic "*A*-phase" ground state. Also, the change of C/T in $UPd_2Al_3H_{1.30}$ in the field is much larger than the change observed in, e.g., UBe_{13} which is considered as non-magnetic. A system where it is now believed that magnetic correlations make a significant contribution to C/T at low temperatures, $CeCu_6$, has [Stewart *et al.*, 1988] a much larger (65%) decrease in C/T ($T \rightarrow 0$) in 14.5 T. In Figure 4-11, it is interesting to notice that our hydrides for $x > 0.6$ get into the sequence of magnetic HFS, but stay far away from the nonmagnetic series.

Another possible interpretation of our data is that the hydrogen goes into the lattice inhomogeneously even though we estimated it about 10 % near the surface by an X-ray measurements for $x = 1.30$ (the penetration depth of an X-ray depends on not only the element of a light source but also the material, e.g., mass absorption coefficient and density of the material, on which the X-ray is shed [Cullity, 1978]). The hydrogen simply first broadens out the magnetic anomaly and then, with increasing x, destroys long range order resulting in short range magnetic correlations. Thus, the entropy remains constant, the anomaly in M vs. H is washed out by disorder, χ (1.8 K) and C/T at low temperatures are enhanced by the short range correlations, and are in contrast to $CeCu_6$ not very strongly affected by an applied field.

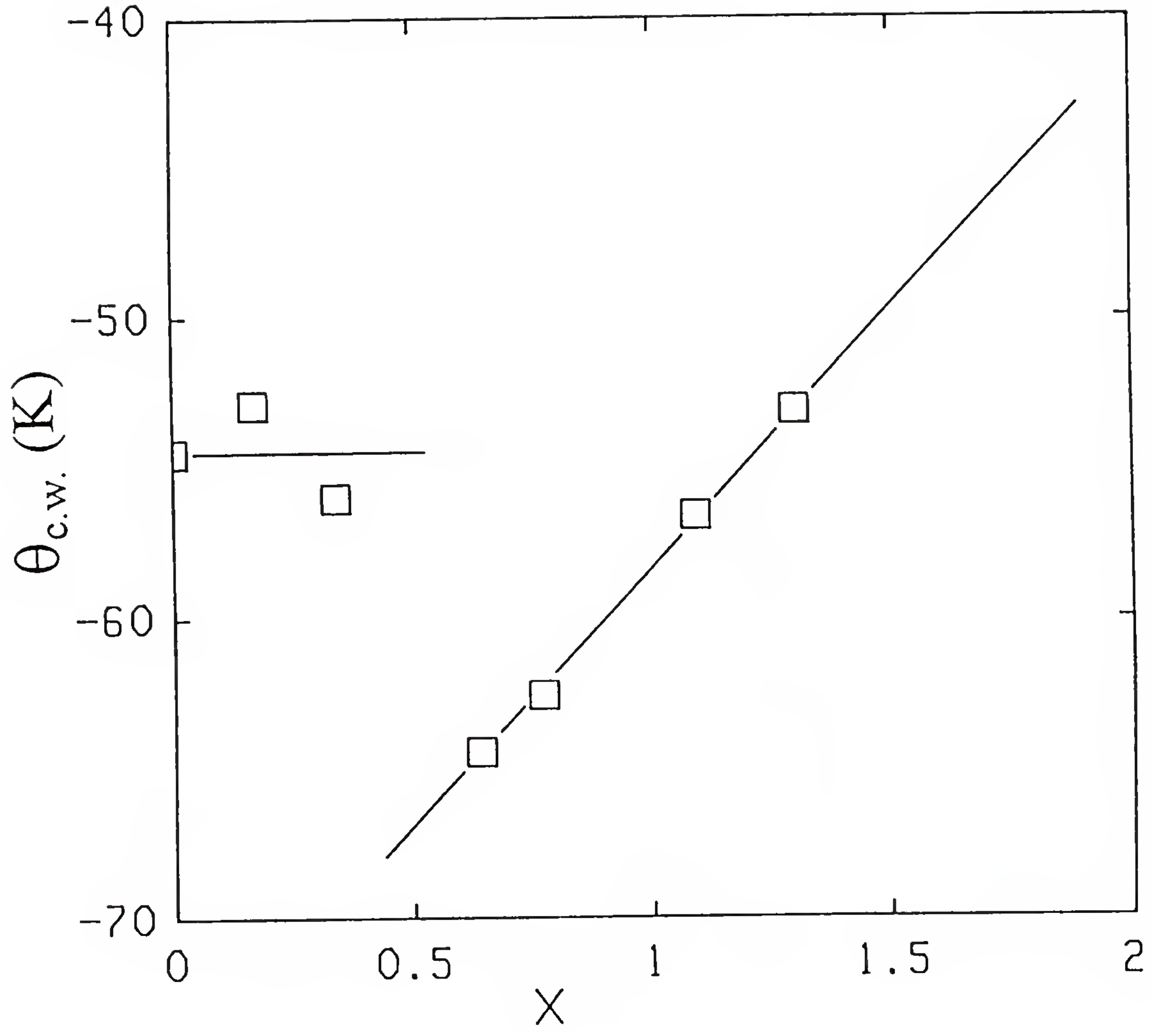

Figure 4-13. Curie-Weiss temperature $\theta_{c.w.}$ vs. concentration x for $UPd_2Al_3H_x$. $\theta_{c.w.}$ is approximately constant for $x < 0.5$ and changes linearly for $x > 0.5$ up to our maximum $x = 1.30$. Note that there seems to be an abrupt change of the magnetic intersite interaction around $x = 0.5$. The lines are guides to the eye.

As we have shown in Figures 4-14 and 4-15, the behavior of χ ($T = 0$) and γ ($T = 0$) vs. hydrogen concentration seems to give a similar trend as we have seen in the $\theta_{\mathrm{C.W.}}$ vs. hydrogen concentration x. Perhaps, the abrupt change of the $\theta_{\mathrm{C.W.}}$ (indicating a change in magnetic correlations) for $x > C_C$ may cause the increase of χ ($T = 0$) and γ ($T = 0$). From this relation, it seems to us that the low temperature behavior (or increase) of C/T and χ with hydrogen concentrations may be more closely related to the magnetic correlations rather than the enhancement of the effective mass.

In order to try to distinguish if the upturn in C/T for our high doped $UPd_2Al_3H_X$ samples is due to magnetic effects or larger m* formation, the neutron scattering experiments with the similar concentration of deuteride $UPd_2Al_3D_X$ (see section 4.1.4) would be an excellent method of resolving whether $UPd_2Al_3H_{1.30}$ is a material with a large effective mass corresponding to a $\gamma > 700$ mJ/mole-K or a system whose properties are dominated by (short) range magnetic correlations. Also M vs. H measurements at low T up to higher magnetic fields than 5.5 T are desirable to resolve the above question.

Crystalline Electric Field Effects. We have seen that the peak in χ of $UPd_2Al_3H_X$ decreases approximately *linearly* with increasing hydrogen uptake. There have been several interpretations about this peak in the host system UPd_2Al_3 [Geibel *et al.*, 1991b]: Firstly, the peak scales with the characteristic temperature T^* for on-site moment compensation in the Kondo lattice, which has been shown [Mignot *et al.*, 1988] nicely in $CeRu_2Si_2$ with varying pressures. We have tried to fit our results based on the scaling temperature T^*, however it was not successful. What we can do is to fit the χ vs. T data with a parameter T^*, i.e., $\chi(T,T^*)$ but no scaling behavior such as $\chi(T/T^*)$ with x [Kim

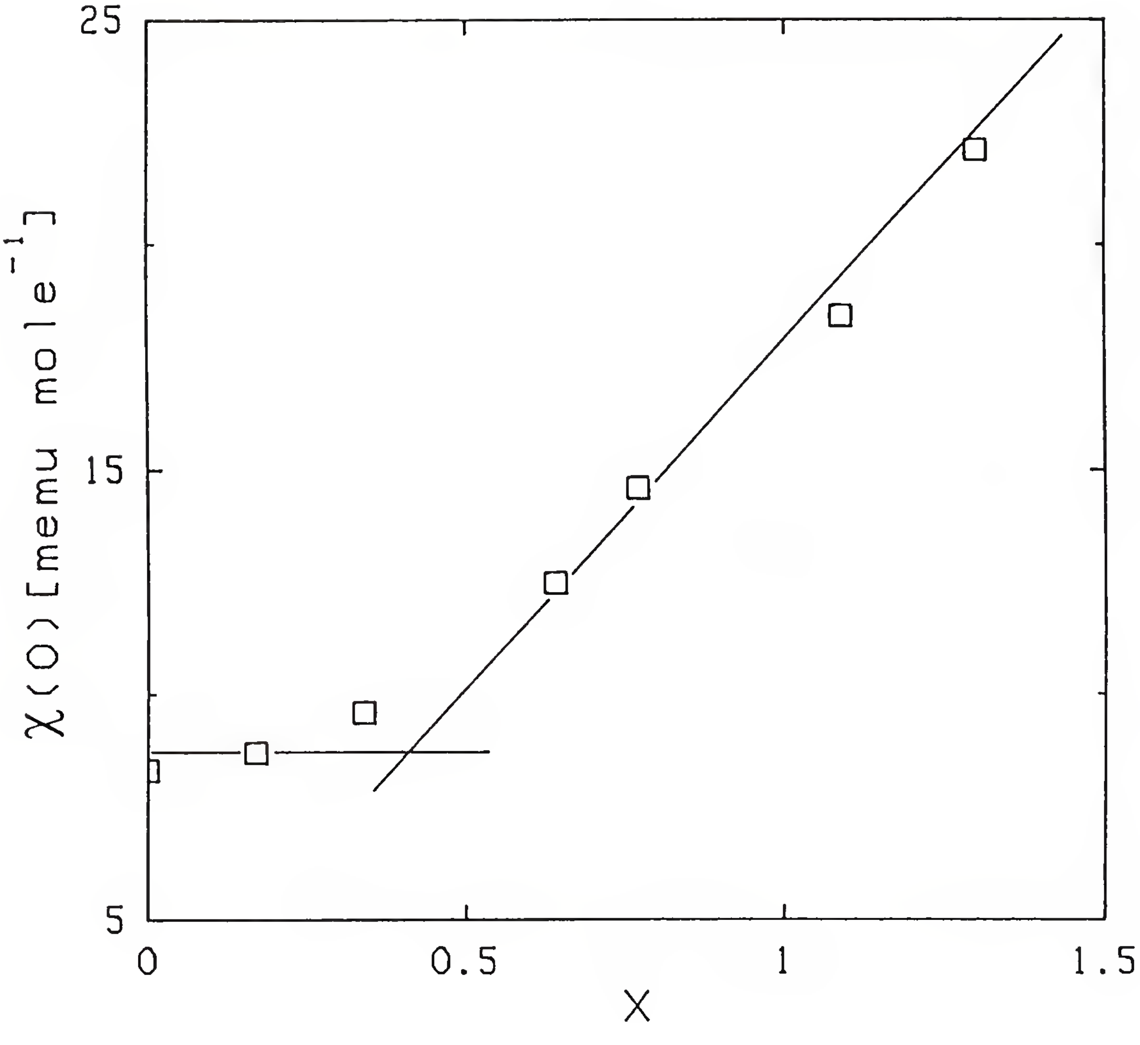

Figure 4-14. Magnetic susceptibility χ (as $T \to 0$) vs. concentration x for $UPd_2Al_3H_x$. χ(0) is approximately constant for x < 0.5 and changes linearly for x > 0.5 up to our maximum x = 1.30.

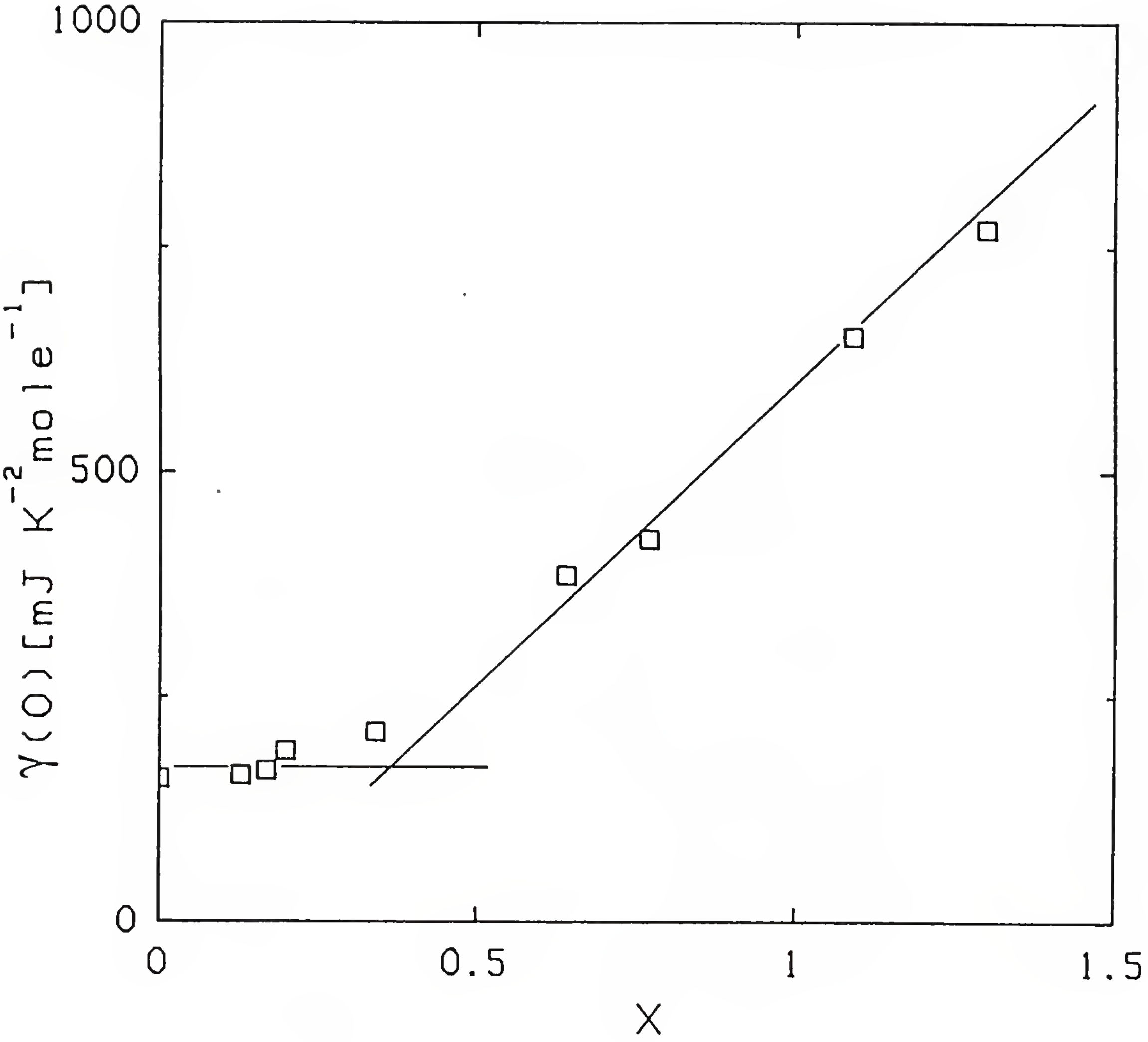

Figure 4-15. γ (C/T as $T \rightarrow 0$) vs. concentration x for $UPd_2Al_3H_x$. γ (0) is approximately constant for x < 0.5 and changes linearly for x > 0.5 up to our maximum x = 1.30.

W.W. and Stewart, 1995]; Secondly, the peak is due to the thermal depopulation of excited CEF levels, e.g., the case of the isostructural 'singlet ground' system $PrNi_5$ [Barthem *et al.*, 1988]. It seems that two low lying singlets in UPd_2Al_3 are probable from the interpretation of several results [Böhm *et al.*, 1993; Geibel *et al.*, 1994], i.e., $5f^2$ or U^{4+}. However the theoretical fitting based on a singlet ground state configuration fails to contain the AFM transition in the specific heat. It has also been claimed in this system that CEF is inversely proportional to the ordered moments at T_N and the intersite interaction of local moments [Schank *et al.*, 1993]. If there is such a proportionality, the peak should increase in our case as we dope more hydrogen, but wesee an opposite result. Thirdly, the peak is due to magnetic short range correlations. This has been applied to similar anomalies in UPt_3 [Franse *et al.*, 1984], URu_2Si_2 [Schlabitz *et al.*, 1986], and $CeRu_2Si_2$ [Mignot *et al.*, 1988]. It may be further supported by the magnetic field dependence of the peak in $UPd_2Al_3H_X$ for $x < 0.8$. For instance, as shown in Figure 4-16 for $x = 0.64$, the peak monotonically decreases to lower temperature and the magnitude of χ at the same T increases as we increase the magnetic field. It seems to us that the field destroys the (antiferro-) magnetic short range correlations giving rise to the above phenomena.

Non-Fermi Liquid Behavior. There has been reported [Kim W.W. *et al.*, 1993; Maple *et al.*, 1995] non-Fermi liquid behavior in doping experiments on UPd_2Al_3, particularly with Th on the U-site. Interesting trend in our hydrided system is, as we dope more hydrogen, that the hydrided system approaches the characteristics of non-Fermi liquid behavior (see Figures 4-17 and 4-18). We think the ln T dependence of $\Delta C/T$ and $-T^{1/2}$ dependence of χ can be achieved at low temperatures by charging more hydrogen.

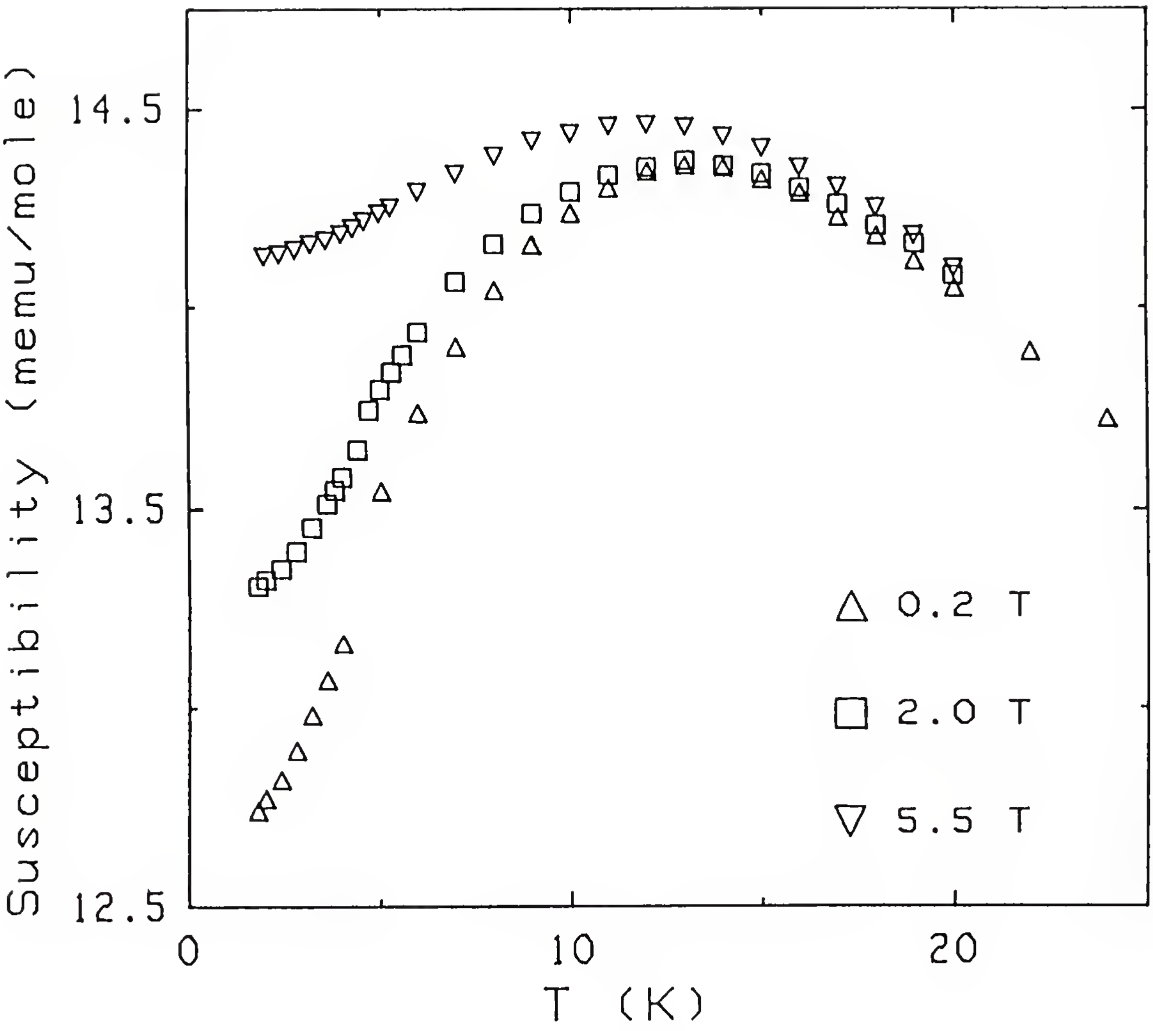

Figure 4-16. Magnetic susceptibility χ vs. temperature *T* for $UPd_2Al_3H_{0.64}$ in magnetic field. Note the enhancement of χ at low *T* and the shift to low *T* of the peak.

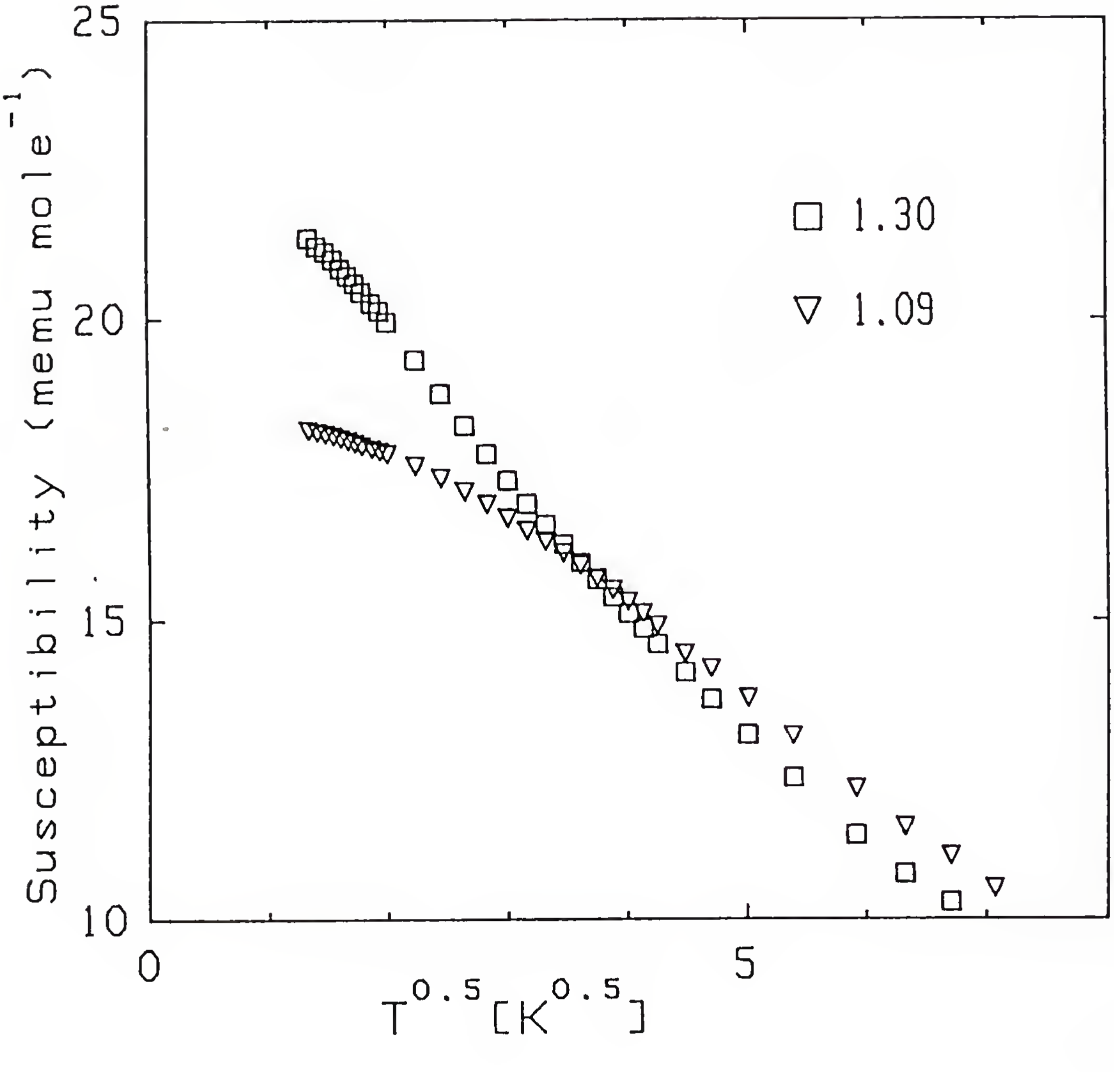

Figure 4-17. Magnetic susceptibility χ vs. $T^{1/2}$ of $UPd_2Al_3H_X$ for x = 1.09 and 1.30. As we increase x, χ approaches non-Fermi liquid behavior indicating a divergence of χ at low T.

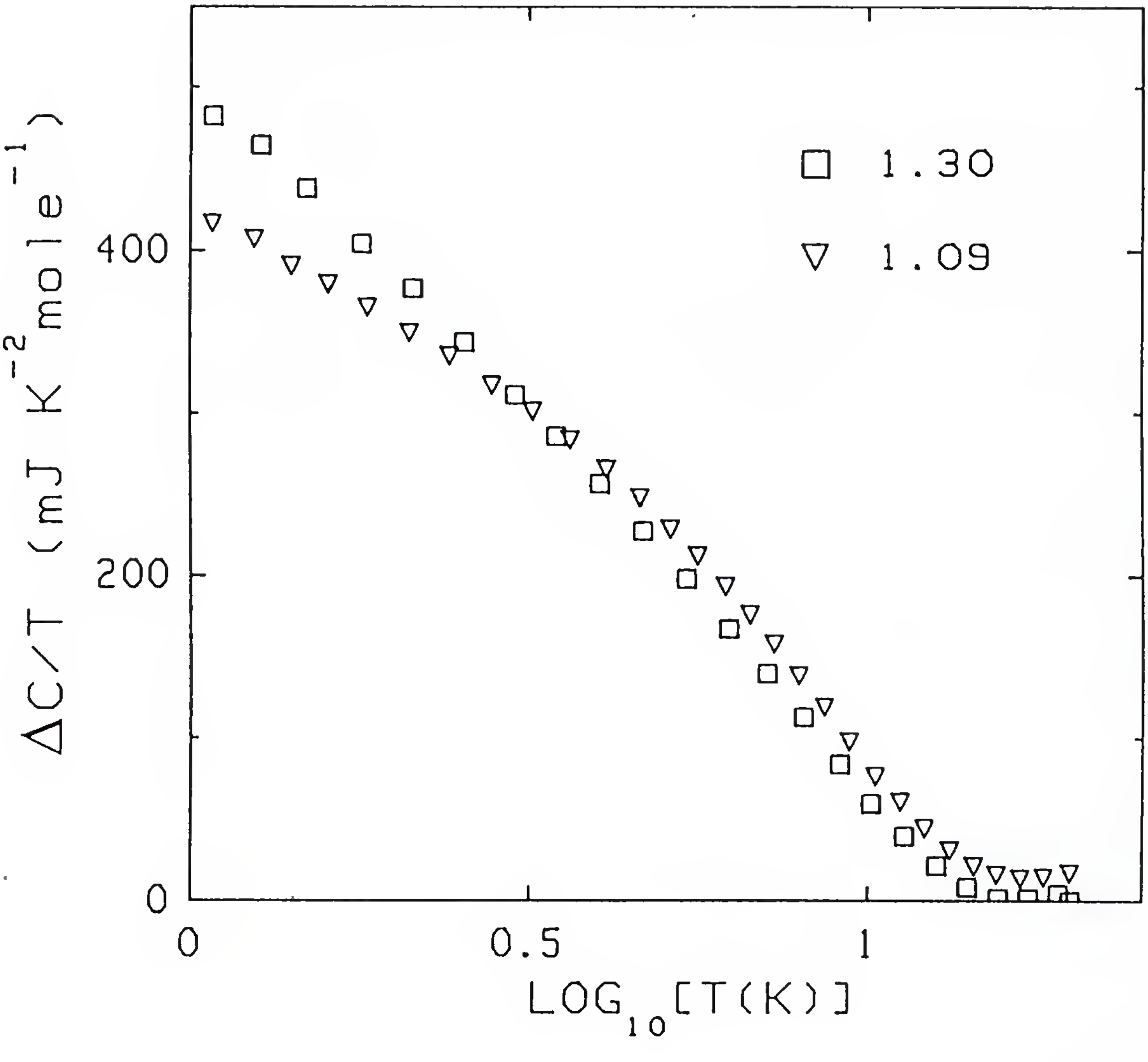

Figure 4-18. 5f electronic contribution to specific heat divided by *T*, *ΔC/T*, vs. ln *T* of $UPd_2Al_3H_X$ for x = 1.09 and 1.30. As we increase x, *ΔC/T* approaches non-Fermi liquid behavior indicating its divergence in the ln *T* scale for *T* → 0. We subtract the electronic and phonon contribution from the total specific heat resulting in *ΔC* after measuring the specific heat of $ThPd_2Al_3$.

Thus, we are now exerting much effort to increase the hydrogen concentration higher than 1.30 to check this idea by paying attention especially to developing the passivation method at higher temperatures with CO_2. If we succeed in keeping more hydrogen in $UPd_2Al_3H_X$, it then will be interesting to elucidate the ground state of the hydrided system to find out what causes non-Fermi-liquid-like behavior.

4.5.2.2 Superconducting state

As may be seen in Figures 4-10 and 4-19, hydrogen suppresses the SC of UPd_2Al_3 and causes broader transition. A more sensitive measurement technique is that of ac susceptibility χ_{ac}, even though it measures T_C onset and is not a bulk measurement. Superconducting onset transition temperatures so determined are shown in Table 4-1, where the data T_C^{onset} = 1.73 K for the x = 0.13 sample, 1.37 K for x = 0.17, and 1.33 K for x = 0.20 show a good deal of scatter. This scatter carries over into our determination of other superconducting parameters, see the thermodynamic critical field, $T_C(0)$, data [Cort *et al.*, 1981] and the critical field slope at T_C data in Table 4-1.

Thus, we can only say that hydrogen depresses T_C by 20 mK/%H at low concentration of hydrogen. As we mentioned in the section 4.5.2.1, it seems to us that some possible interpretations of the depression of superconductivity are: firstly, the pair breaking of 5f electrons due to newly introduced 1s(H); secondly new creation of scattering centers due to the interstitial hydrogen proton.

More exact determinations of these and related parameters such as coherence length ξ_o must await achieving a more monotonic set of behavior as a function of x for

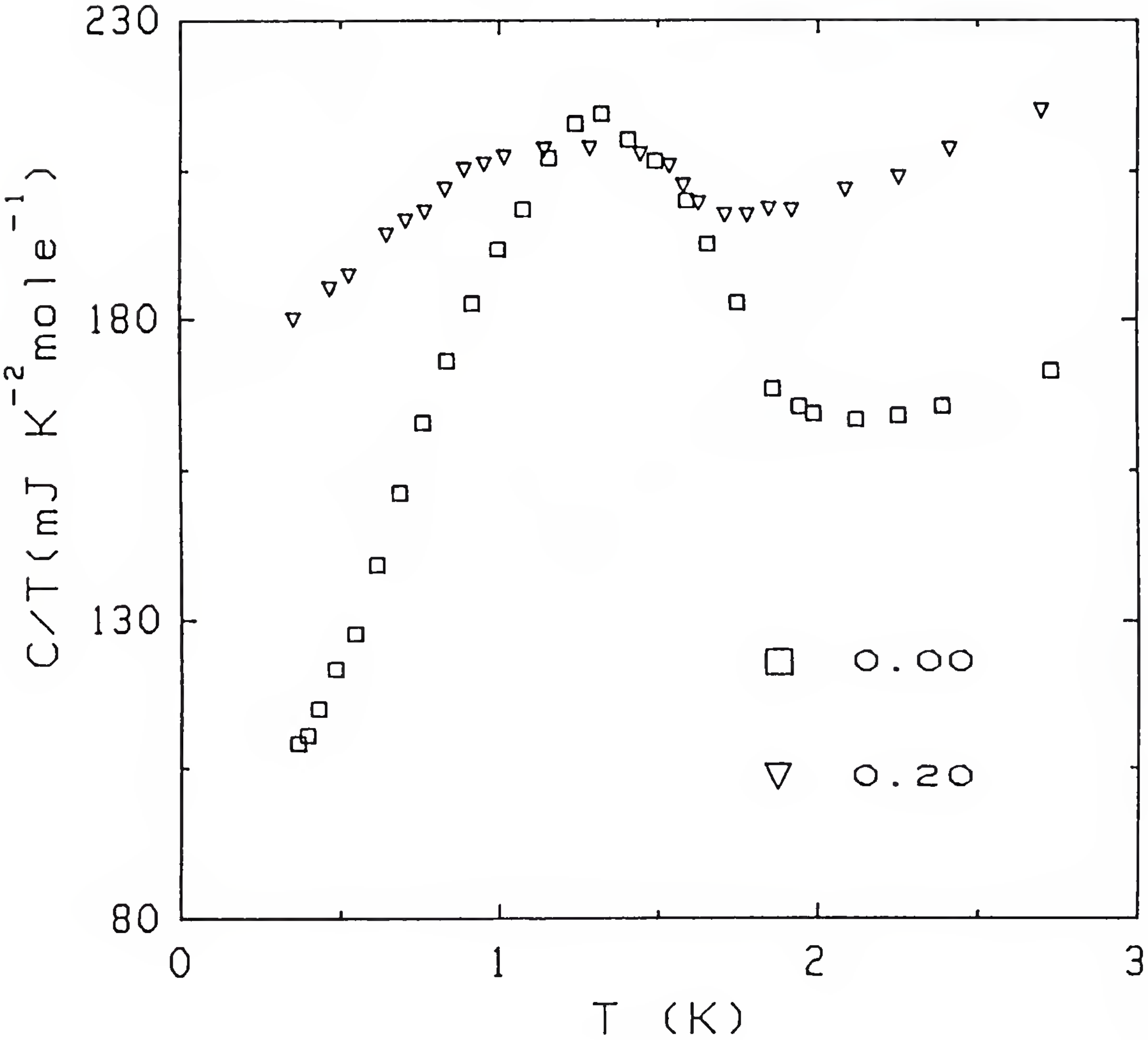

Figure 4-19. Specific heat of $UPd_2Al_3H_X$ as *C/T* vs. *T* at low temperatures. The T_C^{onset} and ΔC at T_C^{onset} are suppressed and a broader anomaly in the specific heat bump has been found for higher concentration x.

low doping levels. Although annealing of the ground powder before hydriding will make some improvement, the real key to narrower superconducting transitions and lower scatter in the measured superconducting parameters probably lies in the method of hydriding. Dehydriding the samples from x = 1.30 down to x = 0.13 will intrinsically cause inhomogeneity possibly due to an inhomogeneous distribution of temperature in hydridewhen we heat the hydride. Thus, hydriding at lower pressures to have a low concentrations of samples after a full activation, and remaining for a long period at one pressure on the x vs. P_{H2} slope (even though it is very steep) should lead to better homogeneity for each low concentration. Another possible way in the future to increase the homogeneity can be firstly to find a temperature T_{mis} above which there is no miscibility gap in concentration (see Figure 4-1), then hydride the activated sample followed by poisoning the surface of the hydride at $T > T_{mis}$ (however, there is a limitation in maximum concentration we can get, because the equilibrium pressure of hydrogen becomes higher as we increase T).

In summary, we have several distinctive effects of hydrogen on UPd_2Al_3 in the normal state. Firstly, we found that the shift of the peak in χ to lower temperatures for hydrogen uptake can be used as a calibration for x < 1.0 to know the hydrogen concentration in this hydride. Secondly, both the increase in both $\chi(0)$ and $\gamma(0)$ with hydrogen uptake and the Sommerfeld free-electron behavior of these in the Fisk plot seem to suggest that the increase in both $\chi(0)$ and $\gamma(0)$ is due to the enhancement of the effective mass m*. Thirdly, magnetic correlations are proposed as a possible origin of the behavior in both $\chi(0)$ and $\gamma(0)$ based on the observed relations among $\theta_{C.W.}$, $\chi(0)$, and $\gamma(0)$

with hydrogen doping. $\theta_{\mathrm{c.w.}}$, $\chi(0)$, and $\gamma(0)$ are relatively constant for hydrogen concentration $x < C_C$ implying that there is no change in the magnetic intersite correlations. The approximately linear enhancement of $\chi(0)$ and $\gamma(0)$ for $x > C_C$ seems to originate from a change of the magnetic intersite correlations, which is observed from the abrupt change of $\theta_{\mathrm{c.w.}}$ inferred from χ measurements. Fourthly, we can understand the dependence of $\theta_{\mathrm{c.w.}}$, $\chi(0)$, and $\gamma(0)$ on the critical concentration C_C in terms of the model of the so called two electron-subsystems in UPd_2Al_3, where we assumed that $5f^T$ is a superposition of $5f^L$ and $5f^1$ and the central position of the 1s(H) having a well defined momentum was off from the central position of $5f^L$. Fifthly, the peak in χ for UPd_2Al_3 seems to be due to short range magnetic correlations as evidenced by the decrease of the peak for hydrogen uptake in χ measurements with increasing magnetic fields. Lastly, as we dope more hydrogen into UPd_2Al_3, the hydrided system seems to approach the NFL regime. Thus, it is desirable to find out what the ground state is in the more hydrided system ($x > 1.30$) to answer the origin of not only the NFL behavior in this hydrided systems but also of the enhancement in both $\chi(0)$ and $\gamma(0)$.

For SC, the data are not as reliable as that in the normal state because of the broadening of the transition temperature. Perhaps, the observed T_C decrease for hydrogen uptake may be explained by the pair breaking of 5f electrons due to newly introduced 1s(H) and new creation of scattering centers due to the interstitial hydrogen proton.

CHAPTER 5
SUMMARY AND CONCLUSIONS

In this chapter we summarize the results from Chapters 3 and 4 , then give conclusions. The first and second parts deal with the NFL behavior and its origin in $U_XTh_{1-X}Ru_2Si_2$ for $0.07 \leq x \leq 0.17$ and $U_{0.9}M_{0.1}Ni_2Al_3$ (M = Y, Th, and Pr), respectively. The third part covers the effects of hydrogen on UPd_2Al_3. We also discuss future studies which would help us to understand those systems further.

5.1 $U_XTh_{1-X}Ru_2Si_2$ for $0.07 \leq x \leq 0.17$

Earlier work in URu_2Si_2 and its doped system by other groups was reviewed in Sections 3.2.1 and 3.2.2, respectively. The NFL behavior observed by Amitsuka and Sakakibara in $U_XTh_{1-X}Ru_2Si_2$ for $x \leq 0.07$ was summarized in Section 3.2.3 along with their new interpretation of the ground state being a magnetic doublet rather than a nonmagnetic doublet.

In Section 3.2.4, we observed T_A in ρ measurements (see Figure 3-3), below which the intersite interactions between local magnetic moments occur in $U_XTh_{1-X}Ru_2Si_2$ for $0.1 \leq x \leq 0.17$ at low temperatures of $T < 2$ K. Also, the monotonic increase of resistivity with temperature for $0.3\text{ K} < T < 20\text{K}$ for $0.01 \leq x \leq 0.17$ and the anomaly at T_A for $0.1 \leq x \leq 0.17$ contradicts the single-site TCKE interpretation, instead implying correlated scattering or the onset of coherence.

From the specific heat measurements in $U_XTh_{1-X}Ru_2Si_2$ for $0.07 \le x \le 0.17$, we basically observed a ln T dependence of C_{5f}/T implying the NFL behavior. For x = 0.07 the ln T dependence of C_{5f}/T is limited to one decade in temperature. The temperature dependence expands for more U concentrations and exhibits a weak saturation from the ln T behavior for $0.14 \le x \le 0.17$ indicating intersite correlations (see Figure 3-5). The decrease of T_K with decreasing concentrations for $0.07 \le x \le 0.17$ as shown in Table 3-1, where intersite correlations are dominant over the on-site interactions as evidenced by the behavior of T_{RKKY} and T_K in Doniac's phase diagram (see Figure 3-7) and the existence of T_A in the ρ measurements, implies that T_{RKKY} is still dominant over T_K as we decrease x further. Also, the specific heat decreased monotonically for increasing fields. Subsequently these systems seem to transform from the magnetic intersite correlation regime to the Fermi liquid regime, where a single-site interaction is induced, in high magnetic field, e.g., observed in $U_{0.1}Th_{0.9}Ru_2Si_2$ at H = 14 T (see Figure 3-6) caused by the destruction of the weak intersite interactions between local magnetic moments. For only x = 0.14, we obtained the relation $T_A \approx 3\ T_a$, where there is a peak anomaly in C/T at T_a.

From χ_{dc} measurements, we observed a spin glass anomaly for $0.07 \le x \le 0.17$ in the FC and ZFC measurements (see Figure 3-8) using the polycrystalline samples. For some concentrations, the ZFC χ flattens at low temperatures below around 3 K indicating a possibility of an anomaly (may be due to intersite correlation) for $T < 1.8$ K.

As a future work, the confirmation of the possible relation between T_m and T_A, i.e., $T_A \approx 3T_m$ using single crystalline samples is desirable to determine the origin of T_m and the logarithmic behavior of $U_{0.01}Th_{0.99}Ru_2Si_2$ in χ. Also, it is desirable to measure specific heat and magnetization at several fields to check the scaling behavior in this system.

5.2 $U_{1-x}M_xNi_2Al_3$ {M = Th, Pr, and Y}

Earlier work in UNi_2Al_3 by other groups was reviewed in Section 3.3.1. In Section 3.3.2, we discussed doping experiments on UNi_2Al_3 with Pr, Th, La, Ce, and Y on the U-site. A diverging behavior for $U_{0.9}M_{0.1}Ni_2Al_3$ (M = Th, Pr, La, and Y) at low temperatures was exhibited in C/T down to 0.3 K (see Figure 3-15) and in χ down to 1.8 K. We found the new system $U_{0.9}M_{0.1}Ni_2Al_3$ (M = Th, Pr, and Y) which exhibits the NFL behavior in thermodynamic, transport, and magnetic properties. The ln T dependence of C_{5f}/T is observed in the system (see Figure 3-16), and we were able to get T_K as 77, 69, and 53 K for the 10 % Pr, Th, and Y doped samples respectively when we applied the TCKE model to the specific heat data. The $T^{1/2}$ (Th and Pr doped ones) and ln T (Y doped one) dependencies in χ were observed as shown in Figures 3-19 and 3-20, and the different behavior seems to be due to the atomic size of the dopants.

The linear T dependence of the resistivity in the nonmagnetic Th- and Y-doped systems at least for $1.0 \text{ K} \leq T \leq 20$ was found as shown in Figure 3-21, while the Pr-doped sample exhibited the same behavior in a less wide range which may be related to the magnetic nature of Pr. Also, the monotonic increase of resistivity with temperature (at least for $0.3 \text{ K} < T \leq 20$ K) along with the mentioned linearity of ρ can not be explained by the single-ion TCKE, but rather seems to be related to the onset of coherence and the correlated scattering at low temperatures.

Also, it is unlikely that one expects the TCKE as an origin of the NFL behavior in the U-concentrated systems (90 % of U). There is little magnetic field dependence (2 % *suppression* at 14 T and at 1 K— there should be about an order of one increase of C/T in such a field according to the theory) observed in the Th 10 % sample, even though the data can be fitted to the theory in the specific heat and magnetic susceptibility measurements. The broad upturn above T_N in the parent system and the change of T_N without the broadening of the AFM transition , e.g., in $U_{1-X}Th_XNi_2Al_3$ for $x \leq 0.005$ (see Figure 3-22), may rule out the possibility of the disorder interpretation as an origin of the NFL behavior. The NFL behavior observed in $U_{0.9}M_{0.1}Ni_2Al_3$ (M = Th, Pr, and Y) did not follow the scaling properties as discussed in section 2.2.2, which were suggested as an evidence of a long range magnetic phase transition at $T = 0$ K. However, the fact that the NFL behavior follows the destruction of magnetic order observed in the specific heat measurements (see Figure 3-22) seems to tell us that the NFL behavior may be due to the proximity to magnetic instability. In other words, the doping makes the magnetic parent system approach a critical point, where a Kondo-compensated nonmagnetic state and the long range magnetic order are nearly degenerate.

5.3 $UPd_2Al_3H_X$

We reviewed some basic physics of hydrided systems in Section 4.1 while keeping in mind the electronic and magnetic properties of those systems. After we discussed the work of other groups in UPd_2Al_3 in Section 4.2, we described the experimental apparatus (see Figure 4.6) of our hydriding system in Section 4.3. The activation and poisoning (or passivation) of our sample were emphasized in Section 4.4. Before we discussed the hydrogen effects on our system, we briefly summarized the hydrogen effects on U (for the sake of a possible argument) to understand the hydride of the compound in Section 4.5.1.

We have several distinctive effects of hydrogen on UPd_2Al_3 in the normal state as shown in Figures 4-8 and 4-10. Hydrogen doping depressed the AFM transition and enhanced both $\chi(0)$ and $\gamma(0)$.

Firstly, we found that the approximately linear shift of the peak in χ to lower temperatures for hydrogen uptake can be used as a calibration for $x < 1.0$ to find out the hydrogen concentration in this hydride.

Secondly, the increase in both $\chi(0)$ and $\gamma(0)$ along with the decrease of μ_{eff} for more hydrogen uptake, being combined with the Sommerfeld free-electron behavior of these physical values in the Fisk plot (see Figure 4-11), seemed to suggest that the increase in both $\chi(0)$ and $\gamma(0)$ is due to the enhancement of the effective mass by hybridization between 5f and 1s(H) electrons added to the Fermi level.

Thirdly, magnetic correlations are proposed as a possible origin of the coupled behavior in both $\chi(0)$ and $\gamma(0)$ based on the observed relations in $\theta_{C.W.}$, $\chi(0)$, and $\gamma(0)$ for hydrogen doping. $\theta_{C.W.}$, $\chi(0)$, and $\gamma(0)$ are relatively constant for hydrogen concentration $x < C_C$ implying that there is little change in the magnetic intersite correlations. The enhancement of $\chi(0)$ and $\gamma(0)$ for $x > C_C$ seems to originate from a change of the magnetic intersite correlations which was observed from the abrupt change of $\theta_{C.W.}$ inferred from χ measurements for $x > C_C$, see Figures 4-13, 4-14, and 4-15. About a 25 % decrease in *C/T* at 14 T for $x = 1.30$ as well as the positions of the hydrides for $0.64 \leq x \leq 1.30$ in the

Fisk plot (see Figure 4-11) may support the magnetic correlation hypothesis in the hydrides with a high concentration of hydrogen. Also, short magnetic correlations in the hydrides are suggested based on not only the inhomogeneity of the system, but also the decrease of the peak position in χ along with the increase of χ below the peak for increasing field (see Figure 4-16).

Fourthly, as we dope more hydrogen into UPd_2Al_3, the hydrided system seems to approach the NFL regime. Thus, it is desirable to find out what the ground state is in the more hydrided system ($x > 1.30$) to discover the origin of both the NFL behavior in this hydrided systems and of the enhancement in both $\chi(0)$ and $\gamma(0)$.

For the superconducting state, the data are not as reliable as that in the normal state because of the broadening of the transition temperature. The observed decrease of T_C for hydrogen uptake can be explained by the creation of the scattering center due to the interstitial hydrogen proton.

Several experimental measurements including XPS and neutron scattering are desirable to understand the hydrided system $UPd_2Al_3H_X$. Also, we need to improve the homogeneity of the hydrided sample, and increase the maximum concentration of hydrogen by improving the poisoning method to give an answer to the possible origin of the NFL behavior. As we described in the Appendix, there are several possible HFS which we can study with this hydrogen doping technique to understand the parent systems and even induce a new ground state. We hope our work becomes a starting point in a new field of study in HFS.

APPENDIX
PRELIMINARY RESULTS OF $UNi_2Al_3H_X$, $CeCu_{2.2}Si_2H_X$, AND UPt_3H_X ; WORK FOR THE FUTURE

We have tried to investigate hydrogen effects on several heavy fermion systems including the systems in Chapter 4. Although not all systems we tried showed a possible hydrogenation, some did indicate the hydrogen effects in our experimental conditions. Therefore, in this chapter, we would like to display preliminary experimental data on $UNi_2Al_3H_X$, $CeCu_{2.2}Si_2H_X$, and UPt_3H_X with short comments to stimulate other physicists, who may have an insight or interest in this newly developing area.

A.1 $UNi_2Al_3H_X$

Since we have seen more or less consistent hydrogen effects on $UPd_2Al_3H_X$, we expected to find another hydriding system in $UNi_2Al_3H_X$, because both parent systems have the same crystalline structure of hexagonal $PrNi_2Al_3$. The X-ray results of the lattice parameters show changes of about –0.15 % along the c-axis and +0.19 % along the *a*-axis. The corresponding concentration of hydrogen is 0.39 within ±5 % from measurements of the pressure change.

We display *C/T* vs. *T* of $UNi_2Al_3H_X$ for x = 0.0, 0.22, 0.30, and 0.39 in Figure A-1. Even though the low temperature magnetic transition is broadened with hydrogen doping, we clearly see the peak of the transition decreases with more hydrogen uptake. For x = 0

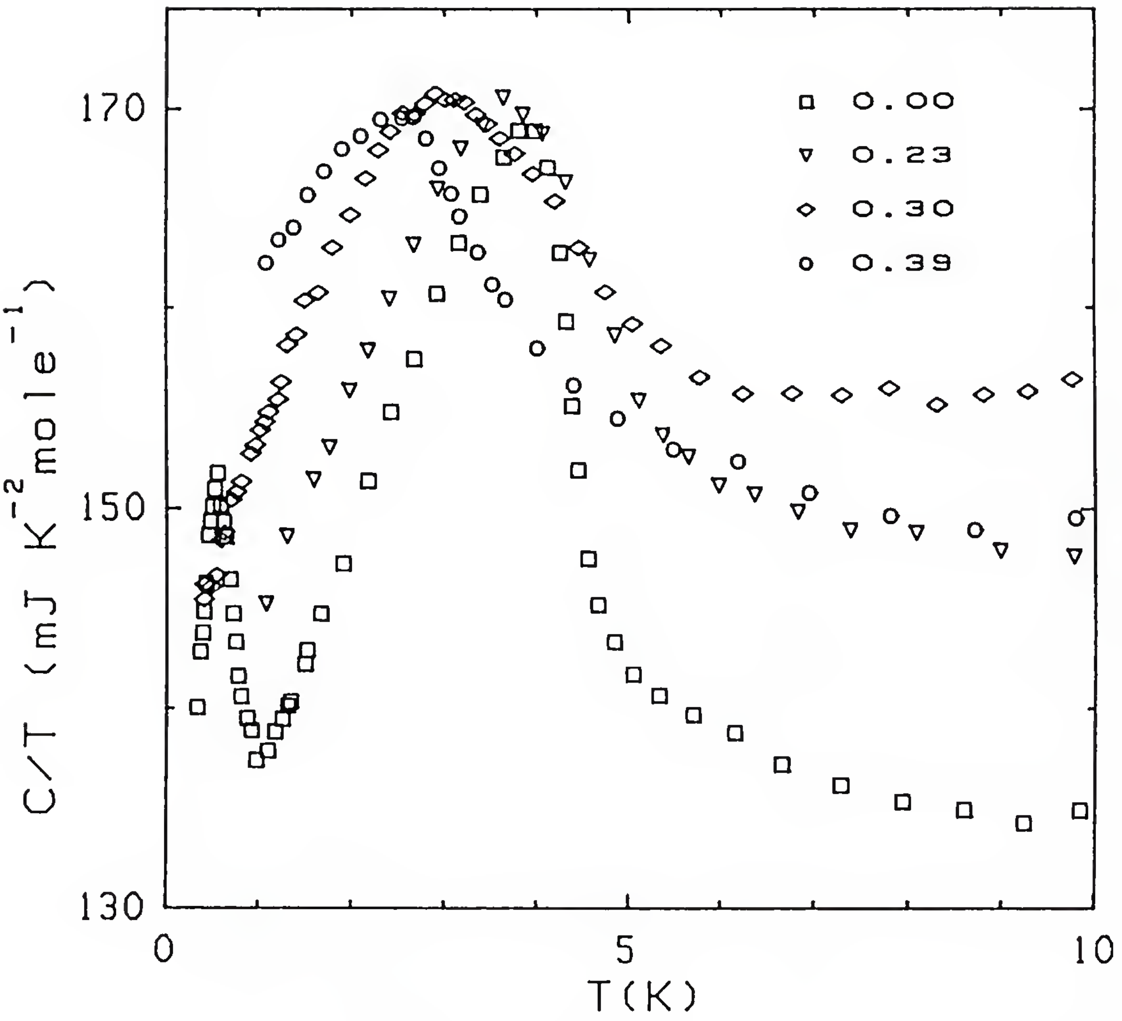

Figure A-1. Specific heat of $UNi_2Al_3H_x$ as C/T vs. T with x = 0.0 (chunk), 0.23 (pellet), 0.30 (pellet), and 0.39 (pellet) for 0.3 K ≤ T ≤ 10 K. The position of peak anomaly in the pellet for x = 0.0 (not shown) is same as that of the chunk with a broadened transition width. The negative slope for T > 6 K is suppressed as we dope with hydrogen.

(chunk), we found a broad superconducting transition from magnetic ac susceptibility, χ_{ac}, measurements down to 0.3 K, while we see a distinct anomaly at the same transition from the specific heat measurements. There is no bulk superconducting transition from specific heat measurements for x = 0.30 down to the lowest temperature of 0.3 K we can reach, shown in Figure A-1. However, the onset of T_C, T_c^{onset}, is about 0.67 K from χ_{ac} measurements.

In Figure A-2, we display magnetic dc susceptibility, χ_{dc}, as a function of temperature for x = 0.30 in different magnetic fields. First of all, the peak of T_N decreases for more hydrogen uptake as was observed from the specific heat results. Thus, we see that hydrogen in $UNi_2Al_3H_X$ depresses magnetic correlations as it does in the homologue system $UPd_2Al_3H_X$. Also, the high temperature anomaly at around 100 K for the parent system shifts to low temperatures with a discontinuous change of slope in χ_{dc} vs. T at 100 K for a magnetic field of H = 0.1 T. We at this point are not sure whether the abrupt change of slope is intrinsic or just an inhomogeneity of hydrogen doping for x = 0.30.

We applied magnetic fields to see any field induced change in both anomalies at low and high temperatures. For x = 0.3, the peak at low temperature, T_N^{peak}, increases from 3.8 K (at H = 0.1 T) to 4.5 K (at H = 5.5 T). The high temperature peak, T_h^{peak}, also increases with increasing magnetic field (however, we do not see any magnetic field dependence of the T_N^{peak} and T_h^{peak} for the parent system up to H = 5.5 T). It is interesting to note that hydrogen destroys the AFM order, however it is recovered by increasing magnetic fields as also observed in T_h^{peak}. In contrast, we have seen suppression

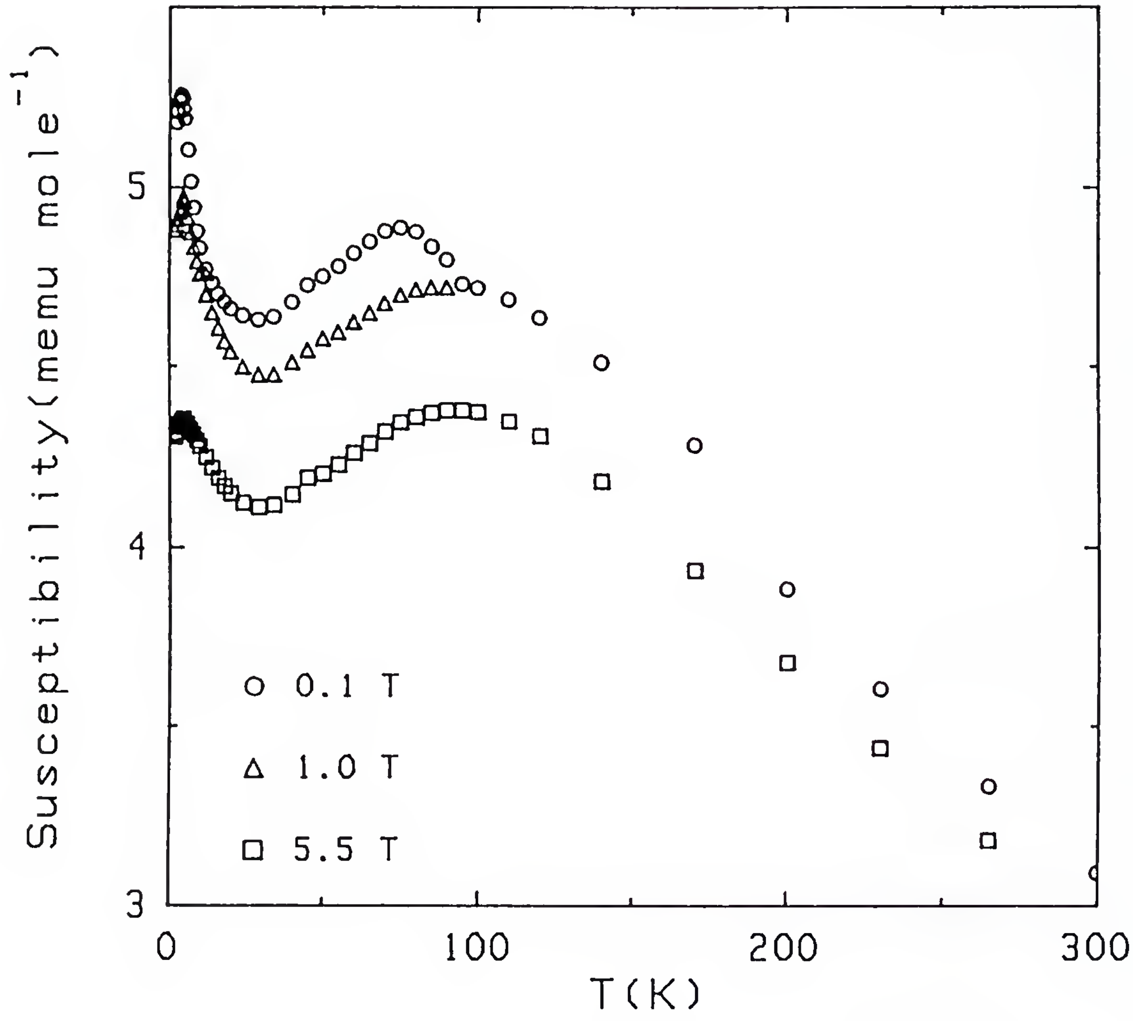

Figure A-2. Magnetic susceptibility χ_{dc} of $UNi_2Al_3H_{0.30}$ as a function of temperature in different magnetic fields. The peaks at low and high temperatures shift to higher temperatures with increasing magnetic field. The data points at 1.0 T (triangles) for $T >$ 100 K, not shown, are almost same with those at 0.1 T.

of the T_h^{peak} in hydrided UPd_2Al_3 in magnetic field as described in section 4.5.2.1. The absolute values of χ_{dc} decrease for both the parent system UNi_2Al_3 and its hydrogen doped systems with increasing magnetic field. The magnetic field H = 1.0 T destroys the abnormal change of slope completely.

If we compare the hydrogen effects on T_N between UNi_2Al_3 and UPd_2Al_3 from the specific heat measurements, shown in Figures A-1 and 4-10, we see that the decrease of T_N, can be approximately determined by the position of the anomaly, per hydrogen in UNi_2Al_3 is less sensitive than in UPd_2Al_3 by a factor of 3. It seems that the more localized moments magnetism in UPd_2Al_3 relative to the (more) dilute magnetism in UNi_2Al_3 can be responsible for the behavior implying more moment compensation in UPd_2Al_3 rather than in UNi_2Al_3.

A.2 $CeCu_{2.2}Si_2H_X$

$CeCu_{2.2}Si_2$ is the first superconducting heavy fermion system discovered with T_C = 0.65 K [Steglich *et al.*, 1979a; Assmus *et al.*, 1984] and $T_N \approx 0.6$ K [Nakamura *et al.*, 1988] with a tetragonal crystalline structure. We observed the change of the lattice parameters after doping hydrogen about x = 0.07 into the parent system; $\Delta a = +0.6$ %, $\Delta c = -0.7$ % (our parent system of $CeCu_{2.2}Si_2$ has a = 9.858 Å and c = 4.114 Å in the lattice parameters). The possible origin of the low affinity of hydrogen to this tetragonal system may be due to the crystalline structure being different from the hexagonal one (as shown in UPd_2Al_3 and the well-known hydrogen storage system $LaNi_5$). Even though we did not observe any hydrogen effects in specific heat measurements (not shown) within ±3 % between the parent and the hydrided systems, we observed an enhancement of χ_{dc} at low temperatures by about 40 %, shown in Figure A-3, and more saturation at lower magnetic fields in magnetization vs. magnetic field measurements at 1.8 K for the hydrided system, shown in Figure A-4.

A.3 UPt_3H_X

UPt_3 is one of the most studied heavy fermion systems, because it displays several interesting features in the phase diagram [Lin, 1993]. It has $T_C = 0.5$ K [Stewart *et al.*, 1984a], and there is an AFM transition at $T_N = 5$ K with ordered moments of (0.02 ± 0.01) μ_B lying in the basal plane [Aeppli *et al.*, 1988, 1989] in the hexagonal crystalline structure. We succeeded in hydriding the system up to x = 0.17, and the corresponding hydrogen doped system shows a change of the lattice parameters: $\Delta a = +0.35$ % and $\Delta c = +0.10$ %. Before we go on, we need to mention that there is a significant anisotropy in undoped UPt_3 in χ_{dc}. We display the experimental results in Figure A-5, and there is a difference of absolute values in χ_{dc} and a change in the anomaly at around 20 K in temperatures. However, after we ground the chunk, there is firstly a shift of the peak anomaly to lower temperatures and secondly an upturn at low temperatures as shown in Figure A-5. This behavior is not surprising in the polycrystalline sample, if we remember

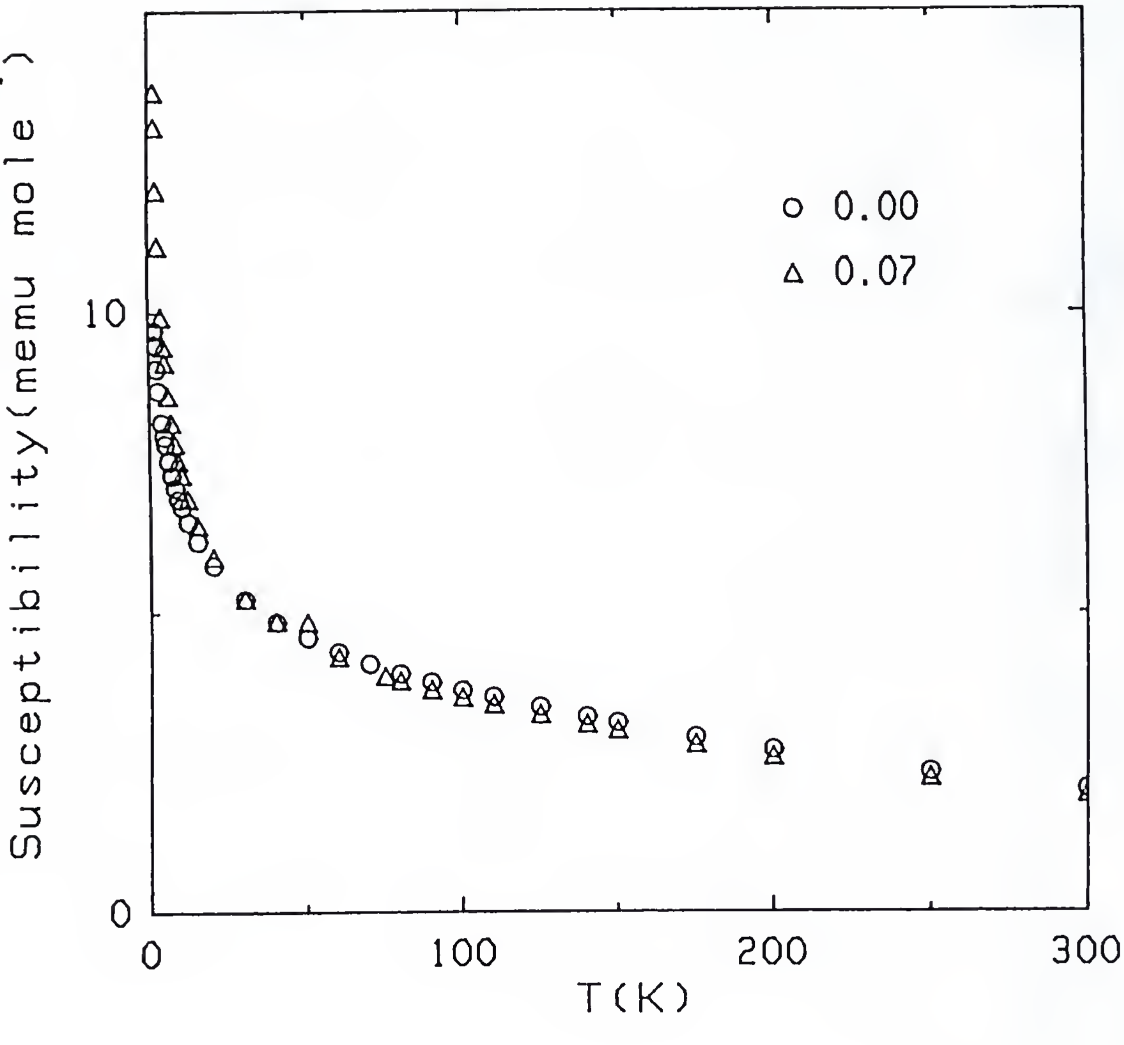

Figure A-3. Magnetic susceptibility χ of $CeCu_{2.2}Si_2H_x$ as a function of temperature at H = 0.5 T between 1.8 K and 300 K for x = 0.0 and 0.07 (both systems are pellets).

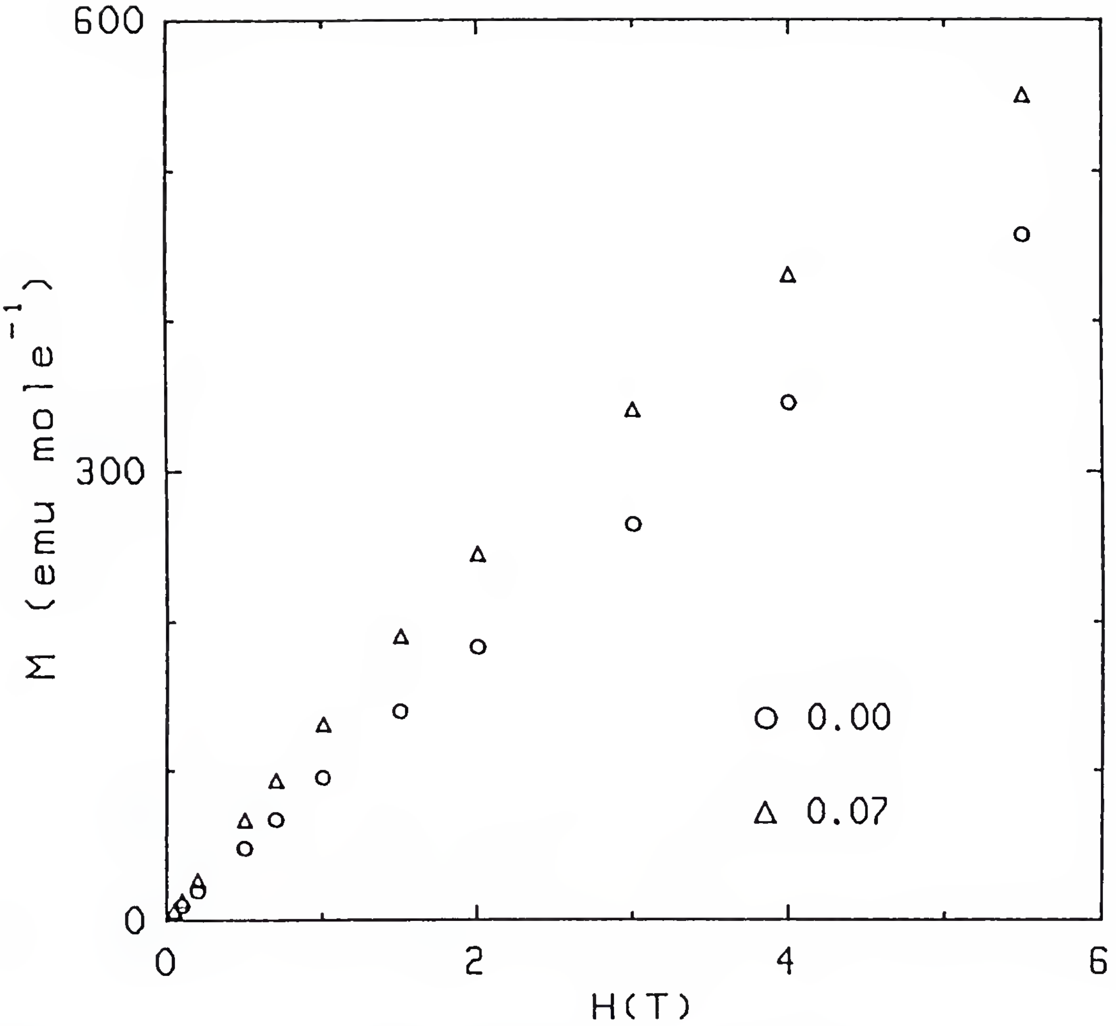

Figure A-4. Magnetization M of $CeCu_{2.2}Si_2H_x$ as a function of magnetic field at $T = 1.8$ K for x = 0.0 and 0.07 (both systems are pellets). There is much saturation at low field ($H < 3$ T) for x = 0.07 than for its parent system.

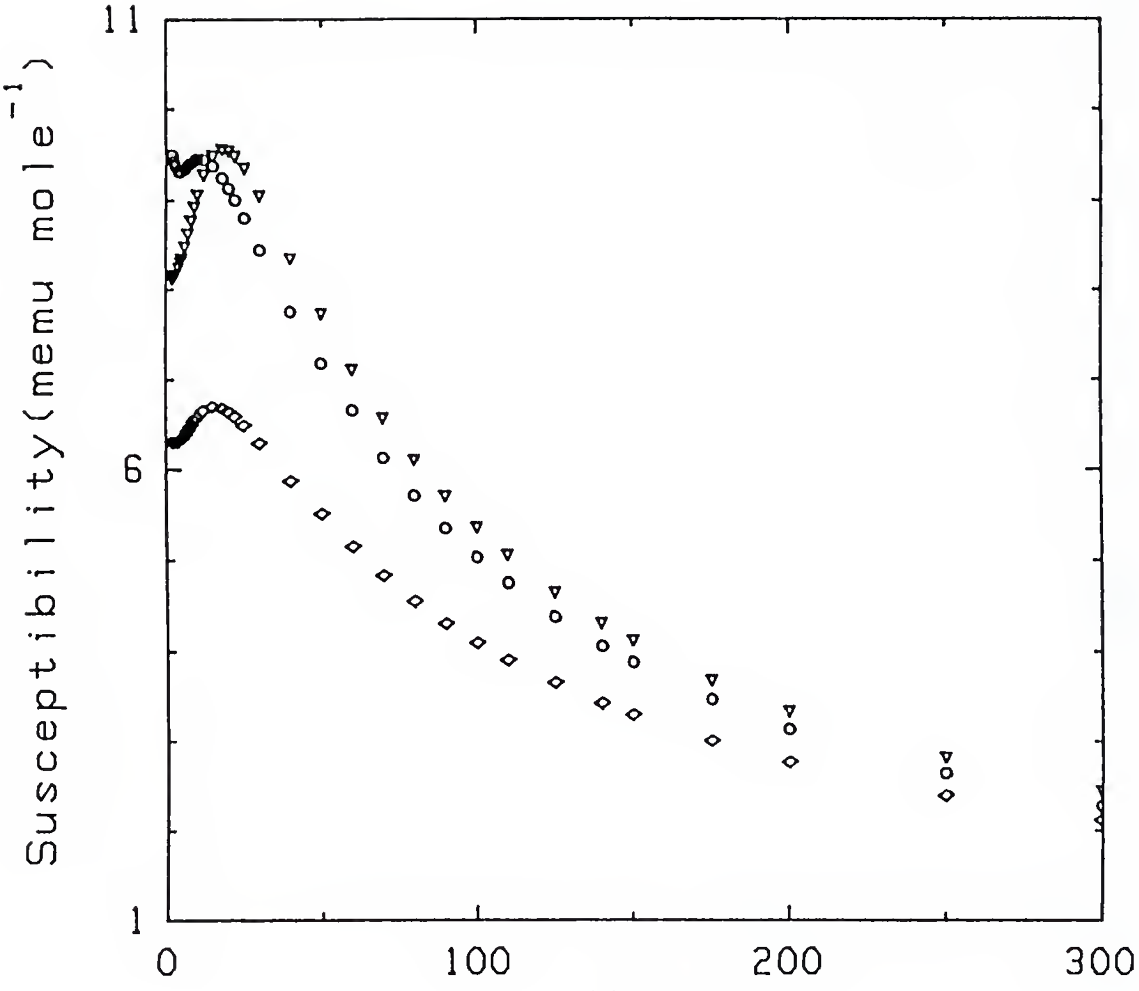

Figure A-5. Magnetic susceptibility χ of the polycrystalline sample of UPt_3 as a function of temperature at H = 0.5 T between 1.8 K and 300 K. As we see, there exists an anisotropy in the chunk (deltas and diamonds): The delta symbols represent the measurements of the preferential growth orientation of the sample perpendicular to the magnetic field. The diamond symbols represent the measurements of the preferential growth orientation of the sample parallel to the magnetic field, and there exists an upturn in χ with decreasing temperature for 1.8 K < T < 2.2 K. The circle symbols represent measurements of the powdered sample.

that there is such a peak as shown (delta simbol) in Figure A-5 along *a*b-plane and a monotonic decrease with temperature without the peak along the c-axis in single crystalline sample [Frings *et al.*, 1983].

For x = 0.17, the peak anomaly in χ_{dc} at 11 K in the parent pellet (or powdered sample) shifts to lower temperatures than 8 K followed by the shoulder, then an upturn below around 5 K as shown in Figure A-6. When we measured the specific heat of the hydrided system, we were very excited because of a broad anomaly at around 6 K, see Figure A-7. Since there was no bulk observation of the AFM transition at T_N = 5 K, this forced us to measure the pellet of the parent system, shown also in Figure A-7. As we see, the parent pellet also shows abnormal data which may be natural in the powdered system if we see again the χ_{dc} data at low temperatures (in contrast to the pellet result, the chunk of UPt_3 exhibits an upturn at low temperatures in the specific heat which is due to spin fluctuations at low temperatures, not shown here). Thus, we are investigating whether the anomaly seen in the specific heat measurements is related to hydrogen-induced magnetic ordering or just a stress effects due to the grinding.

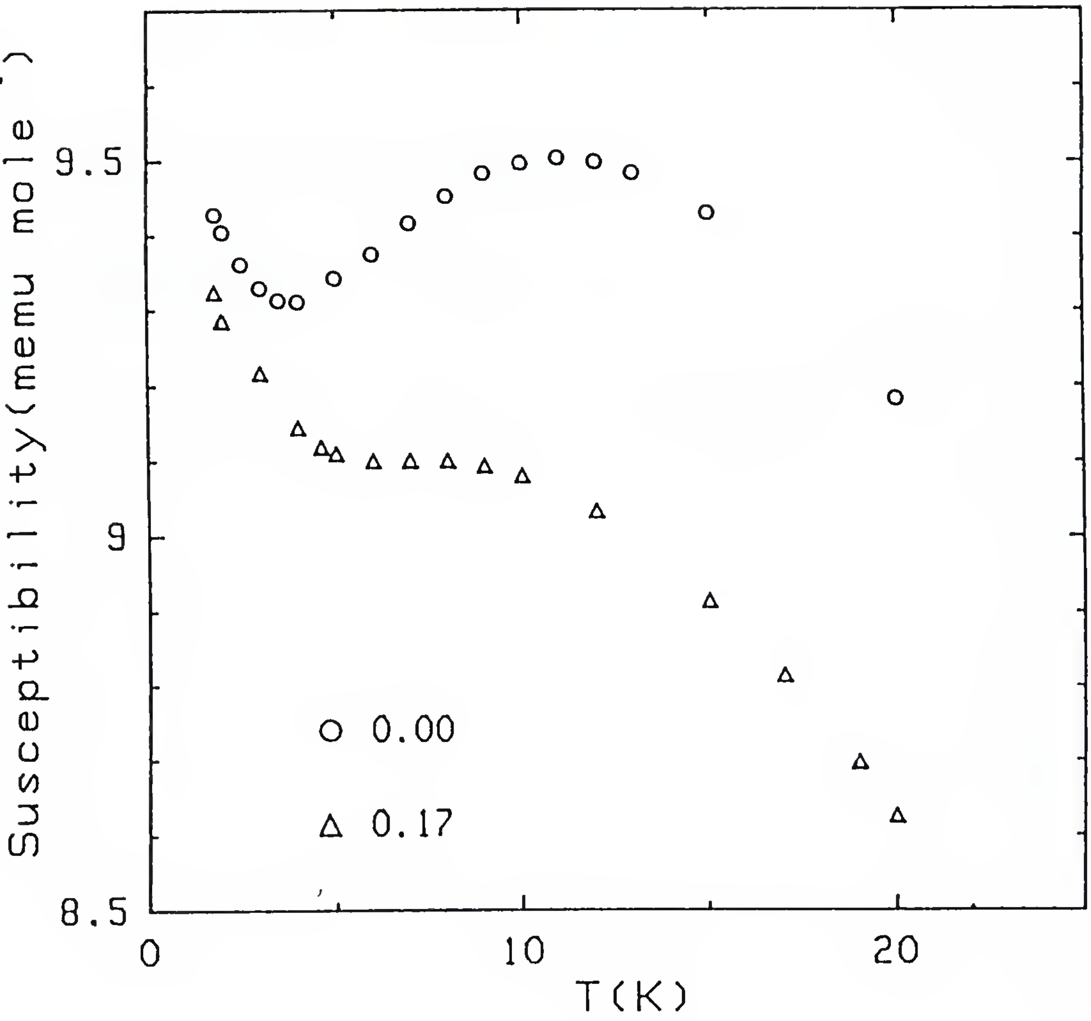

Figure A-6. Magnetic susceptibility χ_{dc} of UPt_3H_x for x = 0.0 and 0.17 (both systems are pellets) as a function of temperature at H = 0.5 T between 1.8 K and 20 K. The peak anomaly at around 11 K shifts to lower T and is smeared out leaving a shoulder as we dope with more hydrogen.

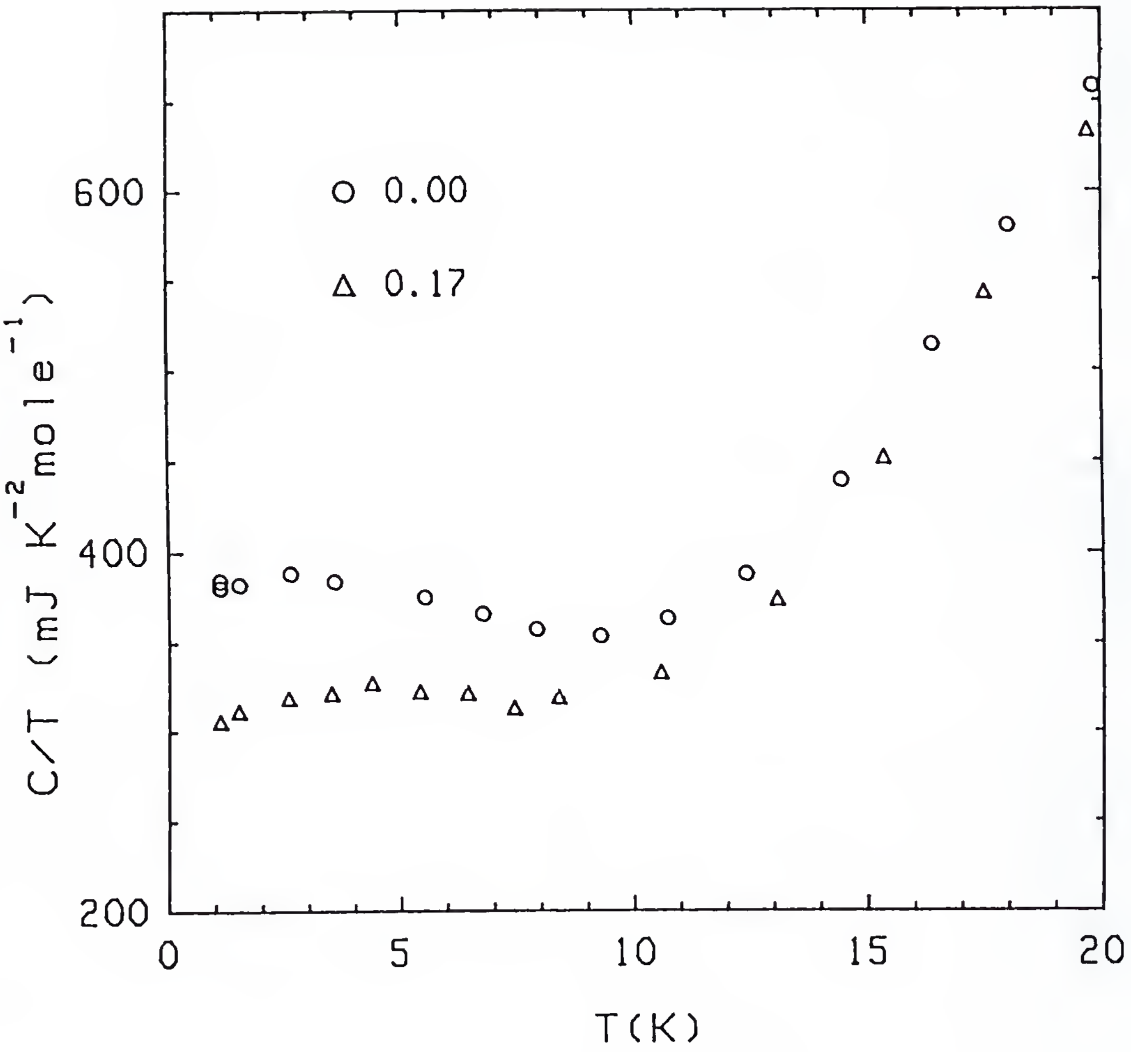

Figure A-7. Specific heat of UPt$_3$H$_x$ as *C/T* vs. *T* with x = 0.0 and 0.17 (both systems are pellets) for 1.0 K ≤ *T* ≤ 20 K. The broad peak at around 5 K is especially interesting, even though the powdered parent system also shows such a very weak anomaly.

REFERENCES

Aarts J. and Volodin A.P., Physica B **206-207**, 43 (1995).

Abrikosov A.A., Physics **2**, 5 (1965).

Aeppli G., Bishop D., Broholm C., Bucher E., Siemensmeyer K., Steiner M., and Stüsser N., Phys. Rev. Lett. **63**, 676 (1989).

Aeppli G., Bucher E., Broholm C., Kjems J.K., Baumann J., and Hufnagl J., Phys. Rev. Lett. **60**, 625 (1988).

Affleck I. and Ludwig A.W.W., Nucl. Phys. B **360**, 641 (1991).

Alefeld G. and Völkl J., *Topics in Applied Physics; Hydrogen in Metals I & II*, edited by G. Alefeld and J. Völkl, (Springer, Berlin 1978) **28-29**.

Alekseeviskii N.E., Mitin A.V., Nzhankovskii V.I., Firsov V.I., and Khlybou E.P., JETP Lett. **41**, 410 (1985).

Aliev F.G., Vieira S., Villar R., Martinez J.L., Seaman C.L., and Maple M.B., Physica B **206-207**, (1995).

Aliev F.G., Vieira S., Villar R., van der Meulen H.P., Bakker K., and Andreev A.V., JETP Lett. **58**, 762 (1993).

Amato A., Feyerherm R., Gygax F.N., Schenck A., Weber M., Caspary R., Hellmann P., Schank C., Geibel C., Steglich F., MacLaughlin D.E., Knetsch E.A., and Heffner R.H., Europhys. Lett. **19**, 127 (1992a).

Amato A., Geibel C., Gygax F.N., Heffner R.H., Knetsch E.A., MacLaughlin D.E., Schank C., Schenck A., Steglich F., and Weber M., Z. Phys. B - Condensed Matter **86**, 159 (1992b).

Amitsuka H., Hidano T., Honma T., Mitamura H., and Sakakibara T., Physica B **186-188**, 337 (1993).

Amitsuka H. and Sakakibara T., J. Phys. Soc. Jpn **63**, 736 (1994).

Amitsuka H., Tateyama K., Paulsen C.C., Sakakibara T., and Miyako Y., J. Magn. Magn. Mater. **104-107**, 60 (1992).

Andraka B., Physica B **199-200**, 239 (1994a).

Andraka B., Phys. Rev. B **49**, 348 (1994b).

Andraka B., Phys. Rev. B **49**, 3589 (1994c).

Andraka B., Fraunberger G., Kim J.S., Quitmann C., and Stewart G.S., Phys. Rev. B **39**, 6420 (1989).

Andraka B. and Stewart G.R., Rev. Sci. Instrum. **54**, 1529 (1991).

Andraka B. and Stewart G.R., Phys. Rev. B **47**, 3208 (1993).

Andraka B. and Tsvelik A., Phys. Rev. Lett. **67**, 2886 (1991).

Andrei N. and Destri C., Phys. Rev. Lett. **52**, 364 (1984).

Assmus W., Herrmann M., Rauchschwalbe U., Riegel S., Lieke W., Spille H., Horn S., Weber G., Steglich F., and Cordier G., Phys. Rev. Lett. **52**, 469 (1984).

Bachmann R., Di Salvo F.J. Jr., Geballe T.H., Greene R.L., Howard R.E., King C.N., Kirsch H.C., Lee K.N., Schwall R.E., Thomas H.U., and Zubeck R.B., Rev. Sci. Instrum. **43**, 205 (1972).

Barthem V.M.T.S., Gignoux D., Naït-Saada A., Schmitt D., and Creuzet G., Phys. Rev. B **37**, 1733 (1988).

Blackledge J.P., *Metal Hydrides*, edited by W.M. Mueller, J.P. Blackledge, and G.G. Libowitz (Academic Press, New York 1968).

Boer F.R.de, Franse J.J.M., Louis E., Menovsky A., Mydosh J.A., Palstra T.T.M., Rauchschwalbe U., Schlabitz W., Steglich F., and de Visser A., Physica B **138**, 1 (1986).

Boer F.R.de, Klaasse J.C.P., Veenhuizen P.A., Böhm P.A., Bredl C.D., Gottwick U., Mayer H.M., Pawlak L., Rauchschwalbe U., Spille H., and Steglich F., J. Magn. Magn. Mater. **63-64**, 91 (1987).

Bogenberger B. and Löhneysen H.v., Phys.Rev. Lett. **74**, 1016 (1995).

Böhm A., Grauel A., Sato N., Schank C., Geibel C., Komatsubara T., Weber G., and Steglich F., Int. J. Mod. Phys. **7**, 34 (1993).

Brandt N.B. and Moshchalkov V.V., Adv. Phys. **33**, 373 (1984).

Brison J.P., Ravex A., Flouquet J., Fisk Z., and Smith J.L., J. Magn. Mgan. Mater. **76** & **77**, 525 (1988).

Broholm C., Kjems J.K., Buyers W.J.L., Mattews P., Palstra T.T.M., Menovsky A.A., and Mydosh J.A., Phys. Rev. Lett. **58**, 1467 (1987).

Buschow K.H.J., *Handbook on the Physics and Chemistry of Rare Earths*, edited by K.A. Gschneidner Jr. and L. Eyring, (Elsevier Science Publishers B.V., Amsterdam 1984), **6**.

Buschow K.H.J. and van Mal H.H., J. Less-Common Metals **29**, 203 (1972).

Caspary R., Hellmann P., Keller M., Sparn C., Wassilew C., Köhler R., Geibel C., Schank C., Steglich F., and Phillips N.E., Phys. Rev. Lett. **71**, 2146 (1993).

Cort B., Stewart G.S., Snead C.L. Jr., Sweedler A.R., and Moehlecke S., Phys. Rev. B **24**, 3794 (1981).

Cox D.L., Phys. Rev. Lett. **59**, 1240 (1987a).

Cox D.L., *Theoretical and Experimental Aspects of Valence Fluctuations and Heavy Fermions,* edited by L.C. Gupta and S.K. Malik (Plenum, New York 1987b).

Cox D.L., J. Magn. Magn. Mater. **76-77**, 53 (1988a).

Cox D.L., Physica C **153**, 1642 (1988b).

Cox D.L., Physica B **186-188**, 1642 (1993).

Crow J.E. and Sweedler A.R., Rev. Sci. Instrum. **144**, 1398 (1973).

Cullity B.D., *Elements of X-ray Diffraction*, 2nd edition (Addison-Wesley Publishing, London 1978).

Date M. and Kindo K., J. Phys. Soc. Jpn. **62**, 1482 (1993).

Dalichaouch Y., de Andrade M.C., and Maple M.B., Phys. Rev. B **46**, 8671 (1992).

Desgranges H.U., J. Phys. C **18**, 5481 (1985).

Dobrosavljevic V., Kirkpatrick T.R., and Kotliar G., Phys.Rev. Lett. **69**, 1113 (1992).

Doniach S., Physica B **91**, 231 (1977).

Doniach S., Phys. Rev. B **35**, 1814 (1987).

Ejima T., Suzuki S., Sato S., Sato N., Fujimori S-i., Yamada M., Sato K., Komatsubara K., Kasuya T., Tezuka Y., Shin S., and Ishii T., J. Phys. Soc. Japan **63**, 2428 (1994).

Fernandes J.C., Continentino M.A., and Guimaraes A.P., Solid State Commun. **55**, 1011 (1985).

Feyerherm R., Amato A., Gygax F.N., Schenck A., Geibel C., Steglich F., Sato N., and Komatsubara T., Phys. Rev. Lett. **73**, 1849 (1994).

Franse J.J.M., Frings P.H., de Visser A., and Menovsky A., Physica B **126**, 116 (1984).

Frieske H. and Wicke E., Ber. Bunsenges. Physik. Chem. 77, 50 (1973).

Frings P.H., Franse J.J.M., de Boer F.R., and Menovsky A., J. Magn. Magn. Mater. **31-34**, 240 (1983).

Fulde P., Keller J., and Zwicknagl G., Solid State Phys. **41**, 1 (1988).

Fulde P. and Loewenhaupt M., Adv. Phys. **34**, 589 (1986).

Gajewiski D.A., Allenspach P., Seaman C.L., and Maple M.B., Physica B **199-200**, 419 (1994).

Geibel C., Ahlheim U., Bredl C.D., Diehl J., Grauel A., Helfrich R., Kitazawa H., Köhler R., Modler R., Lang M., Schank C., Thies S., Steglich F., Sato N., and Komatsubara T., Physica C **185-189**, 2651 (1991a).

Geibel C., Schank C., Jährling F., Buschinger B., Grauel A., Lühmann T., Gegenwart P., Helfrich R., Reinder P.H.P., and Steglich F., Physica B **199-200**, 128 (1994).

Geibel C., Schank C., Thies S., Kitazawa H., Bredl C.D., Böhm A., Rau M., Grauel A., Caspary R., Helfrich R., Ahlheim U., Weber G., and Steglich F., Z. Phys. B - Condensed Matter **84**, 1 (1991b).

Geibel C., Thies S., Kaczorowski D., Mehner A., Grauel A., Seidel B., Ahlheim U., Helfrich R., Petersen K., Bredl C.D., and Steglich F., Z. Phys. B - Condensed Matter **83**, 305 (1991c).

Gratz E., Bauer E., Barbara B., Zemirli S., Steglich F., Bredl C.D., and Lieke W., J. Phys. F **15**, 1975 (1985).

Grauel A., Böhm A., Fisch H., Geibel C., Köhler R., Modler R., Schank C., Steglich F., Weber G., Sato N., and Komatsubara T., Phys. Rev. B **46**, 5818 (1992).

Grauel A., Böhm A., Köhler R., Modler R., Geibel C., Sato N., Komatsubara T., Weber G., and Steglich F., Int. J. Mod. Phys. 7, 30 (1993).

Grewe N. and Steglich F., *Handbook on the Physics and Chemistry of Rare Earths*, edited by K.A. Gschneidner Jr. and L. Eyring (Elsevier, Amsterdam 1991), **14**.

Gruen D.M., J. Chem. Phys. **23**, 1708 (1955).

Grunzweig-Genossar J., Kuznietz M., and Meerovici B., Phys. Rev. B **1**, 1958 (1970).

Heisenberg W., Z. Phys. **49**, 619 (1928).

Hill H.H., *Plutonium 1970 and other Actinides*, edited by W.N. Miner (The Metallurgical Society of the AIME, New York 1970).

Inada Y., Aono H., Ishiguro A., Kimura J., Sato N, Sawada A., and Komatsubara T., Physica B **199-200**, 119 (1994).

Ingersent K., Jones B.A., and Wilkins J.W., Phys. Rev. Lett. **69**, 2594 (1992).

Isaacs E.D., Mcwhan D.B., Kleiman R.N., Bishop D.J., Ice G.E., Zschack P., Gaulin B.D., Mason T.E., Garrett J.D., and Buyers W.J.L., Phys. Rev. Lett. **65**, 3185 (1990).

Jee C.S., Andraka B., Kim J.S., Li H., Meisel M.W., and Stewart G.R., Phys. Rev. B **42**, 8630 (1990).

Kim J.S., Ph.D. Dissertation, University of Florida, Gainesville (May 1992).

Kim J.S., Andraka B., and Stewart G.R., Phys. Rev. B **44**, 6921 (1991).

Kim J.S., Andraka B., and Stewart G.R., Phys. Rev. B **45**, 12081 (1992).

Kim J.S. and Stewart G.R., Phys. Rev. B **49**, 327 (1994).

Kim W.W., Kim J.S., Andraka B., and Stewart G.S., Phys. Rev. B **47**, 12403 (1993).

Kim W.W. and Stewart G.S., Phys. Rev. B **50**, 9948 (1994).

Kim W.W. and Stewart G.R., Physica B **206-207**, 448 (1995).

Kim W.W., Stewart G.R., and Andraka B., Physica B **199-200**, 384 (1994).

Kohori Y. and Kohara T., Physica B **199-200**, 135 (1994).

Kondo J., Prog. Theor. Phys. **32**, 37 (1964).

Krimmel A., Fischer P., Roessli B., Maletta H., Geibel C., Schank C., Grauel A., Loidl A., and Steglich F., Z. Phys. B **86**, 161 (1992).

Kyogaku M., Kitaoka Y., Asayama K., Sato N., Sakon T., Komatsubara T., Geibel C., Schank C., and Steglich F., Physica B **186-188**, 285 (1993).

Lamoise A.M., Chaumont J., Meunier F., and Bernas H., J. Physique Lett. **36**, L-305 (1975).

Landau L.D., Sov. Phys. JETP **3**, 920 (1956).

Lee P.A., Rice T.M., Serene J.W., Sham L.J., and Wilkins J.W., Comm. Cond. Matt. Phys. **12**, 99 (1986).

Lin S.W., Ph.D. Dissertation, University of Wisconsin, Milwaukee (August 1993).

Löhneysen H.v., Pietrus T., Portisch G., Schlager H.G., Sieck M., and Trappmann T., Phys. Rev. Lett. **72**, 3262 (1994).

Ludwig A.W.W. and Affleck I., Phys. Rev. Lett. **67**, 3160 (1991).

Lynton E.A., *Superconductivity*, (Methuen, London 1962).

van Mal H.H., Chemie-Ing.-Techn. **45**, 80 (1973).

Maple M.B., de Andrade M.C., Herrmann J., Dalichaouch Y, Gajewski D.A., Seaman C.L., Chau R., Movshovich R., Aronson M.C., and Osborn R., J. Low Temp. Phys. **99**, 223 (1995).

Maple M.B., Chen J.W., Dalichaouch Y., Kohara T., Rossel C., and Torickachvili M.S., Phys. Rev. Lett. **56**, 185 (1986).

Mason T.E., Gaulin B.D., Garrett J.D., Tun Z., Buyers W.J.L., and Isaacs E.D., Phys. Rev. Lett. **65**, 3189 (1990).

Mignot J.-M., Flouquet J., Haen P., Lapierre F., Puech C., and Voiron J., J. Magn. Magn. Matte. **76-77**, 97 (1988).

Mihalik M., de Visser A., Bakker K., Tai L.T., Menovsky A.A., Hendrikx R.W.A., Gortenmulder T.J., Matas S., and Sato N., Physica B **186-188**, 507 (1993).

Mihály L. and Zawadowski A., J. Phys. Lett. (Paris) **39**, L483 (1978).

Miyako Y., Kawarazaki S., Amitsuka H., Paulsen C.C., and Hasselbach K., J. Appl. Phys. **70**, 5791 (1991).

Mydosh J.A., Phys. Scripta **119**, 260 (1987).

Nakamura H., Kitaoka Y., Yamada H., and Asayama K., J. Magn. Magn. Mater. **76-77**, 517 (1988).

Naughton M.J., Dickinson S., Samaratunga R.C., Brooks J.S., and Martin K.P., Rev. Sci. Instrum. **54**, 1529 (1983).

Nozieres P., *Theory of Interacting Fermi Systems* (W.A. Benjamin, Inc. NewYork 1963).

Nozières Ph., J. Low Temp. Phys. **71**, 205 (1974).

Nozières Ph., Ann. Phys. Fr. **10**, 19 (1985).

Nozières Ph. and Blandin A., J. Physique **41**, 193 (1980).

Okada I. and Yosida K, Prog. Theor. Phys. **49**, 1483 (1973).

Ott H.R. and Fisk Z., *Handbook on the Physics and Chemistry of the Actinides*, edited by A.J. Freeman and G.H. Lander (Elsevier Science Publishers B.V., Amsterdam 1987), **3**.

Ott H.R., Rudigier H., Felder E., Fisk Z., and Batlogg B., Phys. Rev. Lett. **55**, 1595 (1985).

Ott H.R., Rudigier P., Fisk Z., and Smith J.L., Phys. Rev. Lett. **50**, 1595 (1983).

Ott H.R., Rudigier H., Fisk Z., Willis J.O., and Stewart G.R., Solid State Commun. **53**, 235 (1984).

Palstra T.T.M., Menovsky A., van den Berg J., Dirkmaat A.J., Kes P.H., Niewenhuys G.J., and Mydosh J.A., Phys. Rev. Lett. **55**, 2727 (1985).

Paolasini L., Paixão J.A., Lander G.H., Burlet P., Sato N., and Komatsubara T., Phys. Rev. B **49**, 7072 (1994).

Park J.-G., J. Phys. Condens. Matter **6**, 3403 (1994).

Park J.-G., Roy S.B., and Coles B.R., J. Phys. Condens. Matter **6**, 5937 (1994).

Parks R.D., *Superconductivity*, (Marcel Dekker, New York 1969).

Pines D. and Nozieres P., *The Theory of Quantum Liquids: Normal Fermi Liquids* (Addison-Wesley Publishing Company, Inc. 1989).

Radwanski R.J. and Franse J.J.M., Int. J. Mod. Phys. 7, 38 (1993).

Ramirez A.P., Batlogg B., Bucher E., Cooper A.S., Phys. Rev. Lett. **57**, 1072 (1986).

Rauchschwalbe U., Physica B **147**, 1 (1987).

Rauchschwalbe U., Lieke W., Bredl C.D., Steglich F., Aarts J., Martini K.M., and Mota A.C., Phys. Rev. Lett. **49**, 1448 (1982).

Rose-Innes A.C. and Rhoderick E.H., *Introduction to Superconductivity*, 2nd edition (Pergamon Press, New York 1980).

Roy S.B., Pradhan A.K., and Chaddah P., J.Phys. Condens. Matter. **6**, 253 (1994).

Rundle R.E., J. Am. Chem. Soc. **73**, 4172 (1951).

Sacramento P.D. and Schlottmann P., Phys. Rev. B **40,** 431 (1989a).

Sacramento P.D. and Schlottmann P., Phys. Lett. A **142,** 245 (1989b).

Sacramento P.D. and Schlottmann P., Physica B **163,** 231 (1990).

Sacramento P.D. and Schlottmann P., Phys. Rev. B **43,** 13294 (1991a).

Sacramento P.D. and Schlottmann P., J. Phys. Condensed Matter **3**, 9687 (1991b).

Sampathkumaran E.V., Z. Phys. B **90**, 195 (1993).

Sandrock G.D., *Hydrides for Energy Storage*, edited by A.F. Andresen and A.J. Maeland (Pergamon, Oxford 1978).

Sato N., Sakon T., Takeda N., Imamura K., Inada Y., Aono H., and Komatsubara T., Physica B **186-188**, 195 (1993).

Sato N., Sakon T., Takeda N., Komatsubara T., Geibel C., and Steglich F., J. Phys. Soc. Japan **61**, 32 (1992).

Schank C., Jährling F., Grauel C., Borth R., Helfrich R., Lühmann T., Reinders P.H.P., Geibel C., and Steglich F., J. of Alloys & Compounds **213-214**, 509 (1994).

Schank C., Jährling F., Tegel U., Geibel C., Grauel A., Böhm A., Borth R., Helfrich R., Jaeckel D., Weber G., and Steglich F., Int. J. Mod. Phys. **7**, 46 (1993).

Schlabitz W., Baumann J., Pollit B., Rauchswalbe U., Mayer H.M., Ahlheim U., and Bredl C.D., Z. Phys. B - Condensed Matter **62**, 171 (1986).

Schlapbach L., *Topics in Applied Physics; Hydrogen in Intermetallic Compounds I*, edited by L. Schlapbach (Springer-Verlag, New York 1992), **67**.

Schlapbach L., *Topics in Applied Physics; Hydrogen in Intermetallic Compounds II*, edited by L. Schlapbach (Springer-Verlag, New York 1988), **63**.

Schlottmann P., Phys. Rep. **181**, 1 (1989).

Schlottmann P., J. Phys. Condensed Matter **3**, 6617 (1991c).

Schlottmann P. and Sacramento P.D., Adv. Phys. **42,** 641 (1993).

Schröder A., Lussier J.G., Gaulin B.D., Garret J.D., Buyers W.J.L., Rebelsky L., and Shapiro S.M., Phys. Rev. Lett. **72**, 136 (1994).

Seaman C.L., Maple M.B., Lee B.W., Ghamaty S., Torikachvili M.S., Kang J.-S., Liu L.Z., Allen J.W., and Cox D.L., Phys. Rev. Lett. **67**, 2882 (1991).

Shirber J.E. and Morosin B., Phys. Rev. B **12**, 117 (1975).

Signore P.J.-C., Ph.D. Dissertation, University of Florida, Gainesville (May 1995).

Silin V.P., Sov. Phys. JETP **6**, 387 (1958).

Steglich F., Aarts J., Bredl C.A., Lieke W., Meschede D., Franz W., and Schäfer J., Phys. Rev. Lett. **43**, 1892 (1979a).

Steglich F., Ahlheim U., Böhm A., Bredl C.D., Caspary R., Geibel C., Grauel A., Helfrich R., Köhler R., Lang M., Menher A., Modler R., Schank C., Wassilew C., Weber G., Assmus W., Sato N., and Komatsubara T., Physica C **185-189**, 379 (1991).

Steglich F., Bredl C.A., Loweonhaupt M., and Schotte K.D., J., Phys. (Paris) **40**, C5-301 (1979b).

Steglich F., Geibel C., Gloos K., Olesch G., Schank C., Wassilew C., Loidl A., Krimmel A., and Stewart G.R., J. Low Temp. Phys. **95**, 3 (1994).

Steglich F., Geibel C., Modler R., Lang M., Hellmann P., and Gegenwart P., J. Low Temp. Phys. **99**, 267 (1995).

Stewart G.R., Rev. Sci. Instrum. **54**, 1 (1983).

Stewart G.R., Rev. Mod. Phys. **56**, 755 (1984)

Stewart G.S., Andraka B., Quitmann C., Treadway B., Shapira Y., and McNiff E.J., Phys. Rev. B **37**, 3344 (1988).

Stewart G.R., Fisk Z., Willis J.O., and Smith J.L., Phys. Rev. Lett. **52**, 679 (1984a).

Stewart G.R., Fisk Z., and Wire M.S., Phys. Rev. B **30**, 482 (1984b).

Stewart G.R., Giorgi A.L., Willis J.O., and O'Rourke J., Phys. Rev. B **34**, 4629 (1986).

Sticht J. and Kübler J., Z. Phys. B - Condensed Matter **87**, 299 (1992).

Stoner E.C., Proc. R. Soc. A **165**, 372 (1938).

Stritzker B. and Wühl, H., *Topics in Applied Physics; Hydrogen in Metals II*, edited by G. Alefeld and J. Völkl (Springer, Berlin 1978) **29**.

Suhl H., Phys. Rev. A **138**, 515 (1965).

Switendick A.C., *Topics in Applied Physics; Hydrogen in Metals I*, edited by G. Alefeld and J. Völkl (Springer, Berlin 1978) **28**.

Switendick A.C., J. Less-Common Met. **88**, 157 (1982).

Torre A.L.d.l., Visani P., Dalichaouch Y., Lee B.W., and Maple M.B., Physica B **179**, 208 (1992).

Tsvelik A.M., J. Phys. C **18**, 159 (1985).

Tsvelik A.M., J. Phys. Condens. Matter **2**, 2833 (1990).

Tsvelik A.M. and Reizer M., Phys. Rev. B **48**, 9887 (1993).

Tsvelik A.M. and Wiegmann P., Z. Phys. B **54**, 201 (1984).

Tsvelik A.M. and Wiegmann P. B., J. Stat. Phys. **38**, 125 (1985).

Uemura Y.J. and Luke G.M., Physica B **186-188**, 223 (1993).

Varma C.M., Littlewood P.B., Schmitt-Rink S., Abrahams E., and Ruckenstein A.E., Phys. Rev. Lett. **63**, 1996 (1989).

de Visser A., Bakker K., Tai L.T., Menovsky A.A., Mentink S.A.M., Nieuwenhuys G.J., and Mydosh J.A., Physica B **186-188**, 291 (1993).

de Visser A., van der Meulen H.P., Tai L.T., and Menovsky A.A., Physica B **199-200**, 100 (1994).

de Visser A., Nakotte H., Tai L.T., Menovsky A.A., Mentink S.A.M., Nieuwenhuys G.J., and Mydosh J.A., Physica B **179**, 84 (1992).

van Vucht J.H.N., Kuijpers F.A., and Bruning H.C.A.M., Philips. Res. Repts. **25**, 133 (1970).

Walter U., Schlabitz W., Loewenhaupt H., and Loong C.-K., Phys. Rev. B **33**, 7875 (1986).

Ward J.W., *Handbook on the Physics and Chemistry of the Actinides*, edited by A.J. Freeman and C. Keller (Elsevier Science Publishers B.V., Amsterdam 1985a), **3**.

Ward J.W., Physica B **130**, 510 (1985b).

Ward J.W., Cox L.E., Smith J.L., Stewart G.R., and Wood J.H., J. Phys. (Paris) **40**, C4 (1979).

Wicke E., Brodowsky H., and Züchner, *Topics in Applied Physics; Hydrogen in metals II*, edited by G. Alefeld and J. Völkl (Springer-Verlag, New York 1978), **29**.

Wiegmann P.B. and Tsvelik A.M., JETP Lett. **38**, 591 (1983).

Wiesinger G. and Hilscher G., *Handbook of Magnetic Materials*, edited by K.H.J. Buschow (Elsevier Science Publishers B.V., Amsterdam 1991), **6**.

Yoshimori A., Prog. Theor. Phys. **55**, 67 (1976).

BIOGRAPHICAL SKETCH

Weonwoo Kim was born on February 13, 1962, Young-Wol, Kang-Won Province, Korea. He moved to Choon-Chun city in 1977 where he graduated from Choon-Chun High School in 1980. He then entered the Korea University in Seoul, the capital city of Korea, in 1980 and received a Bachelor of Science with a major in physics in 1984, and a Master of Science with a major in statistical physics in 1986. He then moved to Gainesville, Florida, in August 1988, since that time on he has been working toward the Doctor of Philosophy degree at the University of Florida.

I certify that I have read this study and that in my opinion it conforms to acceptable standards of scholarly presentation and is fully adequate, in scope and quality, as a dissertation for the degree of Doctor of Philosophy.

G. R. Stewart

Gregory R. Stewart, Chair
Professor of Physics

I certify that I have read this study and that in my opinion it conforms to acceptable standards of scholarly presentation and is fully adequate, in scope and quality, as a dissertation for the degree of Doctor of Philosophy.

Timothy J Anderson

Timothy J. Anderson
Professor of Chemical Engineering

I certify that I have read this study and that in my opinion it conforms to acceptable standards of scholarly presentation and is fully adequate, in scope and quality, as a dissertation for the degree of Doctor of Philosophy.

J. K. Ing

Kevin J. Ingersent
Assistant Professor of Physics

I certify that I have read this study and that in my opinion it conforms to acceptable standards of scholarly presentation and is fully adequate, in scope and quality, as a dissertation for the degree of Doctor of Philosophy.

Pradip Kumar

Pradeep Kumar
Professor of Physics

I certify that I have read this study and that in my opinion it conforms to acceptable standards of scholarly presentation and is fully adequate, in scope and quality, as a dissertation for the degree of Doctor of Philosophy.

N S Sullivan

Neil S. Sullivan
Professor of Physics

I certify that I have read this study and that in my opinion it conforms to acceptable standards of scholarly presentation and is fully adequate, in scope and quality, as a dissertation for the degree of Doctor of Philosophy.

Yasumasa Takano
Associate Professor of Physics

This dissertation was submitted to the Graduate Faculty of the Department of Physics in the College of Liberal Arts and Sciences and to the Graduate School and was accepted as partial fulfillment of the requirements for the degree of Doctor of Philosophy.

August, 1995

Dean, Graduate School

LD
1780
1995
.K497

UNIVERSITY OF FLORIDA
3 1262 08553 7156